DHR51 as a coordinator of heme biosynthesis and steroid hormone production to time metamorphosis in *Drosophila melanogaster*

by

Brian Terry Phelps

A thesis submitted in partial fulfillment of the requirements for the degree of

Doctor of Philosophy

in

Molecular Biology and Genetics

Department of Biological Sciences

University of Alberta

Abstract

Development from a juvenile to an adult animal is driven by pulses of steroid hormones released at precise developmental times. Inputs from the environment, timing cues, and nutritional factors are all coordinated to produce a steroid hormone pulse. Insects and in particular, the fruit fly *Drosophila melanogaster*, have long been used to study the actions of steroid hormones, how steroid hormones are made, and signaling pathways that regulate steroid hormone production. In *Drosophila*, the primary steroid hormone, ecdysone, is synthesized from cholesterol in a specialized endocrine gland called the prothoracic gland. Multiple highly expressed cytochrome P450 enzymes are involved in synthesizing ecdysone. Ecdysone is then released into the larval body to initiate developmental transitions such as larval molts and metamorphosis. Each cytochrome P450 enzyme requires heme as a cofactor to function. The prothoracic gland must also have a high demand for heme due to the high levels of cytochrome P450 enzymes. Mutations that disrupt late stages of heme biosynthesis cause the prothoracic gland to accumulate red autofluorescent heme precursors due to an attempt to increase heme biosynthesis. This unique accumulation of red autofluorescent heme precursors is only seen in two other tissues, which also happen to highly express cytochrome P450 enzymes, highlighting the importance of heme in the prothoracic gland for cytochrome P450 enzymes. Due to the connection between heme and cytochrome P450 enzymes, I hypothesize that heme is an important input into regulating ecdysone production in the prothoracic gland and that heme biosynthesis and ecdysone production are coordinately regulated during the final larval stage to produce a major ecdysone pulse to initiate metamorphosis.

To understand the importance of heme and heme regulation in the prothoracic gland, my first aim was to identify a heme sensor that can detect when cellular heme levels are low and

upregulate heme biosynthesis in response. My primary candidate for a heme sensor was the nuclear receptor DHR51, *Drosophila* hormone receptor 51, which is capable of reversibly binding heme *in vitro*. To determine whether DHR51 acts as a heme sensor, I used qPCR to determine that loss-of-*DHR51* attenuated the expression of the rate-limiting enzyme in the heme biosynthesis pathway when cellular heme levels were low. RNA-Seq and heme measurements of *DHR51*-RNAi larvae provided evidence that loss-of-*DHR51* disrupted heme homeostasis, lowering cellular heme levels. However, I was unable to determine whether heme binding is relevant *in vivo* and whether DHR51 functions as a heme sensor as predicted. In addition to DHR51's apparent role in maintaining heme homeostasis, DHR51 is also necessary for ecdysone production. qPCR and RNA-Seq identified that *DHR51*-RNAi in the prothoracic gland reduced the expression of most of the ecdysone biosynthetic enzyme genes, which led to a reduced ecdysone titer that was measured with an ecdysone enzyme immunoassay. I provided evidence that DHR51 regulated ecdysone production through the circadian rhythm, the day-night cycle, as *DHR51*-RNAi disrupted the expression of core circadian rhythm genes. I commissioned the production of a DHR51 antibody that can be used in future chromatin immunoprecipitation experiments to identify direct target genes of DHR51 to determine whether DHR51 binds to heme biosynthetic genes, circadian rhythm genes, or ecdysone biosynthetic genes. Since heme and ecdysone are primarily produced during the night, I propose that DHR51 coordinates heme biosynthesis and ecdysone production in the prothoracic gland via the circadian rhythm.

Acknowledgments

I want to give a special thanks to Dr. Kirst King-Jones for accepting me into his lab and for guiding me on my research projects. I always appreciated the critical feedback on my projects, presentations, and writing as the comments helped me to grow and perform better as a researcher and communicator. I would also like to thank my committee members Dr. Heather McDermid and Dr. Andrew Waskiewicz for putting up with my long reports and long meetings, as well as providing useful feedback on my projects and for suggestions for future experiments.

I am very thankful for all the past members of the King-Jones lab for answering all my questions and helping me when I was just starting, especially Dr. Qiuxiang Ou. I would also like to thank the current members of the King-Jones lab for providing feedback on my projects and helping me with CRISPR-related techniques. I want to specifically thank Pendleton Cox, Dr. Jie Zeng, and Sattar Soltani for all the coffee breaks and science discussions that we had. Also, I thank Sattar again for saving me many trips to the university just to change the food for my fly cages.

Lastly, I would like to thank my friends and family that helped me to maintain my sanity during my program. My friends provided an escape from my work when I needed it and also provided helpful discussions related to my research. I specifically want to thank my mom and Binh Le for all their support; they helped me to cope with all my stresses nearing the end of my program and were patient with me when I needed to prioritize lab work.

Table of Contents

List of figures

List of Tables

Abbreviations

20E	20-hydroxyecdysone
7dC	7-dehydrocholesterol
act	*actin*
ALA	Aminolevulinic acid
Alas	*Aminolevulinate synthase*
ana	*anachronism*
BDGP	Berkeley *Drosophila* Genome Project
BLAST	Basic Local Alignment Search Tool
bp	base pair
BRG	Brain-ring gland
Cas9	CRISPR-associated nuclease
cDNA	Complementary DNA
ChIP	Chromatin immunoprecipitation
clk	*clock*
CRISPR	Clustered regularly interspaced short palindromic repeats
CRS	*Circadian regulatory sequence*
cry	*cryptochrome*
C_t	Threshold cycle
cyc	*cycle*
CyO	*Curly O* (*of Oster*) (2^{nd} chromosome balancer)
DBD	DNA-binding domain
DGRC	*Drosophila* Genomics Resource Center
DHR51	*Drosophila* hormone receptor 51
dib	*disembodied*
dilps	*Drosophila* insulin-like peptides
DNA	Deoxyribonucleic acid
Dronc	*Death regulator Nedd2-like caspase*
DRSC	*Drosophila* RNAi Screening Center
dsf	*dissatisfaction*
EcR	*Ecdysone receptor*

EIA	Enzyme immunoassay
ERK	Extracellular signal-regulated kinase
esg	*escargot*
FeCH	*Ferrochelatase*
GAL4	Galactose-responsive transcription factor
GFP	*Green fluorescent protein*
gRNA	Guide RNA
hr	hour
Hr51	Hormone receptor 51
HRP	Horseradish peroxidase
hs	heat shock
IIS	Insulin/Insulin-like growth factor signaling
InR	*Insulin-like receptor*
kDa	Kilodaltons
L1	First instar
L2	Second instar
L3	Third instar
LBD	Ligand-binding domain
MAPK	Mitogen-activated protein kinase
min	minute(s)
miRNA	Micro RNA
ml	millilitres
Mmp1	*Matrix metalloproteinase 1*
mRNA	Messenger RNA
Nc	*See Dronc*
nm	nanometer
NO	Nitric oxide
Nos	*Nitric oxide synthase*
Npc1a	*Niemann-Pick type C-1a*
Nplp4	*Neuropeptide-like precursor 4*
NR2E3	Nuclear receptor subfamily 2 group E member 3

nvd	*neverland*
Pbgs	*Porphobilinogen synthase*
PBS	Phosphate-buffered saline
PCR	Polymerase chain reaction
per	*period*
PG	Prothoracic gland
PGC-1α	*Peroxisome proliferator-activated receptor-gamma coactivator 1alpha*
phm	*phantom*
phm22	*phm-GAL4* – strong prothoracic gland *GAL4* expression of
PNR	Photoreceptor cell-specific nuclear receptor
PPOX	Protoporphyrinogen oxidase
PTTH	Prothoracicotropic hormone
qPCR	Quantitative real-time PCR
RG	Ring gland
RNA	Ribonucleic acid
RNAi	RNA interference
RORE	*Retinoid-related orphan receptors element*
rp49	*Ribosomal protein 49*
RPKM	Reads per kilobase of transcript per million mapped reads
rpm	revolutions per minute
RT	Room temperature
sad	*shadow*
shd	*shade*
s-LNv	small ventral lateral neurons
SOE	Splicing by overlap extension
spo	*spook*
spok	*spookier*
spz5	*spatzle5*
srl	*spargel*
sro	*shroud*
svp	*seven up*

tim	*timeless*
tll	*tailless*
TOR	Target of Rapamycin
tor	*torso*
Tsc1	*Tuberous sclerosis complex 1*
UAS	Upstream activation sequence
unf	*unfulfilled* (*DHR51*)
UV	Ultraviolet
VDRC	Vienna *Drosophila* Resource Center
w	*white*
w^{1118}	*white* mutant allele – used as a control genotype
WT	Wild type
ZT	Zeitgeber time (On a 12 hour light:dark cycle, lights turn on at ZT0 and lights turn off at ZT12)

Chapter 1

Introduction

1.1 General Introduction

1.1.1 Steroid hormones regulate developmental timing

Steroid hormones are signaling molecules in animals that are released as pulses at precise times to regulate a variety of processes, such as metabolism, immune responses, sexual development, and reproduction. Steroid hormones are lipid-based hormones synthesized from cholesterol or other suitable sterols. In humans, there are five main groups of steroid hormones: glucocorticoids and mineralocorticoids, which are primarily made in the adrenal cortex, and androgens, estrogens, and progestogens, which are made primarily in the ovaries and testes. Once these hormones are synthesized, they are released into the bloodstream where they travel to affect target tissues. Glucocorticoids regulate glucose metabolism and have anti-inflammatory and immunosuppressive effects in the immune system. Mineralocorticoids help balance salt and water levels in the body. The sex hormones comprising the androgens (such as testosterone), estrogens, and progestogens are more commonly known.

In humans, sex hormones play fundamental roles in sex differentiation. Sex determination occurs during embryogenesis to begin development of the gonads. Sex determination is regulated by transcription factors based on the presence or absence of the Y chromosome (Biason-Lauber. 2016). If testes begin to develop, testosterone is produced, which further develops the gonads and causes the epididymis, vas deferens, and prostate to differentiate. If testes do not develop or testosterone is not produced, then the default program will lead to ovarian development. This can be seen in mice, where genetically male mice that do not produce testosterone are phenotypically female (Birk, et al. 2000).

The sex hormones are also critical during puberty, a transition from childhood to adulthood. During puberty, secondary sexual characteristics further develop and the gonads

mature such that they are capable of reproduction. Hormonal signals from the brain to the gonads promote sex hormone production and the beginning of puberty. During puberty, males highly produce the androgen testosterone and females produce estrogens to help develop male and female secondary sex characteristics, respectively. Testosterone in males increases muscle mass, induces growth of body and facial hair, and influences a male body shape. In females, estrogens develop the breasts, influence a female body shape, and initiates the menstrual cycle (Tanner. 1986). Estrogen helps to regulate the menstrual cycle by aiding to thicken the uterus lining. Levels of progestogens, such as progesterone, begin to increase to prepare the uterus for implantation, but if implantation does not occur, progesterone levels decrease, resulting in menstruation. In general, progestogens help to maintain pregnancies.

Knowledge of these hormones and how they work have allowed for the development of anabolic steroids, which can be used to treat patients with chronic wasting conditions or treat patients that do not produce sufficient testosterone, but anabolic steroids have also been abused for their ability to increase muscle mass. Estrogens and progestin have been developed for use in birth control pills and hormone replacement therapy to treat symptoms associated with menopause. In general, for humans, ten years after birth, production of the sex hormones begin to increase which marks the onset of puberty, when juveniles develop into a mature, reproductive adult and develop secondary sex characteristics. The onset of this developmental transition is at the heart of my research. What inputs are affecting developmental timing? How does the body determine when the time is right and that there are enough resources to progress development? It has been documented that the onset of puberty is years earlier now in humans than several decades ago (Brudevoll, et al. 1979; Soliman, et al. 2014). One of the various factors that seem to be linked to the earlier onsets of puberty is nutrition. Although there is some understanding of

what factors affect developmental timing and the molecular processes that regulate the onset of puberty, there is still much to learn.

The fruit fly, *Drosophila melanogaster*, has proven to be a highly valuable model organism for studying how steroid hormones are synthesized and how steroid hormone synthesis is regulated. *Drosophila*, in combination with *Bombyx mori* (the silkworm) and *Manduca sexta* (the tobacco hornworm), have a long history of being used to study steroid hormone research (Butenandt and Karlson. 1954), ranging from studying steroid hormone production, to the actions of steroid hormones, and to the regulation of steroid hormone production. In addition, *Drosophila* also provided a useful model because the levels of steroid hormones have been mapped throughout the animals' lifespan, up to adulthood (Richards. 1981; Warren, et al. 2006). *Drosophila* primarily uses the steroid hormone ecdysone to progress development. Like the sex hormones in humans during puberty, ecdysone initiates the onset of metamorphosis, a process in which a juvenile larva transitions to a mature, reproductive adult fly. In addition to metamorphosis, ecdysone is used to initiate larval molts. While there are other steroid hormones in flies such as makisterone A, these other hormones have similar roles to ecdysone and their production is dependent on the available sterols in the diet (Redfern. 1984). Collectively, these steroid hormones are called ecdysteroids, but I will use the term "ecdysone" for simplicity since ecdysone use is favored in *Drosophila*.

Ecdysone pulses progress development by initiating larval molting and metamorphosis. Ecdysone titers increase as a pulse of ecdysone is released prior to hatching and larval molts (Richards. 1981). This is why ecdysone is known as the "molting hormone". As mentioned previously, ecdysone titers have been mapped throughout the *Drosophila* life cycle (Figure 1-1A). *Drosophila* has a life cycle of approximately ten days at 25°C and can be slowed by

lowering the temperature. The embryonic stage lasts for about one day and first instar larvae (L1) hatch after a pulse of ecdysone. The first (L1) and second instar (L2) stage each last one day. During this time, larvae spend most of their time eating. Ecdysis, or molting, is the process whereby larvae shed their cuticle once it has been outgrown. Molting between the larval instar stages are preceded with a pulse of ecdysone. After the L2 stage, larvae reach the final third instar (L3) stage. L3 larvae initially spend their time eating, but minor ecdysone pulses during the L3 stage cause behavioural changes and the L3 larvae begin wandering about 32 hours after the L2/L3 molt (Warren, et al. 2006). Approximately 48 hours after the L2/L3 molt (five days after egg laying), the larvae begin puparium formation and metamorphosis, which is triggered by a major pulse of ecdysone. Adult flies eclose when they are 9-10 days old. Larval timing is important for my research, but the most important times revolve around the L3 stage; the L2/L3 molt takes place when larvae are about three days old and the L3 stage ends two days later when puparium formation occurs on day five.

1.1.2 Steroid hormones regulate gene expression

Steroid hormones affect development by changing cell behaviour. Steroid hormones are released into the blood, in humans, or the hemolymph, in *Drosophila*, and travel around the body. Once at target cells, steroid hormones are thought to freely diffuse across the plasma membrane because steroid hormones are lipophilic, although recent work claims that a membrane transporter is necessary for ecdysone import to better regulate steroid hormone uptake and cellular concentrations (Okamoto, et al. 2018). Once in the cell, there are two pathways for steroid hormones to regulate the cell. Classic steroid hormone signaling involves binding to a steroid hormone nuclear receptor, typically in the cytoplasm. The ligand-bound nuclear receptor then translocates into the nucleus, binds DNA, and regulates gene expression (the genomic

pathway). In general, nuclear receptors are ligand-dependent transcription factors (nuclear receptors will be discussed in more detail in the next section). Nuclear receptors can also work in a rapid response, non-genomic signaling pathway whereby a steroid hormone binds to the nuclear receptor and immediately affects signal transduction. Crosstalk between the genomic and non-genomic pathways provides the full steroid hormone response (Wilkenfeld, et al. 2018). However, I will only focus on the classic steroid hormone signaling pathway.

The genetic response to steroid hormones was studied in *Drosophila* using how cultured salivary glands responded to ecdysone. Cultured salivary glands were used because the salivary glands contain polytene chromosomes, that is, chromosomes that undergo multiple rounds of replication without mitosis (endoreplication). These polytene chromosomes contain thousands of connected strands of DNA that are easily observed. When the cultured salivary glands were exposed to ecdysone, puffs in the polytene DNA strands were observed (Clever and Karlson. 1960). These observed puffs were sites of active gene transcription for downstream genes that responded to ecdysone. The Ashburner model was proposed to explain the hierarchical response to ecdysone (Ashburner. 1974). In short, ecdysone quickly induced transcription of a relatively small set of early genes (or puffs) that encoded transcription factors, which were later identified as nuclear receptors. These early transcription factors then induced the expression of a large number of late genes. In addition, early gene protein products would inhibit their own expression and ecdysone would initially inhibit late gene expression until sufficient concentrations of early gene protein products were produced. Later modifications to the model were made, such as early-late genes, which are induced by both ecdysone and early gene protein products (Ashburner and Richards. 1976). Ashburner established the general mechanism of steroid hormone action in *Drosophila*. Further research tested tissues *in vivo* to determine how spatial

and temporal differences could result in how tissues responded differently to ecdysone. This early work established *Drosophila* L3 larvae as the main focus for ecdysone and steroid hormone research. The Ashburner model became a model for understanding how steroid hormones work in general to regulate cellular changes and in turn, development of an organism.

1.1.3 Mechanisms of nuclear receptors

Nuclear receptors were found to be the mediators of the action of ecdysone that induced the puffs described in the Ashburner model. Once ecdysone is taken up into the target tissue, the cytochrome P450, Shade, adds a hydroxyl group to ecdysone to form the biologically active form of the hormone, 20-hydroxyecdysone (20E) (Petryk, et al. 2003). 20E then binds to the nuclear receptor EcR (Ecdysone receptor) (Koelle, et al. 1991). Upon ligand binding, EcR forms a heterodimer with the nuclear receptor ultraspiracle (usp), which then binds to DNA and regulates gene expression (Yao, et al. 1992). The early genes in the Ashburner model were also found to encode nuclear receptors, such as E75 (Eip75b – Ecdysone-induced protein 75b) (Segraves and Hogness. 1990). A similar mechanism for steroid hormone action is also observed with human sex hormones. The nuclear receptor, Androgen receptor, primarily binds its main ligand, testosterone, and the nuclear receptor, Estrogen receptor, binds estrogens. Upon ligand binding, the androgen receptor forms a homodimer, translocates from the cytoplasm into the nucleus, and regulates gene expression (Li and Al-Azzawi. 2009). Like EcR, the estrogen receptor is already in the nucleus prior to ligand binding, but upon ligand binding, the estrogen receptor dimerizes and begins to regulate gene expression (King and Greene. 1984). This highlights the fundamental role that nuclear receptors play in steroid hormone signaling. In addition to mediating the steroid hormone response in cells, the nuclear receptors E75, βFtz-F1, and DHR4 in *Drosophila* are required to regulate gene expression of enzymes that synthesis ecdysone (Bialecki, et al. 2002;

Parvy, et al. 2005; Ou, et al. 2011). It is important to understand how nuclear receptors function due to the connection between steroid hormones and nuclear receptors.

Nuclear receptors make up a superfamily; there are 21 nuclear receptors in *Drosophila*, 48 nuclear receptors in humans, and over 270 nuclear receptors in *Caenorhabditis elegans* (Zhang, Z., et al. 2004; Sluder and Maina. 2001). Nuclear receptors are ligand-dependent transcription factors that are characterized by a highly conserved N-terminal DNA-binding domain (DBD) and a less conserved C-terminal ligand-binding domain (LBD) joined together by a hinge region. The DBD is composed of two Cys-4 zinc fingers. The first zinc finger provides DNA-binding specificity while the second zinc finger allows for weak dimerization in the DBD (nuclear receptors are reviewed in (King-Jones and Thummel. 2005)). Nuclear receptors generally recognize small lipophilic molecules such as steroid hormones, retinoic acid, and thyroid hormone (Mangelsdorf, et al. 1995). However, orphan nuclear receptors do not bind a ligand, or at least, have no known ligand. The LBD comprises 11 – 13 α-helices that are involved in ligand binding and dimerization (King-Jones and Thummel. 2005).

Two main types of nuclear receptors will be discussed that can give a general understanding of how nuclear receptors can function (Figure 1-2). Type I nuclear receptors generally reside in the cytoplasm and upon ligand binding, Type I nuclear receptors form homodimers and translocate into the nucleus. The homodimer can then bind to a DNA hormone response element, recruit a co-activator, and induce transcription of the nuclear receptor's target genes. Type II nuclear receptors generally exist as heterodimers that stay bound to DNA in the nucleus and in the absence of a ligand, recruit a co-repressor to inhibit target gene transcription. Ligand binding causes a conformation change that adjusts the position of an α-helix, which causes the co-repressor to be ejected and recruitment of a co-activator, allowing for activation of

the target gene (reviewed in (Sever and Glass. 2013)). However, there are many exceptions to how nuclear receptors can work, like the nuclear receptors that function as monomers. Nuclear receptors can also be regulated through post-translational modifications (Berrabah, et al. 2011).

1.1.4 Ecdysone is produced in the prothoracic gland by Cytochrome P450s

My main interest is not how steroid hormones act, but how steroid hormones are synthesized and how that synthesis is regulated. Ecdysone is produced in the prothoracic gland (PG), a larval endocrine tissue (Figure 1-1B). Like the larval salivary glands, the PG also contains polytene chromosomes. The PG is part of a tripartite tissue called the ring gland (RG). The ring gland consists of the corpus allatum, corpus cardiaca, and the prothoracic gland. The RG sits next to the brain and is innervated by brain-derived neurons, which can signal to the RG. The entire RG is typically used for experiments because the tissues within the RG cannot be easily separated and the PG makes up the majority of the RG. Ecdysone is synthesized from sterols, preferentially cholesterol. Since *Drosophila* cannot *de novo* synthesize cholesterol, cholesterol must be taken up in the diet. Ecdysone-producing enzyme genes were initially identified in a mutant screen for disrupted larval cuticle patterning (Nusslein-Volhard, et al. 1984; Jurgens, et al. 1984; Wieschaus, et al. 1984). A major ecdysone pulse during the embryonic stage is needed for the formation of the larval cuticle (Fristrom and Liebrich. 1986). Therefore, mutations that disrupt ecdysone production would disrupt cuticle differentiation. This basis was used to identify many of the genes involved in synthesizing ecdysone.

The first enzyme in the ecdysone production pathway is encoded by the gene *neverland* (*nvd*) (Figure 1-1C) (Yoshiyama, et al. 2006). Neverland is a Rieske-domain oxygenase-like protein. The Rieske domain binds an iron-sulfur cluster (2Fe-2S). Neverland converts cholesterol into 7-dehydrocholesterol (7dC). 7dC then enters the “Black “Box” and is converted to 5β-

ketodiol by a series of unknown steps. None of the ecdysone intermediates have been identified in the Black Box because the intermediates are unstable, however, there have been a few enzymes found to work within the Black Box. The genes that encode enzymes in the Black Box are *shroud (sro*), *spook* (*spo*) / *spookier* (*spok*), and *Cyp6t3* (Niwa, et al. 2010; Namiki, et al. 2005; Ono, et al. 2006; Ou, et al. 2011). *sro* encodes a short-chain dehydrogenase/reductase, which takes part in oxidation and/or reduction reactions. *Spo*, *Spok*, and *Cyp6t3* encode for cytochrome P450 enzymes, which are monooxygenases that add one hydroxyl group to their substrate. The difference between *spook* and *spookier* is that *spook* is specifically expressed during the embryonic stages while *spookier* is expressed during larval stages. 5β-ketodiol is then converted to ecdysone by three cytochrome P450 enzymes. These cytochrome P450 enzymes are encoded by *phantom* (*phm*), *disembodied* (*dib*), and *shadow* (*sad*) (Warren, et al. 2004; Warren, et al. 2002). Once ecdysone is synthesized, ecdysone is released into the hemolymph and transported to target tissues that convert ecdysone to the biologically active hormone, 20-hydroxyecdysone (20E), via the cytochrome P450 enzyme encoded by *shade* (*shd*) (Petryk, et al. 2003). The majority of the ecdysteroidogenic enzymes are cytochrome P450 enzymes. Similarly, vertebrates also synthesize steroid hormones from cholesterol using mainly cytochrome P450 enzymes (Hanukoglu. 1992). Cytochrome P450s are proteins that contain a heme cofactor (hemoproteins) and their name is derived from their maximum absorbance when reduced and bound by carbon monoxide at 450 nm during spectrophotometry (Mak and Denisov. 2018).

The King-Jones lab was initially interested in studying how steroid hormone-producing enzymes are regulated and identifying the signaling pathways involved. Our focus has recently shifted to examining heme and heme regulation, as well as iron homeostasis in the PG. The connection between all of these components is that the cytochrome P450 enzymes require heme

as a cofactor to be functional. Heme is a porphyrin ring that contains a ferrous iron at its core. Heme is most well-known for being a cofactor for hemoglobin that binds oxygen and transports oxygen throughout the body in the blood. Heme, of course, has other roles, such as being a cofactor for cytochrome P450 enzymes, but heme can also function as a signaling molecule, which will be discussed in Chapter 1.1.6. Heme, and consequently iron, became of interest for two main reasons.

The first reason is that cytochrome P450s are expressed at incredibly high levels in the PG in order to produce sufficient ecdysone for developmental pulses. Even shortly after the L2/L3 molt, when ecdysone levels are relatively low, the expression of the ecdysteroidogenic genes were so high that they appeared to max out the signal in a microarray (Ou, et al. 2016). With initially high expression, the expression of these genes only increased throughout the L3 stage as ecdysone was being synthesized for a major ecdysone pulse (Parvy, et al. 2005; McBrayer, et al. 2007; Ou, et al. 2016). The two most extreme cases are *phm* and *dib* that were induced 180 times and 100 times, respectively, at the end of the L3 stage compared to expression in early L3 larvae. The other ecdysteroidogenic genes were more moderately induced. The very high expression of ecdysteroidogenic genes outlines the necessity of the cytochrome P450 enzymes in the PG and the extent that these enzymes are expressed. Since each cytochrome P450 requires heme as a cofactor, it can be reasoned that the PG also has a very high demand for heme. The issue is that heme is cytotoxic and can cause oxidative damage to the cell (Larsen, et al. 2012). The cytotoxicity of heme is why the free heme pool (free heme is heme not bound by a protein) is relatively small. We hypothesized that heme must be dynamically regulated in the PG so that heme levels can match the demand for the cytochrome P450 enzymes for the PG to successfully produce an ecdysone pulse due to the high demand for heme and the cytotoxicity of heme. One

of the main aims of this thesis, which will be discussed in more detail later in the introduction, is to examine how heme homeostasis is regulated in the PG.

The second reason our lab became interested in heme regulation in the PG is that there is a unique phenotype associated with disrupting the heme biosynthesis pathway in the PG (Huynh, in revision). This phenotype will be explained later in Chapter 1.1.6, but briefly, late heme precursors accumulate in the cell when the heme biosynthesis pathway is blocked at later steps and the accumulated heme precursors dye the PG a reddish colour and the PGs autofluoresces red when exposed to UV light. This phenotype highlights the importance of heme in the PG. In fact, a heme biosynthesis mutant only caused observable red autofluorescence in three tissues: the prothoracic gland, the gut, and the oenocytes. As an interesting side note, these three tissues all have high expression of cytochrome P450 genes. The PG expresses cytochrome P450 genes for steroid hormone production. The gut uses cytochrome P450s for detoxification (Chung, et al. 2009). Oenocytes use cytochrome P450s to synthesis hydrocarbons for waterproofing the larval cuticle (Qiu, Y., et al. 2012). That being said, fat body and malpighian tubules were also found to express many cytochrome P450 genes but are not found to have red autofluorescence in a heme pathway mutant. These two reasons listed above are why our lab began investigating heme and heme regulation in the PG and ultimately how it relates to ecdysone production. Before discussing heme regulation in more detail, I first want to give an overview of known pathways that regulate ecdysone production.

1.1.5 Ecdysone is regulated by interconnected pathways

Recently, in the history of studying ecdysone, researchers are beginning to identify the pathways and transcription factors involved in initiating ecdysone production (Figure 1-3). The main focus has been on the major ecdysone pulse that triggers metamorphosis at the end of the

third instar. A small brain-derived neuropeptide called prothoracicotropic hormone (PTTH) was one of the first signaling molecules that were found to stimulate ecdysone production and, consequently, metamorphosis (Kawakami, et al. 1990; Kataoka, et al. 1991). PTTH was later found to be used in *Drosophila* as well and is made by PTTH-producing neurons in the brain that directly innervate the PG (McBrayer, et al. 2007). Ablating the PTTH-producing neurons was found to significantly reduce ecdysteroidogenic gene expression. Although PTTH initiates metamorphosis, PTTH is not necessary for metamorphosis, as many larvae with ablated PTTH-producing neurons were viable, but development was delayed. PTTH seems to be necessary for proper developmental timing, and since larvae missing the PTTH signal are still viable, this points to other signaling pathways involved in ecdysone production. PTTH signals via the PTTH receptor Torso, a receptor tyrosine kinase (Rewitz, et al. 2009). Torso then activates the MAPK (mitogen-activated protein kinase) Ras/Raf/ERK pathway via phosphorylation. One of the targets of the Ras/Raf/ERK pathway in the PG is the nuclear receptor DHR4 (*Drosophila* hormone receptor 4), which is a negative regulator of the ecdysteroidogenic gene *Cyp6t3* (Ou, et al. 2011).

The Torso/Ras/Raf/ERK pathway is remarkably similar to one that exists in humans and other vertebrates. A neuropeptide, aptly named kisspeptin, starts a long chain of signals to initial puberty, similar to how PTTH initiates metamorphosis in *Drosophila*. Kisspeptin is synthesized in neurons in the hypothalamus and kisspeptin's expression increases during puberty. Kisspeptin is sent to GnRH (gonadotrophin releasing hormone) neurons in the hypothalamus, where kisspeptin is recognized by the kisspeptin receptor and stimulates GnRH release via ERK1/2 activation. GnRH travels to the anterior pituitary and stimulates the release of the gonadotrophic hormones luteinizing hormone (LH) and follicle stimulating hormone (FSH). LH and FSH are

then sent to the gonads and stimulate the release of estrogens and progesterone in females and testosterone in males (d'Anglemont de Tassigny and Colledge. 2010). These sex hormones then cause changes associated with puberty.

Besides the Torso/Ras/Raf/ERK pathway, multiple other signaling pathways regulate ecdysone production. The insulin/insulin-like growth factor signaling (IIS) pathway responds to *Drosophila* insulin-like peptides (dilps) via the Insulin-like receptor (InR) to regulate final body size and determine when critical weight has been attained (Colombani, et al. 2005; Mirth, C., et al. 2005). Critical weight is a checkpoint that marks the minimum weight needed to undergo metamorphosis successfully. Without attaining critical weight, larvae will not undergo metamorphosis, regardless of age. The TGFβ/Activin pathway regulates the expression of *InR* and *torso* via dSmad2 (Smox – Smad on X) to enable the PG to become receptive to dilps and PTTH (Gibbens, et al. 2011). Loss-of-*dSmad2* resulted in a significant decrease in ecdysone production. The last pathway that I will mention is the TOR (Target of rapamycin) pathway. The TOR pathway accesses the nutrients in the cell, such as the availability of amino acids. Disruption of the TOR pathway in the PG delays development and increases the body size of larvae (Layalle, et al. 2008). These signaling pathways are intertwined and their inputs together trigger ecdysone production and metamorphosis at the appropriate developmental time. Our lab is beginning to investigate heme and iron to determine whether these molecules are one of the nutritional inputs used to regulate ecdysone production. As such, I am also studying how heme biosynthesis is regulated within the PG.

1.1.6 Heme biosynthesis and mutations

Heme is an essential molecule for life. Heme is a cofactor for hemoproteins (proteins that bind heme) that have a variety of roles, in addition to oxygen transport as mentioned earlier.

Hemoproteins function in the electron transport chain to aid in electron transport, as diatomic gas sensors, as nitric oxide synthase to produce nitric oxide, and of course cytochrome P450 enzymes that aid in detoxification and steroid hormone production (Klatt, et al. 1992; White, K. A. and Marletta. 1992; Reinking, et al. 2005; Kim, et al. 2012). Heme is also capable of acting as a signaling molecule to influence other processes such as transcription. Heme is involved in miRNA processing, the circadian rhythm, and in maintaining heme homeostasis, in regulating itself (Faller, et al. 2007; Ogawa, et al. 2001; Yin, et al. 2007; Raghuram, et al. 2007). Heme is synthesized by eight highly evolutionarily conserved enzymes from succinyl-CoA and glycine (Figure 1-4). Heme synthesis takes place in the mitochondria and cytoplasm. *Alas* encodes the first enzyme in the heme biosynthesis pathway and is the rate-limiting step, at least in vertebrates, but Alas is likely also rate-limiting in *Drosophila* due to the high conservation of the heme biosynthesis pathway and the large induction in *Alas* expression when heme levels decrease (as will be discussed later). After step four of the heme biosynthesis pathway, a porphyrin ring is formed that has a unique ability to autofluoresce red when exposed to air and UV light (Nagababu and Rifkind. 1998). Ferrochelatase, the last enzyme in the heme biosynthesis pathway, incorporates a ferrous iron into the porphyrin ring to form heme, which abolishes the autofluorescent property of the porphyrin ring.

Mutations that disrupt the heme biosynthesis pathway resulted in larvae that had red autofluorescent guts, oenocytes, and prothoracic glands (Figure 1-5). One such mutation that I frequently used to reduce cellular heme levels is the *PPOX* mutation (courtesy of Arash Bashirullah, University of Wisconsin-Madison). PPOX is the penultimate enzyme in the heme biosynthesis pathway. In addition to red autofluorescence, *PPOX* mutant larvae are L3 arrested, that is, the larvae reach the L3 stage and never initiate puparium formation and metamorphosis.

These L3 arrested larvae will continue to live as L3 larvae for weeks. The red autofluorescence is due to the accumulation of late heme precursors (precursors that have formed the porphyrin ring structure) since PPOX has reduced activity in *PPOX* mutant larvae. Late heme precursors accumulate to high levels because the cell recognizes that cellular heme levels are low and upregulates the heme biosynthesis pathway to compensate (Qiuxiang Ou, unpublished). *Alas*, which very likely encodes the rate-limiting enzyme, is highly induced to produce more heme, but the block later in the heme pathway causes a large accumulation of autofluorescent late heme precursors instead. This observed phenotype in *Drosophila* is remarkably similar to humans that have mutations in the heme biosynthesis pathway, which results in a group of disorders called porphyria.

Porphyrias are a group of rare disorders whose symptoms vary based on which enzyme in the heme biosynthesis pathway is defective. There are two main types: acute (primarily affecting the nervous system) and cutaneous. Acute porphyrias are characterized by acute attacks that are typically due to inducing heme biosynthesis, such as taking drugs that are metabolized by cytochrome P450s. Another trigger of acute porphyria attacks is associated with hormonal changes in women as some women experience symptoms just before and a couple of days into menstruation (Kauppinen and Mustajoki. 1992). Acute attacks typically result in abdominal pain, vomiting, and neuropathy, while severe attacks can cause seizures, psychosis, paralysis, coma, and eventually, death. During these attacks, *Alas1* is upregulated, similar to *Drosophila*. I will note that humans have two copies of *Alas*; *Alas1* is ubiquitously expressed and regulated by a negative feedback loop with heme, while *Alas2* is expressed specifically in erythrocytes and is regulated more by iron availability than heme. Acute porphyrias are typically caused by mutations early in the heme biosynthesis pathway, which led to an accumulation of early heme

precursors that are neurotoxic. Severe acute attacks can be treated by administering heme. Cutaneous porphyrias are characterized by an increase of heme precursors in the blood and typically affect the skin. These precursors react with light and can cause skin lesions and fragile skin. For this reason, cutaneous porphyria patients typically avoid the sun and stay covered up (Porphyria reviewed in (Edel and Mamet. 2018)). Similar to the autofluorescence observed in *Drosophila*, redness and red autofluorescence in the urine and feces, teeth, and blood is associated typically with patients with cutaneous porphyrias (Balwani and Desnick. 2012). The accumulation of autofluorescent heme precursors in some porphyria patients is remarkably similar to that seen in *Drosophila* larvae. This may mean that *Drosophila* larvae could serve as a model for porphyria.

1.1.7 Regulation of heme biosynthesis

The King-Jones lab became interested in heme biosynthesis and regulation, and how heme interacts with ecdysone production in the PG. Cells are somehow able to sense that cellular heme levels are low and upregulate *Alas* in response. My work was focused on identifying the heme sensor that acted in this manner, to detect that cellular heme levels are low and increase heme biosynthesis in response. Just as a note, there is a single *Alas* gene in *Drosophila*, similar to ALAS1, which is ubiquitously expressed. The heme sensor in vertebrates has been identified as the nuclear receptor, Rev-erbα (Wu, et al. 2009). Nuclear receptors typically bind hormones, but heme was found to be a ligand for Rev-erbα (Raghuram, et al. 2007; Yin, et al. 2007). Rev-erbα acts as a heme sensor by directly binding heme and regulating heme homeostasis. Upon heme binding, Rev-erbα recruits nuclear receptor corepressor (NCoR) and represses *PGC-1α*. PGC-1α is a coactivator for *Alas1* expression (Handschin, et al. 2005). When cellular heme levels drop,

Rev-erbα is free of heme and can no longer repress *PGC-1α* expression (Wu, et al. 2009). PGC-1α then induces *Alas1* expression, restoring the cellular heme content.

The heme sensor in *Drosophila* is unknown, however. Two nuclear receptors out of 21 in *Drosophila* have been shown to bind heme *in vitro*, E75 and DHR51 (*Drosophila* hormone receptor 51) (Reinking, et al. 2005; de Rosny, et al. 2008). The E75 LBD was expressed in *E. coli* and upon purification, appeared a deep red colour, indicating E75 carried a chromophore that was later identified as heme. E75 also had an absorption spectra consistent with other heme-containing proteins (Reinking, et al. 2005). The hinge region and LBD of DHR51 was expressed in *E. coli* with added hemin. The resulting absorption spectra of the purified DHR51 indicated that DHR51 bound to heme, but with less affinity compared toE75. Unlike E75, DHR51 could be purified without being bound by heme and did not display the characteristic absorption spectra of a heme-containing protein (de Rosny, et al. 2008). E75 (Eip75B – ecdysone-induced protein 75B) is the *Drosophila* homolog of Rev-erbα, although, E75 has a significantly higher affinity for heme compared to Rev-erbα. While Rev-erbα reversibly binds heme, heme is required for E75 protein stability and apo-E75 was undetectable, however, this does not rule out E75 acting as a heme sensor. E75 can act as a redox sensor as E75 heterodimerization with the nuclear receptor DHR3 (*Drosophila* hormone receptor 3) was dependent on the oxidation state of the heme iron. Additionally, diatomic gases, nitric oxide (NO) and carbon monoxide (CO), also regulated E75 binding to DHR3, suggesting E75 could also be a gas sensor (Reinking, et al. 2005). The other heme sensor candidate, DHR51, is the *Drosophila* homolog of NR2E3/PNR (photoreceptor cell-specific nuclear receptor). NR2E3 regulates photoreceptor development and mutations in NR2E3 cause enhanced S-cone syndrome and autosomal dominant retinitis pigmentosa (Haider, et al. 2000; Gerber, et al. 2000; Coppieters, et al. 2007). DHR51 was found

to have an affinity for heme comparable to Rev-erbα *in vitro*, suggesting that DHR51's interaction with heme is reversible (de Rosny, et al. 2008). Although NO and CO can bind to DHR51's heme ligand, it seems less likely that DHR51 is a gas sensor compared to E75 because a gas sensor would be expected to tightly bind heme and remain bound to detect gas levels. DHR51 became my primary candidate for a heme sensor in *Drosophila* based on the vertebrate heme sensor being a nuclear receptor, how Rev-erbα acts as a heme sensor, and how DHR51 has an affinity for heme that suggested that the interaction between DHR51 and heme would be reversible, unlike E75.

1.1.8 Previous research on DHR51

As previously mentioned, DHR51 is a nuclear receptor that has been shown to bind heme *in vitro* (de Rosny, et al. 2008). Mutations in *DHR51* caused a proportion of the *Drosophila* population to be pupal lethal (15% - 75% depending on the combination of mutant alleles), raising the possibility that the pupal lethality was caused by insufficient ecdysone titers. Of the *DHR51* mutants that did eclose as adult flies, many adults failed to expand their wings (30% - 100%) (Sung, et al. 2009). Since many mutant adults were unable to fulfill wing expansion, *DHR51* is also named *unfulfilled* (*unf*). In addition, *DHR51* mutant adults were near sterile, but this phenotype was unable to be rescued with the expression of a *DHR51* cDNA so the sterility could potentially not be due to loss-of-*DHR51* even though two independent mutant alleles caused fertility defects (Sung, et al. 2009). *In situ* hybridization showed that during the larval stages, *DHR51* was primarily expressed in the central nervous system, including the mushroom body (which is the center for learning and memory), and to a lesser extent in the ventral nerve cord. This expression pattern is more closely related to the *Caenorhabditis elegans* homolog, *fax-1* (*fasciculation of axons defective*), which is expressed specifically in a small subset of

neurons compared to NR2E3 that is specific to photoreceptors (Much, et al. 2000; Wightman, et al. 2005). In the mushroom body, DHR51 regulates neuron development and is involved in neuronal re-extension and pathfinding (Lin, et al. 2009; Bates, et al. 2010). DHR51 acts through the TOR (Target of Rapamycin) pathway for the developmental regrowth of mushroom body neurons (Yaniv, et al. 2012).

DHR51 is also required in pacemaker neurons to regulate the free-running clock, which maintains the circadian rhythm without any external cues (Beuchle, et al. 2012). DHR51 directly binds to *period*, which encodes a core protein for the circadian rhythm, and enhances *period* transcription in combination with CLOCK, another core protein for the circadian rhythm (Jaumouille, et al. 2015). Briefly, CLOCK and CYCLE activate the transcription of *period* and *timeless*. PERIOD and TIMELESS form a negative feedback loop and inhibit the activity of CLOCK and CYCLE, thus forming the circadian rhythm (the circadian rhythm will be discussed in more detail in Chapter 4.1.3) (Yu, W. and Hardin. 2006). Interestingly, E75, together with CLOCK and DHR51 all contribute for maximum *period* expression, which suggested that E75 and DHR51 could potentially work together. Rev-erbα also regulates the circadian rhythm by regulating *Bmal1* (the human homolog of *cycle*) (Preitner, et al. 2002). Heme regulation is under the control of the circadian rhythm and Rev-erbα could potentially be the connection between heme biosynthesis and the circadian rhythm since *Alas1* follows circadian expression (Kaasik and Lee. 2004). Rev-erbα demonstrated that a heme sensor could also coordinate with the circadian rhythm.

DHR51 is the *Drosophila* homolog of NR2E3/PNR. Both DHR51 and NR2E3 are considered orphan nuclear receptors. NR2E3 has specific expression in the retina and is important for retina development (Chen, F., et al. 1999; Haider, et al. 2000). NR2E3 has a wide

range of activities, making NR2E3 difficult to use to gain an understanding of how DHR51 could function. For example, NR2E3 functions as a dual repressor/activator (Cheng, et al. 2004; Chen, J., et al. 2005; Haider, et al. 2009). NR2E3 is also capable of forming homodimers with itself, heterodimers with Rev-erbα, and even protein interactions with a non-nuclear receptor transcription factor, such as CRX (Cone-rod homeobox) (Roduit, et al. 2009; Cheng, et al. 2004; Peng, et al. 2005). The heterodimer interactions were determined by yeast two-hybrid assays. NR2E3 and DHR51 have only been observed in the nucleus and given that NR2E3 is a dual repressor/activator, NR2E3 may function like a Type II nuclear receptor, in that these nuclear receptors only seem to have nuclear subcellular localization (Chen, J., et al. 2005; Beuchle, et al. 2012; Yaniv, et al. 2012).

1.1.9 Aims of this thesis

DHR51 is my primary candidate for a heme sensor in the *Drosophila* PG. In this sense, DHR51 may be more functionally equivalent to Rev-erbα than to NR2E3. Previous research has demonstrated that DHR51 can likely reversibly bind heme *in vitro*, which suggested that heme could be DHR51's natural ligand. However, it is unknown whether heme binding is relevant *in vivo*. In addition, heme has been demonstrated to be a ligand for nuclear receptors and that the vertebrate heme sensor is a nuclear receptor. Most research on DHR51 has focused on DHR51's role in the mushroom body and circadian rhythm, and further experiments on DHR51 ligand binding have been unexplored.

The goal of this thesis is to determine whether DHR51 acts as a heme sensor to regulate heme biosynthesis and whether DHR51 coordinates heme biosynthesis and ecdysone production in the PG of L3 larvae. I have broken up my thesis into two main aims. My first aim was to identify whether DHR51 acts as a heme sensor to maintain heme homeostasis and whether heme

binding is biologically relevant. My hypothesis is that DHR51 acts as a heme sensor by recognizing cellular heme levels by directly binding heme and regulating *Alas* accordingly (Figure 1-6). Under normal cellular heme levels, DHR51 is bound by heme and does not affect *Alas* expression. When cellular heme levels decline, DHR51 is freed from heme and upregulates *Alas* expression either directly or by regulating a regulator of *Alas*, thus increasing cellular heme levels and maintaining heme homeostasis. The second aim of my thesis was to identify whether DHR51 regulates ecdysone production and through what mechanism. Based on the importance of heme in the PG, I hypothesize that DHR51 coordinately regulates heme and ecdysone biosynthesis to ensure that the cytochrome P450 enzymes have sufficient heme to produce a major ecdysone pulse at the end of the L3 stage to initiate metamorphosis at the correct developmental time. During my program, I commissioned the production of a DHR51 antibody with the hopes that it could be used in chromatin immunoprecipitation (ChIP) to identify direct DHR51 target genes. My quality control measures for the DHR51 antibody are included in Appendix A.

1.2 Figures

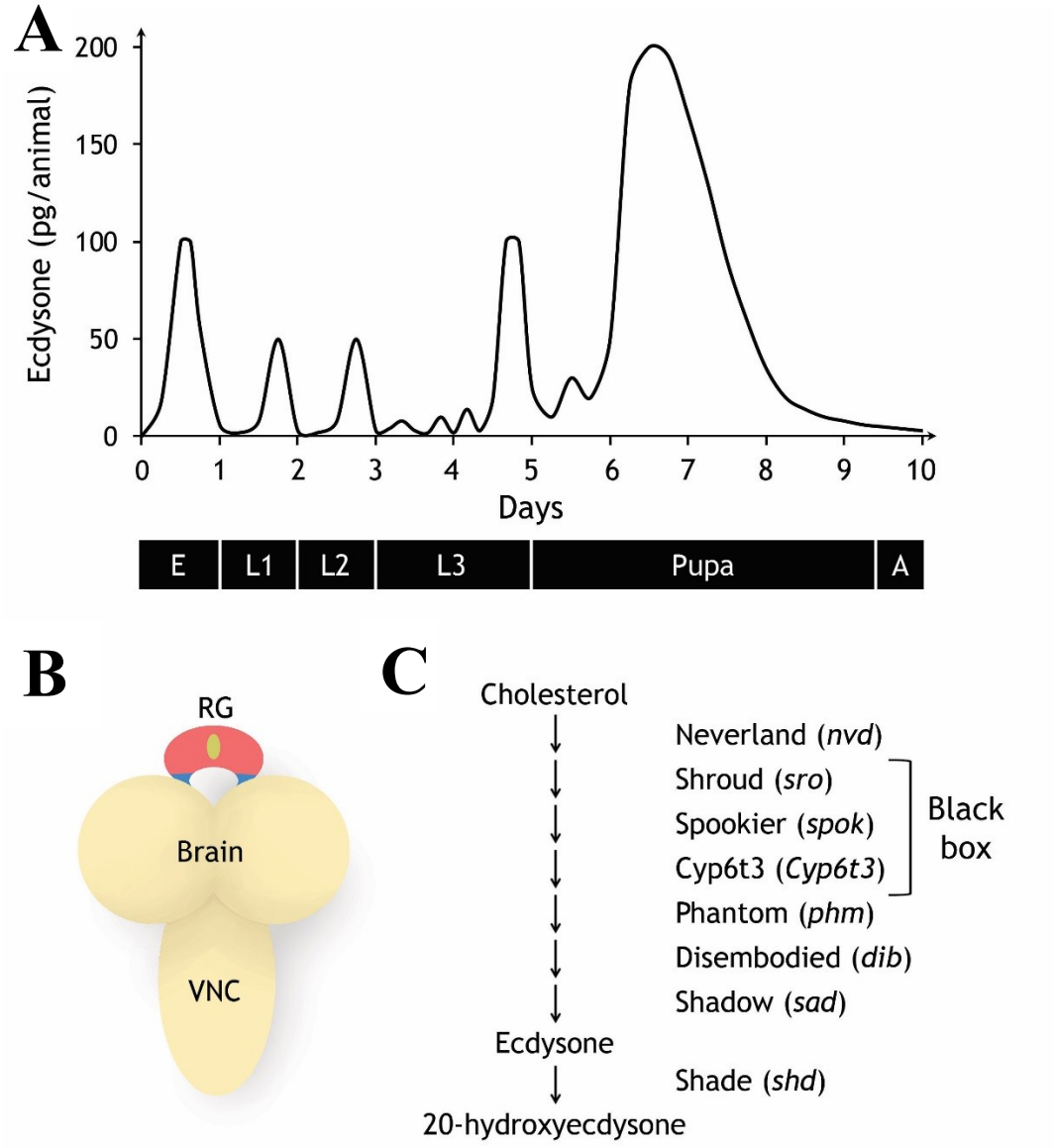

Figure 1-1. Ecdysone production in *Drosophila melanogaster*. A) Ecdysteroids (labeled ecdysone for simplicity) titers have been mapped through the lifespan of *Drosophila*. Ecdysone pulses are released prior to major developmental transitions, such as hatching, larval molts, and metamorphosis. The ecdysone titer from L3 larvae is based on (Warren, et al. 2006) and ecdysone titers at other stages are relative to (Riddiford. 1993). E = embryo. L1/L2/L3 = first/second/third instar larva. A = adult. B) Ecdysone is synthesized in the prothoracic gland (red), which is one part of the tripartite ring gland (RG) along with the corpus allatum (gold) and corpus cardiaca (blue). VNC = ventral nerve cord. C) Ecdysone is synthesized from cholesterol by a series of enzymatic steps by the enzymes on the right (*gene name*). The black box contains uncharacterized intermediates due to their instability and contains the rate-limiting enzyme for ecdysone production. Ecdysone is released into the hemolymph, taken up by target tissues, and converted to the biologically active form, 20-hydroxyecdysone. Ecdysone biosynthesis is reviewed in (Niwa and Niwa. 2014).

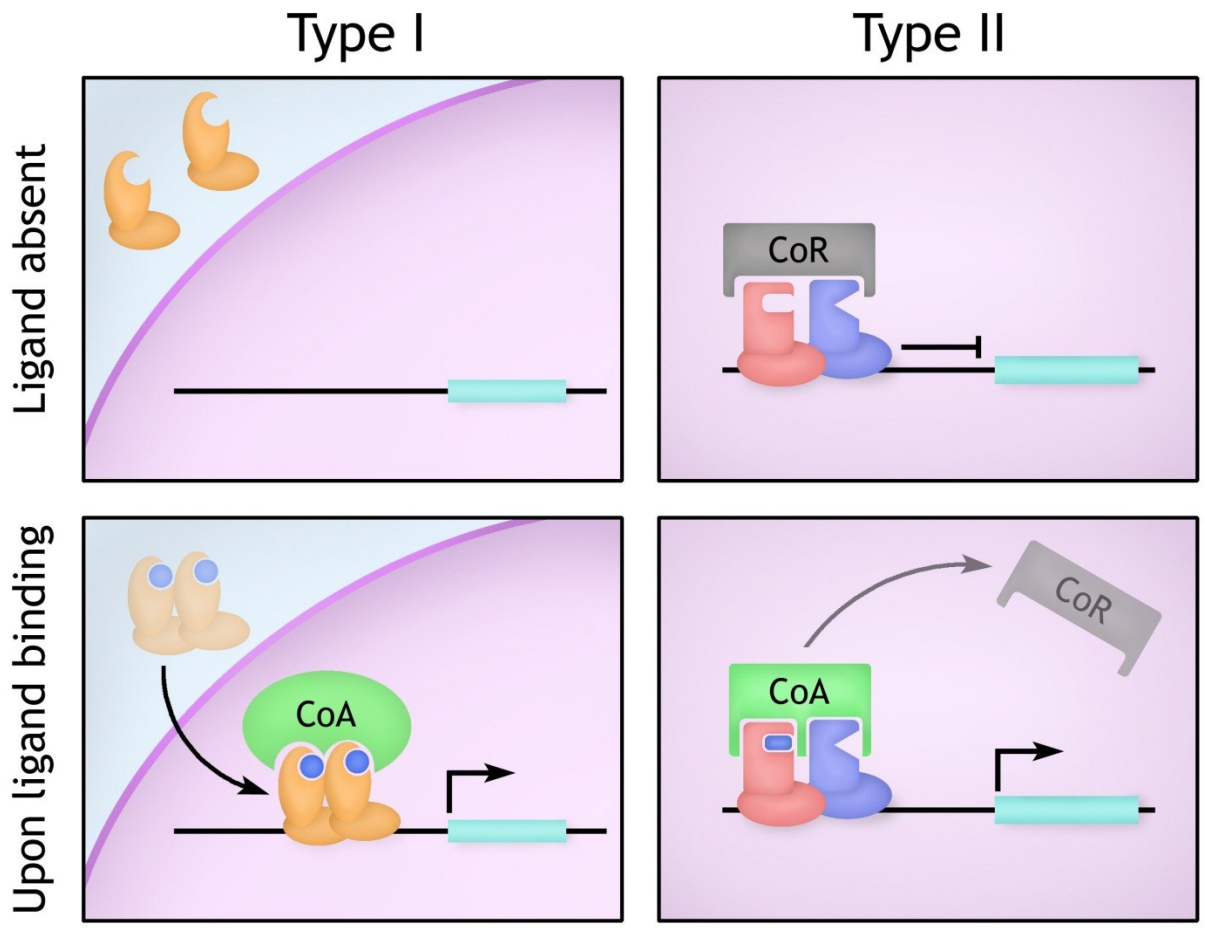

Figure 1-2. General mechanisms of Type I and Type II nuclear receptor function. The two main types of nuclear receptors are shown, Type I (left panels) and Type II (right panels). In the absence of a ligand, Type I nuclear receptors (orange) tend to reside in the cytoplasm (blue background). Upon ligand binding (blue circle) to the ligand-binding domain, Type I nuclear receptors form homodimers and translocate into the nucleus (purple background). Once in the nucleus, the nuclear receptor homodimer binds DNA via the DNA-binding domain, recruits a co-activator (CoA), and activates transcription of target genes (teal rectangle). Type II nuclear receptors remain within the nucleus and form heterodimers (red and blue). In the absence of a ligand, the nuclear receptor heterodimer recruits a co-repressor (CoR) and inhibits target gene expression. Upon ligand binding (blue rectangle) to the ligand-binding domain, a conformational change ejects the co-repressor and a co-activator is recruited. Target gene expression is then activated. Nuclear receptors are discussed in (Sever and Glass. 2013).

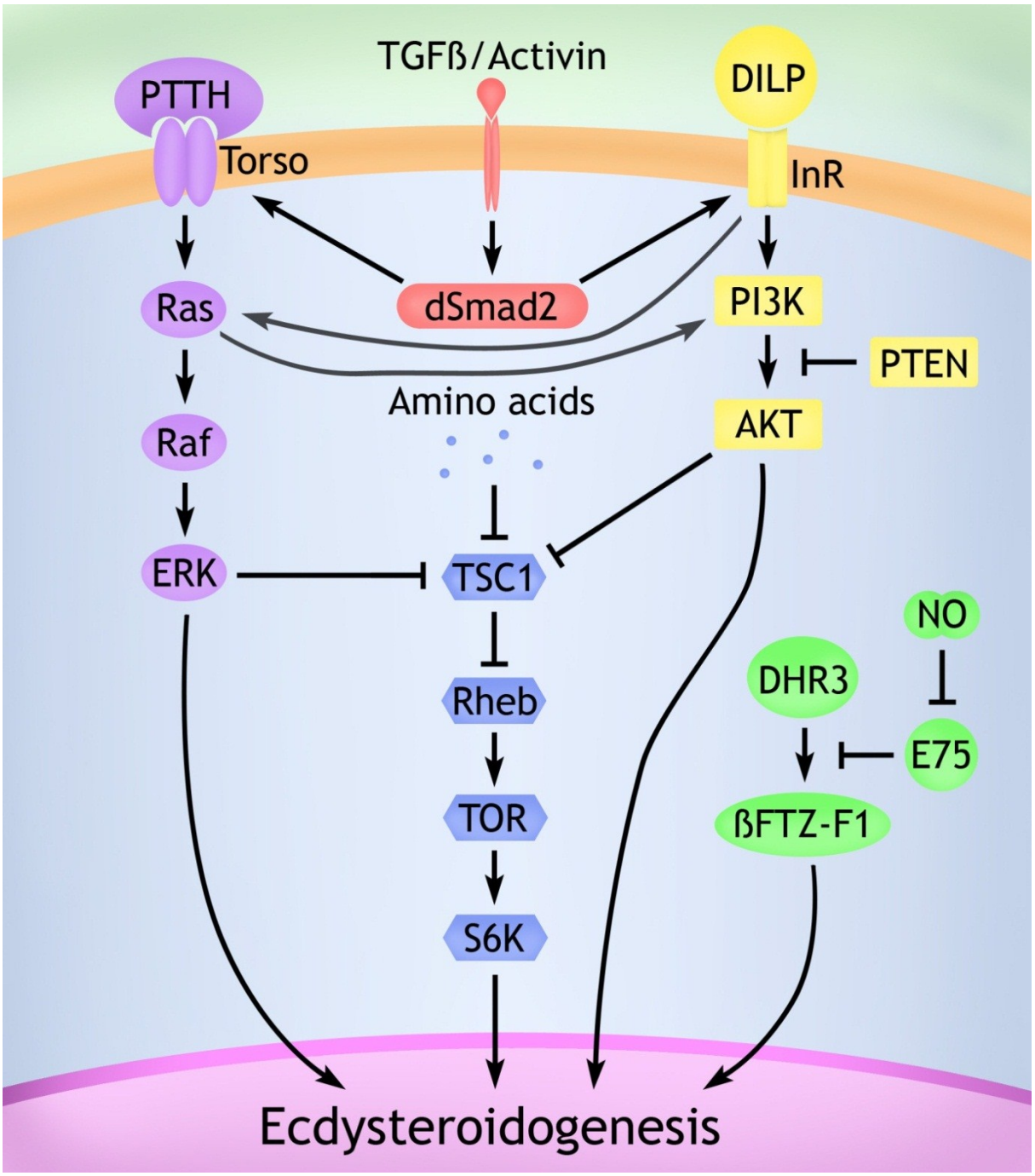

Figure 1-3. Signaling pathways that regulate ecdysteroidogenesis in the *Drosophila melanogaster* prothoracic gland. Above is a simplified view of the main signaling pathways and how the pathways interact with each other to regulate ecdysone production (ecdysteroidogenesis) in late third instar larvae. The Torso/Ras/Raf/ERK (MAPK) pathway proteins are shown in purple. The TGFβ/Activin pathway is shown in red. The insulin/insulin-like growth factor signaling (IIS) pathway is shown in yellow. The TOR pathway is shown in blue. NO/E75/DHR3/βFTZ-F1 signaling is shown in green. PTTH = prothoracicotropic hormone. NO = nitric oxide. Ecdysone signaling pathways are discussed in (Mirth, C. K. and Shingleton. 2012) and (Christesen, et al. 2017).

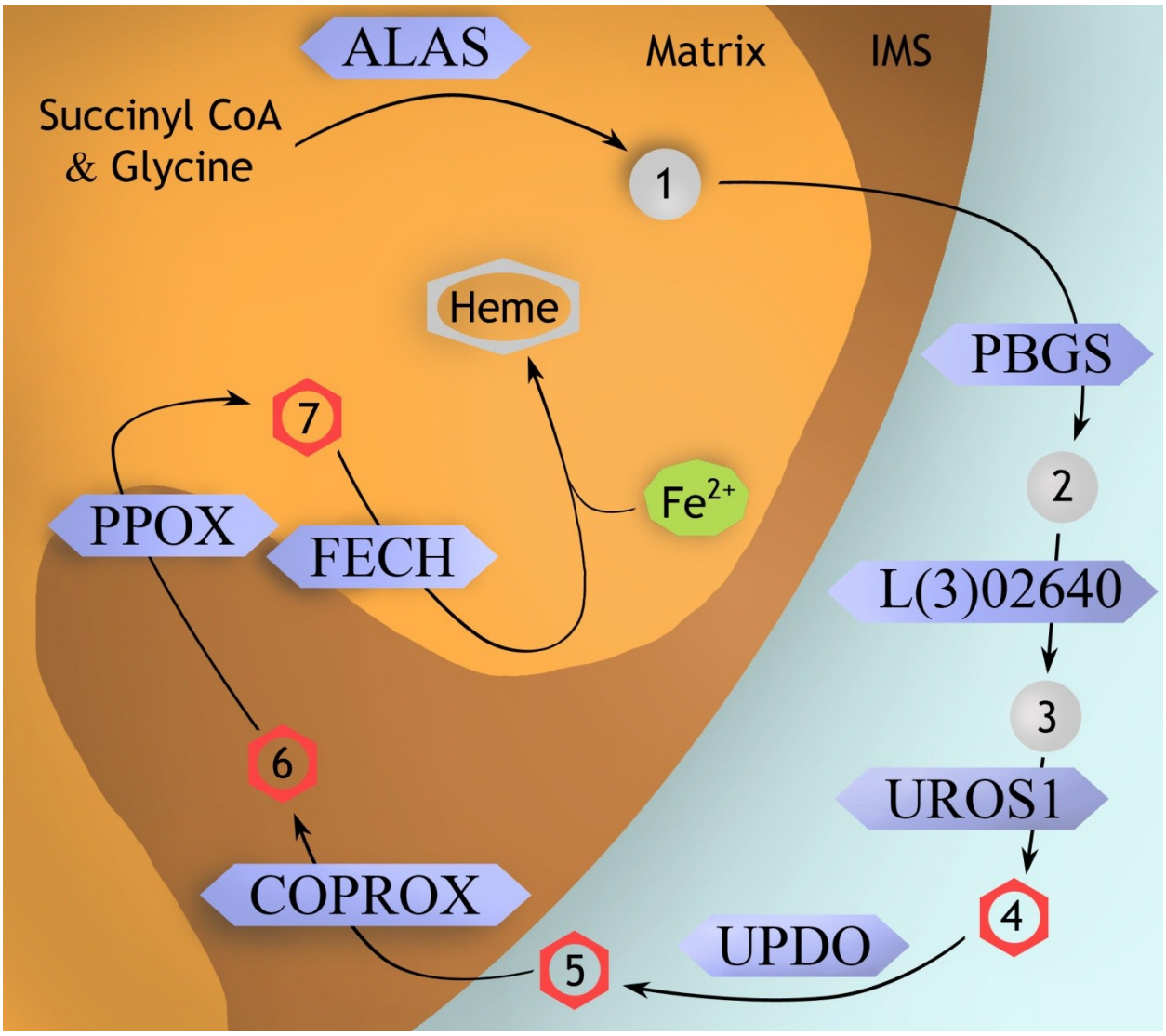

Figure 1-4. Heme biosynthesis in *Drosophila melanogaster*. Heme is synthesized by eight highly conserved enzymes in the mitochondria and cytoplasm from succinyl CoA and glycine. Heme precursors are numbered. Once a porphyrin ring is formed (red ringed hexagons), heme precursors are able to autofluorese red when exposed to UV light. When iron (Fe^{2+}) is inserted into the porphyrin ring in the last step of heme biosynthesis, the autofluorescence is lost. ALAS = Aminolevulinate synthase (ALAS1 or ALAS2 in mammals). PBGS = Porphobilinogen synthase (ALAD in mammals [aminolevulinic acid dehydratase]). L(3)02640 = Lethal (3) 02640. (HMBS = hydroxymethylbilane synthase). UROS1 = Uroporphyrinogen III synthase 1 (UROS). UPDO = uroporphyrinogen decarboxylase (UROD in mammals). COPROX = Coproporphyrinogen oxidase (CPOX). PPOX = Protoporphyrinogen oxidase. FECH = Ferrochelatase. IMS = intermembrane space. Heme synthesis is reviewed in (Khan and Quigley. 2011) and (Sun, et al. 2015).

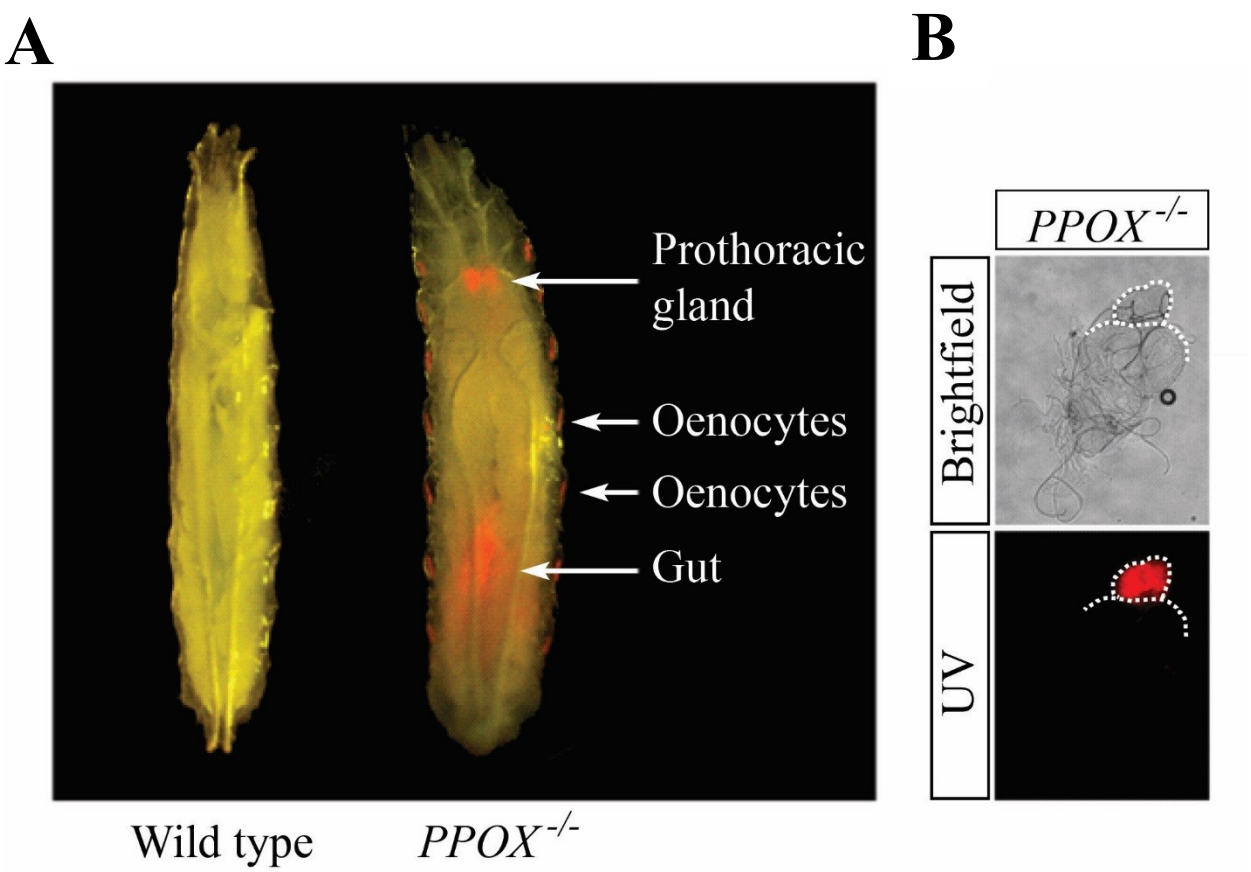

Figure 1-5. Mutations in late heme biosynthetic enzymes like *PPOX*$^{-/-}$ cause an accumulation of red autofluorescent heme precursors in specific tissues. A) L3 larvae viewed under UV light. Late heme precursors autofluoresce red and can be seen in the gut, oenocytes, and the prothoracic gland. Photo credit to Dr. Qiuxiang Ou. B) A brain-ring gland from a *PPOX*$^{-/-}$ L3 larvae. The top panel is a brightfield image and the bottom panel was viewed with UV light that causes late heme precursors to autofluoresce red in the prothoracic gland. The ring gland and part of the brain hemispheres are outlined with a white dotted line.

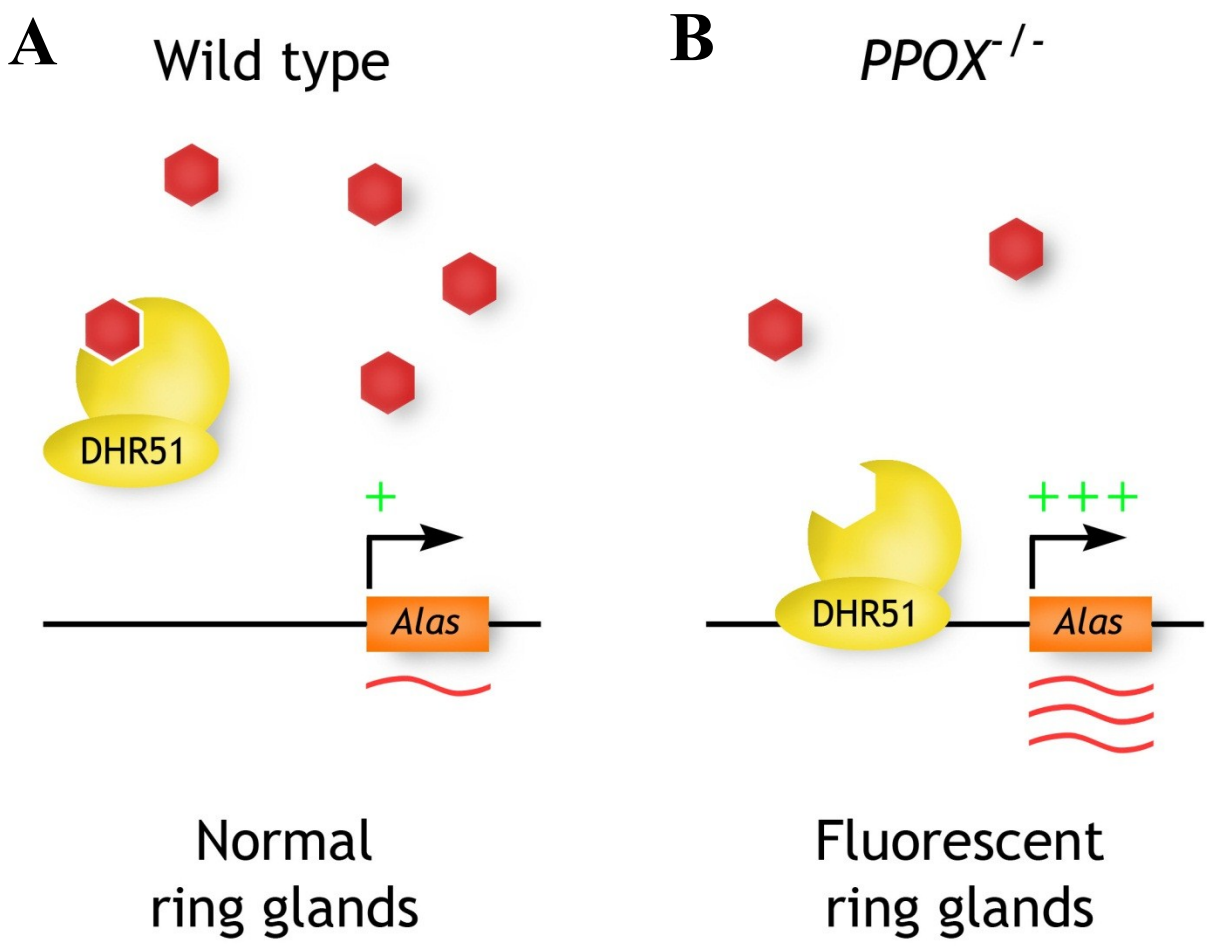

Figure 1-6. My hypothesis for how DHR51 regulates *Alas* expression under various concentrations of cellular heme levels in the prothoracic gland. A) When cellular heme levels are normal (wild type background), DHR51 is bound by heme (red hexagons) and inert with respect to *Alas* expression. *Alas* is expressed at basal levels. B) When cellular heme levels are low (such as in a *PPOX* mutant), DHR51 is freed of heme and upregulates *Alas* expression. An accumulation of heme precursors due to the *PPOX* mutation results in ring glands that have red autofluorescence. It is unknown whether DHR51 directly binds to *Alas*, but is shown that way for simplicity. Red curvy lines are *Alas* mRNA.

Chapter 2

Materials and Methods

2.1 Materials and Methods

2.1.1 *Drosophila* stocks and care

Drosophila melanogaster stocks were reared on standard agar cornmeal medium at 25°C in constant darkness. The media is made by the Fly Kitchen of the *Drosophila* Service Unit at the University of Alberta. All RNAi lines are from VDRC unless otherwise stated. *UAS-DHR51*-RNAi (2) was obtained from Dr. Tzumin Lee, Janelia Research Campus (referred to as *unf* miRNA in the literature) (Lin, et al. 2009). unf^{Z0001}, unf^{XI}, and *UAS-DHR51* cDNA were obtained from Dr. Steven Robinow, University of Hawaii (Sung, et al. 2009). The DHR51 ligand trap was obtained from Dr. Henry Krause, University of Toronto (Palanker, et al. 2006). $PPOX^{13702}$ was gifted by Dr. Arash Bashirullah. *phm22-Gal4* was obtained from Dr. Michael O'Connor, University of Minnesota. cDNA lines and other Gal4 drivers were ordered from Bloomington *Drosophila* Stock Center. *UAS-Flag-DHR51*, *hs-DHR51*, *hs-Flag-DHR51*, and *UAS-Alas*-cDNA were cloned by me and injected into *Drosophila* embryos by BestGene.

2.1.2 Staging developmental time of third instar larvae

Fly crosses were performed in cages and kept at 25°C in constant darkness. Standard agar cornmeal medium was melted down, had water added back, poured into mini-caps, and used as a food source for the cage and as a surface for females to lay embryos. Food caps were changed every morning and evening. Lids with holes to prevent suffocation were placed on the changed out caps and returned to 25°C. Third instar (L3) larvae were staged by examining caps three days after cap collection. Initially, all L3 larvae were discarded. The caps were returned to 25°C for two hours and then re-examined for L3 larvae. Newly molted L3 larvae were transferred to vials and returned to 25°C. Staged L3 larvae would remain at 25°C until the desired developmental stage (hours after L2/L3 molt) and then collected for experiments.

2.1.3 Measuring pupae size

Pupae size was determined by placing experimental and control pupae side-by-side. Images were taken with experimental and control pupae in the same field of view of the camera. Eight to ten comparisons were made using randomly selected pupae. Pupae and larvae were imaged at the same magnification. A representative image was used for each figure. Images were taken with a Leica DFC500 digital camera attached to a Leica MZ16 F fluorescence stereomicroscope.

2.1.4 Sample collection and RNA extraction

L3 larvae were dissected in 1X PBS, then immediately transferred to 200 µl TRIzol (Ambion) on ice. Once all the samples were collected in TRIzol, they were flash-frozen in liquid nitrogen and stored at -80°C. RNA was extracted using a modified RNeasy Mini Kit (Qiagen) protocol. First, samples were thawed, homogenized, and then the volume was brought up to 1 ml with TRIzol. 200 µl of chloroform was added and samples were vortexed for 15 seconds. Samples sat on ice for 1 min before being centrifuged at 13k rpm for 10 min at 4°C. The aqueous phase was transferred to a new microfuge tube and an equal volume of cold 70% ethanol was added. The samples were then transferred to an RNeasy mini spin column and the rest of the protocol was carried out as per the manufacturer's instructions. Samples were centrifuged for 30 seconds at 13k rpm. The flow-through was discarded. 700 µl of RW1 was added to the column, which was then centrifuged for 30 seconds at 13k rpm. The flow-through was then discarded. The column was washed twice with 500 µl of Buffer RPE. The first wash was centrifuged for 30 seconds at 13k rpm and the second wash was centrifuged for 2 min at 13k rpm. The column was transferred to a new collection tube and centrifuged for 2 min to dry the membrane. Approximately 20 µl of RNA-free water was used to elute the RNA. The RNA concentration

was measured with a Qubit 2.0 Fluorometer (Invitrogen) using the Qubit RNA HS Assay Kit (Invitrogen, Q32852). RNA integrity was measured using an Agilent RNA 6000 Nano chip (RNA 6000 Nano Kit) and ran on an Agilent 2100 Bioanalyzer.

2.1.5 cDNA synthesis

cDNA was synthesized from extracted RNA samples using a High Capacity cDNA Reverse Transcription Kit (Applied Biosystems, #4368813) following the manufacturer's instructions. Up to 1 µg of RNA was used for cDNA reactions (up to a maximum volume of 14.2 µl). A cDNA synthesis master mix was prepared (2.0 µl of 10X RT Buffer, 0.8 µl of 25X dNTP Mix [100 µM], and 2.0 µl of 10X Random primers per reaction). The master mix was aliquoted to 0.2 ml PCR tubes. Up to 14.2 µl of RNA was added to the 0.2 ml PCR tubes with aliquoted master mix (if less RNA was used, water was added to bring the final volume to 20 µl). 1 µl of reverse transcriptase was added to each tube. The reactions were then placed in a thermal cycler and the following program was run: 25ºC for 10 min, 37ºC for 2 hours, 85ºC for 5 seconds. cDNA was then diluted 1 in 20 with water per 1 µg of RNA that was added to the cDNA synthesis reaction. Unused RNA was flash froze in liquid nitrogen and stored at -80°C. cDNA was stored at -20°C.

2.1.6 Quantitative real-time PCR (qPCR)

2.1.6.1 Primer validation

qPCR Primers were designed with the Universal ProbeLibrary Assay Design Center (Roche Life Science) and ordered from Integrated DNA Technologies (IDT). All qPCR primers were validated before use and compared to the housekeeping gene, *rp49*. 3.2 µM primer mixes were made (1.6 µM of the forward and reverse primer). cDNA from wild type flies was diluted 1:4 five times. qPCR was done in triplicate with either SYBR Green qPCR Master Mix (Kapa

Biosystems, KK4601) or Luna Universal qPCR Master Mix (New England BioLabs, M3003L) using 5 µl of 2X master mix, 2.5 µl of 3.2 µM primer mix and 2.5 µl of cDNA per reaction. Reactions were run on either a StepOnePlus Real-time PCR system (Applied Biosystems) or a QuantStudio 6 Flex Real-time PCR system (Applied Biosystems) using a relative standard curve followed by a melt curve. Primer analysis relative to *rp49* was done in the provided software for the instrument, checking the amplification plot, standard curve, and melt curve. All primers are listed in Table 2-1.

2.1.6.2 qPCR protocol and analysis

cDNA samples were diluted 1:20 per 1 µg of RNA. qPCR reactions were set up similar to primer validations. The comparative C_t ($\Delta\Delta C_t$) quantification program was used to analyze the samples. All samples were normalized to *rp49*. Each biological sample was collected in triplicate and three technical replicates were included per sample. Fold change was calculated using the $\Delta\Delta C_t$ method and plotted with the confidence interval (alpha = 0.05) in Excel 2013.

2.1.7 Immunofluorescence

Larval tissues were dissected quickly and stored in ice-cold PBS. Dissected tissues were fixed in 4% formaldehyde for 20 min. Samples were washed three times with PBST (PBS + 0.3% Triton X100) for 5 min. Samples were permeabilized in PBST for 30-60 min, rocking at room temperature (RT). Samples were then blocked in PBTB (PBST + 5% goat serum) for 60 min, rocking at RT. Samples were incubated with the primary antibody in PBTB overnight at 4°C. The next day, samples were washed three times in PBST and then incubated with the secondary antibody for 60 min at RT. Samples were washed once with PBST for 10-15 min and then stained with Hoechst DNA stain for 5 min. Samples were washed twice with PBST for 5 min. Samples were mounted with VECTASHIELD Mounting Medium (Vector Laboratories)

and sealed with a coverslip and nail polish. Samples were viewed on a Nikon C2si Confocal Microscope. Confocal and brightfield images were taken.

2.1.8 Food rescue experiments

Standard agar cornmeal medium was melted down. Some water was added back to the medium to account for evaporation. The desired ingredient was then thoroughly mixed into the medium while it was still melted. For sterol rescue experiments, 33 mg/ml of 20E dissolved in 95% ethanol was added to standard media in a 1:100 dilution (final concentration is 330 μg/ml of 20E). An equal amount of 95% ethanol was used as a control medium. 10 mg/ml of 7dC dissolved in 95% ethanol was added to standard medium in a 1:100 dilution (final concentration is 100 μg/ml of 7dC). 7dC food was prepared in the dark, as it is light sensitive. 10 mM of hemin dissolved in 50 mM NaOH was added to standard media in a 1:10 dilution (final concentration is 1 mM of hemin). An equal amount of 50 mM NaOH was used as a control. A range of final concentrations of 100 nM to 80 mM hemin was tested, 1 mM was settled on for rescue experiments. The liquid medium was then poured into vials and allowed to solidify and cool.

Once the food has solidified and cooled, 50 embryos were transferred to each vial and stored at 25°C. Larvae were checked every two or four hours once the larvae were near pupariation to monitor pupariation and rescue extent. Once larvae formed prepupae, the amount of time after egg laying was noted, the pupae were counted and marked on the outside of the vial. Pupation curves could then be compared between genotypes and food types by plotting the fraction of the population that has pupariated at every individual time. Genotypes that resulted in larval arrested phenotypes were scored for the developmental stage (larval, pupal, and/or adult).

2.1.9 Ecdysone measurements

Ecdysone/20E were measured using a 20-Hydroxyecdysone Enzyme Immunoassay (EIA) Kit (Bertin Pharma, #A05120.96 wells). Third instar larvae were staged. Five to seven larvae were used per sample depending on the size of the larvae (more larvae that were younger were collected than older, larger larvae). Larvae were rinsed in distilled water, dried on a Kimwipe, transferred to a 1.5 ml microfuge tube, flash frozen, and stored at -80°C. Ecdysone was extracted with 500 µl of methanol and homogenized. Samples were spun for 5 min at maximum speed (13k rpm). The supernatant was transferred to a new 1.5 ml microfuge tube. Larval samples were re-extracted with 500 µl of methanol and lightly vortexed. Samples were spun again and the supernatant was pooled with the previous supernatant. Samples were extracted a third time with 100% ethanol and lightly vortexed. Samples were spun and the supernatant was pooled with the previous supernatant. The extracts were completely dried with a SpeedVac (Thermo Savant, SPD111V). The dried extracts were dissolved in 110 µl of EIA buffer (provided by the kit) for at least two hours at RT or overnight at 4°C. Once samples were dissolved in EIA buffer, the manufacturer's protocol was followed, including the appropriate controls, standards, and data analysis. An 8-point 20E standard was prepared ranging from 39.1 pg/ml of 20E to 5000 pg/ml by diluting the 5000 pg/ml standard by 1 in 2 with ultrapure water. The mouse anti-rabbit precoated plate (provided by the kit) was washed 4 times with wash buffer (provided by the kit). Before adding reagents and samples, the plate was inverted and shaken to remove the last drops of wash buffer. 100 µl of EIA buffer was added to the non-specific binding control wells and 50 µl of EIA buffer was added to the maximum binding wells. 50 µl of the 20E standard was pipetted into wells in duplicate. 50 µl of the 20E quality control was added to the appropriate wells. 50 µl of each sample was added to the appropriate well in duplicate. 50 µl of the 20E

tracer was added to every well except for the blank wells. 50 µl of the 20E antiserum was added to every well except for the blank wells and non-specific binding wells. The plate was then covered with the cover sheet and incubated overnight at 4ºC. To develop the plate, the plate was first emptied and washed 5 times with wash buffer. After the last wash, the plate was blotted on paper towel. 200 µl of Ellman's reagent was added to each of the wells. The plate was covered with aluminum foil and incubated in the dark at RT. Absorbance at 415 nm was read using a Synergy H1 microplate reader (BioTek). The plate was finished developing once the maximum binding wells had an absorbance of at least 0.200 arbitrary units after the blank had been subtracted. Reagents were dissolved in Ultra-Pure Water EIA Grade (Bertin Pharma, #A07001.1L) when appropriate (including the 20-hydroxyecdysone Quality Control, #A10120).

2.1.10 Heme precursor autofluorescence

Protoporphyrin heme precursors will naturally autofluoresce red when exposed to air and UV light. To view autofluorescent ring glands, larvae were dissected in 1X PBS and stored in ice-cold 1X PBS. The tissues could either be fixed and stained for immunofluorescence or directly added to mounting media and covered with a coverslip. Samples were then viewed with the Nikon C2si Confocal Microscope using the red filter or with epifluorescence and brightfield. Heme precursor autofluorescence in images were changed to a red colour when taken with epifluorescence.

2.1.11 Heme measurements

2.1.11.1 Measuring heme content

Total heme (free heme and protein-bound heme) was measured using oxalic acid and heat. A high concentration of oxalic acid, only with heat, will remove iron from heme, resulting in a fluorescent porphyrin ring. Third instar larvae were staged to the appropriate time. Nine

whole body larvae or 50 brain-ring glands (BRGs) per sample were collected in 100 µl of PBS, flash froze in liquid nitrogen, and stored at -80°C. BRGs were dissected for 1 hr before being flash frozen and stored. BRGs were later pooled after thawing and the PBS volume was reduced to 100 µl. Samples were homogenized, spun down, and the supernatant was transferred to a new tube. Protein concentrations of the samples (the resulting supernatant) were tested with a Qubit 2.0 Fluorometer (Invitrogen) using the Qubit Protein Assay Kit (Invitrogen, Q33211).

A hemin standard ranging from 1 nM to 0.1 nM (using 1:2.5 dilution steps) was made using hemin (Sigma-Aldrich, H9039-1G) dissolved in DMSO. 100 µl of each concentration was used. 1000 µl of 2M oxalic acid (Aldrich Chemistry, 194131-250G) (dissolved in water) was added to each sample, hemin standard, and negative controls (no samples). The content of each tube was split in half, one tube was used as a control (no heat) and the other was used as an experimental (samples were heated). Oxalic acid was not exposed to the samples for more than ten min prior to boiling. Experimental tubes were covered in foil and heated at 95°C for 30 min on a heating block. No heat controls were transferred to 37°C and not boiled. 200 µl of each tube was pipetted into a 96 well microplate (Corning Life Sciences, #3631). Samples were done in duplicate. Fluorescence intensity was measured on a Synergy H1 microplate reader (BioTek). The plate was excited at 400 nm and emission was read at 608 nm and 662 nm. 608 nm results in a stronger signal, but is less specific to heme and 662 results in a lower signal, but more specific to heme (Sinclair, et al. 2001).

2.1.11.2 Analysis of heme measurements

All samples and hemin standards were blanked against a no sample control (oxalic acid with either DMSO for the hemin standard or PBS for the samples). A hemin standard curve was constructed and read at both 608 nm and 662 nm. The standard curve was created using the

difference between the "experimental" (heated) fluorescent reading and no heat control fluorescent reading at each concentration. Only the linear portion of the standard was used and the other points outside the linear range were removed. The difference between the experimental samples fluorescent reading and no heat controls were also found for each sample using the same method for the hemin standard. This difference in fluorescence was then converted to a heme concentration using the hemin standard curve. The heme concentration of each sample was then normalized to the amount of protein in each sample. Heme levels were also determined by a ratio between the fluorescence intensity between the experimental samples and the no heat control samples. Fluorescence was corrected by comparing against an appropriate blank. Samples with normal heme levels would be expected to have a higher ratio due to low background fluorescence in the no heat control, while low heme samples would have significantly higher background fluorescence due to heme precursor accumulation, resulting in a lower experiment to no heat control ratio.

2.1.12 Next-generation RNA sequencing (RNA-Seq)

Approximately 50 ring glands were used per sample to reach at least 100 ng of RNA in 5 µl. RNA was extracted from 44 hr post L2/L3 molt w^{1118} and $PPOX^{-/-}$ (#13702) larvae using the protocol in Chapter 2.1.4 Sample collection and RNA extraction. Samples were done in duplicate. The RNA concentration was measured with a Qubit 2.0 Fluorometer (Invitrogen) using the Qubit RNA HS Assay Kit (Invitrogen, Q32852). RNA integrity was measured using an Agilent RNA 6000 Nano chip (RNA 6000 Nano Kit, 5067-1511) and ran on an Agilent 2100 Bioanalyzer.

cDNA synthesis and library construction were done using the Encore Complete RNA-Seq IL Multiplex System 1-8 (NuGEN, #0312) following the manufacturer's protocol as follows.

2 µl of A1 was added to 0.2 ml PCR tubes. 5 µl of 20 ng/µl of total RNA was added to A1 in the 0.2 ml PCR tubes. The tube was mixed and placed in a prewarmed thermal cycler and incubated at 65ºC for 5 min to anneal the primers. The tubes were immediately returned to ice. A master mix which combined 2.5 µl of A2 and 0.5 µl of A3 per reaction was prepared. 3 µl of the master mix was added to each PCR tube and mixed. The PCR tubes were returned to the prewarmed thermal cycler and incubated at 40ºC for 30 min for first strand cDNA synthesis. The tubes were then placed on ice. A master mix which combined 63 µl of B1 and 2 µl of B2 per reaction was prepared. 65 µl of the master mix was added to each first strand cDNA reaction tube and mixed. The tubes were returned to the thermal cycler and incubated at 16ºC for 60 min for second strand cDNA synthesis. 45 µl of B3 was added to each reaction and the samples were then stored at -20ºC. Following cDNA synthesis, samples were fragmented via sonication with a Covaris S-Series System sonicator using the settings listed in Table 2-2. cDNA was fragmented to approximately 275 bp fragments. To purify the cDNA, 180 µl of an Agencourt RNAClean XP bead suspension was added to 100 µl of fragmented cDNA and mixed. Each sample was split into two 140 µl aliquots. The cDNA fragments were incubated at RT for 10 min. The tubes were transferred to a magnetic plate and the binding buffer was removed and discarded. 200 µl of fresh 70% ethanol was added and allowed to sit for 30 seconds before being removed. The ethanol wash was then repeated. The cDNA was then air dried for 10 min. 12 µl of water was added to the first aliquot of beads and the beads were resuspended. The first aliquot was added to the second aliquot of dried beads and then mixed. The beads then sat at RT for 3 min before being transferred back to the magnetic plate. The eluate was then transferred to a new 0.2 ml PCR tube and placed on ice. For the end repair, a master mix was made that combined 2.5 µl of ER1 and 0.5 µl of ER2 per reaction. 3 µl of the master mix was added to 10 µl of each sample

and mixed. The tubes were then placed in a thermal cycler at 25ºC for 30 min followed by 70ºC for 10 min. After, the tubes were placed on ice. For the ligation, 3 µl of the appropriate Ligation Adaptor Mix (L2) was added to each sample and a unique barcode was assigned to each sample to be used on a single flow cell lane. A master mix was then prepared which contained 6.5 µl of D1, 6.0 µl of L1, and 1.5 µl of L3 per reaction. The master mix was mixed slowly to avoid making bubbles. 14 µl of the master mix was added to each reaction tube and mixed slowly. The reaction tubes were then placed in the thermal cycler at 25ºC for 30 min. Once completed, the tubes were placed on ice. For the first strand selection, a master mix was prepared with 69 µl of SS1 and 1 µl of SS2 per reaction. 70 µl of the master mix was added to 30 µl of each sample and mixed. The tubes were placed in a prewarmed thermal cycler and run at 72ºC for 10 min. Once completed, the tubes were returned to ice. 180 µl of prepared Agencourt RNAClean XP beads were added to the first strand selection reaction products and mixed. Each sample was split into two 140 µl aliquots. The samples were incubated at RT for 10 min. The samples were transferred to a magnetic plate for 5 min and the binding buffer was removed and discarded. The samples were washed twice with fresh 70% ethanol. The samples then air dried for 10 min. The tubes were removed from the magnetic plate and 25 µl of nuclease-free water was added to the first aliquot and mixed. The first aliquot was added to the second and mixed. The samples then sat at RT for 3 min. The tubes were returned to the magnetic plate for 3 min. 21.5 µl of the eluate was removed and transferred to a new 0.2 ml PCR tube. For the second strand selection, a master mix was made that combined 2.5 µl of SS3 and 1.0 µl of SS4 per reaction. 3.5 µl of the master mix was added to 21.5 µl of each sample and mixed. Tubes were placed in a prewarmed thermal cycler and incubated at 37ºC for 30 min, followed by 95ºC for 30 seconds. The tubes were returned to ice. For library amplification, a master mix was made that contained 42 µl of P1, 8 µl

of P2, 4 µl of P4, and 1 µl of P3 per reaction. P3 was added at the last moment and the master mix was mixed slowly to avoid bubbles. 55 µl of the master mix was added to 25 µl of each sample. The tubes were placed in a prewarmed thermal cycler and the following program was ran:

i) 94ºC for 30 seconds
ii) 55ºC for 30 seconds
iii) 72ºC for 1 min
iv) Repeat steps i-iii for 5 cycles
v) 94ºC for 30 seconds
vi) 63ºC for 30 seconds
vii) 72ºC for 1 min
viii) Repeat steps v-vii for 15 cycles
ix) 72ºC for 5 min
x) Hold at 4ºC

Once the reaction was completed, the tubes were returned to ice or stored at -20ºC. To purify the amplified library, 96 µl of prepared Agencourt RNAClean XP beads were added to each reaction tube and mixed by pipetting. The samples were incubated at RT for 10 min. The tubes were transferred to a magnetic plate and allowed to sit for 5 min. The binding buffer was removed and discarded. The samples were washed twice with fresh 70% ethanol. The samples were then air dried and then removed from the magnetic plate. The samples were resuspended in 30 µl of nuclease-free water. The samples were incubated at RT for 5 min and then transferred to the magnetic plate for 2 min. 25 µl of the eluate was transferred to a fresh tube. Once library construction was done, sample quality was checked using an Agilent High Sensitivity DNA 1000 Kit (5067-4626). Sample quantity was determined with the Qubit, using the Qubit dsDNA BR Assay Kit (Invitrogen, Q32850). Samples were sent to Delta Genomics to sequence on an Illumina Hi-Seq 2500 Sequencing System. Raw data was analyzed on Arraystar 4.0 (DNAstar) and data analysis was carried out in Microsoft Access 2013.

2.1.13 Analysis of the circadian rhythm

All flies were entrained to a 12 hour light:dark cycle. Larvae that were to be dissected were raised in a 12 hour light:dark cycle. All fly stocks, cages, and caps were stored at 25°C under a 12 hour light:dark cycle. Food caps were changed twice daily, at the beginning and end of the day. Larvae were staged at the L2/L3 molt between ZT0-ZT4 (when lights turn on to when lights have been on for four hours). Larvae were dissected two days later every six hours at ZT1, ZT7, ZT13, and ZT19 (almost three days after being staged at the L2/L3 molt). Larvae dissected at ZT13 and ZT19 (lights are turned off between ZT12 and ZT24) had minimal light exposure. RNA was then extracted according to Chapter 2.1.4 Sample collection and RNA extraction. qPCR was done according to Chapter 2.1.6 Quantitative real-time PCR (qPCR) using a 384 well plate.

2.1.14 DHR51 antibody production and quality control

2.1.14.1 Antibody production

GenScript was commissioned to produce a rabbit antibody against DHR51 that would hopefully be able to work in for chromatin immunoprecipitation (ChIP). A polyclonal antibody was raised in rabbits using a protein antigen of the sequence:

```
                                  394    MAVKWAK NLPSFARLSF RDQVILLEES
421 WSELFLLNAI QWCIPLDPTG CALFSVAEHC NNLENNANGD TCITKEELAA DVRTLHEIFC
481 KYKAVLVDPA EFACLKAIVL FRPETRGLKD PAQIENLQDQ AHVMLSQHTK TQFTAQIARF
541 GRLLLMLPLL RMISSHKIES IYFQRTIGNT PMEKVLCDMY KN
```

This sequence includes the annotated ligand-binding domain and the remaining C-terminal of the protein. The peptide was conjugated to a carrier and then used in the primary immunization. Each rabbit was injected subcutaneously with 0.2 mg of the DHR51 peptide conjugated to KLH (Keyhole Limpet Hemocyanin). Freud's Complete Adjuvant was used. A pre-immune serum was

collected a day before the primary immunization. The first booster was administrated subcutaneously 14 days after the primary immunization with 0.2 mg of DHR51 peptide conjugated with KLH, along with Freud's Incomplete Adjuvant. 100 µl of serum was collected 21 days after the primary immunization to test the immune response with an ELISA (enzyme-linked immunosorbent assay). 28 days after the primary immunization, a second booster was carried out similar to the first booster. 35 days after the primary immunization, 10-20 ml of serum per rabbit was removed in a production bleed. Another production bleed was carried out 49 days after the primary immunization. A test bleed was sent to me after the third immunization for in-house testing. Two post-immune serums were sent, along with the corresponding pre-immune serum. Specificity was tested via western blotting. Once the antibody was tested, a fourth immunization was done and the final antibody underwent antigen-specific affinity purification.

2.1.14.2 Protein extraction and western blot

Whole body L3 *hs-DHR51* cDNA larvae were heat shocked at 37.5°C for 1 hr, then moved to 25°C to recover for 3 or 6 hrs. Control larvae were not heat shocked or recovered for 0 hrs following heat shock. Protein was extracted from 5 whole body larvae in 300 µl of RIPA buffer (150 mM NaCl, 1% Nonidet P-40, 0.5% Sodium deoxycholate, 0.1% SDS, 50 mM Tris-HCl pH 8.0, 2 mM EDTA, cOmplete protease inhibitor cocktail tablet [Roche, 11873580001]). Samples were homogenized, vortexed, and placed on a shaker for 2 hrs at 4°C. Samples were centrifuged at 14k rpm for 20 min at 4°C and then transferred to a new tube on ice. A small aliquot was taken to measure protein concentration on a Qubit 2.0 using the Qubit Protein Assay Kit (Invitrogen, Q33211). An equal volume of 2X Laemmli loading buffer (4% SDS, 10% 2-

mercaptoethanol [added fresh], 20% Glycerol, 0.004% Bromophenol blue, 0.125M Tris-HCl, final pH of 6.8). Samples were boiled at 100°C for 5-10 min.

The western gel was made up of a 7.5% separating gel and 4% stacking gel. Once the gel was made and properly set up, equal amounts of protein (20-30 μg) were loaded onto the SDS-PAGE gel, along with a PageRuler Plus Prestained Protein Ladder, 10-250 kDa (Thermo Scientific, 26619). The gel was run at 120V for 10 min, then 175V for 40 min. Once the SDS-PAGE gel was done running, the gel was transferred to 1X transfer buffer (25 mM Tris, 190 nM Glycine, 20% Methanol) (a wet transfer) for 10-15 min. Blotting paper, sponge, and a nitrocellulose transfer membrane (Bio-Rad, 1620146) were also presoaked in 1X transfer buffer before creating a sandwich stack for the actual wet transfer. The transfer was done at 100V for 1 hr. After, the membrane was quickly washed with distilled water and stained with Ponceau S for 1 min to access protein transfer. Ponceau S was washed off with distilled water once, followed by two washes of 1X TBST (TBS + 0.1% Tween 20). The membrane was blocked in blocking solution (TBST + 5% w/v non-fat milk) for 1 hr at RT. Primary antibody was then added to the membrane and incubated overnight at 4°C. DHR51 rabbit serum was used at 1:300-500. Purified rabbit DHR51 antibody was used at 1:500. The membrane was washed three times for 10 min with TBST, followed by incubation with the secondary antibody for 1 hr at RT. Goat anti-rabbit HRP (GenScript, A01827) was used at 1:5000 or at 1:8000. The membrane was washed five times for 5 min with TBST. HRP was detected with the SuperSignal West Pico PLUS Chemiluminescent Substrate kit (Thermo Scientific, 34579) following the manufacturer's instructions. A working solution of 1:1 stable peroxide solution to luminol/enhancer solution was prepared (using 100 μl of working solution per cm^2 of membrane). The blot was incubated with the working solution for 5 min at RT in the dark. The working solution was removed and the

membrane was covered in a plastic wrap protein side up. The membrane was exposed to X-ray film in a dark room for an appropriate amount and time and developed. DHR51 is predicted to have a size of 63.3 kDa based on its amino acid sequence but appeared to be present at 70 kDa, which has been reported previously (Rabinovich, et al. 2016).

2.1.14.3 Pull-down assay

L3 *hs-Flag-DHR51* cDNA larvae were heat shocked for 1 hr at 37.5°C. They were then moved to 25°C and allowed to recover for 0 hr, as a control, or 4 hrs. 300 µl of ice-cold lysis buffer was added to 5 whole body larvae, which were then homogenized, vortexed, and put on a shaker for 2 hrs at 4°C. This experiment was repeated using a denaturing (see RIPA buffer in Chapter 2.1.14.2) and non-denaturing lysis buffer (20 mM Tris-HCl pH 8.0, 137 mM NaCl, 1% Nonidet P-40, 2 mM EDTA, cOmplete protease inhibitor cocktail tablet [Roche, 11873580001]). The samples were centrifuged at 14k rpm for 1-2 hrs at 4°C. The supernatant was transferred to a new tube on ice. A small volume was removed for protein measurement using the Qubit as described previously. 8 µl was removed to be used as the total lysate sample (crude cell extract) on the gel. Equal amounts of 2X Laemmli buffer was added to the samples. Samples were boiled at 95-100°C for 10 min.

Protein G beads (Dynabeads, Invitrogen, 10004D) were washed three times with lysis buffer for 1 min at RT, using a 1:1 lysis buffer : bead solution. 50 µl of prepared beads were added to 200 µl of crude cell extract (of 1-5 mg/ml) to pre-clear the extract. Samples were incubated with the prepared beads at 4°C for 1 hr on a rocker. Beads were removed using a magnetic field and the supernatant was transferred to a new tube. 1-5 µg of the primary antibody was added to the cell lysate and incubated at 4°C for 1-3 hrs on a shaker. 4 µg of Rabbit anti-DHR51 was used for testing the antibody. Rabbit anti-Flag (Cell Signaling Technology, 14793S)

was used at 1:50. 50 µl of prepared beads were added to the samples and incubated at 4°C for 1-3 hrs. Beads were placed in a magnetic strip and the supernatant was removed (which was saved for the "absorbed fraction"). The beads were washed three times in lysis buffer for 2 min. Beads were resuspended in 30 µl of 2X SDS Laemmli buffer (1:1 of lysis buffer to 2X Laemmli buffer). Samples were incubated at 95-100°C for 5 min. Beads were removed via a magnetic strip and the supernatant was used to load an SDS-PAGE gel as described previously. Crude extract and absorbed fractions were also prepared and loaded. The western blot and detection were performed as described previously in Chapter 2.1.14.2. Flag-DHR51 was either detected with Rabbit anti-Flag at 1:1000 or Rabbit anti-DHR51 at 1:400. A secondary Goat anti-Rabbit HRP antibody (GenScript, A01827) was used at 1:7000.

2.1.14.4 Sonication optimization

Sample collection, lysis, and sonication

Six whole body w^{1118} larvae were quickly cut in half and inverted in 1X PBS and stored in ice-cold 1X PBS for less than 1 hr. Tissues were quickly spun down and the supernatant was removed. Tissues were resuspended in 1 ml of A1 buffer (60 mM KCl, 15 mM NaCl, 15 mM HEPES pH 7.6, 4 mM $MgCl_2$, 0.5% Triton X-100, 0.5 mM DTT, Protease inhibitor cocktail tablet). Tissues were rotated for 5 min at RT and then spun for 5 min at 4k rpm. The supernatant was removed and tissues were resuspended in 500 µl A1 buffer with a final volume of 1% formaldehyde. Tissues were fixed for 10 min at RT on a shaker, protected from the light. The reaction was quenched with the addition of 2.5M glycine for a final glycine concentration of 125 mM and rotated for 5 min at RT. Tissues were spun at 4k rpm for 5 min at 4°C and the supernatant was removed. Tissues were washed three times for 10 min on a shaker at RT. The first wash was with A1 buffer, the second with Washing Buffer A (10 mM HEPES pH 7.6, 10

mM EDTA pH 8.0, 0.5 mM EGTA pH 8.0, 0.25% Triton X-100), and finally with Washing Buffer B (10 mM HEPES pH 7.6, 200 mM NaCl, 1 mM EDTA pH 8.0, 0.5 mM EGTA pH 8.0, 0.01% Triton X-100). Tissues were resuspended in 1 ml of RIPA buffer (140 mM NaCl, 10 mM Tris-HCl pH 8.0, 1 mM EDTA, 1% Triton X-100, 0.1% SDS, 0.1% Sodium deoxycholate, Protease inhibitor cocktail tablet) and homogenized. Samples were rotated for 5 min at 4°C, then spun at 4k rpm for 5 min at 4°C and the supernatant was removed. Samples were resuspended in ~300 µl of RIPA buffer with 20% SDS added for a final concentration of 1% SDS (SDS was critical for sonication efficiency). Samples were rotated for 20 min at 4°C. Samples were sonicated for 5-30 min for determining the optimal time to get ~300 bp fragments. Samples were sonicated on high power, using a 30s on / 30s off setting using the Diagenode Bioruptor. Samples were rotated for 10 min at 4°C in a new tube, followed by centrifugation for 3 min at 13k rpm at 4°C. The supernatant was transferred to a new tube.

Reverse crosslinking

2 µl of 10 mg/ml of RNase was added per 300 µl of sample and incubated at 37°C for 30 min. Samples were incubated with 5 µl of 10 mg/ml Protease K overnight at 37°C. To reverse the crosslink, samples were incubated at 65°C for at least 6 hrs. Samples were extracted with phenol-chloroform, using an equal volume with the samples. Samples were mixed and spun at 13k rpm for 3 min at RT. The aqueous phase was transferred to a new tube. Samples were then ethanol precipitated and resuspended in 14 µl of water. Samples were run on a 1.5% agarose gel at 80V. Once samples were finished running, the gel was imaged.

2.1.14.5 Chromatin immunoprecipitation, followed by qPCR

(One version of the protocol that did not work)

Day 1

The attempted protocol was a mix between Thomas Danielsen's protocol, who did ChIP in Dr. Kim Rewitz lab with *Drosophila* ring glands, and a DHR51 ChIP protocol in S2 cells (Jaumouille, et al. 2015). *hs-Flag-DHR51* cDNA larvae were heat shocked for 1 hr at 37.5°C and allowed to recover at 25°C for 4 hrs. Samples were collected, fixed, and sonicated as above in Chapter 2.1.14.4. Samples were sonicated for 10 min, using the same settings described previously. Once the chromatin extracts were transferred to new tubes following the sonication and spin, the extracts were stored overnight at -80°C.

Day 2

Chromatin extracts were thawed on ice for at least 1 hr. Meanwhile, Protein G magnetic beads were prepared; 100 µl of beads were prepared per replicate. The appropriate amount of beads was taken out and the supernatant was removed. The beads were washed three times in lysis buffer and resuspended in a 1:1 ratio of beads : lysis buffer. 100X BSA was added to the beads to block the beads and rotated at 4°C for 1 hr. The BSA lysis buffer was then removed and washed three times in lysis buffer. The beads were resuspended in lysis buffer to create prepared beads. 50 µl of prepared beads were added to thawed chromatin extracts on ice and rotated for 4 hrs at 4°C. The beads were removed and 10% of the chromatin extract was saved as Input for the ChIP control. The remaining 90% would be used for the actual ChIP. 1-5 µg of Rabbit anti-DHR51 antibody was added to the ChIP samples or 1:50 of Rabbit anti-Flag antibody. ChIP samples were rotated overnight at 4°C, while Inputs were left at 4°C.

Day 3

50 µl of prepared beads from the previous day were added to the ChIP samples and rotated at 4°C for 4 hrs. After, the supernatant was removed with help from a magnetic bar and washed 4 times with 1 ml of cold lysis buffer. The samples were rotated at 4°C for 5 min

between washes. After washing, the beads were washed twice with cold TE buffer (10 mM Tris-HCl pH 8.0, 1 mM EDTA). 100 µl of Elution Buffer 1 (10 mM EDTA, 1% SDS, 50 mM Tris-HCl pH 8.0) was added to each bead sample and incubated for 10 min at 65°C. The supernatant was removed and transferred to a new tube. 150 µl of Elution Buffer 2 (TE with 0.67% SDS) was added to the beads. The supernatant was transferred to the same tube with Elution Buffer 1. ChIP samples were incubated overnight at 65°C to reverse the crosslinks. 1 µl of 10 mg/ml of Proteinase K was added to the Input, as well as 5 µl of 20% SDS, for every 100 µl of Input volume. The Inputs were incubated at 60°C overnight.

Day 4

Inputs were incubated at 70°C for 20 min. 250 µl of a Proteinase K mix (0.5 µl 20 mg/ml glycogen, 10 µl of 10 mg/ml Proteinase K, in TE) was added to each ChIP sample and incubated at 50°C for 2 hrs. Inputs were moved to ice after their 20 min incubation. 1.25 µl of 4 mg/ml RNase was added to Inputs per 100 µl and incubated at 37°C for 2 hrs. After both incubations, ChIP and Input samples were moved to RT and 55 µl of 4M LiCl was added to ChIP samples. 500 µl of phenol-chloroform was added to ChIP samples and an equal volume was added to the Inputs. Samples were mixed by pipetting and centrifuged at 13k rpm for 3 min at RT. The aqueous phase was transferred to a new tube. The samples were then ethanol precipitated. ChIP DNA was resuspended in 25 µl of water and Input DNA was resuspended in 600 µl of water.

qPCR

qPCR was performed on ChIP and Input DNA samples following the protocol in Chapter 2.1.6 Quantitative real-time PCR (qPCR). Data were analyzed using a % input method, as well as a fold enrichment method compared to a mock ChIP with no primary antibody (according to the ChIP Analysis page on thermofisher.com).

2.1.15 Cloning transgenes

2.1.15.1 DHR51 Transgenes

The goal was to clone *UAS-Flag-DHR51* cDNA (in a pUAST plasmid), *hs-DHR51* cDNA, and *hs-Flag-DHR51* cDNA (in a pCaSpeR-hs-act plasmid) and transform these plasmid constructs into *Drosophila* embryos. pUAST-*DHR51* was a kind gift from Dr. Steven Robinow (Sung, et al. 2009). The pUAST-*DHR51* plasmid was sequence verified using primers listed in Table 2-3 and verified with an EcoRI restriction digest. *Flag-DHR51* cDNA was generated via PCR using pUAST-*DHR51* as a template and a 5' primer to add the *Flag* tag sequence. *Flag-DHR51* was blunt-end ligated into pBS (pBluescript) cut with EcoRV. pBS had been run on an agarose gel to confirm the digestion and gel extracted using the QIAquick Gel Extraction Kit (Qiagen, 28704), while the PCR product was purified using the QIAquick PCR Purification Kit (Qiagen, 28106). Ligated fragments were transformed into *DH5α Escherichia coli* and plated onto agar LB medium containing ampicillin. Colonies that grew overnight were than used to create an overnight culture containing liquid LB and ampicillin that was then purified the next day using the QIAprep Spin Miniprep Kit (Qiagen, 27106). pBS-*Flag-DHR51* was verified with a BamHI digestion and sequencing. Both pBS-*Flag-DHR51* and pUAST were digested with KpnI and NotI. pBS-*Flag-DHR51* was run on a gel and the *Flag-DHR51* fragment was gel extracted and ligated with the cut pUAST fragment. After, the ligated plasmid was transformed into *DH5α E. coli*. Colonies that grew were used to set up an overnight culture containing liquid LB and ampicillin and were purified the next day with a miniprep. pUAST-*Flag-DHR51* plasmids were verified by gel electrophoresis after NotI and KpnI digestion and sequencing.

Flag-DHR51 cDNA and *DHR51* cDNA were cloned into pCaSpeR to generate a heat shock-inducible transgene. pCaSpeR-*Flag DHR51* was cloned similarly to pUAST-*Flag-*

DHR51. Primers were used to add a NotI site and *Flag* tag to the 5' end and a SpeI site to the 3' end. This PCR fragment was cloned into EcoRV cut pBS. Once pBS-*Flag-DHR51* was obtained, it was digested with NotI and SpeI and the insert was purified, while pCaSpeR was cut with NotI and XbaI. The fragments were ligated together, transformed into *DH5α E. coli*, and eventually purified with a miniprep. The resulting pCaSpeR-*Flag-DHR51* plasmid was confirmed via sequencing and digestion with NcoI.

pCaSpeR-*DHR51* was subcloned with pUAST-*DHR51*. pCaSpeR was cut with NotI and XbaI, while pUAST-*DHR51* was cut with NotI and partially digested with XbaI by reducing the digestion time and using a less optimal restriction enzyme buffer. The *DHR51* fragment was gel extracted and ligated into pCaSpeR. The pCaSpeR-*DHR51* plasmid was confirmed via digestion with EagI and sequencing.

The three plasmids, pUAST-*Flag-DHR51*, pCaSpeR-*Flag-DHR51*, and pCaSpeR-*DHR51*, were purified using the QIAGEN Plasmid Midi Kit (12143) following the manufacturer's instructions. A single colony of *E. coli* transformed with one of the plasmids was used to prepare a starter culture in 5 ml of LB and the appropriate antibiotic. The culture was incubated at 37ºC for 8 hours. 200 µl of the starter culture was transferred to 100 ml of fresh LB with the appropriate antibiotic, which was then incubated at 37ºC overnight. 50 ml of the culture was transferred to a 50 ml falcon tube and centrifuged at 4k rpm for 15 min at 4ºC. The remaining 50 ml of culture was added to the same tube and centrifuged again. The supernatant was discarded and the pellet was resuspended in 4 ml of Buffer P1. 4 ml of Buffer P2 was then added and the tube was inverted six times and incubated at RT for 5 min. 4 ml of chilled Buffer P3 was then added, the tube was inverted 6 times, and then incubated on ice for 15 min. The tube was then centrifuged at 11k rpm for 45 min at 4ºC. A column (QIAGEN-tip 100) was

equilibrated with 4 ml of Buffer QBT that flowed through the column via gravity and emptied into a 50 ml falcon tube. After the centrifuge, the supernatant was applied to the QIAGEN-tip 100 column and allowed to flow through via gravity. The column was then washed twice with Buffer QC. The plasmid was eluted with 5 ml of Buffer QF into a 15 ml falcon tube. DNA was precipitated by adding 3.5 ml of RT isopropanol to the plasmid. The tube was mixed and centrifuged at 13k rpm at 4ºC for 30 min. The DNA pellet was washed with 2 ml of RT 70% ethanol and centrifuged at 13k rpm at 4ºC for 10 min. The pellet was air dried for 10 min and dissolved in nuclease-free water and stored at -20ºC. The purified plasmids were sent to BestGene for injections into *Drosophila* embryos. Lines screened for injection were then sent back.

2.1.15.2 Alas transgene

pOT2-*Alas* was ordered from DGRC (*Drosophila* Genomics Resource Center), which comes from the BDGP (Berkeley *Drosophila* Genome Project) Gold cDNAs (FI09607). The plasmid was confirmed via PstI digestion and gel electrophoresis. The *UAS-Alas*-cDNA was cloned via Gateway cloning. PCR primers were designed to amplify *Alas* from pOT2-*Alas* and CACC was added to the 5' end to facilitate entry into the pENTR/D Topo entry vector. The protocol was done following the manufacturer's protocol. Approximately 8 ng of the *Alas* cDNA PCR product was added to 1 µl of the Topo entry vector, which includes the topoisomerase enzyme, so that the DNA is present in a 1:1 ratio. 1 µl of a salt solution was added and the total reaction was brought up to 5 µl with nuclease-free water. The reaction was incubated for 5 min at RT before being transformed into One Shot TOP10 *E. coli*. SacI and NotI digestion and sequencing was used to confirm the pENTR-*Alas* plasmid. The LR clonase reaction was done with pBID-UASC-G, sent by Dr. Brian McCabe, Columbia University, which contained a UAS

promoter (Wang, J. W., et al. 2012). The resulting pBID-UASC-G *Alas* plasmid was confirmed via EagI digestion and sequencing. The plasmid was sent to BestGene for injection into the fly strain #8622-*attP2*, which used the phiC31 system for site-directed insertion onto the 3rd chromosome.

2.1.16 DHR51 CRISPR

2.1.16.1 Endogenous Flag tag for *DHR51*

The goal was to knock-in an N-terminal and a C-terminal Flag tag to the endogenous *DHR51* locus with homology-directed repair. The construct was cloned into the pHD-*DsRed* vector and used DsRed as a selectable marker after injections (Gratz, et al. 2014). The strain that was to be injected, *vasa-Cas9* Strain #51323, was sequenced prior to gRNA construction. The general strategy used a protocol from Gratz *et al.* 2015 for targeting gRNA (guide RNA) sites (Gratz, et al. 2015). The gRNA sequences used for the N-terminal tag targeted the sequences 5'-CCGCCAAAGCTCAACAAAATGAA-3' and 5'-ACACCCACGATTAATTAGGACGG-3' (the underlined sequences are the PAM sites). The gRNA sequences used for the C-terminal tag targeted the sequences 5'-TCTATTTTCAGCGCACTATTGGG-3' and 5'-CCAAGCTGGTTTCGCTACCGTCC-3'. gRNA was cloned into the expression vector pCFD4 according to the website crisprflydesign.org. Gibson Assembly was done with slight modifications: having a reaction temperature of 40°C to aid annealing, increased incubation time (30 min), diluting the Gibson reaction before transformation (1 in 3), and adding 20-30 µl of the Gibson reaction due to the Gibson reaction being inefficient for me. Other reaction parameters are according to the manufacturer's instructions. 50-100 ng of the vector was used with a two to three-fold excess of the insert for the Gibson reaction. The DNA was added to 10 µl of Gibson assembly master mix (2X) and nuclease-free water was used to bring the total reaction volume to

20 µl. The reaction was incubated at 40°C for 30 min. The reaction was then used to transform *E. coli*. pCFD4-gRNA was confirmed via BbsI digestion and sequencing.

A less direct approach was taken to clone the pHD-*DsRed Flag-DHR51* construct due to complications with the Gibson Assembly reactions. Overlapping PCR primers were designed to amplify multiple regions: *DsRed*, the pHD backbone, the *DHR51* 5' homology arm, a *DHR51* 3' homology arm, and finally, a small piece of genomic DNA between the gRNA cut sites. Gibson Assembly was not successful with combining these five PCR fragments, so Gene SOEing (Splicing by Overlap Extension) was used in the initial stages to reduce the number of PCR fragments before Gibson Assembly. Gene SOEing worked best when done in a two-step PCR reaction. The first was a smaller reaction which used no primers for 20 cycles to combine two fragments that had short (15-30 bp) overlaps. A second PCR reaction that used the product of the first PCR reaction as a template and had primers anneal to the end of each original DNA fragment so the entire combined fragment would be amplified was performed. This was done for 30 cycles. Two separate gene SOEing was done to combine the inter-gRNA cut site fragment with the *DsRed* fragment, as well as combine the *DsRed* fragment with the *DHR51* 3' homology arm. The individual fragments were then blunt-end ligated into EcoRV cut pBS. Subcloning was then used to cut *DsRed* in the middle of the fragment and pBS, one plasmid was used as an insert, and the other the destination vector. Note: This was done for the N-terminal tag, for the C-terminal tag, the inter-gRNA cut site fragment was successfully gene SOEd with the *DsRed*-3' homology arm fragment and cloned into EcoRV cut pBS. Either way, the end result was a pBS plasmid with three combined DNA fragments (inter-gRNA cut site, *DsRed*, and a *DHR51* 3' homology arm). At this point, the plasmid was sequenced to confirm correct SOEing of the fragments. These three combined fragments were then amplified via PCR and combined with the

DHR51 5' homology arm with a Gibson reaction. The four combined fragments were amplified via PCR and another Gibson reaction was done with the PCR fragment of the pHD backbone. The now fully assembled five fragment plasmid containing *DHR51* 5' and 3' 1 kb homology arms, *DsRed*, and an added Flag tag was transformed into *E. coli*. The final product was then confirmed with a restriction digest and sequencing.

The final pHD-*DsRed Flag-DHR51* plasmids and pCFD4-*DHR51* 2xgRNA plasmids were sent to GenetiVision for injection into *Drosophila* embryos, Strain #51323. Unfortunately, no transformants were identified by GenetiVision during the screening for both the N-terminal and C-terminal tags. Another round of injections was done by Nhan Huynh from our lab. Viable larvae that were injected were transferred to fresh food shortly after hatching. Once these larvae made it to adulthood, they were crossed to w^{1118} adults of the opposite sex. G_1 progeny were screened for the DsRed marker but I did not identify any positive transformants during the screening process. As of now, the transformation has not been completed.

2.1.16.2 DHR51 conditional CRISPR

GenetiVision was hired to create a fly strain that has a 2xgRNA transgene against *DHR51*. The two target sites chosen were 5'-CCCGGATTAAGGGTCAGAACCTG-3', which targets before the first zinc finger of the DNA-binding domain, and 5'-TACGGAATCCTAGCCTGCAATGG-3', which targets the first zinc finger of DHR51 (Sung, et al. 2009). The two gRNAs were both cloned into pCFD5, which allows for ubiquitous gRNA expression in the animals and injected into *Drosophila* v^1 (*vermilion*) embryos. The embryos that were injected also had an *attP2* site that allowed for site-directed insertion of the *pCFD5-DHR51* 2xgRNA onto the third chromosome via the PhiC31 integrase system. Three independent insertion lines of *DHR51* 2xgRNA (3m, 6m, and 12m) flies were obtained which should all have

the same sequences of gRNA and same insertion site. The resulting *DHR51* 2xgRNA flies were then balanced and then shipped. The *DHR51* 2xgRNAs were then crossed to *Act5C-Cas9* (Bloomington #54590) and *Spok-eCas9* (Huynh, et al. 2018) for tissue-specific CRISPR *DHR51* mutations.

2.1.17 Statistical analysis

All qPCR and fold change data were analyzed with a two-tailed unpaired Student's t-test. P-values less than 0.05 were considered statistically significant. Student's t-tests were calculated in Microsoft Excel 2010 and 2013.

To determine whether the overlap in misregulated genes between *phm>DHR51*-RNAi (1) and *phm>FeCH*-RNAi was significant in the RNA-Seq data set, a Chi-squared test was done. The expected values were calculated using the totality of the RNA-Seq data (15771 genes). The Chi-squared test was calculated in Microsoft Excel 2010 and 2013 using the CHISQ.TEST function. The significance of the Pearson and Spearman's rank correlations were calculated with a regression analysis in Microsoft Excel 2010 and 2013. P-values less than 0.05 were considered statistically significant.

2.2 Tables

Table 2-1. qPCR primers. Primers are listed as pairs. Sequences are listed from 5' to 3'. F = For = Forward. R = Rev = Reverse.

Primer Name	Primer sequence	Comments
qRP49-F#105	CGGATCGATATGCTAAGCTGT	Used for normalization
qRP49-R#105	GCGCTTGTTCGATCCGTA	
DHR51 Forward qPCR #46	AAGCACTACGGAATCCTAGCC	
DHR51 Reverse qPCR #46	GATGAGCTTTGTCCACCACA	
Alas Forward qPCR	ACCAACGGAACGTCTCCTAC	Heme pathway
Alas Reverse qPCR	CTTCGACGGGGAAACCTT	
Pbgs (ALAD) qPCR For	GAATCGCCTGAAGGAGCAC	Heme pathway
Pbgs (ALAD) qPCR Rev	AAGAGCAGCACCGACGAC	
l(3)02640 (PBGD) qPCR For	ATAGCCTCGCTTCCAAAGG	Heme pathway
l(3)02640 (PBGD) qPCR Rev	ACACCGTCAAATGGGGATAC	
FeCH qPCR For	CTGGCCGAGATCGAAAAG	Heme pathway
FeCH qPCR Rev	TGAGTAAATATGGAGTTAAAGCTGGA	
neverland_F	CCCTCACCTAGGAGCCAACT	Ecdysone biosynthesis
neverland_R	GGCATATAACACAGTCGTCAGC	
shroud_F	CGAATCGCTGCACATGAC	Ecdysone biosynthesis
shroud_R	TAGGCCCTGCAGCAGTTTAG	
spookier_F	GCGGTGATCGAAACAACTC	Ecdysone biosynthesis
spookier_R	CGAGCTAAATTTCTCCGCTTT	
Cyp6t3 (Forward)	GGTGTGTTTGGAGGCACTG	Ecdysone biosynthesis
Cyp6t3 (Reverse)	GGTGCACTCTCTGTTGACGA	
phantom_F	GGCATCATGGGTGGATTT	Ecdysone biosynthesis
phantom_R	CAAGGCCTTTAGCCAATCG	
disembodied_F	GTGACCAAGGAGTTCATTAGATTTC	Ecdysone biosynthesis
disembodied_R	CCAAAGGTAAGCAAACAGGTTAAT	
shadow_F	CAAGCGGATATTTGTAGACTTGG	Ecdysone biosynthesis
shadow_R	AAGCCCACTGACTGCTGAAT	

Torso Forward qPCR Rewitz	TCCAACTCTACCCACAACATCAC	(Rewitz, et al. 2009)
Torso Reverse qPCR Rewitz	CAGATTCACCGCTCCCATTT	
esg Forward qPCR	CCGGATTGCCAAATCTTA	RNA-seq validation
esg Reverse qPCR	ATGGAACTGCTGATGTTTGGT	
Mmp1 Forward qPCR	GTTTCCACCACCACACAGG	RNA-seq validation
Mmp1 Reverse qPCR	GCAGAGGCGGGTAGATAGC	
Thor Forward qPCR	CCAGATGCCCGAGGTGTA	RNA-seq validation
Thor Reverse qPCR	AGCCCGCTCGTAGATAAGTTT	
Nc Dronc Forward qPCR	CAACAGTGTGGAGGGAAAAGA	RNA-seq validation
Nc Dronc Reverse qPCR	TGCATATCGACCACAGATCC	
Ana Forward qPCR	ACTTGCGACCAGGCAGAC	RNA-seq validation
Ana Reverse qPCR	CTTAAACGGTTCTGTTCGGTAAA	
Nplp4 Forward qPCR	TGCTGGTTGTCGTTTTCG	RNA-seq validation
Nplp4 Reverse qPCR	TCCGGAGTAGGCGTATGG	
Period E1 qPCR For	CTATACACAGACACGTGCATACACCGAC	(Jaumouille, et al. 2015)
Period E1 qPCR Rev	CGGCTTCTTTGCTCATTATCATCAACGAATC	
Period E5 (CRS) qPCR For	CCAGTGCCAGTGCGAGTTC	(Jaumouille, et al. 2015)
Period E5 (CRS) qPCR Rev	GATGCCAAGTGTCAATCCAAGC	
Period RORE qPCR For	CATCCAATCTGGGTCAGAGCA	(Jaumouille, et al. 2015)
Period RORE qPCR Rev	AGCTGAAAATACCAAGGTGCAATG	
Period E8 qPCR For	CAAGCCATGATTCATGAACATGAATGGCAG	(Jaumouille, et al. 2015)
Period E8 qPCR Rev	CTTCACGTTGCTCGCCAATAGTATTGTG	
Lim1 out qPCR For	GCCTGGTGGGCCATAAATCCA	(Jaumouille, et al. 2015)
Lim1 out qPCR Rev	ATACCAGTGTTTGGCGGAAAGTGT	
Timeless For. qPCR #133	ATGGTGGCATCTGTGTACGA	Circadian rhythm

Timeless Rev. qPCR #133	CCGAGGCCAAAGAGACATT	
Period For. qPCR #61	TGAGAGCGAGAGCGAGTGTA	Circadian rhythm
Period Rev. qPCR #61A	CATGGTGCTTAGGTTCTCCAG	
EGFP qPCR R67F	GAAGCGCGATCACATGGT	Ligand trap
EGFP qPCR R67R	CCATGCCGAGAGTGATCC	
GAL4 DBD Forward qPCR	GTGAATAAAGATGCCGTCACAG	Ligand trap
GAL4 DBD Reverse qPCR	CAATGTTAGAGGCATATCAGTCTCC	

Table 2-2. Covaris S-Series System sonicator settings. Table adapted from the Encore Complete RNA-Seq Library System user guide. Settings used for sonication of RNA-Seq samples.

Parameter	Value
Duty cycle	10%
Intensity	5
Cycles/burst	200
Time	180 seconds
Temperature (water bath)	6-8°C
Power mode frequency	Sweeping
Degassing mode	Continuous
Sample volume	120 µl
Water (fill/run)	S2 – level 12 E210 – level 6
AFA intensifier	Yes

Table 2-3. Primers used for cloning and CRISPR. Primer sequences are listed 5' to 3'. F = For = Forward. R = Rev = Reverse.

Primer name	Primer sequence	Comment
Fp DHR51	CCGCCAAAGCTCAACAAAATGAATAAGG	DHR51 PCR
Rp DHR51	CGAGTTAACTAGTTCTTATACATGTCACAGAGC	DHR51 PCR
NotI DHR51 Forward	ATCGCGGCCGCATGAATAAGGAAGAAAATTCCTCC	DHR51 cloning
DHR51 SpeI Reverse	TGTACTAGTCTAGTTCTTATACATGTCACAGAGC	DHR51 cloning
Flag tag DHR51 N terminal	ATCGCGGCCGCATGGATTACAAGGATGACGATGACA AGGATTACAAGGATGACGATGACAAGGATTACAAG GATGACGATGACAAGATGAATAAGGAAGAAAATTC CTCC	DHR51 cloning (Flag tag)
pUAST Forward	ACTGCAACTACTGAAATCTGCCAAG	Sequence insert
pUAST Reverse	TAATGTCACACCACAGAAGTAAGG	Sequence insert
pCaSpeR Forward	GATCCACATCTGCTGGAAGG	Sequence insert
pCaSpeR Reverse	AACTGCAACTACTGAAATCTGCC	Sequence insert
DHR51 Forward (middle)	GCAGCTTTCCCATGTTCAACG	Sequencing
DHR51 Reverse (middle)	AAGAGCTGACGGAGGAGACAC	Sequencing
Alas Topo Forward	CACCATGCAGTGTCCGTTCTTGAACC	Alas gateway cloning
Alas Reverse	GGCAACTATGCTGCAAGCGAG	Alas cloning
5' Hr51 Forward Genomic	GTCGCCTCTCCACGATTG	gRNA genomic sequencing
5' Hr51 Reverse Genomic	TGGGCATTTTACAATTGATCCAG	gRNA genomic sequencing
3' Hr51 Forward Genomic	GTGCCTCAAGGCGATAGTTC	gRNA genomic sequencing

3’ Hr51 Reverse Genomic	TTTGATTCGCTGTACGTAATCC	gRNA genomic sequencing
N-term gRNA#1 (pCFD4)	TATCCGGGTGAACTTCGTTCATTTTGTTGAGCTTTGG GTTTTAGAGCTAGAAATAGCAAG	gRNA construction
N-term gRNA#2 (pCFD4)	CTATTTCTAGCTCTAAAACTCCTAATTAATCGTGGGT GTCGACGTTAAATTGAAAATAGG	gRNA construction
C-term gRNA#1 (pCFD4)	TATCCGGGTGAACTTCGTCTATTTTCAGCGCACTATT GTTTTAGAGCTAGAAATAGCAAG	gRNA construction
C-term gRNA#2 (pCFD4)	GCTATTTCTAGCTCTAAAACAGCTGGTTTCGCTACCG TCCGACGTTAAATTGAAAATAGG	gRNA construction
pHD-dsRed Forward	CGAGGCTCTTCCGTCAATCGAGTTC	CRISPR plasmid
pHD-dsRed Reverse	CTGGCAGTTCCCTACTCTCGCATGG	CRISPR plasmid
dsRed (LoxP) Forward	GCCCTTCGCTGAAGCAGGTG	CRISPR plasmid
dsRed (LoxP) Reverse	CGCCTTATGCATGGAGATCTTTACTAGTGC	C-term CRISPR plasmid
dsRED (LoxP) Gibson Reverse	CATATCACTTTTTTTATTTTCCTATCTTATCGCCTTAT GCATGGAGATCTTTACTAGTGC	N-term CRISPR plasmid
N-term 5 Homology Forward	ACTCCCCATGCGAGAGTAGGGAACTGCCAGCGAAA GCGCCGACATCACAAAGG	N-term CRISPR plasmid
N-term 5 Homology Reverse	ATAATCACCGTCATGGTCTTTGTAGTCCATTTTGTTG AGCTTTGGCGCACTGC	N-term CRISPR plasmid
N-term InterCRISPR Forward + Flag	ATGGACTACAAAGACCATGACGGTGATTATAAAGAT CATGACATCGATTACAAGGATGACGATGACAAGATG AATAAGGAAGAAAATTCCTCCGAAAC	N-term CRISPR plasmid + Flag tag
N-term	GCAAGAATTCCACCTGCTTCAGCGAAGGGCGCGTCC	N-term

InterCRISPR Reverse	TAATTAATCGTGGGTGTAAGAAAC	CRISPR plasmid
N-term 3 Homology Forward	GATAAGATAGGAAAATAAAAAAAGTGATATGTTAAAGAAAAAAACGGAAAGG	N-term CRISPR plasmid
N-term 3 Homology Reverse	CCCTTGAACTCGATTGACGGAAGAGCCTCGCCGGTGGTAATGGGTGGTGC	N-term CRISPR plasmid
C-term 5 Homology Forward	ACTCCCCATGCGAGAGTAGGGAACTGCCAGCGTCAGCTCTTCCAGTCCCACC	C-term CRISPR plasmid
C-term 5 Homology Reverse + Flag	CTACTTGTCATCGTCATCCTTGTAATCGATGTCATGATVTTTATAATCACCGTCATGGTCTTTGTAGTCGTTCTTATACATGTCACAGAGCACCTTTTCCATGGGCGTGTTGCCAATAGTGC	C-term CRISPR plasmid + Flag tag
C-term InterCRISPR Forward	GACATCGATTACAAGGATGACGATGACAAGTAGTTAACTCGAGCTTTAAGTTACAAC	C-term CRISPR plasmid
C-term InterCRISPR Reverse	GCAAGAATTCCACCTGCTTCAGCGAAGGGCAACCAGCTTGCTTGTATAGAAATATAC	C-term CRISPR plasmid
C-term 3 Homology Forward	GCACTAGTAAAGATCTCCATGCATAAGGCGTCGCTACCGTCCCATAGAAGCC	C-term CRISPR plasmid
C-term 3' Homology Reverse the 2nd	CCCTTGAACTCGATTGACGGAAGAGCCTCGAGCCAGAAGATTTTTGTTGGCTTTG	C-term CRISPR plasmid (first not specific)
3' Homology N-term Rev.	TGGAATGGAAAGACAAAGTCAGG	Sequencing CRISPR
5' Homology C-term For.	CCTGCTGAACGCAATCCAATG	Sequencing CRISPR
3' Homology C-term Rev.	TTTCGCCAACAAGAAGAGATACG	Sequencing CRISPR
dsRed Middle For.	AAGAAGACTATGGGCTGGGAG	Sequencing CRISPR
DHR51 Genomic Reverse	TATTTCACGCACAATTTCCCAAC	PCR Confirmation of injection lines

dsRed Reverse PCR	ACGAAGTTATGATCGCAGGTG	PCR Confirmation of injection lines

Chapter 3

DHR51 as a regulator of *Alas* to maintain heme homeostasis

3.1 Introduction

3.1.1 DHR51 in the prothoracic gland

The King-Jones lab was interested in examining nuclear receptors for their role in heme regulation because the vertebrate heme sensor is a nuclear receptor. DHR51 was a prime candidate for a heme sensor in the prothoracic gland (PG) because DHR51 showed a comparable affinity for heme as Rev-erbα and heme binding to DHR51 was likely reversible *in vitro*. E75 had a much higher affinity for heme compared to DHR51 and heme was required for E75 protein stability (de Rosny, et al. 2008; Reinking, et al. 2005). Since it seemed like E75 required heme, E75 could more likely act as a redox or gas sensor than a heme sensor. The dissociation constant (K_d) of DHR51 and heme was found to be 0.43 μM *in vitro*, while other transcription factors that reversibly bind heme, such as Bach1 and Rev-erbα and Rev-erbβ have K_d values of 0.1 μM and 2-3 μm, respectively (de Rosny, et al. 2008; Ogawa, et al. 2001; Raghuram, et al. 2007). E75 was estimated to have a K_d in the nanomolar range (de Rosny, et al. 2008). The affinity for heme suggested that DHR51 could potentially be more functionally equivalent to Rev-erbα than E75, thus DHR51 could function as a heme sensor.

Before I joined the lab, Qiuxiang Ou, a then PhD student in the King-Jones lab, did preliminary tests with DHR51 to determine whether DHR51 had a role within the PG. Two independent *UAS-DHR51*-RNAi lines were used to disrupt *DHR51*. These two RNAi lines targeted different sequences of *DHR51* to minimize the probability of off-target effects, when RNAi silences unintentional gene targets (any gene other than *DHR51*). RNAi was expressed specifically in the PG with *phantom22-GAL4* (*phm22* or *phm>* for short) (I will use the notation of *phm>gene*-RNAi to indicate RNAi targeting a specific gene of interest). *phm>DHR51*-RNAi (1) (VDRC #37618) resulted in an L3 arrest, where larvae make it to the L3 stage and remain as

L3 larvae for weeks and never form pupae. The prolonged L3 stage allowed larvae to remain in the food eating longer, which caused the larvae to grow larger than normal. *phm>DHR51*-RNAi (2), which is a miRNA-based RNAi line from Dr. Tzumin Lee's lab (Lin, et al. 2009), resulted in a minor developmental delay into puparium formation and the L3 larvae were slightly larger compared to control L3 larvae due to a prolonged feeding phase (the *DHR51*-RNAi phenotypes will be discussed in more detail in Chapter 3.2.1). Both *DHR51*-RNAi lines disrupted larval development when expressed in the PG, which suggested that DHR51 has a developmental role in the PG.

My hypothesis was that DHR51 acts as a heme sensor to upregulate *Alas* when cellular heme levels are low within the PG. Under normal conditions, heme is bound to DHR51 and DHR51 is inactive with respect to *Alas*. When cellular heme levels drop, DHR51 is freed from heme and DHR51 upregulates *Alas* (Figure 1-6). I will note that this is a different mode of function compared to Rev-erbα which was active when bound to heme whereas I am proposing that DHR51 is inactive when bound to heme and heme is an inverse agonist for DHR51. This is based on preliminary experiments by Qiuxiang Ou and my data that will be discussed in this chapter support this model for DHR51. If DHR51 is functional when unbound by heme due to low cellular heme levels, which results in *Alas* upregulation, disrupting DHR51 function when cellular heme levels are low should result in *Alas* not being upregulated. If *Alas* is not upregulated when cellular heme levels are low, red autofluorescence should not noticeably accumulate due to less of an accumulation of late heme precursors.

Our lab had access to multiple RNAi lines that disrupted heme biosynthesis and resulted in large red autofluorescent RGs, which is a characteristic of low cellular heme levels and *Alas* upregulation. These lines included *spz5*-RNAi (*spz5* [*spatzle 5*] encodes a neurotrophin, but the

observed low heme phenotype is now suspected to be caused by an off-target of the RNAi), *Nos*-RNAi (*Nitric oxide synthase*, which encodes a protein that produces nitric oxide) (Caceres, et al. 2011), and RNAi lines that target genes that encodes for enzymes in the heme biosynthesis, *PPOX*-RNAi and *FeCH*-RNAi. Qiuxiang disrupted *DHR51* function in these RNAi lines that disrupted heme biosynthesis to determine whether DHR51 was required for *Alas* upregulation. Qiuxiang found that expressing *DHR51*-RNAi (1) with either *PPOX*-RNAi or *spz5*-RNAi rescued the red autofluorescence in the PG normally caused by *PPOX*-RNAi or *spz5*-RNAi alone (Ou, unpublished). She also found that *Alas*-RNAi was able to rescue *PPOX*-RNAi and *spz5*-RNAi similarly to *DHR51*-RNAi (1) in the PG, which demonstrated that the accumulation of heme precursors was dependent on *Alas* upregulation when cellular heme levels were low. Since *DHR51*-RNAi (1) and *Alas*-RNAi similarly reduced the accumulation of red autofluorescent heme precursors, this indicated that DHR51 could be necessary for *Alas* induction when cellular heme levels are low and that DHR51 might be active when cellular heme levels are low. However, we later became concerned that using two *UAS*-RNAi lines could be diluting the GAL4 at each *UAS* promoter, lowering the efficiency of each RNAi lines. In addition to this uncertainty, this experiment was only conducted with one *DHR51*-RNAi line, so it is possible that an off-target, an unintended target of the *DHR51*-RNAi, was responsible for *Alas* expression being attenuated in a low heme background. For my experiments, I used a second *DHR51*-RNAi line (*DHR51*-RNAi (2)) that targets an independent sequence compared to *DHR51*-RNAi (1) due to concerns about a potential off-target of *DHR51*-RNAi (1). In addition, I developed *DHR51* CRISPR lines that can disrupt DHR51 in a tissue-specific manner (conditional or somatic CRISPR), independently of RNAi.

3.1.2 Conditional CRISPR

I wanted to disrupt *DHR51* in the PG with a technique other than RNAi, since the RNAi lines could have potential off-targets and *phm>DHR51*-RNAi (1) and (2) caused different developmental phenotypes (L3 arrest compared to a minor delay, respectively). This would allow me to determine the true effect of loss-of-*DHR51* in the PG. *DHR51* mutants affect the whole body and the mutant phenotypes from the *DHR51* mutants that I received differed in severity to the published phenotypes (this will be discussed in Chapter 3.2.1). A variation of CRISPR was used to disrupt *DHR51* independent of RNAi. CRISPR has been found to have very few, if any, off-target edits, although the investigation of the rate of CRISPR off-targets is still ongoing (Bassett, et al. 2013; Gratz, et al. 2014). CRISPR (Clustered Regularly Interspaced Short Palindromic Repeats), in general, is explained more in depth in Appendix A.1.1. Briefly, CRISPR is a fast and easy genome-editing technique adapted from the immune system of bacteria (Ishino, et al. 1987). In a type II CRISPR system, Cas9 (CRISPR-associated nuclease) binds foreign RNA and uses the RNA to target complementary DNA sequences to cut foreign DNA. CRISPR has since been modified to use Cas9 to bind engineered guide RNAs (gRNAs) to target host DNA sequences of interest in order to cut the DNA and cause mutations through inefficient repair by nonhomologous end joining (NHEJ), which can cause insertions and deletions, or homologous recombination. CRISPR has been used successfully in causing mutations in *Drosophila (Bassett, et al. 2013; Gratz, Cummings, et al. 2013; Yu, Z., et al. 2013)*.

The specific variant of CRISPR that I used was conditional (or somatic) CRISPR. Conditional CRISPR works similarly to the *UAS*-GAL4 system to edit a target gene in a tissue-specific manner. In fact, the first conditional CRISPR in *Drosophila* used the *UAS*-GAL4 system to accomplish this. A tissue-specific *GAL4* driver was used to express *UAS-Cas9* in the desired

tissue. gRNA to target the DNA sequence of interest was expressed with a ubiquitous promoter (Xue, et al. 2014). Thus, gRNA could only combine with Cas9 to edit DNA wherever Cas9 was expressed. However, *UAS-Cas9* led to lethality when highly expressed in the PG, even in the absence of a gRNA (Huynh, et al. 2018). The lethality of overexpressing *Cas9* with GAL4 was independent of Cas9 endonuclease activity (Port, et al. 2014). To circumvent the lethality, *Cas9* was directly expressed with the PG-specific promoter from *Spok*. *Spok-Cas9* provided a viable balanced heterozygous stock that could be used for conditional CRISPR in the PG (Huynh, et al. 2018). Thus, conditional CRISPR using *Spok-Cas9* and ubiquitously expressed *DHR51* gRNAs would provide another method to disrupt *DHR51* specifically in the PG, independent from RNAi.

3.1.3 Tools for testing DHR51 ligand binding capability

Nuclear receptors are transcription factors that contain an N-terminal DNA-binding domain (DBD), as well as a C-terminal ligand-binding domain (LBD). Upon ligand binding, the nuclear receptor undergoes a conformational change that can result in altered protein interactions. For some nuclear receptors, conformational changes can result in dimerization, translocation between the cytoplasm and nuclear, or the recruitment of co-regulators. In order to identify potential ligands of nuclear receptors or when nuclear receptors may be active, 18 LBDs of nuclear receptors were fused to the DBD of GAL4 (Palanker, et al. 2006). This approach is referred to as a ligand trap. The LBD of a specific nuclear receptor attached to the DBD of GAL4 created a ligand trap fusion protein that targeted a known sequence (*UAS*) and reporter gene, like *UAS-EGFP* (see Figure 3-1A for an example using the DHR51 ligand trap). The ligand trap fusion proteins are produced using a heat shock promoter to allow temporal control of expression. Since the LBD and ligand binding can regulate the activity of a nuclear receptor, in

theory, these ligand trap fusion proteins would also be regulated by the LBD. The GAL4 DBD in these ligand trap fusion proteins lacks the GAL4 activation domain, so GAL4 activation should be dependent on the nuclear receptor LBD. So, when an endogenous nuclear receptor is activated in the presence of a ligand, like EcR with 20E during a major ecdysone pulse, the GAL4 DBD-EcR LBD ligand trap fusion protein (EcR ligand trap fusion protein) should also be activated and express the reporter gene. This allows for *in vivo* testing of the ligand binding ability of nuclear receptors. Of these 18 ligand trap fusion proteins created, nine were found to have activated a reporter during larval development (Palanker, et al. 2006). Of these, the EcR ligand trap fusion protein was responsive to its ligand, 20E. Exogenous 20E induced more tissues to express the reporter gene and reporter gene expression was higher compared to when exogenous 20E was not added. This indicated that the EcR ligand trap fusion protein had higher activity and responded to its 20E ligand. Disrupting ecdysone production decreased reporter gene expression, which indicated that the EcR ligand trap fusion protein was less active without its 20E ligand. (Palanker, et al. 2006). This set of experiments showed that the activity of the GAL4 DBD could be regulated through ligand binding to the LBD.

In general, when nuclear receptors dimerize, they form strong protein-protein interactions between the LBDs, but there are also weak interactions through the DBD (King-Jones and Thummel. 2005). The strong interactions between the LBDs could potentially still allow for proper dimerization with the ligand trap fusion protein that only contains the nuclear receptor LBD. Palanker *et al*. tested protein-protein interaction between the DHR3 ligand trap fusion protein and E75B, an isoform of E75 that is missing the DBD and acts as a repressor (Segraves and Hogness. 1990). E75B binds to DHR3 and repress DHR3 activity (White, K. P., et al. 1997). The DHR3 ligand trap fusion protein was found to be active in many larval tissues and ectopic

expression of E75B decreased the activity of the DHR3 ligand trap fusion protein in many of the tissues where DHR3 was active (Palanker, et al. 2006). The DHR3 ligand trap fusion protein demonstrated that ligand trap fusion proteins could potentially still form necessary nuclear receptor dimers.

Nine out of the 18 ligand trap fusion proteins did not show any activity at the times and developmental stages tested, despite that the ligand trap fusion proteins were found to be produced (Palanker, et al. 2006). The DHR51 ligand trap fusion protein was among those that did not show activity. There are a variety of reasons why these fusion proteins could seem inactive. The first is that Palanker *et al*. only tested for activation of the reporter gene and some of these nuclear receptors are known to function as repressors, such as E75 and DHR4 (White, K. P., et al. 1997; King-Jones, et al. 2005). NR2E3, the vertebrate homolog of DHR51, functions as a dual repressor/activator (Cheng, et al. 2004; Chen, J., et al. 2005; Haider, et al. 2009). Although DHR51 induced *period* transcription, DHR51 could also potentially function as a dual repressor/activator similar to NR2E3 (Jaumouille, et al. 2015). If so, the DHR51 ligand trap fusion protein could have been functioning as a repressor under the time or conditions that were initially tested in *Palanker et al*. Secondly, the presence and/or absence of a potential ligand could render one of the ligand trap fusion proteins inactive at the time and stages examined. Based on my hypothesis that DHR51 acts as a heme sensor, DHR51, and therefore the DHR51 ligand trap fusion protein, would be inactive under normal heme levels and would only be activated when cellular heme levels are low. Other possible explanations for not seeing reporter gene expression with the ligand trap fusion proteins are that the fusion proteins failed to dimerize or recruit co-regulators or that the ligand trap proteins are just non-functional.

3.1.4 Identifying the *Drosophila* heme sensor

Even though the vertebrate heme sensor has been identified, I still aimed to determine whether DHR51 acted as a heme sensor in *Drosophila*. *Drosophila* has proven to be a powerful tool to study nuclear receptors and how nuclear receptors function in relation to steroid hormones, both as upstream regulators and downstream responders to the action of steroid hormones. The PG in *Drosophila* can also potentially be used as a model to study heme and heme regulation. Qiuxiang Ou conducted a secondary screen based on a whole genome RNAi screen in the PG using RNAi lines that resulted in L3 arrests or major delays when expressed in the PG to identify genes that disrupted heme biosynthesis (Ou, unpublished) (Danielsen, et al. 2016). If heme biosynthesis was disrupted, then presumably larvae would not have functional cytochrome P450 enzymes to synthesize ecdysone, leading to developmental defects. The red autofluorescence phenotype observed in the PG when heme biosynthesis was disrupted provided a fast and fairly reliable way to determine whether a gene product was involved in heme regulation in some way. Qiuxiang identified approximately 20 genes, that when knocked down with RNAi in the PG, resulted in reduced heme levels (Ou, unpublished). Many of these genes have no previously known roles in heme biosynthesis. This secondary screen is an example of one way *Drosophila* can be used to study heme regulation and identifying the heme sensor is a critical step to determine how heme is regulated in *Drosophila* and the PG. In addition, determining whether DHR51 is a heme sensor and that heme is DHR51's natural *in vivo* ligand could aid in understanding further DHR51 function, both in the development of neurons and controlling the circadian rhythm. NR2E3 is an orphan nuclear receptor, so if DHR51 binds heme *in vivo*, NR2E3 could possibly also bind heme, which would provide further insight into NR2E3 function.

3.2 Results

3.2.1 Loss-of-*DHR51* phenotypes

Before investigating DHR51's function as it relates to heme and heme regulation, it is first important to understand the loss-of-*DHR51* phenotype and the tools available to study DHR51 function. In general, loss-of-*DHR51*, either through mutations or *DHR51*-RNAi, resulted in developmental defects, mainly affecting the L3 and pupal stages. Loss-of-*DHR51* caused developmental defects such as delays during the L3 stage, L3 arrests, and pupal lethality. These types of developmental defects are classic phenotypes of ecdysone-deficient animals, as ecdysone is required to initiate developmental transitions at the proper time. Interestingly, disruption of the heme biosynthesis pathway can also cause developmental defects as heme is required for the function of cytochrome P450 enzymes that synthesize ecdysone, which can explain why *PPOX* mutant larvae were L3 arrested. This could mean that the developmental defects seen in loss-of-*DHR51* animals could be due to impaired ecdysone production either by reducing ecdysone production directly or indirectly by decreasing heme biosynthesis or both. Although developmental defects do not necessarily mean that the ecdysone titer had been reduced.

My main tools that I used to disrupt *DHR51* are the *DHR51*-RNAi lines (1) and (2). In order to confirm that these RNAi lines silence *DHR51*, I compared whole body knockdown of *DHR51* via RNAi with *DHR51* mutants. RNAi was expressed in whole body animals using a ubiquitous *GAL4* driver (*actin-GAL4* or *act>*). *act>DHR51*-RNAi (1) resulted in major pupal lethality and some shriveled larvae that died on the side of the vial (Table 3-1). *act>DHR51*-RNAi (2) also resulted in pupal lethality, but the phenotype was less severe and some adults were observed, although the adults seemed to die soon after eclosing. This suggested that whole

body *DHR51*-RNAi caused developmental defects. These phenotypes, especially the phenotype caused by *phm>DHR51*-RNAi (2), are similar to *DHR51* mutant phenotypes. However, the *DHR51* mutant phenotypes are a little more complex, as will be explained.

The *DHR51* mutant alleles, unf^{Z0001} and unf^{XI} (*DHR51* is also known as *unfulfilled* [*unf*]), were sent by Dr. Steven Robinow. The mutant allele unf^{Z0001} is the result of a missense mutation that causes an amino acid substitution of a glycine residue in the first zinc finger domain of the DBD of DHR51 (Sung, et al. 2009). The equivalent mutation is also found in the human homolog, NR2E3, where a p.G56R mutation created a dominant negative protein that caused autosomal dominant retinitis pigmentosa (Escher, et al. 2009). unf^{Z0001} was reported to have 75% of animals unable to eclose (pupal lethality) and the adult flies that did eclose did not fulfill wing expansion (hence the name *unfulfilled*). unf^{Z0001} flies had fertility issues and could not be kept as a homozygous stock, but the fertility defect was not able to be rescued by expression of an *unf* transgene while the other mutant phenotypes could be rescued (Sung, et al. 2009). However, when I received the unf^{Z0001} flies, I did not notice any defects (pupal lethality, wings that did not expand, or sterility) and made a homozygous stock that kept for years (data not shown). I never confirmed the presence or absence of the missense mutation, so I could have received the wrong stock.

The unf^{XI} allele was made through homologous recombination and disrupted the 5' donor splice site on the boundary of intron 2, resulting in a premature stop codon. The stop codon occurred between the two zinc fingers of the DBD. unf^{XI} was reported to only have 44% of animals unable to eclose, 17% of adults with unexpanded wings, and 39% of flies were normal (Sung, et al. 2009). A slightly less severe fertility defect was also described for unf^{XI}, but again, the infertility was unable to be rescued by an *unf* transgene (Sung, et al. 2009). When I received

the *unf*^{XI} flies balanced over the balancer chromosome *CyO*, I never saw *unf*^{XI} adults. Only once the stock was rebalanced over *CyO GFP* were *unf*^{XI} adults observed. The *unf*^{XI} animals in the *unf*^{XI} / *CyO GFP* stock also seemed to have a similar or lesser degree of pupal lethality as was published. Another defect I noticed was that once *unf*^{XI} adults eclosed, they would frequently and quickly get stuck in the food, similar to what I observed in whole body *DHR51*-RNAi (2) larvae (Table 3-1). *unf* mutants were noted to be "poorly coordinated" (Sung, et al. 2009). Also, many *unf*^{XI} adults failed to fulfill wing expansion. I was able to confirm the presence of the *unf*^{XI} allele due to the creation of an XbaI restriction enzyme recognition site (data not shown). I only used the *unf*^{XI} allele when I needed a *DHR51* mutant because I confirmed the presence of the mutant allele and the mutant phenotype matched what was previously published. The *unf*^{XI} phenotype is remarkably similar to *act>DHR51*-RNAi which suggested that the *DHR51*-RNAi was targeting *DHR51*.

Based on the observed phenotypes of *unf*^{XI} either balanced with *CyO* or *CyO GFP*, *unf* mutant phenotypes appeared to be sensitive to background genetic factors or environmental influences. This was also noted when the *unf* mutant alleles were described, as differences in the severity of the *unf* mutant phenotype in two *unf*^{XI} / *Df(2R)2426* (a *DHR51* deficiency line) *Drosophila* populations were found when set up independently of each other (21.1% uneclosed adults compared to 3.6% uneclosed adults with the same genotype) (Sung, et al. 2009). A third *unf* mutant allele was published by Dr. Oren Schuldiner, Weizmann Institute of Science, *unf*^{LL04325}, which was a *piggyBac* insertion mutation that was inserted into the first intron of *DHR51*. *unf*^{LL04325} was identified as homozygous lethal and affected the morphology of the adult mushroom body, as did the previous two *unf* mutant alleles (Yaniv, et al. 2012). Upon receiving this stock, *unf*^{LL04325} larvae were homozygous viable and personal communications with Dr.

Schuldiner confirmed that *unf*^{LL04325} larvae were viable after crosses that removed a *GAL4* driver after the *GAL4* driver was initially added, despite that the *piggyBac* insertion in *DHR51* was still present. The original insertion of *unf*^{LL04325} before *GAL4* was added has unfortunately been lost. I did not observe any developmental defects in the *unf*^{LL04325} line. This provided further evidence that the *DHR51* mutants might be susceptible to background genetic factors.

In order to validate that DHR51 had a role within the PG, I disrupted DHR51 function with *DHR51*-RNAi using *phm22-GAL4*. Knocking down *DHR51* in the PG with *phm>DHR51*-RNAi (1) resulted in an L3 arrest of the larvae (Figure 3-2A). These larvae remained as L3 larvae, which continued to feed for weeks instead of wandering out of the food and beginning metamorphosis. The continuation of feeding likely explains their larger body size. Contrary to their larger size, their RGs were smaller compared to the control, which was also noted by Qiuxiang Ou (Figure 3-2B). While *phm>DHR51*-RNAi (2) did not result in an L3 arrest, it did cause a minor developmental delay into puparium formation by approximately 14 hours and resulted in larger larvae and pupae than the control (Figure 3-2A). Since *phm>DHR51*-RNAi (2) larvae are delayed, the larvae spent more time eating compared to their control counterparts, explaining the increase in body size, but *phm>DHR51*-RNAi (2) larvae do eventually begin wandering, which is why they are smaller compared to *phm>DHR51*-RNAi (1) larvae. When the RGs of *phm>DHR51*-RNAi (2) larvae were examined, the RGs were similar in size to control RGs (Figure 3-2B). The discrepancy in the aberrant developmental phenotype, L3 arrest compared to a minor developmental delay, and ring gland size in *phm>DHR51*-RNAi larvae could be due to one of the off-targets predicted to occur in the *DHR51*-RNAi (1) line. In support of this, each *DHR51*-RNAi line reduced *DHR51* expression to similar levels (Figure 3-2C). Since both *DHR51*-RNAi lines caused developmental defects when expressed in the PG, this

suggested that DHR51 had a developmental role within the PG. Due to one of the RNAi lines potentially having off-targets, I designed *DHR51* conditional CRISPR lines to disrupt *DHR51* to confirm the actual phenotype of loss-of-*DHR51* in the PG, independently of RNAi.

With the relatively recent advent of CRISPR and explosion of CRISPR techniques, I used Conditional CRISPR as a way to verify the PG *DHR51*-RNAi phenotypes, as well as the *DHR51* mutant phenotypes. Conditional CRISPR uses ubiquitously expressed gRNA against the gene of interest alongside tissue-specific *Cas9* expression (Xue, et al. 2014). Conditional CRISPR allows for creating tissue-specific mutations. Together with GenetiVision, we designed two gRNAs that target *DHR51* at the DNA sequence that corresponded to just before the first zinc finger and at the first zinc finger of the DBD. GenetiVision then cloned, injected, and screened for the flies with the 2xgRNA constructs. Three lines that ubiquitously expressed *DHR51* 2xgRNA (3m, 6m, and 12m) were received.

To first determine the phenotype of larvae expressing whole body *DHR51* 2xgRNA and to confirm the *DHR51* / *unf* mutant phenotypes, each *DHR51* 2xgRNA line was crossed to *act-Cas9*, which expressed *Cas9* throughout the body in larvae to mimic *act>DHR51*-RNAi and *DHR51* mutant animals. *act-Cas9>DHR51* 2xgRNA 6m and 12m behaved similarly in all experiments, so they will be collectively referred to as 6/12m. *act-Cas9>DHR51* 2xgRNA 6/12m were found to have an approximate day and a half delay in eclosion compared to control *act-Cas9>*w^{1118} larvae (Table 3-1). At least part of that delay occurred prior to puparium formation, but I have yet to quantify how long puparium formation was delayed in the 6/12m lines. Once *act-Cas9>DHR51* 2xgRNA adults eclosed, they quickly became stuck in the food at the bottom of the vial and had unexpanded wings, much like unf^{X1} mutant adults (Figure 3-3A). The few adults that did not get stuck in the food seemed to move very slowly, if at all and had tremor-like

symptoms. *act-Cas9>DHR51* 2xgRNA 3m resulted in a more severe phenotype, where eclosion was delayed by approximately 4 days, with the majority of the delay before puparium formation (Table 3-1). Once adults eclosed, they also got stuck in the food and had unexpanded wings, similar to the 6/12m lines (Figure 3-3A). In addition, *act-Cas9>DHR51* 2xgRNA 3m animals had ~20% pupal lethality. I did not test to determine whether *act-Cas9>DHR51* 2xgRNA adults had fertility defects like in unf^{Z0001} and unf^{XI} adults. The phenotypes observed in the *act-Cas9>DHR51* 2xgRNA lines closely matched what was observed in unf^{XI} mutants and *act>DHR51*-RNAi (2) larvae, although I had not timed unf^{XI} larval development to determine whether these larvae were delayed. The three *DHR51* 2xgRNA lines were able to reproduce the *DHR51* loss-of-function phenotypes when expressed in the whole body. The *DHR51* 2xgRNA 3m line resulted in a much more severe phenotype.

With the *DHR51* 2xgRNA lines, I attempted to validate the *phm>DHR51*-RNAi phenotypes. *Cas9* was specifically expressed in the PG through the use of *Spok-Cas9* (Huynh, et al. 2018). *Spok-Cas9>DHR51* 2xgRNA 3m caused a three and a half day developmental delay for eclosion (Table 3-1). *Spok-Cas9>DHR51* 2xgRNA 3m larvae were delayed by at least a day into puparium formation, but this delay needs to be more accurately quantified. The larvae that were delayed were larger compared to the controls, likely due to prolonged feeding, and produced larger pupae (Figure 3-3B). *Spok-Cas9>DHR51* 2xgRNA 3m larvae phenocopied the delay observed in *phm>DHR51*-RNAi (2) larvae, but was more severe, which indicated that *DHR51* 2xgRNA 3m could be more efficient at disrupting *DHR51* than *DHR51*-RNAi (2). Unfortunately, the *Spok-Cas9>DHR51* 2xgRNA 3m phenotype was not recapitulated in *Spok-Cas9>DHR51* 2xgRNA 6/12m flies, as the *Spok-Cas9>DHR51* 2xgRNA 6/12m flies did not have any observable defect, although there may have been a minor day, less than a half day, that

still needs to be accurately quantified (Table 3-1). This was unexpected as the *DHR51* 2xgRNA lines target the same *DHR51* sequence, were inserted into the same genomic location, and into embryos of the same fly strain. As observed in whole body expression of the *DHR51* 2xgRNA lines, the 3m line was more severe than the 6/12m lines, which suggested that the 3m line may somehow be more efficient at disrupting DHR51 function and producing a stronger loss-of-function phenotype. Neither *Spok-Cas9>DHR51* 2xgRNA lines phenocopied the L3 arrest observed in *phm>DHR51*-RNAi (1) larvae, which provided further support that the L3 arrest phenotype is likely caused by an off-target of the *DHR51*-RNAi (1) line. Together, the *DHR51* 2xgRNA lines were able to validate the *DHR51*-RNAi and unf^{XI} phenotypes when expressed in whole body larvae and *Spok-Cas9>DHR51* 2xgRNA 3m validated the *phm>DHR51*-RNAi (2) phenotype. Despite all the complexities with identifying the exact developmental phenotype of loss-of-*DHR51* animals, it remained clear that there was a developmental defect, which likely resulted in pupal lethality and/or developmental delays. Since the *DHR51* 2xgRNA conditional CRISPR lines were generated late into my program, no further experiments were completed with the conditional CRISPR lines. The majority of the experiments that will be described had used the *DHR51*-RNAi lines.

3.2.2 Determining whether heme is an *in vivo* ligand for DHR51

DHR51 was my primary candidate for a heme sensor in *Drosophila* due to DHR51's demonstrated capability to reversibly bind heme *in vitro* and that the vertebrate heme sensor is a nuclear receptor (de Rosny, et al. 2008; Wu, et al. 2009). To test whether heme binding *in vivo* regulates DHR51 activity, I used a heat shock-inducible DHR51 ligand trap fusion protein. The DHR51 fusion protein had the DBD of GAL4, which can regulate a *UAS-EGFP* reporter gene, combined with the LBD of DHR51 that could regulate the fusion protein's transcriptional

activity upon ligand binding (Palanker, et al. 2006). If heme is the ligand of DHR51, adjusting cellular heme levels should result in differential expression of the reporter gene. As a warning, I ultimately came to the conclusion that the DHR51 ligand trap system was either non-functional or DHR51 does not function as hypothesized, but I will discuss the experiments that led me to that conclusion. According to my hypothesis, DHR51 is activated when cellular heme levels are low; if DHR51 is an activator, the reporter gene would be expressed in a low heme background (such as in *PPOX* mutant larvae) and the reporter gene would not be expressed when cellular heme levels were normal.

I first tested whether the DHR51 ligand trap fusion protein was an activator under low cellular heme levels (Figure 3-1A). The *PPOX* mutation was used to decrease cellular heme levels. Brain-ring gland complexes (BRGs) from 10 day old arrested L3 larvae were dissected from *UAS-EGFP ; PPOX* larvae with and without the *DHR51* ligand trap transgene (larvae were L3 arrested due to the *PPOX* mutation). *EGFP* expression was measured with qPCR. *EGFP* expression was not induced when the *DHR51* ligand trap was expressed in a low heme background (Figure 3-4A). Since the DHR51 ligand trap fusion protein did not induce *EGFP* reporter gene expression in a low heme background, the DHR51 ligand trap fusion protein may not be an activator. However, if DHR51 acts as a heme sensor in the PG, the brain could partly obscure reporter gene expression in the PG. I repeated the above experiment using RGs from 10 day old L3 larvae. Once again, the DHR51 ligand trap fusion protein did not induce *EGFP* reporter gene expression in a low heme background in RGs. Curiously, there was an apparent 50% reduction in *EGFP* expression in RGs when the *DHR51* ligand trap was present compared to when the *DHR51* ligand trap was absent (Figure 3-4B). A reduction in *EGFP* expression was odd because in the absence of the ligand trap, *UAS-EGFP* should not be expressed. The

difference in *EGFP* expression between the two lines could be due to variable leaky expression of *UAS-EGFP* or that the DHR51 ligand trap fusion protein was acting as a repressor to reduce whatever leaky expression there was in the RG. However, when the RGs were examined for EGFP fluorescence, there was no apparent difference in EGFP fluorescence between RGs that had the *DHR51* ligand trap and those that did not when examined with a confocal microscope (data not shown). This data suggested that the DHR51 ligand trap fusion protein does not function as an activator under low cellular heme levels in the BRG or the RG. Palanker *et al*. 2006 also found that the DHR51 ligand trap fusion protein did not function as an activator under normal physiological conditions in the various tissues examined. Palanker *et al*. suspected that DHR51 could be a repressor due to homology to vertebrate NR2E3, which can function as a repressor (PNR – photoreceptor cell-specific nuclear receptor) (Chen, J., et al. 2005). However, NR2E3 can also function as an activator (Cheng, et al. 2004; Haider, et al. 2009). Since the DHR51 ligand trap fusion protein did not act as an activator, both in my experiment and Palanker *et al*.'s experiment, I attempted to test whether the DHR51 ligand trap fusion protein acted as a repressor.

In order to test whether the DHR51 ligand trap fusion protein acted as a repressor under low cellular heme levels, I expressed wild type *GAL4* via heat shock to induce *EGFP* expression (Figure 3-1B). Co-expression of GAL4 and the DHR51 ligand trap fusion protein would then compete to regulate *UAS-EGFP* in a *PPOX* mutant background, which would decrease *EGFP* expression compared to GAL4 alone without the DHR51 ligand trap fusion protein present if the DHR51 ligand trap fusion protein functioned as a repressor. Both the *DHR51* ligand trap and *GAL4* were expressed via heat shock. I dissected RGs from 9 day old arrested L3 *hs-GAL4, UAS-EGFP* ; *PPOX* larvae with and without the *DHR51* ligand trap. *EGFP* reporter gene expression

was reduced by about one third when the *DHR51* ligand trap was present in a *PPOX* mutant background with GAL4 compared to *EGFP* expression with GAL4 in a *PPOX* mutant background without the *DHR51* ligand trap (Figure 3-5A). However, a Student's t-test demonstrated that the difference was barely non-significant (P-value = 0.052). This seemed to suggest that the DHR51 ligand trap fusion protein could be acting as a repressor under low cellular heme levels. However, an alternative explanation was that the DHR51 ligand trap fusion protein was binding to the *UAS*-promoter of *EGFP*, but instead of repressing expression, the DHR51 ligand trap fusion protein could be inert with respect to *EGFP* and just physically block GAL4 binding.

To control for the DHR51 ligand trap fusion protein being inert on the *UAS* promoter, the same experiment was done as above, but a wild type background was included (absence of a *PPOX* mutation). If the DHR51 ligand trap fusion protein was inert and physically blocking GAL4 binding, the presence of the DHR51 ligand trap fusion protein should decrease *EGFP* expression regardless of cellular heme concentrations. If *EGFP* expression was only reduced when heme levels were low, that would argue that the DHR51 ligand trap fusion protein acts as a repressor when cellular heme levels are low. RGs were dissected from L3 larvae 30 hours after the L2/L3 molt to allow for a comparison between larvae with normal and low cellular heme levels. *EGFP* expression via *hs-GAL4* was not decreased by the DHR51 ligand trap fusion protein when heme levels were normal, which suggested that the DHR51 ligand trap fusion protein was not just physically blocking GAL4 binding to the *UAS* promoter. However, DHR51 ligand trap fusion protein repression of *EGFP* in a *PPOX* mutant background in RGs from 9 day old L3 larvae was not reproducible, as *EGFP* expression was unaffected by the DHR51 ligand trap fusion protein in a *PPOX* mutant background in RGs from L3 larvae 30 hours after the

L2/L3 molt (Figure 3-5B). This data did not demonstrate that the DHR51 ligand trap fusion protein acted as a repressor or that it significantly blocked GAL4 binding to the *UAS* promoter. Possible explanations for this are that the lines used lost the *PPOX* mutation, were set up incorrectly, the *DHR51* ligand trap was not being expressed, the DHR51 ligand trap fusion protein was non-functional, or heme may not be the ligand for DHR51.

Alas expression was tested via qPCR to determine whether the *PPOX* mutation was still present in RGs from L3 larvae 30 hrs after the L2/L3 molt that were used in the previous experiment. *Alas* expression was significantly induced in RGs that were expected to have the *PPOX* mutation (Figure 3-6A). *Alas* induction indicated that cellular heme levels were low in the RGs of *PPOX* mutant larvae, which confirmed that the lines I used still had the *PPOX* mutation. Next, I wanted to ensure that *EGFP* was being expressed when *hs-GAL4* was heat shocked. Although not a proper comparison, I compared the controls' relative *EGFP* expression, normalized to *Rp49*, between experiments that tested whether the DHR51 ligand trap fusion protein was an activator and was a repressor in RGs from 9 day old arrested L3 larvae (no *hs-GAL4* compared to *hs-GAL4* present). Comparing these two different experiments showed that *EGFP* expression was 120-fold higher when *hs-GAL4* was present, which suggested that *hs-GAL4* and *UAS-EGFP* are present and that *EGFP* was induced by *hs-GAL4* (data not shown). To confirm that the *DHR51* ligand trap transgene was present in the lines used, genomic DNA was amplified with PCR using a primer targeting *GAL4* and *DHR51*. The resulting PCR product was then sequenced. *DHR51* sequence of the ligand trap began at amino acid #344, relative to the DHR51 reference sequence, and ran for the remainder of the 582 amino acid protein (data not shown). This segment of the protein used for the DHR51 ligand trap spanned the suspected LBD that is from amino acids #398 to #417 (Sung, et al. 2009). The *DHR51* sequence in the DHR51

ligand trap did not result in any amino acid changes relative to Sung *et al*. 2009's *DHR51* sequence (data not shown). To ensure that the DHR51 ligand trap was expressed after heat shock, qPCR using primers targeting the DBD of *GAL4* demonstrated that the ligand trap was expressed following heat shock and a five-hour recovery period (Figure 3-6B). This is consistent with previous work that reported that GAL4-LBD ligand trap fusion proteins were detected via western blots following heat shock (Palanker, et al. 2006). My combined data suggested that the fly lines were made properly and the *DHR51* ligand trap was being expressed. Despite this, there seemed to be no consistent effect on *EGFP* reporter gene expression. At this point, it seemed like the DHR51 ligand trap fusion protein was either non-functional or heme was not a relevant *in vivo* ligand for the DHR51 ligand trap fusion protein. It would have been very difficult to differentiate between these two possibilities and ultimately, not a good use of time, so unfortunately, the *DHR51* ligand trap experiments were dropped. Since I could not use the DHR51 ligand trap to determine whether DHR51 could bind and be regulated by heme, I then sought to determine whether DHR51 regulated *Alas* expression based on cellular heme levels.

3.2.3 DHR51 may be required for *Alas* upregulation

My hypothesis was that when cellular heme levels are low, DHR51 is unbound by heme and induces *Alas* expression, either directly or indirectly and that when heme levels are replete, DHR51 is bound by heme and inactive with respect to *Alas*. To test whether DHR51 is necessary for *Alas* induction when heme levels are low, I knocked down *DHR51* via RNAi specifically in the PG in a low heme background. A *PPOX* mutant background was used to disrupt heme synthesis instead of another RNAi line to avoid potentially diluting GAL4 over two *UAS* promoters like in Qiuxiang Ou's experiment. If DHR51 acts as a heme sensor, a *PPOX*-deficient cell would be unable to detect that heme levels are low in the absence of DHR51, thus *Alas*

expression would not be induced. Without *Alas* induction, red autofluorescent heme precursors would not accumulate. Both *DHR51*-RNAi (1) and *DHR51*-RNAi (2) were used separately to knockdown *DHR51* to account for the possibility of off-target effects. *phm>DHR51*-RNAi was expressed in *PPOX* mutant larvae. RGs from 9 day old arrested L3 larvae were examined (larvae were L3 arrested due to the *PPOX* mutation). RGs were only dissected in 9 day old L3 larvae to allow sufficient time for the heme precursors to accumulate to observable levels. There was a noticeable decrease in the amount of red autofluorescence in the PG as a result of either *phm>DHR51*-RNAi (1) or (2) when expressed in a *PPOX* mutant background compared to a *PPOX*-deficient PG alone (Figure 3-7A). *phm>DHR51*-RNAi (1) in a *PPOX* mutant resulted in a stronger suppression of red autofluorescence in the PG compared to *phm>DHR51*-RNAi (2) in a *PPOX* mutant background, which indicated that there were likely fewer heme precursors that had accumulated in *phm>DHR51*-RNAi (1) PGs. Even though *phm>DHR51*-RNAi (2) in a *PPOX* background resulted in reduced red autofluorescence compared to *PPOX* alone, all RGs examined still had red autofluorescence. *phm>DHR51*-RNAi (1) in a *PPOX* mutant background resulted in some RGs that had faint red autofluorescence (deemed "red" RGs), while others had no detectable red autofluorescence (deemed "white" RGs). Red and white RGs from *phm>DHR51*-RNAi (1) ; *PPOX* larvae were observed in an approximate 1:1 ratio. The reduction in red autofluorescence in the PG when either *DHR51*-RNAi line was expressed in the PG of *PPOX* mutant larvae suggested that heme precursors accumulated to a lesser extent compared to *PPOX*-deficient RGs alone and that *Alas* expression had likely been attenuated. This provided evidence that the accumulation of red autofluorescent heme precursors was dependent on DHR51.

To determine whether *Alas* expression had actually been attenuated in *PPOX*-deficient RGs that expressed *phm>DHR51*-RNAi, I measured *Alas* expression with qPCR in RGs dissected from 9 day old arrested L3 larvae that were *PPOX* mutants or *PPOX* mutants with either *DHR51*-RNAi line expressed in the PG. "Red" and "white" RGs were collected separately in *phm>DHR51*-RNAi (1) ; *PPOX* animals. For a baseline of *Alas* expression, *phm>DHR51*-RNAi (1) RGs were used since wild type larvae already formed pupae when the animals were 9 days old, as *phm>DHR51*-RNAi (1) larvae were L3 arrested. Initially, it was thought that *phm>DHR51*-RNAi did not affect *Alas* expression when heme levels were normal, but later experiments demonstrated that there might be slight induction of *Alas* expression (Figure 3-7C and Figure 3-13A) (*Alas* expression in *DHR51*-RNAi RGs will be discussed in more detail at the end of Chapter 3.2.4). When *DHR51* was knocked down in a *PPOX* mutant background, *Alas* induction was significantly attenuated in RGs compared to *PPOX*-deficient RGs alone (Figure 3-7B). "White" RGs tended to have slightly lower *Alas* expression compared to "red" RGs, but the difference was not statistically significant. While *phm>DHR51*-RNAi (2) in *PPOX* mutant larvae all had faint red RGs and mild to moderate *Alas* induction, however, *Alas* induction was reduced compared to *Alas* induction in *PPOX*-deficient RGs alone. Interestingly, the degree of heme precursor accumulation seemed to be positively correlated with *Alas* induction in a linear fashion. I was able to successfully replicate the results from the above experiment using independently collected samples (data not shown).

I also tested whether DHR51 was necessary for *Alas* induction when heme levels were low in younger L3 larvae, as opposed to 9 day old arrested larvae. RGs were collected from *PPOX* mutant larvae, w^{1118} (control) larvae, *phm>DHR51*-RNAi (1), and *phm>DHR51*-RNAi (1) ; *PPOX* larvae 44 hours after the L2/L3 molt. Collecting larvae at this time allowed for comparing

Alas expression to proper control RGs and the RGs are not from larvae that had been long arrested. Once again, *phm>DHR51*-RNAi (1) attenuated *Alas* induction in RGs from *PPOX* mutant larvae (Figure 3-7C). Unlike the previous experiment using RGs from 9 day old larvae, *Alas* expression was not brought down to basal levels in RGs from *phm>DHR51*-RNAi (1) ; *PPOX* larvae. This could be due to the developmental time when RGs were collected (larvae had not been arrested for several days prior to dissection), because "red" and "white" RGs were not separated because the heme precursors did not have sufficient time to accumulate to observable levels at 44 hours after the L2/L3 molt, or because *Alas* expression levels were compared to *Alas* expression in *phm>w*^{1118} RGs instead of *phm>DHR51*-RNAi (1) RGs. I will also note that *Alas* expression is 2-fold increased in *phm>DHR51*-RNAi (1) RGs compared to *phm>w*^{1118} control RGs. See the end of Chapter 3.2.4 and Figure 3-13A for further details. These experiments demonstrated that loss-of-*DHR51* function attenuated *Alas* induction in *PPOX*-deficient RGs, which suggested *Alas* induction when cellular heme levels are low was dependent on DHR51.

To confirm whether the attenuation of *Alas* upregulation in *PPOX*-deficient RGs was due to loss-of-*DHR51*, I attempted to validate the experiment using a *DHR51* mutant by combining *unf*^{XI}, a *DHR51* mutant allele, with the *PPOX* mutant allele. The *unf*^{XI} allele disrupts a splicing site and is predicted to truncate the DHR51 protein between the two zinc fingers of the DBD (Sung, et al. 2009). *unf*^{XI} ; *PPOX* mutant larvae still displayed red autofluorescent RGs and *Alas* expression was highly induced, similar to *PPOX*-deficient RGs alone (Figure 3-8AB). Note: the *Alas* qPCR on *unf*^{XI} ; *PPOX* RGs was added onto another qPCR, so it was done with improper controls that expressed *GAL4*. Nevertheless, *unf*^{XI} ; *PPOX* RGs were still autofluorescent and *Alas* expression was high. It is unlikely that *Alas* induction when cellular heme levels were low was attenuated by the *unf*^{XI} mutation. However, *unf*^{XI} does not have a clearly defined phenotype

and may be prone to genetic background or environmental effects (Sung, et al. 2009). The UNF^{XI} protein is expected to still retain the first zinc finger of the DBD, so UNF^{XI} could potentially be capable of binding to DNA. unf^{XI} is not a null allele and if anything, unf^{XI} may actually be a gain-of-function mutation (Sung, et al. 2009; Yaniv, et al. 2012). Sung *et al*. also showed that unf^{XI} adults expressed four novel *DHR51* transcripts due to inappropriate splicing, which have yet to be characterized.

To circumvent the uncertainties I had with the unf^{XI} mutation, I planned to use *DHR51*-RNAi (2) (which had a less severe phenotype compared to *DHR51*-RNAi (1)) in combination with *Df(2R)ED2426*, a deficiency that covers *DHR51*, to produce a stronger knockdown of *DHR51*, which would hopefully cause a greater attenuation of *Alas* induction in a *PPOX* mutant background. Using the *DHR51* deficiency line to enhance the *DHR51*-RNAi (2) phenotype was successfully done in a previous study examining neuronal defects due to loss-of-*DHR51* (Lin, et al. 2009). However, when I combined *Df(2R)ED2426* with *phm>DHR51*-RNAi (2) in *PPOX* mutant larvae, *Alas* expression was still highly induced in RGs from 9 day old arrested larvae, similar to *Alas* expression in *phm>DHR51*-RNAi (2) ; *PPOX* RGs (Figure 3-8C). The combination of the *DHR51* deficiency with *phm>DHR51*-RNAi (2) seemed to have no effect on *Alas* induction. Unexpectedly, *Alas* expression was similar between *PPOX*-deficient RGs and *phm>DHR51*-RNAi (2) ; *PPOX* RGs; previously I observed lower *Alas* expression in *phm>DHR51*-RNAi (2) ; *PPOX* RGs than in *PPOX* RGs, as seen in Figure 3-7B. One difference could be a slight difference in the *PPOX* allele severity between the regular *PPOX* mutant line and the *phm22-GAL4 PPOX* line used when I tested the effect on the *DHR51* deficiency (one chromosome has both *phm22-GAL4* and the *PPOX* mutant allele, made through a series of crosses and recombination), as *Alas* expression was approximately 25-30-fold upregulated

compared to only 15-fold, respectively. Another possibility is that *phm22-GAL4* could somehow be influencing *Alas* expression. These experiments may need to be repeated to resolve the discrepancy in *Alas* expression in *PPOX*-deficient RGs with and without *phm22-GAL4*. It may also be better to test *Alas* expression in 44 hour post L2/L3 molt larvae as they are likely more "normal" compared to old L3 larvae that have been arrested for several days. Together, the unf^{XI} mutant did not attenuate *Alas* induction in low cellular heme conditions and the *DHR51* deficiency, *Df(2R)ED2426*, did not aid in further attenuating *Alas* induction in concert with *phm>DHR51*-RNAi (2) in a *PPOX* mutant background. This provided evidence against the hypothesis that DHR51 upregulates *Alas* when cellular heme levels are low.

As will be explained in Chapter 4, loss-of-*DHR51* reduced the expression of the ecdysone biosynthetic genes, many of whose gene products are cytochrome P450 enzymes that require heme as a cofactor to function. One possible explanation for the attenuation of *Alas* upregulation in low cellular heme conditions was that when *DHR51* was knocked down, there was a reduction in ecdysone biosynthetic gene expression, which lowered the demand for cellular heme. This could reduce *Alas* upregulation because heme was not being used up in large quantities for the ecdysteroidogenic cytochrome P450 enzymes. To test this, I knocked down *torso* (*tor*) expression in the PG in *PPOX* mutant larvae. Torso is the receptor for brain-derived prothoracicotropic hormone (PTTH), which initiates metamorphosis by signaling through the Ras/Raf/ERK pathway to stimulate ecdysone biosynthetic gene expression (McBrayer, et al. 2007; Rewitz, et al. 2009). RGs were dissected from larvae 44 hours after the L2/L3 molt, about the time when PTTH is released to the PG. *Alas* expression was compared between *phm>tor*-RNAi ; *PPOX* RGs and *PPOX* RGs alone. *phm>tor*-RNAi in *PPOX*-deficient RGs resulted in a mild attenuation of *Alas* induction compared to *PPOX*-deficient RGs alone, similar to that seen

with *phm>DHR51*-RNAi (2) ; *PPOX* RGs from 9 day old L3 larvae (Figure 3-9A). This result was replicated by Qiuxiang Ou in a similar experiment. These data suggested that at least part of the effect of *DHR51*-RNAi could be due to reduced demand for heme because of a reduction of ecdysone biosynthetic enzymes. However, because *tor* is an upstream receptor, there could also be numerous unknown and unintended downstream consequences that could attenuate *Alas* expression in a low heme background.

To further test how *Alas* might be regulated under low heme conditions, I sought to test Spargel (the *Drosophila* homolog of PGC-1α) by knocking down *spargel* (*srl*) in a *PPOX* mutant background. In mammals, PGC-1α is a co-activator that upregulates *Alas* when heme levels are low, and when heme levels are normal, PGC-1α is repressed by the mammalian heme sensor, Rev-erbα (Wu, et al. 2009). *phm*>s*rl*-RNAi in *PPOX* RGs resulted in a significant attenuation of *Alas* upregulation compared to *PPOX* RGs alone (Figure 3-9B). *Alas* was still upregulated relative to wild type *Alas* expression, but *Alas* expression in *phm*>s*rl*-RNAi ; *PPOX* RGs was less compared to *PPOX* RGs alone. This suggests that Spargel may regulate *Alas* similar to how PGC-1α regulates *Alas1* in mammals. At this time, I cannot say whether Spargel's action on *Alas* is dependent on DHR51, as PGC-1α is dependent on Rev-erbα.

3.2.4 DHR51 RNA-Seq and other heme-deficient ring glands

The previous section provided some evidence that DHR51 may function as a heme sensor and that DHR51 may upregulate *Alas* when cellular heme levels are low. If DHR51 is indeed a heme sensor, then I suspect disrupting DHR51 function should impact cellular heme levels and heme homeostasis. There are three possibilities if DHR51 function is lost: either heme levels increase, decrease, or remain constant. The PG has a very high demand for heme due to the very high levels of cytochrome P450 enzymes for ecdysone production and it seemed most likely that

heme levels would begin to decrease if the heme sensor was lost. Cytochrome P450s could use up free heme and heme levels would not adequately be replenished without a heme sensor. Two methods were used to determine whether loss-of-*DHR51* disrupted heme homeostasis. One method to test whether loss-of-*DHR51* reduced heme levels was with RNA-Seq, where the effect on transcription between *DHR51*-RNAi RGs and RGs with low cellular heme levels, such as RGs expressing *FeCH*-RNAi (FeCH, Ferrochelatase, is the last enzyme in the heme biosynthesis pathway), can be compared. Another method to determine whether loss-of-*DHR51* reduced cellular heme levels was to measures heme levels directly (see Chapter 3.2.5).

Qiuxiang Ou conducted RNA-Seq on RG samples collected from multiple *phm*>RNAi lines 44 hours past the L2/L3 molt that had heme biosynthesis disrupted in the PG. RNAi lines against *Nos* (*Nitric oxide synthase*), *spz5* (*spatzle5*), *FeCH*, and *DHR51* (*DHR51*-RNAi (1)) were compared to the control, *phm*>w^{1118}. *phm*> *nos*-, *spz5-,* and *FeCH*-RNAi all result in a low heme phenotype with red autofluorescent RGs and high *Alas* expression. My primary focus was to analyze the *phm*>*DHR51*-RNAi (1) RNA-Seq data for effects related to heme biosynthesis and ecdysone production. This chapter will focus on how the effects of *DHR51*-RNAi compare to the effects of disrupting heme biosynthesis. How *DHR51*-RNAi affects ecdysone production will be examined in Chapter 4. I aimed to compare the *phm*>*DHR51*-RNAi (1) RNA-Seq data to *phm*>*FeCH*-RNAi to determine whether both RNAi lines had a similar effect on PG cells. Before comparing *phm*>*DHR51*-RNAi (1) to *phm*>*FeCH*-RNAi, I sought to validate the *phm*>*DHR51*-RNAi (1) RNA-Seq results by testing a small handful of *DHR51*-RNAi differentially expressed genes with qPCR in both *DHR51*-RNAi lines and unf^{XI} mutants. Brain-ring gland complexes were dissected from *phm*>*DHR51*-RNAi (1), *phm*>*DHR51*-RNAi (2), unf^{XI} mutant larvae, and the appropriate controls (*phm*>w^{1118} or w^{1118}) 44 hours post L2/L3 molt.

In general, the genes that were upregulated in the RNA-Seq by *DHR51*-RNAi (1) were also upregulated in the qPCR with the other loss-of-*DHR51* lines (Figure 3-10AB). Although not all the genes were significantly upregulated, they were at least trending towards being upregulated. However, the degree of upregulation varied between the RNA-Seq and qPCR, especially for *Nplp4*, which was upregulated 64 fold in the RNA-Seq and only 3 fold in the qPCR. The difference in expression levels could be due to measuring RGs in the RNA-Seq and BRGs in the qPCR. *Alas* only showed very mild effects in the loss-of-*DHR51* lines, consistent with previous qPCRs.

Genes that were downregulated in the *phm>DHR51*-RNAi (1) RNA-Seq data were also downregulated in qPCR of both *DHR51*-RNAi lines and unf^{XI} BRGs, but not quite to the same extent as in the RNA-Seq (Figure 3-10CD). The main exception was *esg*, however, *esg* expression in the RNA-Seq was not considered statistically significant despite the low expression (P-value = 0.18). Differences between the qPCR and RNA-Seq results could be due to measuring BRGs as opposed to RGs. As well, some qPCR samples had high variation, giving less reliable measurements. Both *ana* and *esg* were selected for qPCR validation because their transcripts were enriched in the RG greater than 10-fold compared to the whole body to help account for the extra brain tissue (Ou, et al. 2016). Overall, the qPCR data tended to reproduce the RNA-Seq results in multiple loss-of-*DHR51* lines, but the degree of gene expression differed considerably. This suggested that the RNA-Seq data is reliable to an extent, but genes of interest should be validated with both *DHR51*-RNAi lines with qPCR.

After validating the *phm>DHR51*-RNAi (1) RNA-Seq data, I compared genes that were misregulated between *phm>DHR51*-RNAi (1) and *phm>FeCH*-RNAi RGs to determine whether RGs responded to each of these RNAi lines in a similar manner. I selected genes that were up- or

downregulated more than 3-fold compared to controls and that had an RPKM (reads per kilobase of transcript per million mapped reads) greater than 0.5 in the RNAi line of interest. With these criteria, 273 genes were downregulated and 167 genes were upregulated in RGs dissected from *phm>DHR51*-RNAi (1) L3 larvae (a total of 440 misregulated genes). 428 genes were downregulated and 139 genes were upregulated in RGs as a result of *phm>FeCH*-RNAi (a total of 567 misregulated genes). Gene ontology enrichment analysis of *phm>DHR51*-RNAi (1) RGs did not return anything of interest except for a small grouping of downregulated genes involved in larval development / ecdysone production, but this will be discussed more in Chapter 4. After identifying differentially expressed genes, I compared the genes that were upregulated as a result of *phm>DHR51*-RNAi (1) and *phm>FeCH*-RNAi and the genes that were downregulated in response to both RNAi lines. Between the 440 misregulated genes in *phm>DHR51*-RNAi (1) RGs and 567 misregulated genes in *phm>FeCH*-RNAi RGs, 186 genes were misregulated similarly (46 upregulated genes and 140 downregulated genes in common) (Figure 3-11A). This overlap of 186 genes is highly statistically significant (P-value = 0), which suggested that the PG cells had a similar transcriptional response to both *phm>DHR51*-RNAi (1) and *phm>FeCH*-RNAi. Given the size of the original data set (15771 genes), if *DHR51*-RNAi (1) and *FeCH*-RNAi had completely unrelated effects in the cell, it was expected that approximately 16 genes would overlap in response to both of these RNAi lines due to random chance. A 186 gene overlap is a near 12-fold enrichment over random chance. Even if you were to consider that not all 15771 genes would be expressed in the RG and assume a total of 5000 genes instead, the result was still highly significant, as you would expect approximately 50 genes to overlap due to chance (a 3.7-fold enrichment, P-value = 7.4×10^{-102}, according to a Chi-squared test). This indicated that the cellular response to *phm>DHR51*-RNAi (1) and *phm>FeCH*-RNAi in the RG

was similar, and since *FeCH*-RNAi disrupts heme biosynthesis and results in low cellular heme levels, my analysis suggested that disrupting DHR51 could also reduce cellular heme levels, similar to *FeCH*-RNAi.

Due to the high overlap in gene response to *phm>DHR51*-RNAi (1) and *phm>FeCH*-RNAi, I used another analysis method to determine how similar the cells' response to each of these RNAi lines in the RG were. I used the Pearson correlation and the Spearman's rank correlation to determine how well gene expression from the *phm>DHR51*-RNAi (1) and *phm>FeCH*-RNAi RNA-Seq data sets correlated with each other. A positive correlation between *phm>DHR51*-RNAi (1) and *phm>FeCH*-RNAi would indicate that the RNAi lines had a similar effect on cells in RGs. Both Pearson and Spearman's rank correlations assign a number between -1 and +1. -1 is a perfect negative correlation, +1 is a perfect positive correlation, and 0 is no correlation between two data sets. The Pearson correlation used the expression data in the RNA-Seq data set, which compared the fold changes in gene expression between each of the RNAi lines; whereas the Spearman's rank correlation ranks the data set from 1 to *n* number of genes from highest to lowest fold change, then compares the rankings between the two data sets. In addition to *phm>DHR51*-RNAi (1) and *phm>FeCH*-RNAi, I conducted RNA-Seq on RGs dissected from *PPOX* mutant L3 larvae 44 hours post L2/L3 molt. RGs from *PPOX* mutant larvae were included to determine the extent of the effect of the GAL4 and RNAi in general on gene expression. Genes with an RPKM of greater than 0.1 were used in the correlation analysis to include most genes that may be expressed in the RG (over 7000 genes were obtained).

Firstly, the genes were compared for their correlation between the *phm>FeCH*-RNAi and *PPOX* mutant RG samples. The Pearson correlation was calculated to be 0.358, which indicated a positive, weak to moderate correlation between genes in *phm>FeCH*-RNAi and *PPOX* mutant

RGs. However, the Spearman's rank correlation was 0.554, which indicated a moderate positive correlation (Figure 3-11B). If the loss of either FeCH or PPOX only resulted in a defect of heme production, I would have expected a high correlation when comparing the *phm>FeCH*-RNAi and *PPOX* mutant RNA-Seq data sets. A low to moderate positive correlation between *phm>FeCH*-RNAi and the *PPOX* mutant could mean that there is an effect from either GAL4 or the RNAi that reduced the correlation between these two samples. Possible explanations for the difference between Pearson and Spearman's rank correlation will be discussed in the next paragraph. When *phm>FeCH*-RNAi was compared to *phm>DHR51*-RNAi (1), the Pearson correlation was calculated to be 0.494 and the Spearman's rank correlation was calculated to be 0.558, which indicated a moderate positive correlation between these two RNAi lines (Figure 3-11C). This suggested that the RG *phm>FeCH*-RNAi gene set was slightly more similar to *phm>DHR51*-RNAi (1) than to *PPOX*. Again, this may point to a common effect from either expressing *GAL4* or RNAi in general. When the *phm>DHR51*-RNAi (1) gene data set was compared to the *PPOX* mutant gene data set, the Pearson correlation was 0.291 and the Spearman's rank correlation was 0.305, indicating a weak to moderate correlation (Figure 3-11D). This weak to moderate correlation suggested that the cell had a mildly similar transcriptional response to both *phm>DHR51*-RNAi (1) and *PPOX*, which suggested that loss-of-*DHR51* could reduce cellular heme levels (the correlation between *phm>DHR51*-RNAi (1) and *PPOX* and *phm>FeCH*-RNAi and *PPOX* were only slightly different). All correlation values were found to be highly significant with P-values nearing 0 using a regression analysis. These analyses support the hypothesis that loss-of-*DHR51* could result in low cellular heme levels, possibly due to disrupted heme homeostasis in the PG and that PG cells responded in a similar manner when *DHR51* was knocked down as when heme biosynthesis was disrupted.

There were some unexpected results within the Pearson and Spearman's rank correlation analyses. First, the correlation between *PPOX* and *FeCH*-RNAi resulted in a lower correlation than expected, potentially caused by an effect from *GAL4* expression or RNAi when comparing an RNAi RG to a mutant RG. Also, the *PPOX* RNA-Seq and RNAi RNA-Seq were not done together and were done by two different people. To look at the latter issue, I compared the RPKM of genes from the control samples from both RNA-Seq experiment (w^{1118} compared to *phm*>w^{1118} RGs) to see how well the controls correlated. The comparison between w^{1118} and *phm*>w^{1118} RGs resulted in a Pearson correlation of 0.980 and a Spearman's rank correlation of 0.877, which indicated a high correlation between these two wild type samples (Figure 3-11E). Based on the correlation between the two control samples, there may only be a fairly mild effect of comparing two different RNA-Seq experiments that used RNAi versus mutants.

I decided to look closer at the transcription of the heme biosynthetic genes due to the moderate positive correlation between *phm*>*DHR51*-RNAi (1) and *phm*>*FeCH*-RNAi because other heme biosynthetic genes were upregulated in response to low cellular heme levels besides *Alas*. First, to determine which heme biosynthetic genes and the extent that these genes were upregulated in response to low cellular heme levels in the RG, I examined the RNA-Seq data for all the heme biosynthetic genes in all the lines that caused low heme phenotypes (*Nos*-, *spz5*-, *FeCH*-RNAi, and *PPOX* mutants). The RNA-Seq data showed that four genes in the heme pathway were upregulated to some extent in response to low cellular heme: *Alas* (up 27.3-fold on average), *Pbgs* (up 11.4-fold on average), *l(3)02640* (up 5.4-fold on average), and *FeCH* (up 3.4-fold on average) (Figure 3-12A). These four genes are upregulated in all the heme-deficient RGs, making up a general response to low cellular heme levels. If *DHR51*-RNAi disrupts heme homeostasis and causes lower cellular heme levels, *Pbgs*, *l(3)02640*, and *FeCH* should be

upregulated. *Alas* expression should be unaffected as *Alas* upregulation in response to low cellular heme levels was dependent on DHR51 to some extent. The RNA-Seq showed that *phm>DHR51*-RNAi (1) resulted in *Alas* expression of 1.1-fold compared to the control, *Pbgs* expression increased by 3.0-fold, *l(3)02640* expression increased by 3.3-fold, and *FeCH* expression increased by 2.4-fold (Figure 3-12A). *phm>DHR51*-RNAi (1) also increased the expression of *Pbgs*, *l(3)02640*, and *FeCH*, similar to a general low cellular heme level response, with the exception of *Alas* and that *Pbgs* was not as highly induced in *phm>DHR51*-RNAi (1) RGs compared to other heme-deficient RGs. No change in *Alas* expression was in line with my hypothesis that DHR51 acts as a heme sensor that is required for *Alas* upregulation when cellular heme levels are low and that loss-of-*DHR51* could disrupt heme homeostasis, causing low heme levels. Without DHR51, cells could have low heme levels and be unable to upregulate *Alas* since *Alas* upregulation was dependent on DHR51.

Expression of the heme biosynthetic genes were validated with qPCR in RGs from *phm>DHR51*-RNAi (1) and (2) larvae 68 hours after the L2/L3 molt. *phm>PPOX*-RNAi RGs were used as a positive control. Both *DHR51*-RNAi lines resulted in a significant upregulation of *Pbgs*, *l(3)02640*, and *FeCH* in the RG, similarly to *phm>PPOX*-RNAi in the RG, although the upregulation was to a slightly lesser extent (Figure 3-12B). *Pbgs* expression was not increased as much compared to the other RNAi lines that resulted in low heme phenotypes, possibly because loss-of-*DHR51* does not cause as low of heme levels. Another possible explanation was that DHR51 might also partly regulate *Pbgs* since *Pbgs* had the second highest upregulation in response to low cellular heme levels, however, *Pbgs* was still significantly upregulated in *phm>DHR51*-RNAi RGs. This data together suggested that loss-of-*DHR51* function may decrease cellular heme levels. Upregulation of the heme biosynthetic genes in *DHR51*-depleted

RGs, except for *Alas*, supported my hypothesis that loss of a potential heme sensor in a tissue that has a high demand for heme could disrupt heme homeostasis and result in reduced heme levels due to the cell's inability to upregulate *Alas* in response to lowering cellular heme levels.

One unexpected result from the qPCR of upregulated heme biosynthetic genes was a significant upregulation of *Alas* in *phm>DHR51*-RNAi (1) RGs, and nearly significant in *phm>DHR51*-RNAi (2) RGs (P-value = 0.07). One question that has not yet been answered is "Does loss-of-*DHR51* affect *Alas* expression when cellular heme conditions are normal?" The answer to that question is not straightforward. RNA-Seq data suggested that *Alas* expression was unaffected in *phm>DHR51*-RNAi (1) RGs (1.14-fold change, P-value = 0.82), however, other qPCR experiments suggested there may be mild *Alas* upregulation when *DHR51* was knocked down. I compiled *Alas* expression data from my various experiments and the most consistent response was that loss-of-*DHR51* resulted in a significant 2-fold upregulation of *Alas* expression in RGs (Figure 3-13A). This suggested that DHR51 may regulate *Alas* in some way. An intriguing idea was that if *DHR51*-RNAi caused low cellular heme levels, remaining DHR51 protein could upregulate *Alas* to a small degree. With only a minor depletion of heme and limited DHR51 protein, only a minimal effect on *Alas* expression would be expected. Other evidence that suggested that DHR51 regulates *Alas* was that overexpression of *DHR51* cDNA in the RG reduced *Alas* expression in larvae harboring the *DHR51* transgene. *UAS-DHR51* cDNA (*F1*), obtained from Dr. Steven Robinow (Sung, et al. 2009), was expressed with the ring gland *GAL4* driver, *P0206*. Brain-ring glands were dissected 24 hours after the L2/L3 molt and *Alas* expression was measured with qPCR. Overexpression of *DHR51* in the RG resulted in *Alas* expression at 0.6 times that of the control (Figure 3-13B). *DHR51* overexpression seemed to reduce *Alas* expression, but it was difficult to explain how. Overexpression of *DHR51* could

somehow result in increased cellular heme levels which would repress *Alas* or if DHR51 acts as a heme sensor, DHR51 may be mimicking high cellular heme levels with more DHR51 protein available. If an abundance of DHR51 is present in the cell and bound by heme, heme-bound DHR51 could signal to the cell that heme levels are sufficient or higher than normal, resulting in *Alas* suppression. Another possibility is that DHR51 is actually a repressor of *Alas* when bound by heme, instead of being inactive as initially thought. Further experiments will need to be done to differentiate between these two possibilities.

3.2.5 *DHR51*-RNAi reduced heme levels in larvae

The second method to determine what happens if a heme sensor is lost was to measure heme levels directly (the first method was to compare the transcriptional response between the loss of DHR51, a potential heme sensor, to RNAi lines that caused low heme phenotypes). Measuring heme levels could determine whether loss-of-*DHR51* disrupted heme homeostasis, resulting in reduced cellular heme levels. I attempted to directly measure heme levels in *DHR51*-RNAi larvae to determine whether disrupting a potential heme sensor decreased heme levels as suggested by qPCR of heme biosynthetic genes. There are a variety of heme measurement methods, however, heme is not typically measured in *Drosophila*. I modified a protocol that used high concentrations of oxalic acid (2 M) combined with boiling temperatures to strip iron from heme, which created an autofluorescent porphyrin ring. The autofluorescence from the porphyrin ring can then be measured (Morrison. 1965). Iron is only removed from heme with oxalic acid and heat (the experimental condition), oxalic acid alone cannot remove iron (the background autofluorescence condition). This approach measures total heme (free heme and protein-bound heme). Before heme could be measured in *DHR51*-RNAi larvae, I needed to establish a working protocol and analysis. Firstly, I tested the emission spectrum of hemin (hemin is similar to heme,

but has ferric iron that is bound by chloride). Hemin was excited at 400 nm and a major emission peak at 600 nm and a minor peak at 650-660 nm were observed (Figure 3-14A). This is in line with what was expected. Porphyrins have a major emission peak at 608 nm, which is stronger, but less specific to just porphyrins, and a minor emission peak at 662, which is weaker, but more specific to porphyrins (Sinclair, et al. 2001).

My ultimate goal was to measure heme in RGs that expressed *phm>DHR51*-RNAi, however, I needed to validate my heme measurement protocol first. I initially measured heme in whole body larvae as a proof of principle and then moved to brain-ring glands (BRGs). If heme could be measured in BRGs, I would then attempt to measure heme in RGs. However, I was never able to quantify heme in RGs for reasons that will be discussed later. To ensure my method and analysis for heme measurements worked properly, I measured heme in 5 day old L3 *PPOX* mutant whole body larvae and compared the heme levels to 5 day old L3 w^{1118} whole body larvae, as a control. Heme was quantified two different ways. Each larval sample was split into two; one sample would be treated with oxalic acid and heat (experimental condition), while the other would only be treated with oxalic acid (background condition). First, the fluorescence ratio was calculated from the autofluorescence given off by the porphyrin rings from the experimental samples (oxalic acid and heat) compared to the background autofluorescence of the samples (oxalic acid and no heat). I will refer to the ratio between the autofluorescence observed in the experimental samples to the autofluorescence observed in the background samples as the "fluorescence ratio". Control w^{1118} larvae were expected to have a high fluorescence ratio due to high autofluorescence in the experimental samples since total heme was converted into porphyrin rings and low background autofluorescence (heme precursors did not accumulate). *PPOX* larvae were expected to have a low fluorescence ratio due to high background autofluorescence due to

accumulated heme precursors and high autofluorescence in experimental samples (a small increase in autofluorescence due to low amounts of heme converted to porphyrin rings plus the accumulated heme precursors). When heme was measured in *PPOX* whole body larvae, the fluorescence ratio was calculated to be 2.5, compared to the control w^{1118} whole body larvae that had a fluorescence ratio of 50.0 when measured at each wavelength (Figure 3-14B). This difference was statistically significant (P-value = 8.15×10^{-6} when measured at 608 nm and 5.58×10^{-4} when measured at 662 nm). Obtaining fluorescence ratios as predicted supported the use of the fluorescence ratio to distinguish between samples that had low and normal levels of heme in whole body larvae, although, the difference in heme concentrations is not quantifiable.

The more typical analysis to quantify heme that is normally done in the literature is to measure heme levels by comparing the autofluorescence in the samples to a hemin standard curve to calculate the concentration of heme in each sample and normalize the concentration of heme to the protein content of the sample. When the concentration of heme in each sample was calculated relative to a hemin standard curve (Figure 3-14CD) and normalized to the amount of protein, *PPOX* whole body larvae appeared to have as much heme as w^{1118} control larvae (Figure 3-14E). This unexpected result was also seen when heme levels were measured in 8 day old, arrested whole body *PPOX* L3 larvae, which had accumulated higher levels of heme precursors, compared to 5 day old w^{1118} larvae. The 8 day old *PPOX* larvae had as much or possibly more heme than 5 day old w^{1118} whole body larvae (data not shown). *PPOX* larvae could appear to have more heme than w^{1118} larvae possibly due to the fluorescence not accurately being subtracted from the blank wells or the no heat controls (background samples). There could also be an issue comparing *PPOX* and w^{1118} larvae because, despite being L3 arrested, *PPOX* larvae are smaller and have less fat compared to w^{1118} controls, which could skew the protein to heme

content. The hemin standard could have also caused issues because the hemin standard was initially difficult to replicate and used few points or was not exactly linear. If *PPOX* larvae actually have more heme than w^{1118} larvae, the heme pathway may be appropriately compensated for at the expense of accumulating toxic heme precursors, which then disrupt the cells by creating reactive oxygen species and impairing development.

After measuring heme in whole body larvae, I attempted to measure heme in BRGs as a more accurate way to access heme in the PG. Before measuring heme levels in *phm>DHR51*-RNAi BRGs, I first determined whether my protocol and analysis worked for BRGs that had heme biosynthesis disrupted in the PG. To measure heme in BRGs, I used *phm>PPOX*-RNAi to reduce heme levels in the PG and compared heme levels in BRGs to *phm>*w^{1118} BRGs from 5 day old L3 larvae. When comparing the fluorescence ratio, *phm>PPOX*-RNAi BRGs had a significantly smaller fluorescence ratio compared to *phm>*w^{1118} BRGs, 2.2 compared to 14.2 at 608 nm (P-value = 0.019) and 1.9 compared to 33.3 at 662 nm (P-value = 0.0016) (Figure 3-14F). This data demonstrated that the fluorescence ratio could differentiate between BRGs with heme biosynthesis disrupted in the PG and controls. When the autofluorescence from the samples was compared to the hemin standard curve (Figure 3-14GH) and normalized to the protein content in the wells, no difference in heme content was found between *phm>PPOX*-RNAi and *phm>*w^{1118} BRGs (Figure 3-14I). Since RNAi was used only in the PG, the brain would have had normal heme levels, making it possible that the brain masked a potential heme difference in the PG. This result could also be similar to *PPOX* whole body larvae that had similar amounts of heme per amount of protein. Cells could be compensating for the lack of heme at the cost of accumulating high levels of toxic heme precursors. Based on these

measurements, the fluorescence ratio seemed to be a better analysis to determine whether heme levels were reduced in whole body larvae and in the PG of BRGs.

In my analyses, I found that using a fluorescence ratio between the autofluorescence observed in oxalic acid and heat-treated samples (experimental) compared to the autofluorescence observed in oxalic acid-treated samples with no added heat (background) was more reliable and able to differentiate expected low heme tissues compared to normalizing the amount of heme to protein. Examining the fluorescence ratio was not the usual analysis of heme levels, but I believe it can be used to determine whether heme levels are reduced compared to controls, but the fluorescence ratio cannot accurately measure to what extent heme levels are reduced. If *DHR51*-RNAi reduced heme levels, I would expect a low to moderate fluorescence ratio, opposed to a high fluorescence ratio as seen in w^{1118} controls because *DHR51*-RNAi larvae are expected to have low background autofluorescence (since there were no observed red autofluorescence in loss-of-*DHR51* tissues) and low to moderate autofluorescence once samples are heated in oxalic acid (since I would expect these larvae to have less total heme compared to controls). I expected that *DHR51*-RNAi larvae would have more heme, and therefore, a higher fluorescence ratio compared to *PPOX*-RNAi larvae, but a lower fluorescence ratio compared to w^{1118} controls.

To first investigate whether loss-of-*DHR51* function caused low heme levels in whole body L3 larvae, I knocked *DHR51* down ubiquitously in L3 larvae. *DHR51*-RNAi was expressed with the *actin* (*act*) – *GAL4* driver, which expresses *GAL4* throughout the body. Heme was measured in whole body larvae that were 5 days old. *act>DHR51*-RNAi (1) and (2) and *act>PPOX*-RNAi resulted in a significant reduction in the fluorescence ratio compared to *act*>w^{1118} whole body larvae (Figure 3-15A). The 608 nm and 662 nm fluorescence ratios

yielded similar results between *act>PPOX*-RNAi, *act>DHR51*-RNAi (1), and *act>DHR51*-RNAi (2) larvae. The control, *act>w*^{1118}, had fluorescence ratios of 57 and 59 at 608 nm and 662 nm, respectively, while *act>PPOX*-RNAi had fluorescence ratios of 20 and 28 (P-value = 0.0028 and 0.0046), *act>DHR51*-RNAi (1) had fluorescence ratios of 19 and 22 (P-value = 0.0019 and 0.0022), and *act>DHR51*-RNAi (2) had fluorescence ratios of 27 and 33 (P-value = 0.011 and 0.022) at 608 nm and 662 nm, respectively. *act>PPOX*-RNAi fluorescence ratios were noticeably higher than the fluorescence ratios in whole body *PPOX* larvae (approximately 2), however, in a previous test in whole body *act>PPOX*-RNAi larvae at 5 days old, a fluorescence ratio was calculated to be about 6 (data not shown). Despite this discrepancy, the fluorescence ratios in *act>DHR51*-RNAi and *act>PPOX*-RNAi larvae were significantly lower than the fluorescence ratio in the control and *act>DHR51*-RNAi larvae had similar fluorescence ratios to *act>PPOX*-RNAi larvae. *act>DHR51*-RNAi larvae had a low fluorescence ratio, similar to *PPOX*-RNAi larvae, which suggested that loss-of-*DHR51* reduced heme levels in whole body L3 larvae.

The fluorescence readings of experimental and background samples used to calculate the fluorescence ratio were examined to determine whether the observed autofluorescence followed the trend described in the above two paragraphs for *DHR51*-RNAi tissues (low background fluorescence readings and low – moderate experimental fluorescence readings). The fluorescence readings at 608 nm and 662 nm for the experimental treatment group (oxalic acid and heat) were significantly lower in both *act>DHR51*-RNAi larvae compared to the *act>w*^{1118} control larvae (all P-values < 0.05) (view the dark grey bars in Figures 3-15BC). The experimental fluorescence readings behaved as predicted, which indicated that there could be less overall heme in *act>DHR51*-RNAi larvae. Unexpectedly, the background fluorescence readings at 608 nm and

662 nm in both *act>DHR51*-RNAi larvae were slightly elevated compared to the *act>w*^{1118} control, which was odd because no red autofluorescence was ever observed with any *DHR51*-RNAi line, however the difference was only significantly different in *act>DHR51*-RNAi (1) larvae (view the purple bars in Figures 3-15BC). If *act>DHR51*-RNAi larvae had low heme levels, heme precursor accumulation was not expected because the latter half of the heme pathway was regulated properly as demonstrated in the *DHR51*-RNAi qPCR of heme pathway genes in the RG. Previous heme measurements by me of *act>PPOX*-RNAi larvae yielded a much higher background fluorescence reading and a lower experimental fluorescence reading as what was observed in Figures 3-15BC, which resulted in a much lower fluorescence ratio. However, *act>PPOX*-RNAi larvae in Figure 3-15A had a relatively high fluorescence ratio for a sample with heme synthesis disrupted due to lower background fluorescence readings than previous readings of *act>PPOX*-RNAi larvae. This partly highlights some of the difficulty and variability I observed with the heme measurements. Samples tended to be more reliable when prepared quickly and stored for only a short amount of time. The data presented here used samples that were collected as quickly as possible to ensure that the samples were as reliable as possible.

After calculating the fluorescence ratios in *act>DHR51*-RNAi whole body larvae, I quantified the amount of heme by converting the fluorescence readings to heme concentrations using a hemin standard curve and normalizing the heme concentration to the amount of protein per sample. Based on this analysis, *act>PPOX*-RNAi and *act>DHR51*-RNAi (1) had significantly lower heme levels in whole body L3 larvae compared to *act>w*^{1118} controls (P-value = 0.023 and 0.0064) (Figure 3-15D). *act>DHR51*-RNAi (2) also had a reduction in heme levels compared to *act>w*^{1118} controls, but the difference was not statistically significant due to

high variability between the *act>DHR51*-RNAi (2) samples (P-value = 0.15). High variability was typical with the *DHR51*-RNAi (2) line in my experience. This experiment was the first time that this analysis method showed a significant reduction in heme levels in loss-of-*PPOX* larvae. However, both analysis methods suggested that *act>DHR51*-RNAi reduced whole body heme levels compared to *act>w*^{1118} controls.

After successfully measuring heme in *DHR51*-RNAi whole body larvae, I measured heme levels in BRGs that expressed *DHR51*-RNAi in the PG to determine whether *DHR51*-RNAi reduced heme levels specifically in the PG. BRGs were dissected from larvae 48 hours after the L2/L3 molt. The fluorescence ratio at 608 nm and 662 nm in *phm>DHR51*-RNAi (1) and (2) BRGs was not significantly different from the fluorescence ratio in *phm>w*^{1118} control BRGs, which suggested that the heme levels were normal in *phm>DHR51*-RNAi BRGs (P-value = 0.81/0.69 and 0.57/0.41 at 608 nm / 662 nm) (Figure 3-16A). However, *phm>PPOX*-RNAi BRGs had very low fluorescence ratios at 608 nm and 662 nm, but only had a significant reduction in the fluorescence ratio when measured at 608 nm due to very high *phm>w*^{1118} fluorescence reading variance when measured at 662 nm (P-value = 0.035/0.20). High variation, especially the fluorescence reading at 662 nm, was also found in both *DHR51*-RNAi lines as well. The fluorescence ratio may not be as robust to detect a subtler decrease in heme levels as would be expected for *phm>DHR51*-RNAi BRGs with the brain that has normal heme levels, even though the fluorescence ratio identified *phm>PPOX*-RNAi BRGs as having lower heme levels. When the individual fluorescence readings for the experimental and background *phm>DHR51*-RNAi BRG samples were examined, the readings were indistinguishable from the fluorescence readings from *phm>w*^{1118} control BRGs (data not shown), unlike what was seen in the whole body knockdown analysis.

Fluorescence readings were then converted to a heme concentration via a hemin standard curve and normalized to the protein content per sample. *phm>DHR51*-RNAi (1) and *phm>PPOX*-RNAi BRGs had similar heme levels as *phm>w*^{1118} BRGs, while *phm>DHR51*-RNAi (2) BRGs had higher heme levels (Figure 3-16B). The *phm>PPOX*-RNAi heme measurement mirrored my previous heme measurements with *phm>PPOX*-RNAi that found no decrease in heme levels compared to *phm>w*^{1118} BRGs. Again, this could be due to the large size of the brain that has normal heme levels, as the brain could mask a subtle decrease in heme in the PG. Heme measurements in the RG could solve this discrepancy, however, RG heme measurements required a large amount of tissue for protein normalization, which could pose a technical limitation. The fluorescence ratio offered a potential workaround, but in practice, many RGs would still need to be dissected. Fluorescence readings in BRGs suffered from very low background fluorescence readings, so minor differences compared to the blanks introduced high variability within samples. Dissecting more tissue could raise the background fluorescence readings to provide a more reliable fluorescence ratio, which may help for heme measurements in BRG samples, but ultimately would not solve needing to dissect many RGs to measure heme. Given all this, I was unable to pursue measuring heme only in the RG. Based on the results of these experiments, heme measurements in whole body *DHR51*-RNAi larvae seemed to have reduced cellular heme levels, but it is unclear whether *phm>DHR51*-RNAi reduced heme levels in the PG. However, it remains plausible that DHR51 functions as a heme sensor to maintain heme homeostasis. If loss-of-*DHR51* does indeed reduce heme levels in the PG, restoring normal heme levels through hemin feeding could potentially rescue the *DHR51*-RNAi phenotypes if the developmental defective phenotypes are due to reduced heme levels.

3.2.6 Hemin feeding rescued *phm>PPOX*-RNAi larvae, but not phm>*DHR51*-RNAi larvae

If *DHR51*-RNAi does reduce heme levels in the PG, this could explain developmental defects observed in *phm>DHR51*-RNAi larvae. The L3 arrest phenotype from *phm>DHR51*-RNAi (1) larvae was similar to the L3 arrest phenotype observed in *phm>PPOX*-RNAi (II) larvae (the RNAi transgene is located on the 2nd chromosome) and the half day delay into puparium formation from *phm>DHR51*-RNAi (2) larvae was a milder phenotype compared to the 2 day delay observed in *phm>PPOX*-RNAi (III) larvae (the RNAi is located on the 3rd chromosome). A reduction in cellular heme would reduce ecdysone production because the cytochrome P450 enzymes would not have sufficient heme to be functional. Reductions in ecdysone production can cause developmental defects like larval arrests and delays because ecdysone pulses that trigger developmental transitions would be absent or delayed. To test whether the loss-of-*DHR51* phenotype in the PG was due to reduced cellular heme levels, I attempted to increase heme levels in the PG by feeding *phm>DHR51*-RNAi larvae hemin to determine whether hemin could rescue the developmental defects. However, a hemin-feeding rescue experiment had not been done in *Drosophila,* so I needed to determine whether oral hemin would be transported to the PG and whether hemin was capable of rescuing a low heme phenotype.

The concept for hemin-feeding is similar to feeding 20E to larvae to rescue ecdysone-deficient phenotypes, however, they differ in that 20E target tissues are throughout the body, but hemin would need to target the PG specifically. To find an ideal hemin concentration to use in larval food and whether hemin-feeding caused toxicity, Ami Soni, an undergraduate student, and I tested the viability of *Drosophila* larvae on hemin food using a range of concentrations from 100 nM to 80 mM (which seemed to be reaching hemin's saturation point in 50 mM NaOH).

Hemin was mixed into the normal agar cornmeal medium. Wild type w^{1118} animals raised on media supplemented with 100 nm to 80 mM of hemin showed no signs of decreased viability (Figure 3-17A). Since hemin demonstrated no signs of toxicity, Ami Soni and I decided to use 1 mM of hemin for hemin-feeding rescue experiments because 1 mM was a relatively high concentration and it is easy to work with (not too viscous).

To determine whether hemin feeding could rescue larvae with reduced heme levels in the PG, loss-of-*PPOX* larvae were fed 1 mM hemin. *phm>PPOX*-RNAi (II) and (III) larvae were both partially rescued when raised on hemin food, but *PPOX* mutant larvae were not. When I repeated the hemin-feeding rescue experiments with the *PPOX*-RNAi lines, *phm>PPOX*-RNAi larvae were indeed rescued by ingesting exogenous hemin from their food. *phm>PPOX*-RNAi (II) resulted in a 100% L3 arrest on control food, but when raised on food supplemented with 1 mM hemin, at least 50% of the population was able to make it to adulthood (Figure 3-17B). While *phm>PPOX*-RNAi (III) resulted in an approximate 50 hour delay on control food, this delay was rescued by approximately 24 hours when grown on food supplemented with 1 mM hemin (Figure 3-17C). However, *phm>PPOX*-RNAi (III) larvae were still delayed by about 24 hours compared to *phm>*w^{1118} larvae on hemin food. Similar results were also obtained by another graduate student in the lab, Sattar Soltani.

Ami Soni also investigated whether hemin was able to attenuate *Alas* induction as a result of *phm>PPOX*-RNAi in the RG via qPCR. *Alas* expression in RGs from 5 day old loss-of-*PPOX* L3 larvae raised on control food or 1 mM hemin-supplemented food were mixed and needs to be repeated (Figure 3-17D). *Alas* induction was not observed in *phm>PPOX*-RNAi (II) RGs, despite that the RGs had red autofluorescence. *phm>PPOX*-RNAi (III) resulted in *Alas* induction, but hemin did not attenuate *Alas* expression, even though hemin partially rescued the

developmental delay observed in these larvae. *Alas* expression in *PPOX* mutant RGs was lower (although not significant due to high variance within the samples, P-value = 0.061) when the larvae were grown on 1 mM hemin-supplemented food compared to *Alas* expression in RGs when *PPOX* larvae were raised on the control medium, however, hemin was unable to rescue the mutant phenotype. Hemin was likely unable to rescue *PPOX* mutant larvae because hemin was unable to supplement all tissues in the larvae and toxic heme precursors would still be synthesized in all tissues, albeit to a lower extent compared to *PPOX* larvae on normal food. Taken together, hemin did seem capable of being transported to the PG to rescue *phm>PPOX*-RNAi larvae and may attenuate *Alas* expression in the RG, at least in *PPOX* mutants. This data suggested that hemin can be fed to larvae and be transported to the PG, so hemin can be used to determine whether hemin can rescue *phm>DHR51*-RNAi larvae.

If loss-of-*DHR51* in the PG reduced cellular heme levels, then the larvae could potentially be rescued by hemin feeding. When *phm>DHR51*-RNAi larvae were grown on 1 mM hemin-supplemented food, the *phm>DHR51*-RNAi developmental defects were not rescued (Figure 3-18A). *phm>DHR51*-RNAi (1) resulted in a 100% L3 arrest on control media and the larvae were still 100% L3 arrested on 1 mM hemin-supplemented media. In *phm>DHR51*-RNAi (2) larvae, puparium formation was delayed by approximately 7 hours on control food (normally around half a day delay), but when raised on 1 mM hemin-supplemented media, the delay remained at about 7 hours compared to *phm>w*^{1118} animals on 1 mM hemin-supplemented media. The *phm>DHR51*-RNAi hemin rescue experiment was performed at the same time as the *phm>PPOX*-RNAi (III) rescue attempt (Figure 3-17C), so the same *phm>PPOX*-RNAi data was included in Figure 3-18A as a positive control. *phm>DHR51*-RNAi animals were unable to be

rescued be hemin feeding. This could indicate that loss-of-*DHR51* larvae do not have reduced heme levels or that decreased heme levels are not the only defect in these larvae.

As will be discussed in Chapter 4, *phm>DHR51*-RNAi decreased the expression of the cytochrome P450 enzyme genes, which resulted in reduced ecdysone titers, therefore, increasing heme levels in these ecdysone-deficient larvae would be expected not to rescue the larvae, as the cytochrome P450 genes would still have reduced expression. I added a combination of 20-hydroxyecdysone (20E) and hemin to the food of *phm>DHR51*-RNAi (1) larvae and *phm>w*^{1118} control larvae to determine whether 20E and hemin could rescue *phm>DHR51*-RNAi (1) larvae better than 20E or hemin alone (*phm>DHR51*-RNAi (2) larvae were almost fully rescued from 20E alone, so they were not included). With 20E alone, *phm>DHR51*-RNAi (1) larvae were partially rescued from 100% L3 arrest to some larvae attempting puparium formation. However, 20E- and hemin-supplemented media did not provide a better rescue of *phm>DHR51*-RNAi (1) larvae compared to *phm>DHR51*-RNAi (1) larvae on strictly 20E-supplemented media (Figure 3-18B). This indicated that hemin was unable to rescue *phm>DHR51*-RNAi (1) L3 arrested larvae. The phenotype of *phm>DHR51*-RNAi (1) larvae on 20E-supplemented food will be discussed in detail in Chapter 4.2.3. Ultimately, no conclusions could be drawn from attempting to rescue *phm>DHR51*-RNAi larvae on hemin-supplemented media. Had hemin been able to rescue *phm>DHR51*-RNAi larvae, that would have provided strong evidence that loss-of-*DHR51* decreased cellular heme levels in the PG.

3.2.7 *UAS-Alas* cDNA cloning and expression

Heme measurements suggested that *DHR51*-RNAi could reduce cellular heme levels, but *phm>DHR51*-RNAi larvae were unable to be rescued by hemin feeding. I took another approach to determine whether *DHR51*-RNAi resulted in low cellular heme levels by attempting to induce

red autofluorescence in the RG by ectopically overexpressing *Alas*. Since *phm>DHR51*-RNAi may decrease cellular heme levels in the RG, but *Alas* is not upregulated, *Alas* overexpression may be able to induce heme precursor accumulation and red autofluorescence. There was no *UAS-Alas* cDNA fly stock, so I cloned *UAS-Alas* (described in Chapter 2.1.15.2). Before testing whether increased *Alas* expression could induce red autofluorescence in *phm>DHR51*-RNAi RGs, I tested whether the *UAS-Alas* cDNA line was properly overexpressing *Alas* and to what extent. *phm>Alas* cDNA resulted in 8-fold increased expression of *Alas* compared to $phm>w^{1118}$ in RGs (Figure 3-19A). Overexpression of *Alas* in the RG resulted in no observable phenotypes and upon dissection of the RG, there was no observable red autofluorescence when photographed using a very long exposure (three seconds) (Figure 3-19B). This could be expected because the rest of the heme pathway was functional, so no heme precursors would be expected to accumulate, hence no red autofluorescence would be expected.

After testing *phm>Alas* cDNA, Ami Soni overexpressed *Alas* cDNA and *DHR51*-RNAi in the PG with *phm22-GAL4* to determine whether heme precursor accumulation could be induced in the PG when *DHR51* was disrupted. BRGs from late L3 larvae were dissected and examined for red autofluorescence in the PG. Overexpression of *Alas* cDNA with either *DHR51*-RNAi line did not induce red autofluorescence in the PG, thus heme precursors did not accumulate (Figure 3-19C). Red autofluorescence was only observed in *phm>PPOX*-RNAi (II) RGs and no red autofluorescence was observed in either *phm>DHR51*-RNAi RGs or *Alas* overexpression controls. Unfortunately, no meaningful conclusion could be drawn from this experiment. Heme precursors would likely only accumulate when *Alas* was overexpressed if loss-of-*DHR51* disrupted the latter half of the heme pathway when porphyrin rings form, but based on qPCR data, the latter half of the heme pathway appeared unaffected. If anything, loss-of-*DHR51* would

only affect *Alas*, and possibly *Pbgs*, which encodes the second enzyme in the pathway. Given all this, if loss-of-*DHR51* disrupted heme homeostasis, only the initial steps in the heme biosynthesis pathway would be expected to be compromised.

3.2.8 DHR51 overexpression and subcellular localization

Nuclear receptors have the potential to be localized in the cytoplasm and translocate to the nucleus upon ligand binding (Type I). The Androgen Receptor is an example of a Type I nuclear receptor (Chan and O'Malley. 1976). DHR51 and NR2E3 have only been reported to be observed in the nucleus, however, a range of conditions had not been tested to determine whether either nuclear receptor could be found in the cytoplasm (Chen, J., et al. 2005; Beuchle, et al. 2012; Yaniv, et al. 2012). I wanted to observe DHR51's subcellular localization and determine whether cellular heme levels influence DHR51's localization. If heme is DHR51's ligand, varying the heme levels could potentially affect DHR51's localization. However, some nuclear receptors are always nuclear and ligand binding does not affect subcellular localization (like a Type II nuclear receptor). Before I tested whether varying heme concentrations affected DHR51's subcellular localization, I made transgenic lines that could overexpress FLAG-tagged DHR51 via the *UAS* promoter so that commercially available FLAG antibodies could be used to identify DHR51's subcellular localization. Before discussing DHR51's localization under varying heme levels, I will first discuss making the *UAS-FLAG-DHR51* transgenic flies.

3.2.8.1 FLAG-DHR51 transgene cloning and preliminary testing

(*FLAG-*)*DHR51* transgenic lines were made early in my program for use in various experiments. I designed a *UAS-FLAG-DHR51* line, as well as *heat shock* (*hs*)*-DHR51* (FLAG-tagged and untagged), using N-terminal tags. In Chapter 3.2.8.2, I will discuss using the *UAS-FLAG-DHR51* lines for determining DHR51's localization. The *hs-(FLAG-)DHR51* lines will be

discussed in Appendix A.2.1.1 when I discuss testing a DHR51 antibody that I designed (the antibody was not suitable for immunofluorescence). A *UAS-DHR51* cDNA plasmid and transgenic fly already existed, which I received from Dr. Steven Robinow (Sung, et al. 2009). Sung *et al*. demonstrated that two *DHR51* cDNAs (*F1* and *C1*) were able to rescue the *unf* (*DHR51*) mutant phenotype, which indicated that the DHR51 transgenic protein functioned similarly to endogenous DHR51. Cloning of the (*FLAG-*)*DHR51* cDNA plasmids is described in Chapter 2.1.15.1. Multiple *UAS-FLAG-DHR51* fly stocks were recovered, while only one of each *hs-*(*FLAG-*)*DHR51* line was recovered. Chromosome location of each transgene was identified due to segregation away from either a 2nd or 3rd chromosome dominant marker. The chromosome that each transgene was located on is listed in Table 3-2.

Overexpression of *DHR51* was never examined with qPCR in the *UAS-(FLAG-)DHR51* transgenes, so if any future major experiment is based on these transgenes, testing *DHR51* with qPCR should be done. Instead, I compared the overexpression phenotypes of my *UAS-FLAG-DHR51* transgenes in the PG with the overexpression phenotypes of the *UAS-DHR51* lines that could rescue *unf* mutants. Overexpression of *UAS-DHR51 (F1)* with a strong PG driver (*phm22-GAL4*) resulted in major L1 arrest with a few L2 arrested larvae (~5%, but never accurately quantified) (Figure 3-20) (Table 3-3). *phm>DHR51 (C1)* resulted in a similar phenotype to *phm>DHR51 (F1)*. Overexpression of *DHR51 (F1)* with a weaker RG *GAL4* driver (*P0206*) resulted in a major pupal lethal phenotype with some larvae arrested at the L3 stage. *P0206>DHR51 (C1)* resulted only in an L3 arrest phenotype (Table 3-3). Overexpression of *DHR51* also resulted in smaller RGs. The difference in overexpression phenotypes between the *phm22* and *P0206* drivers could be due to the dosage of *DHR51* and a higher dose of *DHR51* resulted in earlier lethality.

Once the *DHR51* overexpression phenotype was documented, I overexpressed *UAS-FLAG-DHR51* in an attempt to recapitulate the *DHR51* overexpression phenotype to provide support that these transgenes acted similarly. Multiple *UAS-FLAG-DHR51* lines were tested because they were created from random P-element insertions during embryo transformation, so the lines may differ in expression. Overexpression of all *FLAG-DHR51* lines in the PG with a strong PG driver (*phm22-GAL4*) resulted in an L1 arrest, similar to *phm>DHR51* (Table 3-3). Overexpression of *FLAG-DHR51* with a weaker *GAL4* driver (*P0206*) resulted in a later stage arrest compared to overexpression with *phm22-GAL4*, similar to overexpressing *DHR51*. This demonstrated that the *FLAG-DHR51* phenotype was also dose-dependent. *P0206>FLAG-DHR51* generally resulted in a major L2 arrest phenotype, which was more severe compared to *P0206>DHR51*. Since *FLAG-DHR51* and *DHR51* caused similar phenotypes, it seemed likely that the *FLAG-DHR51* was functional.

3.2.8.2 FLAG-DHR51 localized to the nucleus at all heme levels tested

Once the *UAS-FLAG-DHR51* lines were made, FLAG antibodies could then be used to determine DHR51's subcellular localization under normal heme conditions and when heme levels were low (using a *PPOX* mutant) in the PG. I was unable to examine endogenous DHR51 localization because the DHR51 antibody I commissioned (Appendix A) was not suitable for immunofluorescence (data not shown). I was also unable to use a *DHR51-GFP* transgene with a *DHR51* promoter due to *DHR51* having low expression in the PG (Spokony, R. and White, K. (2012.5.22) Spokony insertions). The *DHR51-GFP* may have had faint nuclear localization, but it was difficult to differentiate the fluorescence signal from the background (data not shown). *P0206-GAL4* was used to overexpress multiple *UAS-FLAG-DHR51* lines (*1M*, *4M*, and *8M*) in the RG in a wild type heme backgrounds and low heme backgrounds (*PPOX* mutant

background). BRGs from *P0206>w*^{1118} and *P0206>PPOX* mutant larvae were used as controls. *P0206* expressed *GAL4* in the RG and some areas of the brain. The *P0206* line also expressed *GFP* that localized to the cytoplasm. During preliminary testing, I observed that GFP was not observed in the small *FLAG-DHR51* ring glands, so I used a secondary antibody that had a green fluorescence marker with the *PPOX* mutant brain-ring glands to avoid using a secondary antibody with a red fluorescence marker that could overlap with the red autofluorescence from the heme precursors. However, since young L2 larvae were dissected, the heme precursors did not have sufficient time to accumulate to give off observable red autofluorescence, as seen in the *P0206>PPOX* control RG. Initially, *P0206>FLAG-DHR51 4M* and *8M* were L3 arrested, but later changed to be L2 arrested. *P0206>FLAG DHR51 1M* was included because the phenotype remained L3 arrested so I could observe DHR51 localization under normal heme levels in L3 larvae. I did not make a *FLAG-DHR51 1M* ; *PPOX* line at the time because overexpression of *FLAG-DHR51 4M* and *8M* were still thought to be L3 arrested, therefore, I did not test *FLAG-DHR51 1M* localization in a *PPOX* mutant background.

BRGs were dissected from L2 larvae (except for *P0206>w*^{1118} and *P0206>FLAG-DHR51 1M* larvae, which were dissected from L3 larvae). In all *FLAG-DHR51* lines tested, DHR51 was observed to be solely in the nucleus under normal heme levels (Figure 3-21A). As noted, overexpression of *FLAG-DHR51* reduced ring gland size and GFP was not observed in these ring glands. DHR51 was also observed in the nucleus when *FLAG-DHR51 4M* was overexpressed in a low heme (*PPOX* mutant) background (Figure 3-21B). No FLAG-DHR51 fluorescence was observed in *P0206>FLAG-DHR51 8M ; PPOX* RGs. Given the difference in FLAG-DHR51 fluorescence between the *FLAG-DHR51 4M* and *8M* lines in a *PPOX* mutant background, this experiment needs to be repeated and could also include *FLAG-DHR51 1M* in a

PPOX mutant background. However, I would expect FLAG-DHR51 to have a nuclear localization when heme levels are low, since DHR51 was necessary for *Alas* induction when heme levels were low, so DHR51 would presumably be active in the nucleus. Since BRGs were dissected when the larvae were still young, autofluorescent heme precursors had not had the time necessary to accumulate to give off observable red autofluorescence. Given this, the lines should be tested for *Alas* induction during the L2 stage to ensure the RGs have low levels of heme. Based on this experiment, FLAG-DHR51 localized to the nucleus under normal conditions and, likely, when heme levels were low. If heme is DHR51's natural ligand, DHR51's localization under normal and low levels of heme would suggest that DHR51 is a type II nuclear receptor, always present in the nucleus, regardless of ligand binding.

3.3 Discussion

3.3.1 Loss-of-*DHR51* phenotypes

The exact natures of the *unf* (*DHR51*) mutants are unknown. Homozygous unf^{Z0001} and unf^{XI} animals have a relatively high degree of uneclosed adults (pupal lethality) and adults that do not expand their wings if they eclose. When each *unf* allele was used in combination with a *DHR51* deficiency line, the loss-of-*DHR51* phenotype was less severe than the homozygous *unf* mutants (Sung, et al. 2009). This indicated that unf^{Z0001} and unf^{XI} mutants were likely gain-of-function mutations. The *unf* mutants also seemed sensitive to genetic background and/or environmental factors as the flies I received differed to what was published (in the case of unf^{Z0001}) or the phenotype differed based on the genetic background (unf^{XI} mutants from unf^{XI} / *CyO* versus unf^{XI} */ CyO GFP* stocks) (Table 3-1). The same conclusion was noted in Sung *et al*. 2009 when they independently created two unf^{XI} / *Df(2R)ED2426* (*DHR51* deficiency) lines, where one had 21.1% pupal lethality and the other had 3.6% pupal lethality. Similarly, a *piggyBac* insertion mutation into *DHR51*, $unf^{LL04325}$, resulted in a homozygous lethal phenotype (Yaniv, et al. 2012). Excising the *piggyBac* rescued the lethality, however, the lethality associated with the $unf^{LL04325}$ allele went away after some time, despite the continued presence of the *piggyBac* insertion.

To try and gain a better understanding of the loss-of-*DHR51* phenotype, I attempted to disrupt *DHR51* in whole body animals using conditional CRISPR. Together with GenetiVision, *DHR51* 2xgRNA fly lines were designed that ubiquitously express *DHR51* 2xgRNA. *act-Cas9>DHR51* 2xgRNA 3m phenocopied the unf^{XI} mutant phenotype when balanced with *CyO GFP*, that is, approximately 20-40% pupal lethality was seen in both unf^{XI} and *act-Cas9>DHR51* 2xgRNA 3m, adults failed to expand their wings, and adults frequently became stuck in the food,

likely due to motor defects (Figure 3-3A and Table 3-1). A developmental delay was observed in *act-Cas9>DHR51* 2xgRNA 3m animals, but a delay has never been noted for unf^{XI} larvae. Future work will need to determine whether the *unf* mutants are also developmentally delayed. The *act-Cas9>DHR51* 2xgRNA 6/12m lines had a similar phenotype to unf^{XI} mutants, but was less severe. This data confirmed that loss-of-*DHR51* in the whole body resulted in developmental delays, unexpanded wings, and possibly motor defects causing adults to get stuck in the food. I did not examine the adults for any fertility defects, despite that fertility defects were observed in unf^{Z0001} and unf^{XI} adults. This also demonstrated that DHR51 had a role in development.

The *DHR51* 2xgRNA conditional CRISPR lines were also used to validate the *DHR51*-RNAi phenotypes specifically in the PG using *Spok-Cas9* (Huynh, et al. 2018). *Spok-Cas9>DHR51* 2xgRNA 3m only recapitulated the developmental delay of *phm>DHR51*-RNAi (2) (Figures 3-3B and 3-2A). *Spok-Cas9>DHR51* 2xgRNA 3m adults had fully expanded wings, did not get stuck in the food, and appeared to have no motor defects, so these phenotypes observed in whole body loss-of-*DHR51* animals are likely caused by loss-of-*DHR51* in tissues other than the PG. The *Spok-Cas9>DHR51* 2xgRNA 6/12m lines did not seem to result in any aberrant phenotypes. There is the possibility that the 6/12m lines caused a very minor developmental delay, but these animals need to be accurately timed to determine whether they are actually delayed. No CRISPR lines were able to recapitulate the L3 arrest in *phm>DHR51*-RNAi (1) larvae (Table 3.1), which suggested that the L3 arrest could be due to an off-target of the *DHR51*-RNAi (1) as *DHR51*-RNAi (1) is predicted to have up to 10 off-targets based on the VDRC website. One way to test this possibility is to attempt to rescue the *phm>DHR51*-RNAi (1) phenotype by overexpressing an RNAi-resistant *DHR51* cDNA. If an RNAi-resistant *DHR51* cDNA cannot rescue *DHR51*-RNAi (1) larvae, that would provide strong evidence for the L3

arrest phenotype to be due to an off-target. Despite issues with *DHR51*-RNAi (1), *phm>DHR51*-RNAi (2) and *Spok-Cas9>DHR51* 2xgRNA provided a consistent phenotype, which suggested that loss-of-*DHR51* in the PG resulted in a developmental delay. This provided evidence that DHR51 is required for proper developmental timing, likely by regulating either heme biosynthesis or ecdysone production or both.

It is unclear why the *DHR51* 2xgRNA 3m and 6/12m lines behaved differently. Despite the gRNA targeting the same sequence, that the gRNA was inserted into the same genomic location by phiC31 integrase, and the gRNAs were injected into embryos from the same fly strain, *DHR51* 2xgRNA 3m provided a more severe phenotype when expressed with *Cas9*. qPCR should be used to quantify the reduction in *DHR51* expression to determine the efficiency of the three 2xgRNA lines. If *DHR51* 2xgRNA 3m is a little stronger than *DHR51*-RNAi (2), and *DHR51* 2xgRNA 6/12m are a little weaker, that could explain the difference in phenotype, but not why the difference arose. *phm>DHR51*-RNAi (2) only caused a half day delay, so if *DHR51* 2xgRNA 6/12m provided a slightly weaker delay phenotype, the delay might not be noticeable without accurate quantification. Another possibility is that the fly that gave rise to the *DHR51* 2xgRNA 3m stock could have had a random mutation that makes the animals more susceptible to loss-of-*DHR51*. The *DHR51* 2xgRNA lines were received late in my program, so I was unable to quantify their phenotypes fully. Once the *DHR51* 2xgRNA lines are fully examined, the lines can be used to validate previous experiments that used *DHR51*-RNAi. High priority experiments to validate would be to knockdown *DHR51* with the 2xgRNA in a *PPOX* mutant background and test *Alas* expression to determine whether *Alas* upregulation is dependent on *DHR51*. Heme levels can also be measured in *DHR51* 2xgRNA larvae to determine whether heme levels are indeed reduced in loss-of-*DHR51* larvae.

3.3.2 Heme as an *in vivo* ligand for DHR51

Heme was found to bind to two nuclear receptors, E75 and DHR51, *in vitro* (Reinking, et al. 2005; de Rosny, et al. 2008). E75 had a very high affinity for heme (in the nanomolar range) and apo-E75 was unable to be purified, which made it likely that heme is required for E75 stability. E75 can bind to and inhibit the nuclear receptor DHR3, but the interaction between E75 and DHR3 was dependent on the oxidation state of the iron at the center of heme, as well as diatomic gases (nitric oxide and carbon monoxide) binding to heme in E75 (White, K. P., et al. 1997; Reinking, et al. 2005). Therefore, E75 may more likely be a redox or gas sensor than a heme sensor. Contrary to E75, Rev-erbα, the vertebrate heme sensor and the homolog of E75, reversibly binds heme and did not respond to changes in redox state or binding of diatomic gases, which suggested that Rev-erbα did not function as a redox or gas sensor (Raghuram, et al. 2007). On the other hand, DHR51 had an affinity for heme *in vitro* much more similar to Rev-erbα, 0.43 μM compared to 2-3 μM respectively (de Rosny, et al. 2008; Raghuram, et al. 2007). For these reasons, DHR51 was the prime candidate for a heme sensor in the *Drosophila* PG.

My first approach to determine whether heme binding was biologically relevant for DHR51 activity was to use the ligand trap system. The DHR51 ligand trap fusion protein combined the GAL4-DBD and the DHR51-LBD (Palanker, et al. 2006). Palanker *et al*. demonstrated that many of the nuclear receptor ligand trap fusion proteins were able to activate the expression of a *UAS*-reporter gene. About half of the ligand trap fusion proteins did not activate the reporter gene, but of those, many of the native nuclear receptors were repressors, thus likely so were the ligand trap fusion proteins. DHR51 was among the ligand trap fusion proteins that did not activate a reporter gene, but I hypothesized DHR51 may only function as an activator under low heme conditions or function as a repressor (Figure 3-1). Trying to predict

how exactly DHR51 could function as a nuclear receptor based on the vertebrate homolog, NR2E3, was difficult due to NR2E3's versatility. NR2E3 is as a dual repressor/activator (Cheng, et al. 2004; Chen, J., et al. 2005; Haider, et al. 2009). If DHR51 functioned similarly as a dual repressor/activator, then the DHR51 ligand trap fusion protein could also function as a dual repressor/activator, so both repressor and activator activity of the DHR51 ligand trap fusion protein needed to be tested.

Unfortunately, the DHR51 ligand trap fusion protein did not seem to function as an activator or repressor when heme levels were low or normal (Figures 3-4 and 3-5). One issue that caused me concern when testing whether the DHR51 ligand trap fusion protein was a repressor was the high number of transgenes involved (*UAS-EGFP*, *hs-GAL4*, and the *DHR51* ligand trap, with or without the *PPOX* mutation). However, when I tested the fly lines, they all behaved as expected, indicating that all the transgenes were present and function (Figure 3-6). Typically, to test the repression activity of a transcription factor, most experiments seem to have been done in cell culture to reduce the expression of a constitutively active reporter gene like luciferase. However, I wanted to test DHR51 function specifically in the PG since tissue-context can matter, which has already been shown for DHR51 where DHR51 proteins levels differed in different neurons (in one set of neurons, DHR51 protein levels oscillated with the circadian rhythm, but did not in another set of neurons) (Beuchle, et al. 2012). With the inability for the DHR51 ligand trap fusion protein to influence reporter gene expression, it seemed like the DHR51 ligand trap fusion protein was either non-functional (either the fusion protein does not function or a nuclear receptor binding partner or co-regulator are not properly recruited) or heme was not a relevant ligand for DHR51. To distinguish between these two possibilities would be very difficult and not worth the time investment as I already invested a lot of time to determine whether I could get the

DHR51 ligand trap fusion protein to work. At this point, the *DHR51* ligand trap does not seem like a worthwhile tool to use to study DHR51 function.

Beyond the *DHR51* ligand trap, another way to determine whether heme binding to DHR51 is biologically relevant was to determine whether heme binding affected the subcellular localization of DHR51. Some nuclear receptors reside in the cytoplasm and upon ligand binding, translocate into the nucleus (Type I) (Figure 1-2). If DHR51 behaved in a similar manner, heme binding or release could affect DHR51 subcellular localization. However, the prospect of DHR51 translocating between cellular compartments was unlikely given that NR2E3 seemed to only have a nuclear localization and only mutations caused cytoplasmic localization (Bumsted O'Brien, et al. 2004; Cheng, et al. 2004; Kanda and Swaroop. 2009). In agreement with NR2E3, DHR51 has only been reported with nuclear localization, but it was not clear whether DHR51 could be localized in the cytoplasm if heme levels were changed (Beuchle, et al. 2012; Yaniv, et al. 2012). Originally, overexpression of *FLAG-DHR51* cDNA lines with *P0206-GAL4* (a ring gland GAL4 driver) resulted in an L3 or pupal arrest phenotype. I planned to examine the subcellular localization of FLAG-DHR51 in normal and low heme conditions in PGs from L3 larvae. When I made lines that expressed *FLAG-DHR51* in a *PPOX* mutant background some time later, the overexpression phenotype resulted in an L2 arrest, instead of the previously observed L3 and pupal arrest. The L3 stage was the primary stage I was interested in to model the major ecdysone pulse that triggers metamorphosis. I tried using other RG-*GAL4* drivers like *Mai60-GAL4* and *Feb36-GAL4* to overexpress *FLAG-DHR51* in the PG of larvae, but they also had a similar pattern; overexpression of *FLAG-DHR51* resulted in L3 and pupal arrest phenotypes, and after some time after I made *FLAG-DHR51* lines with the *PPOX* mutation, the phenotype changed to L2 arrest that had small larvae (Table 3-3). I do not know why the *DHR51*

overexpression phenotype seemed to have changed, but it was independent of the *GAL4* driver. The change in phenotype could be more evidence that *DHR51* is susceptible to background/environmental effects, similar to how $unf^{LL04325}$, which was created by a *piggyBac* insertion, was initially identified as lethal, but later became viable (Yaniv, et al. 2012).

Eventually I decided to examine FLAG-DHR51 localization in L2 larvae because DHR51 should behave similarly in L2 larvae as L3 larvae when heme conditions are lowered. FLAG-DHR51 localized to the nucleus during normal and low heme levels, although, FLAG-DHR51 was not observed when heme levels were low in the *FLAG-DHR51 8M* line (Figure 3-21). I do not think FLAG-DHR51 would be absent or degraded during low heme levels because my other experiments suggested that DHR51 was necessary for *Alas* upregulation when heme levels were low, so presumably DHR51 would be active in the nucleus. In addition, *P0206* expresses *GAL4* in areas of the brain, which is why FLAG was also detected in the brain of other samples, but the *FLAG-DHR51 8M* line did not even show expression in the brain. Therefore, I do not think the immunofluorescence experiment worked in the *FLAG-DHR51 8M* sample in a *PPOX* mutant background. The L2 RG samples from larvae with the *PPOX* mutation did not have any observable red autofluorescence because the larvae were relatively young and the autofluorescent heme precursors had not had sufficient time to accumulate to observable levels. Red autofluorescence had been observed in the RG from L2 larvae, but those larvae were L2 arrested. When *Updo* is knocked down via RNAi (*Updo* is the fifth enzyme in the heme biosynthesis pathway), larvae were L2 arrested and had red autofluorescent ring glands (Huynh, in revision). This suggested that a heme sensor was present in the PG even in L2 larvae, which is part of the reason why I ended up examining FLAG-DHR51 localization in PGs from L2 larvae. Nuclear localization of FLAG-DHR51 under varying heme levels is consistent with only nuclear

localization observed previously in DHR51 and NR2E3. If heme is the natural ligand for DHR51, heme does not affect DHR51 localization, as DHR51 remained in the nucleus during various cellular heme concentrations (like a Type II nuclear receptor). I cannot say specifically that DHR51 is a Type II nuclear receptor because Type II nuclear receptors also form heterodimers, typically with the nuclear receptor RXR (Retinoid X receptor) in vertebrates or the *Drosophila* homolog usp (ultraspiracle). Although DHR51 has been shown to form a heterodimer with E75 (Rabinovich, et al. 2016), if DHR51 does function similar to NR2E3, DHR51 could potentially also form homodimers. The ability for DHR51 to form homodimers is also supported by the allele interactions between unf^{Z0001}, unf^{XI}, and transheterozygotes (Sung, et al. 2009). This suggested that DHR51 may not fit into a defined category of nuclear receptor and may be an exception to the classic types of nuclear receptors.

My experiments were unable to demonstrate whether heme is the natural, *in vivo* ligand for DHR51. Another approach to determine whether heme binding is biologically relevant is to test DHR51 protein-protein interactions in varying cellular heme conditions. Upon ligand binding, nuclear receptors undergo a conformational change that affects protein-protein interactions and recruitment of co-regulators (Perissi and Rosenfeld. 2005). To determine whether heme binding affected DHR51 protein interactions, I had planned to do a mass spectrometry (mass spec) experiment under normal and low heme conditions in whole body larvae. However, whole body overexpression of *FLAG-DHR51* was embryonic lethal, regardless of what *GAL4* driver was being used (*tubulin-GAL4*, *actin-GAL4*, *daughterless-GAL4*, and *ubiquitin-GAL4*). Along with this, I also began running out of time in my program to complete the experiment. If *UAS-GAL4* could not be used in whole body larvae, mass spec could be done with *FLAG-DHR51* in cell culture or in whole body *hs-FLAG-DHR51* larvae. However, I was

unable to induce *Alas* upregulation in S2 cells with 1 mM of succinylacetone (an inhibitor of the second enzyme in heme biosynthesis) (discussed in Appendix A.2.1.6). So, if mass spec would be done with DHR51 in cell culture, an appropriate concentration of succinylacetone would need to be found or a different cell type or method to reduce cellular heme levels would need to be used. If mass spec resulted in different protein-protein interactions of DHR51 under normal and low levels of heme, that would provide strong evidence that heme is a relevant *in vivo* ligand for *DHR51*.

3.3.3 DHR51 regulation of *Alas*

Although I was unable to determine whether heme was DHR51's natural ligand *in vivo*, I could determine whether DHR51 regulated *Alas* expression based on cellular heme levels. If DHR51 did regulate *Alas*, that would provide evidence that DHR51 could function as a heme sensor. My hypothesis was that DHR51 upregulates *Alas* expression when heme levels are low (Figure 1-6). To test my hypothesis, I knocked down *DHR51* with RNAi in a low heme background generated by a *PPOX* mutation. Two independent *DHR51*-RNAi lines attenuated *Alas* induction when heme levels were low in the RG and reduced the accumulation of red autofluorescent heme precursors (Figure 3-7). This data suggested that *Alas* induction when heme levels were low was dependent on DHR51. Interestingly, *phm>DHR51*-RNAi (1) in a *PPOX* mutant background resulted in some RGs that accumulated observable red autofluorescence in the RG ("Red"), but other RGs did not ("White"). *Alas* expression was slightly lower in "White" RGs compared to "Red" RGs, but the difference was not statistically significant (P-value = 0.12). I was able to replicate these results with an independent experiment and one thing that I noticed was that "White" RGs consistently had *Alas* less than two-fold upregulated and "Red" RGs consistently had *Alas* greater than two-fold upregulated. Two-fold

upregulation of *Alas* expression may set a boundary or threshold when the latter half of the heme biosynthesis pathway is disrupted where, once crossed, red autofluorescent heme precursors accumulate to observable levels. Once this threshold is crossed, it seemed that *Alas* upregulation and the amount of accumulated heme precursors are positively correlated in a relatively linear manner based on this experiment and observations of other lab members that study other genes where loss of gene function disrupts heme biosynthesis and causes *Alas* upregulation.

I attempted to replicate the above experiment with the unf^{XI} mutation in a *PPOX* mutant background to attempt to validate that specifically DHR51 is required for *Alas* upregulation when heme levels were low. But contrary to *DHR51*-RNAi in a low heme background, unf^{XI} ; *PPOX* larvae still had red autofluorescent RGs and high *Alas* induction in the RG similar to *PPOX*-deficient RGs alone (Figure 3-8AB). However, the exact nature of the unf^{XI} allele is not known, but it seems to have some gain-of-function properties (Sung, et al. 2009; Yaniv, et al. 2012). The unf^{XI} allele is caused by a splicing defect and four novel *DHR51* transcripts were detected on a Northern blot (Sung, et al. 2009). The results of the interaction between unf^{XI} and *PPOX* are difficult to interpret because of the uncertainty of the unf^{XI} allele.

Since *DHR51*-RNAi (2) attenuated *Alas* to a lesser extent as *DHR51*-RNAi (1) in a *PPOX* mutant background and due to uncertainties with the unf^{XI} allele, I attempted to increase *Alas* attenuation in *phm>DHR51*-RNAi (2) RGs in a *PPOX* mutant background by crossing in a *DHR51* deficiency line. This would presumably result in a stronger decrease in DHR51 function and the *DHR51* deficiency would be a true null allele since the entire *DHR51* gene is deleted on one chromosome. If DHR51 function could be decreased further, that should have resulted in a strong attenuation of *Alas* upregulation when heme levels were low. A similar idea was used to enhance the *DHR51*-RNAi phenotype in mushroom body axon lobe extension (Lin, et al. 2009).

However, the deficiency had no effect on *Alas* induction in low heme levels in combination with *DHR51*-RNAi (2) (Figure 3-8C). This suggested that either loss-of-*DHR51* was not responsible for the change in *Alas* expression or the deficiency line did not further reduce DHR51 function within the PG. Lin *et al*. noted that the *DHR51* deficiency did not enhance the stronger *DHR51*-RNAi line phenotype, only the weaker one (*DHR51*-RNAi (2)). However, Lin *et al*. tested *DHR51*-RNAi in the mushroom body, but *DHR51* likely has lower expression in the PG so the weaker *DHR51*-RNAi line (*DHR51*-RNAi (2)) may provide a relatively strong knockdown in the PG and decreasing *DHR51* expression in the PG with the *DHR51* deficiency line had no additional effect. However, if *DHR51*-RNAi (2) did fully suppress DHR51 function and *Alas* upregulation was attenuated, *Alas* was still upregulated when heme levels were low compared to *Alas* expression when heme levels were normal. At least in vertebrates, *Alas1* is regulated by a variety of transcription factors, such as Rev-erbα, PGC-1α (which is also linked to nutrition), and the circadian rhythm (Wu, et al. 2009; Handschin, et al. 2005; Kaasik and Lee. 2004). I would suspect that *Drosophila Alas* is also regulated by many transcription factors and that the heme sensor function is lost, there may be ways to compensate for *Alas* expression through the other transcription factors.

An oddity that I observed in my experiment when I crossed in a *DHR51* deficiency line was that *phm>DHR51*-RNAi (2) did not attenuate *Alas* induction when heme levels were low compared to *Alas* expression in RGs from *phm22-GAL4 PPOX* (*PPOX* mutant larvae that also expressed *GAL4*), unlike in my past experiment (compared Figure 3-8C to 3-5B). This experiment suggested that DHR51 was not involved in *Alas* upregulation when cellular heme levels were low. However, *Alas* expression was lower than normal in *PPOX*-deficient RGs (compare *Alas* in *PPOX* RGs from 9 day old L3 larvae in Figure 3-8C to 3-7B). Typically, *Alas*

is upregulated between 25 to 50 times wild type levels and when I tested *Alas* expression with the *DHR51* deficiency, *Alas* was around 15-fold higher than the control. Previously, I had just used just *PPOX*, but when I tested the deficiency, I used *phm22-GAL4 PPOX⁻ / PPOX⁻* (*PPOX*$^{-/-}$ mutation with one copy of *phm22-GAL4*), so for some reason, *Alas* expression between these two lines differed. One possible idea to examine is that *Alas* expression was higher in younger *phm22-GAL4 PPOX* larvae compared to older *phm22-GAL4 PPOX* larvae (compare *Alas* expression in Figures 3-8C and 3-9). Although this difference could be a coincidence or because *Alas* expression in *phm-GAL4 PPOX* RGs was being compared to *phm>DHR51*-RNAi (1) RGs rather than the appropriate control in older larvae, it may be worth repeating *phm> DHR51*-RNAi (2) with the *DHR51* deficiency line in 5 day old larvae rather than in 9 day old larvae that had been arrested for an extended period. With these experiments together, *DHR51* may be involved in the upregulation of *Alas* when heme levels were low, but further experiments need to be done due to having mixed results with *DHR51*-RNAi. Using the *DHR51* 2xgRNA conditional CRISPR lines would be ideal for testing whether DHR51 is required for *Alas* upregulation when heme levels are low because CRISPR would provide a way to disrupt *DHR51* independently of the *UAS-GAL4* system and RNAi.

An alternative explanation existed for why *DHR51*-RNAi may attenuate *Alas* expression independently of upregulating *Alas* expression when heme levels were low. The majority of heme in the PG is likely used by cytochrome P450 enzymes for synthesizing ecdysone. As will be discussed in the next chapter, DHR51 regulates the expression of the ecdysone biosynthetic genes. *phm>DHR51*-RNAi reduced the expression of the ecdysone biosynthetic genes, which would reduce the demand for heme in the PG as there would be less cytochrome P450 enzymes. If the demand for heme is reduced, heme levels may not be as low in *PPOX* mutant larvae as

heme levels would otherwise be. Reducing the demand for heme may indirectly attenuate *Alas* expression. To test this hypothesis, I expressed *torso*-RNAi in the PG (Torso is an upstream receptor for PTTH that induced the ecdysone biosynthetic genes at the end of the L3 stage) in a *PPOX* mutant background (McBrayer, et al. 2007; Rewitz, et al. 2009). *phm>torso*-RNAi in *PPOX*-deficient RGs attenuated *Alas* expression compared to *Alas* expression in *PPOX* RGs alone (Figure 3-9A). This suggested that *DHR51*-RNAi may indirectly attenuate *Alas* expression in a low heme background by reducing the PG's demand for heme. However, one issue is that Torso is an upstream component of a signaling pathway and knocking down *torso* could have many consequences beyond simply impairing the expression of ecdysone biosynthetic genes. Future experiments could knockdown *phm* or *sad* (cytochrome P450 genes with very high expression in the PG) and access whether loss of a cytochrome P450 enzyme specifically can attenuate *Alas* expression when heme levels are low. However, if loss-of-*DHR51* only attenuated *Alas* expression when heme levels were low due to a decreased demand for heme, that would not explain why loss-of-*DHR51* seemed to decrease heme levels in an otherwise wild type background. Presumably, without the high demand for heme from cytochrome P450 enzymes, heme levels would increase, but that was not seen. Thus, it would seem unlikely that loss-of-*DHR51* only attenuated *Alas* expression when heme levels were low by decreasing the demand for heme by downregulating genes that encode for cytochrome P450 enzymes.

Although it is uncertain whether DHR51 actually regulates *Alas*, I decided to test whether Spargel (*srl*) was involved in upregulating *Alas* when cellular heme levels were low. *srl* is the *Drosophila* homolog of *PGC-1α*. PGC-1α is a co-activator of *Alas1* expression and *PGC-1α* is regulated by the human heme sensor, Rev-erbα (Handschin, et al. 2005; Wu, et al. 2009). *phm>srl*-RNAi in *PPOX*-deficient RGs also significantly attenuated *Alas* expression compared

to *PPOX* alone (Figure 3-9B). This suggested that Srl could have a similar function as PGC-1α in *Drosophila*, although, Srl was not solely responsible for *Alas* induction. It remains unknown whether *srl* is regulated by DHR51 (*DHR51*-RNAi (1) increased *srl* expression by 2-fold in the RNA-Seq but was not considered statistically significant). One worry I had in using RNAi to attempt to attenuate *Alas* expression in *PPOX*-deficient RGs was that *Alas* expression was typically attenuated by about 50% (as seen in *DHR51*-RNAi (2), *torso*-RNAi, and *srl*-RNAi). Since all the RNAi lines I tested attenuated *Alas* expression, I am not sure whether the effect on *Alas* expression was in response to a general RNAi phenomenon or whether the proteins of interest actually regulated *Alas* expression as all the proteins had a plausible connection to *Alas*. To test whether a general RNAi phenomenon was affecting *Alas* expression levels, RNAi against a gene that has no role in heme regulation, like *EGFP*, could be used in a *PPOX* mutant background as a negative control for these sets of RNAi experiments. If *Alas* expression is unaffected in the *PPOX* mutant by an *EGFP*-RNAi line, then that would add confidence that the attenuation of *Alas* was not a general RNAi phenomenon in the other RNAi lines. However, *DHR51*-RNAi (1) was the only RNAi line that attenuated *Alas* expression to near basal levels in a *PPOX* mutant background (Figure 3-7), however, *DHR51*-RNAi (1) does seem to have off-target effects.

My hypothesis was that under normal heme conditions, DHR51 was inert with respect to *Alas* and heme functioned as an inverse agonist for DHR51. Therefore, loss-of-*DHR51* when heme levels were normal would be expected not to affect *Alas* expression, however, *phm>DHR51*-RNAi alone typically resulted in mild *Alas* upregulation in RGs, but not in 100% of experiments (about 2-fold increased expression) (Figure 3-13A). One possibility was that DHR51 was involved in suppressing *Alas* expression when heme levels are normal and then

makes a switch to an activator to induce *Alas* when heme levels drop. If this were the case, that would require revising our model of how DHR51 functions. A switch would occur once heme is freed from DHR51, causing a conformational change that ejects a co-repression and recruits a co-activator. A potential binding partner could also be released when heme levels drop, changing DHR51's activity. If this were the case, one potential binding partner could be E75 since DHR51 and E75 have been shown to work together and can physically interact with each other (Jaumouille, et al. 2015; Rabinovich, et al. 2016). Interestingly, this interaction is conserved between NR2E3 and Rev-erbα (NR1D1) (Cheng, et al. 2004; Mollema, et al. 2011). When heme levels fall, E75 could become unstable and dissociate from DHR51. Another possibility for how *DHR51*-RNAi increased *Alas* expression was that loss-of-*DHR51* reduced cellular heme levels and remaining DHR51 protein or some other factor could contribute to a small increase in *Alas* expression.

Overexpression of *DHR51 (F1)* cDNA in the RG reduced normal *Alas* expression by 40% when *Alas* expression was measured in BRGs by qPCR (Figure 3-13B). A higher reduction in *Alas* expression could potentially be observed if *DHR51* cDNA RG samples were used. Overexpressing *DHR51* and observing a reduction in *Alas* provided additional evidence that DHR51 regulates *Alas* expression. If DHR51 does repress *Alas* expression when heme levels are normal, overexpressing *DHR51* would be expected to repress *Alas* expression even further. However, since loss-of-*DHR51* appeared to reduce cellular heme levels, maybe an abundance of DHR51 may somehow increase heme levels and another protein is responsible to suppressing *Alas* expression when heme levels are high (this assumes that DHR51 is still inert with respect to *Alas* when bound by heme). An experiment to differentiate whether DHR51 is inert or a repressor of *Alas* under normal heme levels could be to disrupt DHR51 function while feeding

larvae hemin. Presumably, an increase in heme in the PG would decrease *Alas* expression; if this is mediated by DHR51, *DHR51*-RNAi would still lead to an increase in *Alas* expression, as seen in *DHR51*-RNAi larvae on normal food because DHR51 would be needed to repress *Alas* expression when heme levels are high. If DHR51 does not regulate *Alas* expression when heme levels are normal or high, hemin feeding should reduce *Alas* expression in *DHR51*-RNAi larvae, as another protein would repress *Alas* when heme levels are high. There is currently not enough data to know how DHR51 is regulating *Alas* when heme levels are low, so further experiments like the one suggested are needed. Chromatin immunoprecipitation (ChIP) can also be used to determine whether DHR51 directly binds to *Alas* under normal and low heme conditions, or to a regulator of *Alas*. As DHR51 seemed to be transcriptionally active when heme levels are low, with respect to *Alas*, identifying how DHR51 functions when heme levels are normal would provide information on how DHR51 functions as a nuclear receptor and how potential binding of a ligand affects DHR51 activity.

3.3.4 DHR51 is involved in maintaining heme homeostasis

If DHR51 functions as a heme sensor, DHR51 would maintain heme homeostasis in the PG. I suspected that loss-of-*DHR51* would ultimately reduce cellular heme levels due to the high demand for heme in the PG by cytochrome P450 enzymes for ecdysone production and the cell's inability to detect low cellular heme levels and upregulate *Alas* in the absence of a heme sensor. I used two approaches to determine whether *DHR51*-RNAi reduced cellular heme levels. The first approach was to use RNA-Seq and compare the cell's response to *phm>DHR51*-RNAi (1) and other RNAi lines that reduced cellular heme levels in the RG, particularly *FeCH*-RNAi. I found a high degree of overlap between genes that were misregulated between *phm>DHR51*-RNAi (1) and *phm>FeCH*-RNAi (Figure 3-11A).

In addition to identifying the overlapping misregulated genes between *phm>DHR51*-RNAi (1) and *phm>FeCH*-RNAi, I examined the correlation, via Pearson and Spearman's rank correlation, between the two RNAi data sets (each data set relative to the *phm>w*^{1118} control) to determine how the majority of the genes in the RG correlated to the other data set (RPKM greater than 0.1, which resulted in over 7000 genes). *phm>DHR51*-RNAi (1) and *phm>FeCH*-RNAi were also individually compared to RNA-Seq data from independently collected RGs from *PPOX* mutant L3 larvae. The correlation analyses between *phm>DHR51*-RNAi (1), *phm>FeCH*-RNAi, and *PPOX* data sets all had a weak to moderate positive correlation (Figure 3-11BCD). Since loss-of-*FeCH* and loss-of-*PPOX* reduced cellular heme levels, this data suggested that loss-of-*DHR51* may also reduce cellular heme levels within the RG. One unexpected result was the weak to moderate correlation between *phm>FeCH*-RNAi and *PPOX*. I would have expected a much higher correlation since both should only disrupt heme biosynthesis. A weak to moderate correlation could indicate that there were additional effects from either GAL4 or the RNAi, but the RGs were collected at different times by different people which could also introduce variation. Also, the strength of the correlation between *phm>FeCH*-RNAi and *PPOX* differed based on the Pearson and Spearman's rank correlation. Differences in the strength of the correlation could arise for various reasons. Some assumptions about the data for the Pearson correlation may not be valid, like if the data were not normally distributed. The Pearson correlation is also more sensitive to outliers in data since it accounts for gene expression values (as opposed to just ranking the genes 1 to *n* number of genes). Lastly, even with the positive trend in the data, that trend may not be linear, which would decrease the value of the Pearson correlation. *DHR51*-RNAi (1) tended to correlate more with *FeCH*-RNAi, but still correlated with *PPOX*. This may suggest that part of the correlation could be due to either the

UAS-GAL4 system or an RNAi phenomenon. However, since *DHR51*-RNAi (1) data set correlated with data sets that had low cellular heme levels, that does provide evidence that loss-of-*DHR51* may decrease cellular heme levels. In addition, DHR51 is a transcription factor that does regulate other cellular processes like ecdysone biosynthesis (discussed in Chapter 4), so a high correlation with *FeCH*-RNAi or *PPOX* was not expected.

Since *DHR51*-RNAi (1) in the PG correlated with *FeCH*-RNAi and *PPOX*-deficient RGs, I examined the expression of the heme biosynthetic genes. I also used *phm>Nos*-RNAi and *phm>spz5*-RNAi (which also reduced cellular heme levels) to determine how the heme biosynthetic genes generally responded to low cellular heme levels. There was a consistent response that the genes that encoded for the first three heme biosynthetic enzymes were upregulated, as well as *FeCH* (Figure 3-12A). *Alas* was upregulated the most, which provided support that *Alas* is likely rate-limiting in invertebrates, followed by *Pbgs*, which encodes the second enzyme, and lastly, *l(3)02640* and *FeCH* were upregulated the least. These genes were found to be upregulated in RGs as a result of *DHR51*-RNAi, with the important exception of *Alas* (Figure 3-12B). This suggested that loss-of-*DHR51* disrupted heme homeostasis, resulting in lower cellular heme levels. However, the degree that these genes were upregulated were lower compared to other low heme phenotypes, but this could indicate that loss-of-*DHR51* does not cause as strong of a reduction in cellular heme levels as loss-of-*FeCH* or loss-of-*PPOX*. This would be similar to *Alas* expression when heme levels are low, as *Alas* expression is not all or nothing, but gradually increases as heme levels lower. It is important to note that *Alas* expression is not increased (or only mildly increased), especially if loss-of-*DHR51* causes low cellular heme levels in the PG. If heme levels are low, *Alas* is typically upregulated, but my previous data suggested that *Alas* upregulation when heme levels were low was dependent on DHR51. So, if

heme levels are truly reduced in the PG due to loss-of-*DHR51*, this provides further support that DHR51 is required for *Alas* upregulation. The RNA-Seq data and qPCR of heme biosynthetic in *phm>DHR51*-RNAi RGs suggested that loss-of-*DHR51* disrupted heme homeostasis and reduced cellular heme levels. This provided evidence that DHR51 is acting as a heme sensor to maintain cellular heme levels.

The second approach to determine whether loss-of-*DHR51* reduced cellular heme levels was to measure heme levels directly. I used a method that measured total heme (free heme plus protein-bound heme) by applying high concentrations of oxalic acid and high temperatures to dissociate iron from the porphyrin ring (Morrison. 1965). I first measured heme in whole body larvae that expressed *DHR51*-RNAi. *act>DHR51*-RNAi (1) and (2) reduced cellular heme levels in whole body larvae, similar to *act>PPOX*-RNAi whole body larvae (Figure 3-15). This suggested that DHR51 is required to maintain heme homeostasis and loss-of-*DHR51* reduced cellular heme levels. It is not quite clear why *act>DHR51*-RNAi decreased whole body heme levels as DHR51 has not been reported to have expression outside of the nervous system (Sung, et al. 2009). However, this does not rule out very low expression for DHR51 in other tissues. As seen in *PPOX* mutant larvae, the gut and oenocytes also autofluorescence red, so these tissues must also have a heme sensor. Heme measurements in whole body larvae expressing *DHR51*-RNAi supported my hypothesis that DHR51 is required to maintain heme homeostasis. The mammalian heme sensor, Rev-erbα, also maintains heme homeostasis, although Rev-erbα works slightly differently. When heme levels are normal, Rev-erbα represses *PGC-1α*, an activator of *Alas1* expression, and when heme levels fall, Rev-erbα relieves its repression of *PGC-1α* (Wu, et al. 2009). Therefore, overexpression of Rev-erbα decreased heme levels in cell culture, while knocking down Rev-erbα increased heme levels in cell culture. Contrary to Rev-erbα, DHR51

may be responsible for upregulating *Alas* when heme levels fall and knocking down *DHR51* reduced heme levels.

After measuring heme levels in whole body larvae expressing *DHR51*-RNAi, I attempted to measure heme in BRG samples expressing PG *DHR51*-RNAi to determine whether DHR51 was required to maintain heme homeostasis in the RG. *phm>DHR51*-RNAi in BRG samples did not reduce heme levels, unlike *phm>PPOX*-RNAi (Figure 3-16). This contradicted *DHR51*-RNAi in whole body larvae, which resulted in lower heme levels. However, it seems plausible that the normal levels of heme in the brain could mask a reduction of heme in the RG. When examining the fluorescence ratio of *phm>DHR51*-RNAi BRGs, a low background fluorescence intensity was expected because loss-of-*DHR51* does not result in red autofluorescence. So, a reduced fluorescence ratio is dependent on low experimental fluorescence intensity, but the much larger brain could mask a reduction in the PG. This is in contract to *phm>PPOX*-RNAi samples that did have a lower fluorescence ratio because these samples had a high background fluorescence intensity due to the accumulation of red autofluorescent heme precursors. So, in *phm>PPOX*-RNAi samples, low heme levels could not be masked by normal heme levels in the brain.

To resolve the issue of the brain masking a reduction in heme levels, heme could be measured solely in RGs, but due to technical limitations, it may not be feasible for one person to dissect all the RGs necessary. The dissected tissues may not be able to be stored for too long at -80°C. For an anecdotal story, during my first attempt to measure heme in *phm>DHR51*-RNAi BRGs, my dissections were interrupted by Christmas vacation. When I returned and finished my dissections, and measured heme levels, every sample was indistinguishable from the others, including the *PPOX*-RNAi samples. From then on, I tried to keep the storage duration to a

minimum. In order to dissect even more RGs (easily over 1000 RGs in total compared to a several hundred BRGs), multiple people may need to be involved in the dissection, staging the larvae to a strict developmental time may need to be relaxed in order to collect more larvae per day, the experiment may need to be performed in duplicate (which may be an issue with *DHR51*-RNAi (2) because I find that line generally has a higher variation between samples), or only test one *DHR51*-RNAi line. Unfortunately, I was unable to quantify heme levels in RGs due to the listed difficulties.

For my heme measurements, I analyzed the data using two methods. The standard analysis method for heme measurements is to compare the fluorescence from the samples to a hemin standard curve to calculate a heme concentration and normalize the concentration to the amount of protein present in each sample. However, only once did this method show a reduction in heme levels and that was when I measured heme in *act>PPOX*-RNAi and *act>DHR51*-RNAi larvae (compare Figure 3-15D to Figures 3-14EI and 3-16B). All other measurements showed no reduction in heme, including early tests when heme was measured in *PPOX* and *act>PPOX*-RNAi larvae. Although this analysis method did not reliably work for me, it did for another lab member, Qiuxiang Ou, when she measured heme levels in *tub>Nos*-RNAi and *tub>spz5*-RNAi whole body larvae (*tub* is *tubulin-GAL4*, a whole body *GAL4* driver) (both *Nos*-RNAi and *spz5*-RNAi reduced cellular heme levels). Qiuxiang used the same method of high concentrations of oxalic acid and heat to measure heme levels, but our exact protocols differed slightly. Qiuxiang did identify decreased heme levels in *tub>Nos*-RNAi and *tub>spz5*-RNAi whole body larvae and that the standard heme measurement analysis worked in *Drosophila* larvae (Ou, unpublished). Also, by comparing my concentrations of heme per amount of protein to Qiuxiang's data, our numbers differed considerably. The analysis that I found to be much more

reliable is what I called the fluorescence ratio, which compared the experimental fluorescence to the background fluorescence. A low fluorescence ratio represents a sample with low cellular heme levels, while a high fluorescence ratio represents a sample with high cellular heme levels. One downside of the fluorescence ratio is that it cannot be used to quantify the amount of heme, the fluorescence ratio only determines whether samples have lower heme than a control.

Given that DHR51 seemed to maintain heme homeostasis and loss-of-*DHR51* decreased heme levels, I attempted to determine whether the *phm>DHR51*-RNAi developmental defects were due to a lack of cellular heme, ultimately impairing ecdysone production as cytochrome P450 enzymes would be non-functional without heme. I planned to feed to *phm>DHR51*-RNAi larvae hemin in an attempt to rescue their developmental defects. However, hemin feeding experiments had not been done in *Drosophila* and it was unknown whether hemin would be transported to the PG. Ami Soni and I demonstrated that hemin feeding was about to rescue *phm>PPOX*-RNAi larvae, which suggested that hemin was indeed transported to the PG and that hemin was capable of rescuing larvae with heme-deficient RGs (Figure 3-17). However, when hemin was fed to *phm>DHR51*-RNAi larvae, hemin was unable to rescue the developmental phenotypes (Figure 3-18). The inability for hemin to rescue *phm>DHR51*-RNAi larvae is likely due to the impaired expression of the ecdysteroidogenic genes (which will be discussed next chapter), so even if heme levels were restored, there would still be a reduced number of cytochrome P450 enzymes to utilize the heme. Thus, ecdysone would not be produced and the larvae would still have developmental defects.

3.3.5 Speculation on the heme sensor

I have provided evidence that supports the hypothesis that DHR51 acts as a heme sensor in the PG, whereby DHR51 aids in *Alas* upregulation when heme levels are low and helps to

maintain heme homeostasis. Further experiments are needed to confirm this hypothesis and will be discussed in Chapter 5.3. One experiment is to perform a chromatin immunoprecipitation of DHR51 to identify direct target genes of DHR51 and determine whether DHR51 DNA binding changes between levels of normal heme compared to low heme. There is still a possibility that E75, the homolog of Rev-erbα, acts as a heme sensor. Initially, I tested *E75*-RNAi in a *PPOX* mutant background and the resulting RGs still accumulated red autofluorescent heme precursors (data not shown). However, with the RNA-Seq data, *E75* expression was correlated to heme levels, similar to how E75 protein levels were correlated with heme levels (Reinking, et al. 2005). *E75* was downregulated in *FeCH*-RNAi RGs by 9.3-fold, *spz5*-RNAi RGs by 6.3-fold, *Nos*-RNAi RGs by 4.2-fold, *PPOX* RGs by 5.5-fold, and *DHR51*-RNAi (1) RGs by 6.2-fold. I will note that it is interesting the *E75* was downregulated in response to *DHR51*-RNAi (1), which could be a further indicator that cellular heme levels are indeed low, however, in mammals, NR2E3 directly regulates Rev-erbα expression, so DHR51 could potentially regulate *E75* in *Drosophila* (Haider, et al. 2009). If E75 were to function as a heme sensor, E75 would repress *Alas* expression when heme levels are replete because *E75* expression correlated with heme levels, and when heme levels drop, E75 would become unstable and relieve its repression of *Alas*. If this were the case, RNAi against *E75* in a low heme background would be expected not to affect *Alas* expression because *E75* expression was already decreased. A relatively easy experiment to test this hypothesis would be to use *E75*-RNAi in a wild type background and measure *Alas* expression. If E75 functions as a heme sensor as described, *Alas* expression should be increased even though heme levels are normal.

Is there a possibility that DHR51 and E75 could work together? Since nuclear receptors tend to form dimers, it would be possible for DHR51 and E75 to form a heterodimer, and there is

evidence that this occurs. While NR2E3 can form homodimers, NR2E3 is also capable of forming a heterodimer with Rev-erbα (Roduit, et al. 2009; Cheng, et al. 2004). A similar interaction was recently demonstrated in *Drosophila*. First, DHR51 and E75 were found to both be involved in regulating *period* and bound to similar promoter regions of *period* (Jaumouille, et al. 2015). While DHR51 and E75 synergistically enhanced *period* expression, E75 decreased DHR51 binding to *period*. The authors claimed that E75 enhanced DHR51 turnover which could increase transcription (Perissi and Rosenfeld. 2005). Later, DHR51 and E75 were found to physically interact with one another (Rabinovich, et al. 2016). The interaction between DHR51 and E75 was sensitive to nitric oxide (NO), where NO disrupts the interaction between DHR51 and E75, similar to how NO disrupts the interaction between E75 and DHR3 (Reinking, et al. 2005; Caceres, et al. 2011). This could mean that NO acts through E75 rather than DHR51 since E75 is common to the interaction between E75 and DHR51 and E75 and DHR3. Also, NO is known to regulate E75 activity by binding to the heme cofactor and while NO does seem capable of binding to the heme cofactor of DHR51 *in vitro*, that has no known physiological role (Reinking, et al. 2005; de Rosny, et al. 2008)

NO is synthesized from Nos (nitric oxide synthase) and as I mentioned previously, *phm>Nos*-RNAi reduced cellular heme levels in the RG, caused red autofluorescence in the RG, and larvae were L3 arrested (Caceres, et al. 2011). However, there was always debate what the actual phenotype of loss-of-*Nos* was because other *Nos* knockdown lines had no aberrant phenotypes. *Nos* was investigated by a previous Master's student in the King-Jones lab, Pendleton Cox, who found that the reduced heme phenotype in *Nos*-RNAi was likely due to an off-target effect of *Nos*-RNAi. However, Pendleton Cox also found what looked to be pulses of NO being produced around 16 to 24 hours after the L2/L3 molt and 40 to 44 hours after the

L2/L3 molt. These NO pulses are around the time of the minor ecdysone pulses during the L3 stage and major ecdysone pulse that initiates metamorphosis. Even if *Nos*-RNAi does not disrupt heme production, the pulses of NO could regulate the interaction between DHR51 and E75 to potentially somehow regulate heme in anticipation or in response to increased ecdysone production. DHR51's interaction with E75 and NO provides one layer of complexity to how DHR51 could function and whether this interaction is necessary for heme regulation is currently unknown. Other layers of complexity could come from post-translational modifications of DHR51. DHR51 shares a conserved phosphorylation and SUMOylation site with NR2E3, but these sites on DHR51 are not yet known to be relevant (Bates, et al. 2015). So, it is possible for DHR51 and E75 to work together; whether DHR51 and E75 actually work together to regulate heme homeostasis is unknown. It does provide an intriguing possibility, but more evidence is necessary to support these speculations. It still remains that DHR51 is likely involved with heme homeostasis, as multiple methods suggested that loss-of-*DHR51* reduced cellular heme levels and DHR51 remains the prime candidate for the heme sensor in the *Drosophila* PG.

3.4 Figures

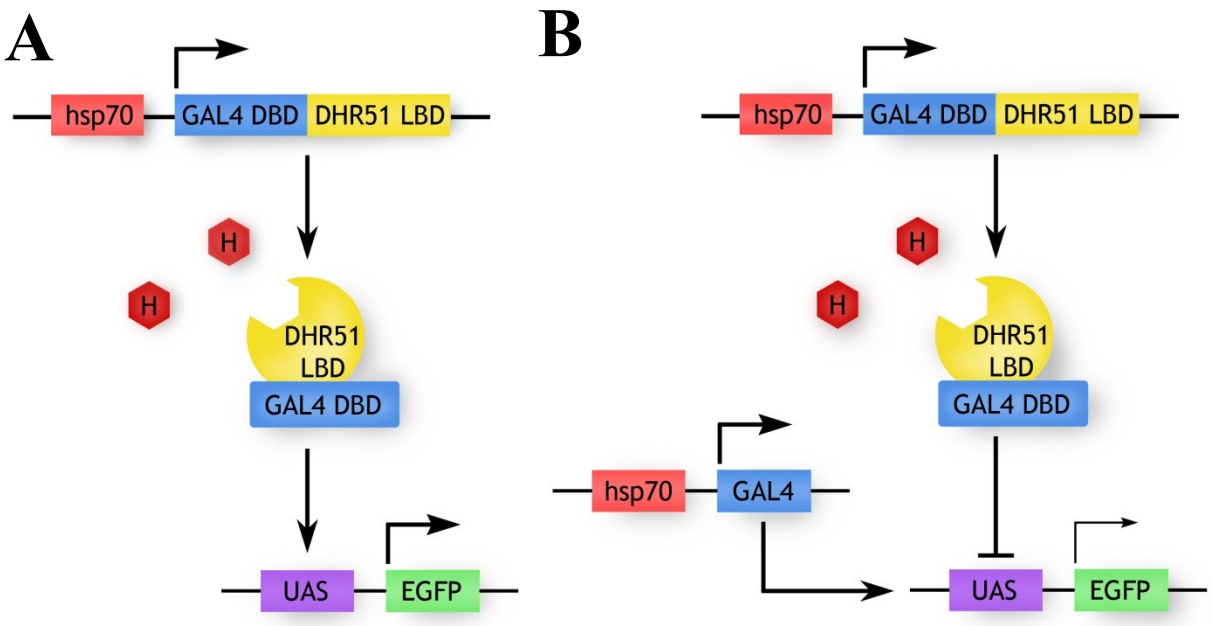

Figure 3-1. My hypothesis for how the DHR51 ligand trap system could work when cellular heme levels are low. A) The DHR51 ligand trap fusion protein acting as an activator. hsp70 = heat shock protein 70 promoter. DBD = DNA-binding domain. LBD = ligand binding domain. UAS = upstream activation sequence. EGFP = enhanced green fluorescent protein. H = heme. The ligand trap transgene is expressed after heat shock and can bind to the UAS promoter of a reporter gene (EGFP in this case). Based on my hypothesis, the DHR51 ligand trap fusion protein is active when heme levels are low and the LBD is not bound to heme. This is also how the ligand trap system works in general but the ligand will vary. B) My setup to determine whether DHR51 is a repressor when unbound by heme. Wild type GAL4 is also expressed via heat shock and competes with the UAS promoter of the reporter gene with the DHR51 ligand trap fusion protein. If the DHR51 ligand trap fusion protein is bound by heme, the fusion protein would be inactive and more EGFP would be observed than when the DHR51 ligand trap fusion protein is unbound from heme.

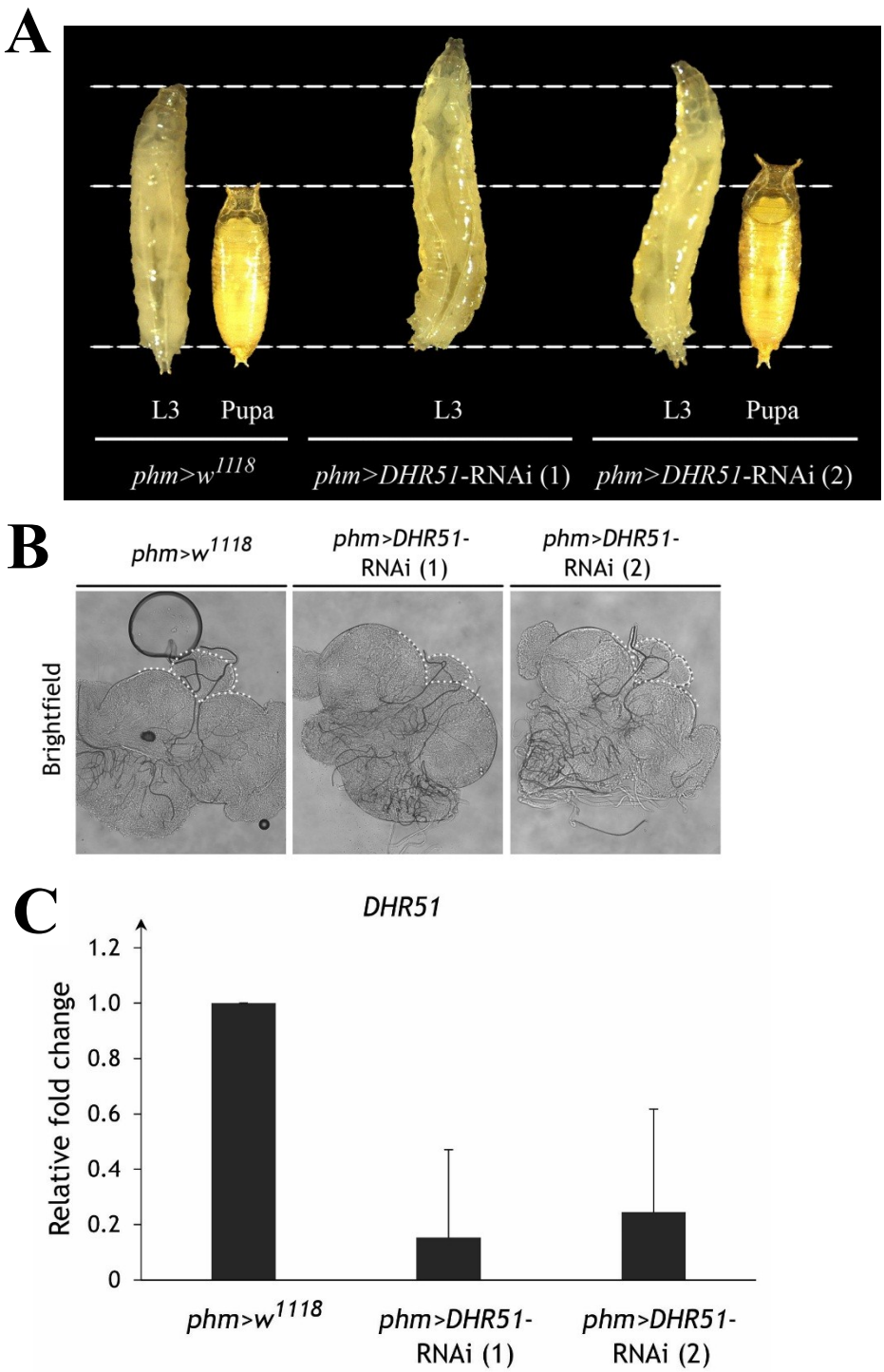

Figure 3-2. *phm>DHR51*-RNAi affected development. A) L3 larvae were imaged 5 days after egg laying. Pupae were imaged 9 days after egg laying. White dashed lines mark the length of control larvae and pupae. B) Brain-ring glands were examined with brightfield microscopy. Brain-ring glands were dissected from 5 day old larvae. Ring glands are outlined in white dotted lines. C) Ring glands were dissected from 44 hour post L2/L3 larvae. qPCR was used to quantify *DHR51* expression in *DHR51*-RNAi lines. *phm>* = *phm22-GAL4*. A Student's t-test was used to determine significance relative to *phm>w*^{1118}.

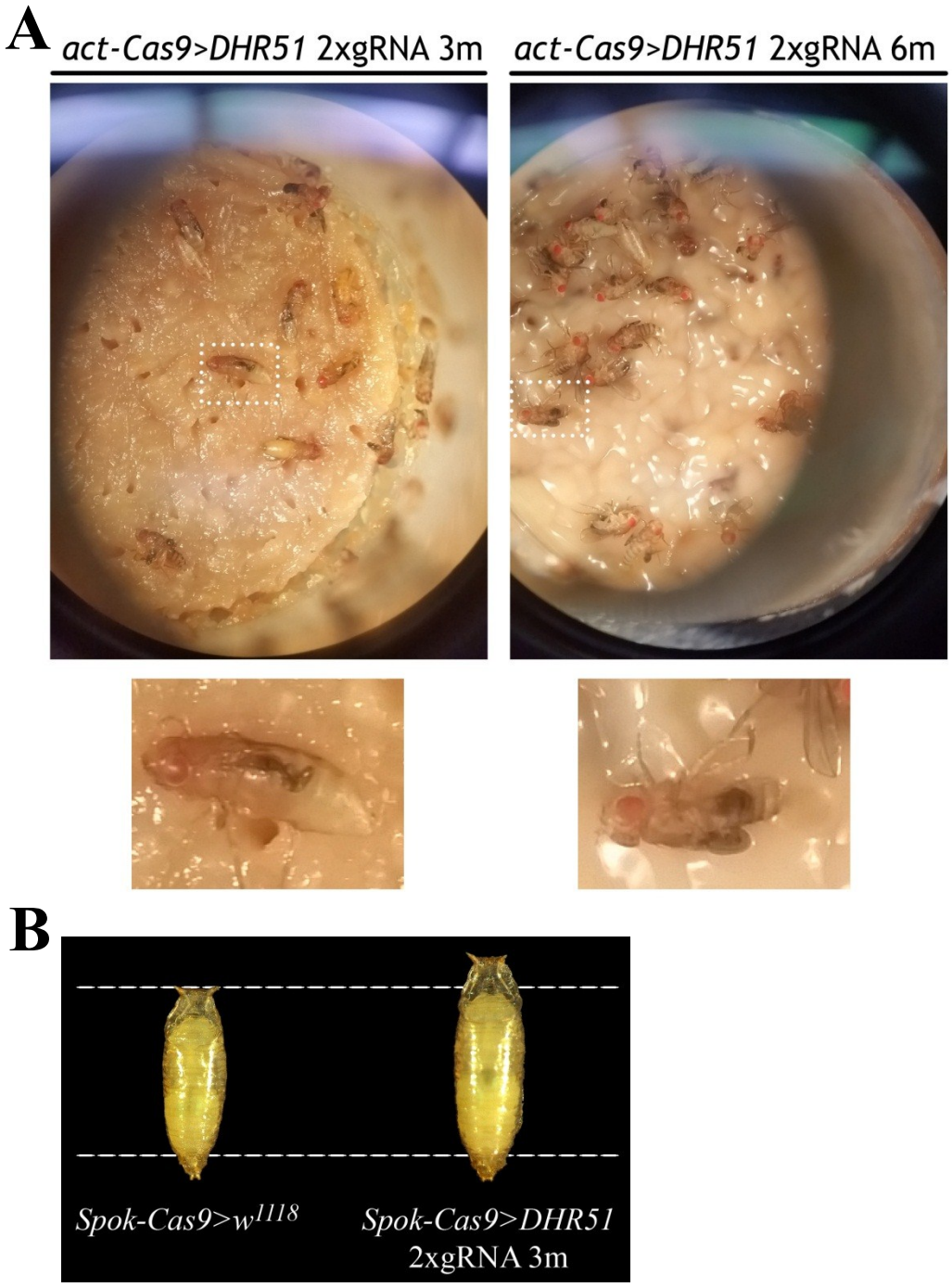

Figure 3-3. *DHR51* 2xgRNA caused developmental defects that phenocopied *unf*^{XI} adults and *phm>DHR51*-RNAi (2) larvae. A) Ubiquitous expression of *Cas9* with the *actin* (*act*) promoter. Adults eclosed, but got stuck in the media shortly after, likely due to motor defects. Many flies had characteristic *unf* mutant wings that failed to expand (see the zoomed in image below the main image. The zoomed in fly is outlined with a dotted white line). *act-Cas9>w*^{1118} flies do not get stuck in the media. B) *Cas9* was specifically expressed in the prothoracic gland with the *Spookier* (*Spok*) promoter. *Spok-Cas9>DHR51* 2xgRNA 3m resulted in a developmental delay and enlarged pupae. No abnormal phenotype was detected in *Spok-Cas9>DHR51* 2xgRNA 6/12m animals.

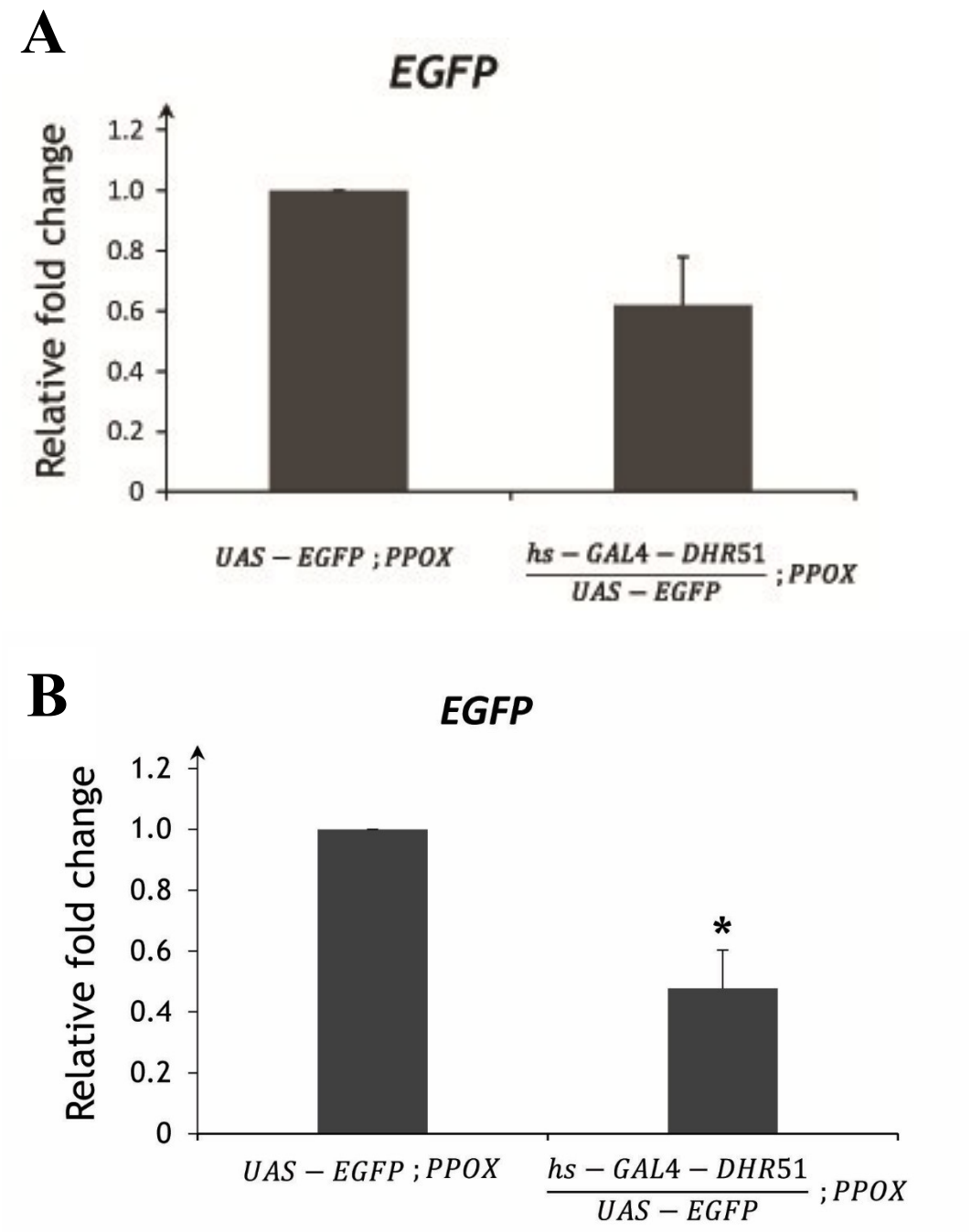

Figure 3-4. The DHR51 ligand trap fusion protein did not activate *EGFP* expression under low cellular heme levels. A) 10 day old arrested L3 were heat shocked for 35 min at 37°C and allowed to recover for 4-5 hours. RNA was extracted from brain-ring gland complexes. B) 10 day old arrested L3 were heat shocked for 1 hour at 37.5°C and allowed to recover for 4-5 hours. RNA was extracted from ring gland samples. *EGFP* expression was measured with qPCR. *hs-GAL4-DHR51* is the *DHR51* ligand trap. *hs* = heat shock. *UAS-EGFP* was heterozygous in all experiments. *PPOX* is the #13702 mutant allele. * = P-value < 0.05. A Student's t-test was used to determine significance relative to *UAS–EGFP ; PPOX*.

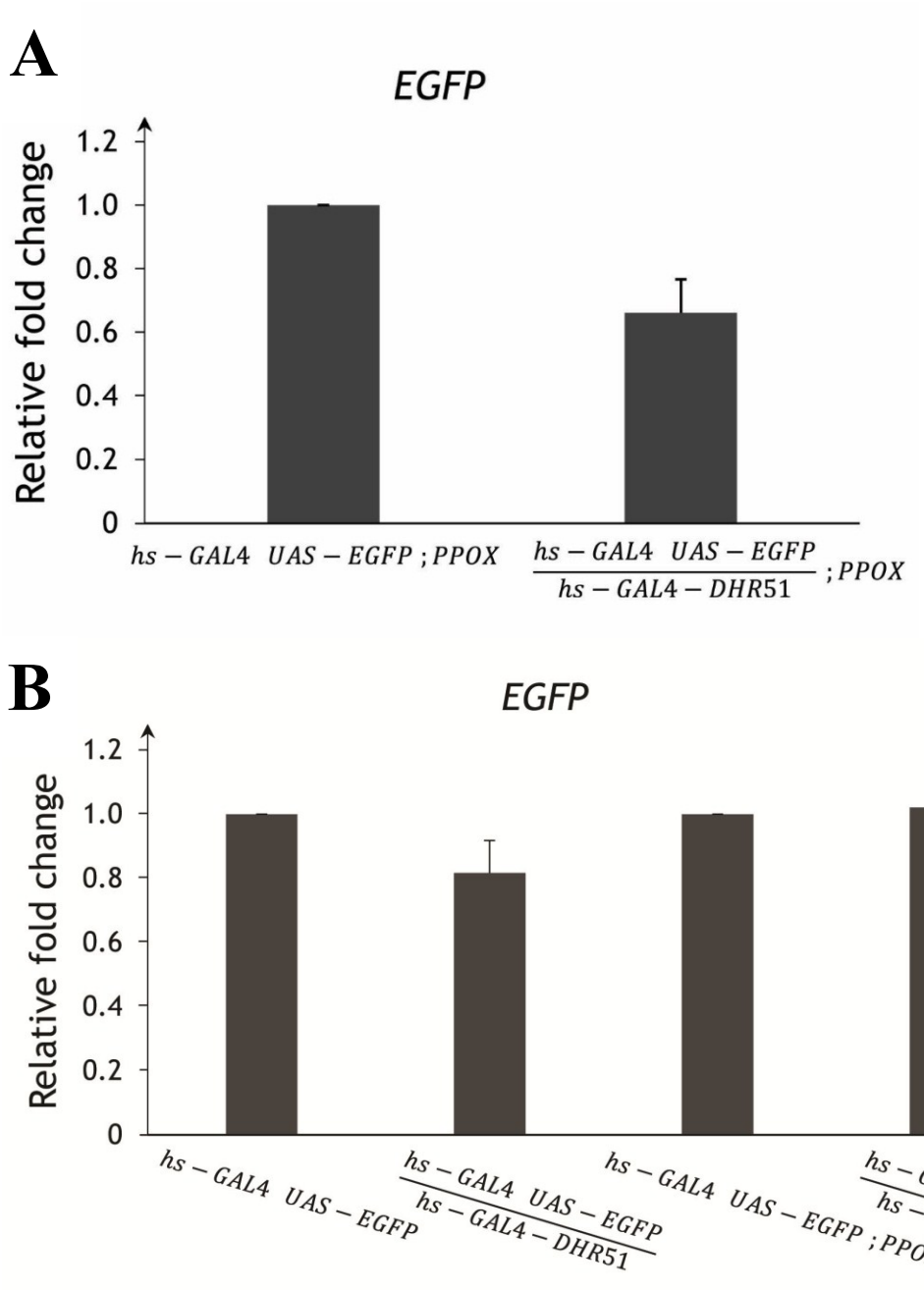

Figure 3-5. The DHR51 ligand trap fusion protein did not repress *EGFP* under low cellular heme levels. A) Arrested 9 day old L3 larvae were heat shocked for 1 hour at 37.5°C and allowed to recover for approximately 5 hours before the ring glands were dissected. A Student's t-test was used to determine significance relative to *hs–GAL4 UAS–EGFP ; PPOX*. B) Larvae were staged at the L2/L3 molt and heat shocked for 1 hour at 37.5°C 24 hours after staging. Larvae were then allowed to recover for 5 hours before ring glands were dissected. Samples were normalized to controls without the ligand trap. *EGFP* expression was measured with qPCR. *hs-GAL4-DHR51* is the *DHR51* ligand trap. *hs* = heat shock. *hs-GAL4 UAS-EGFP* was heterozygous in all experiments. A Student's t-test was used to determine significance relative to the control: *hs–GAL4 UAS–EGFP* or *hs–GAL4 UAS–EGFP ; PPOX*.

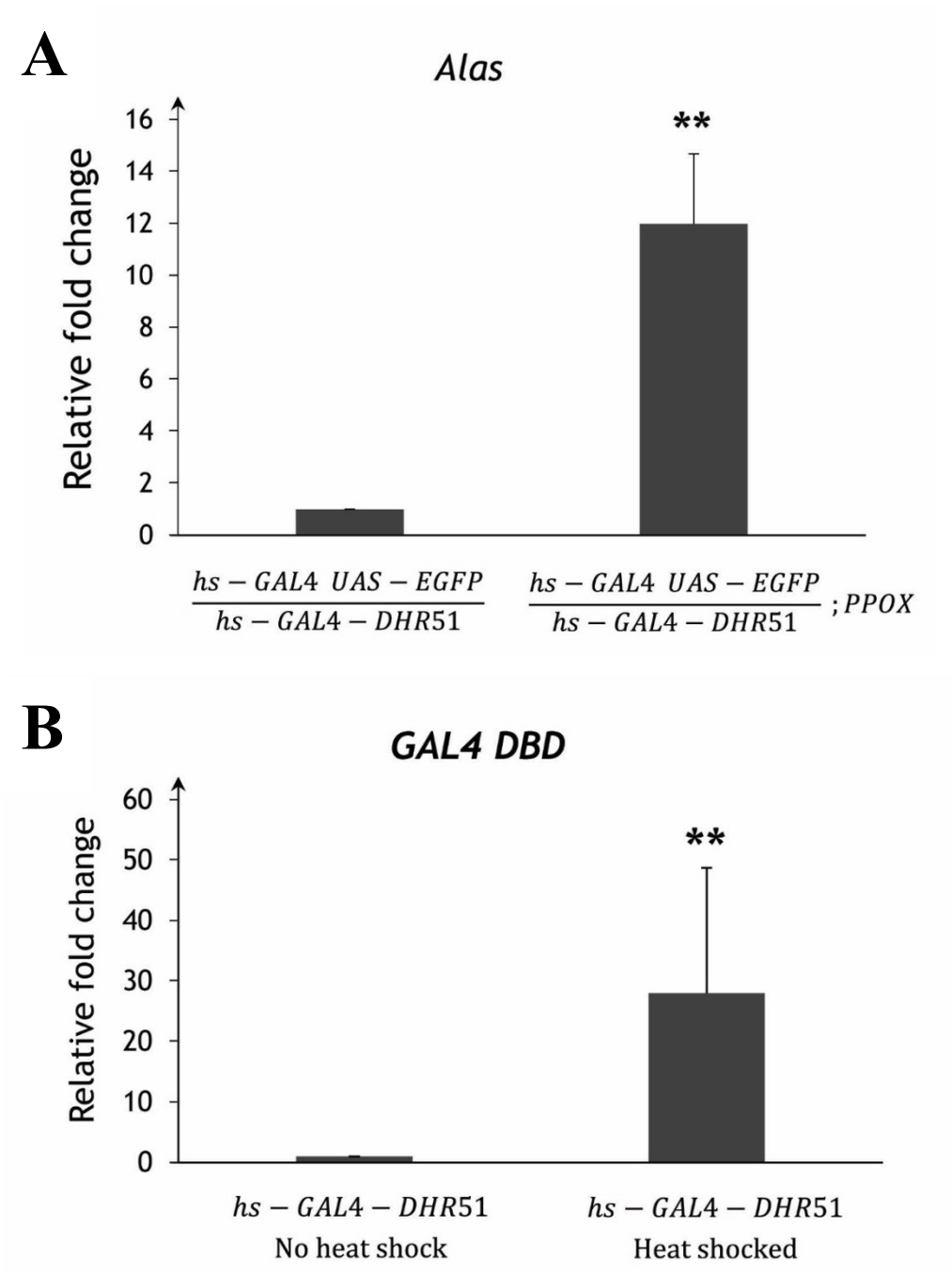

Figure 3-6. DHR51 ligand trap quality control ensured all fly lines were behaving properly. A) qPCR was used to determine that *Alas* expression was induced to confirm the presence of the *PPOX* mutation. RNA was extracted from ring glands from larvae 30 hours after the L2/L3 molt. A Student's t-test was used to determine significance relative to *hs–GAL4 UAS–EGFP / hs–GAL4–DHR51*. B) qPCR was used to determine that the *DHR51* ligand trap was being expressed. Primers were designed to target the *GAL4* DNA-binding domain sequence. Larvae were heat shocked for 1 hour at 37.5°C and allowed to recover for 5 hours. *hs-GAL4-DHR51* is the *DHR51* ligand trap. *hs* = heat shock. ** = P-value < 0.01. A Student's t-test was used to determine significance relative to the no heat shock control.

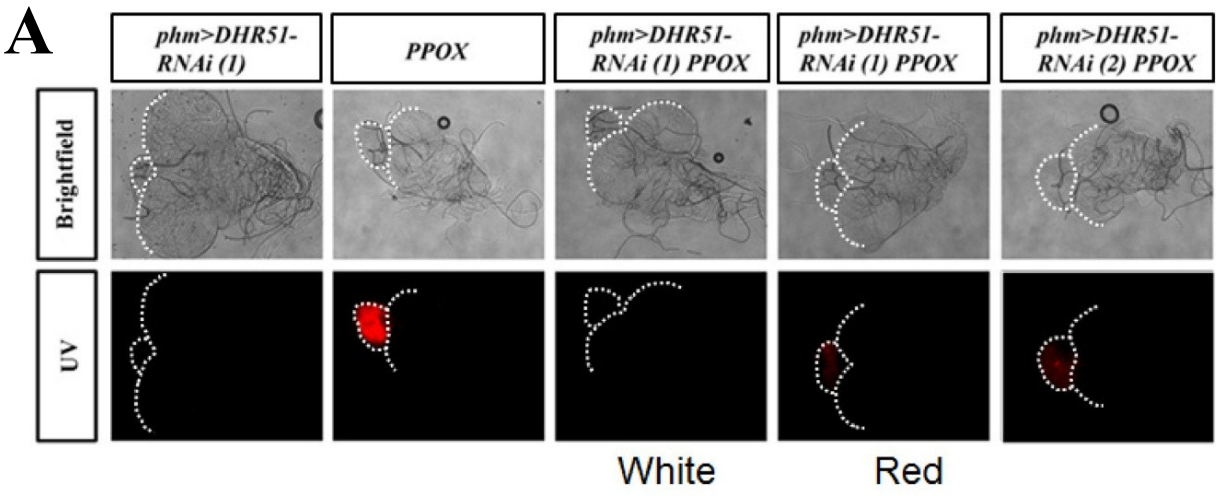

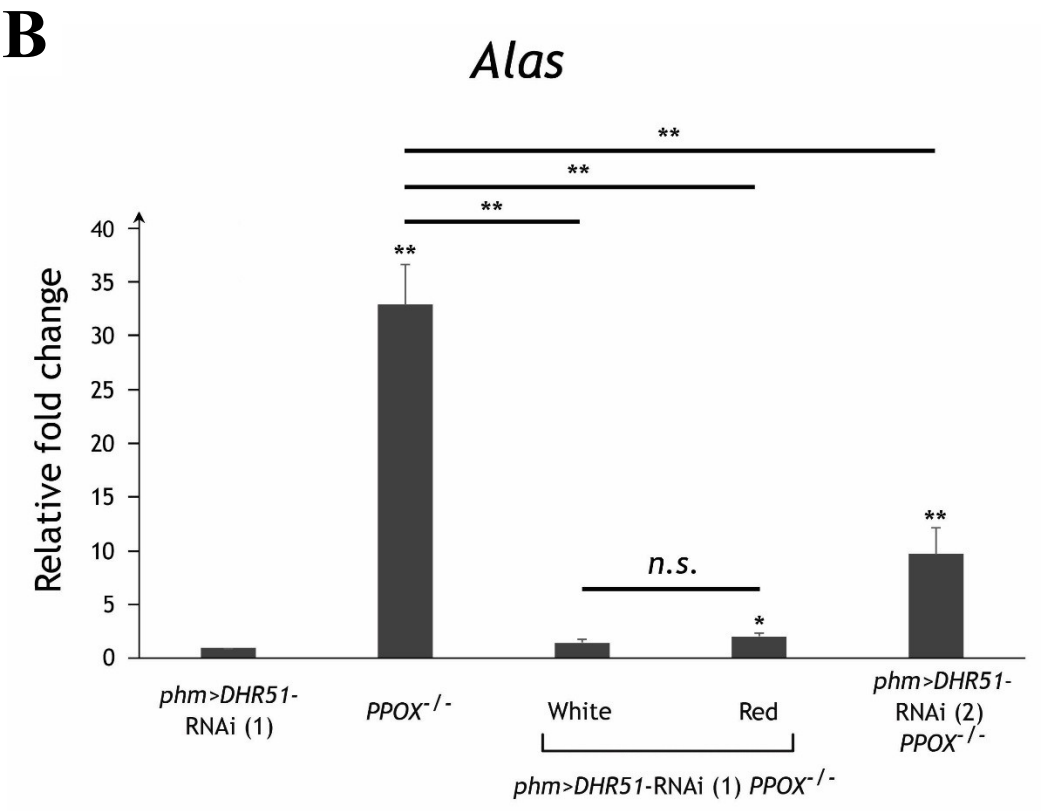

(Legend on next page)

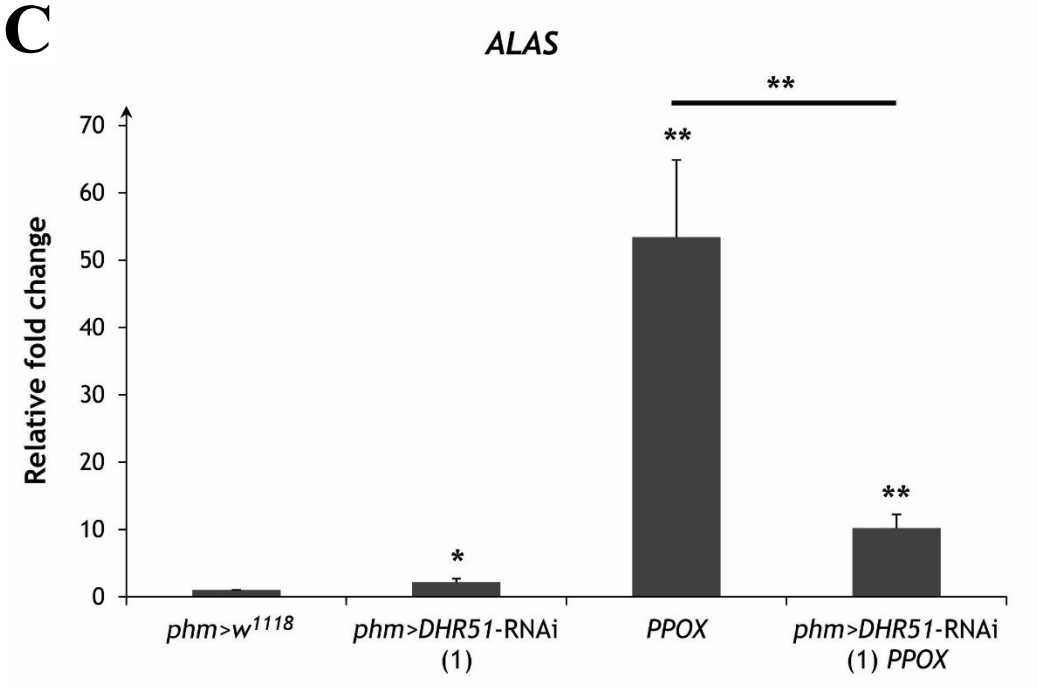

Figure 3-7. *Alas* upregulation in response to low cellular heme levels was dependent on DHR51. A) Brain-ring gland complexes from 9 day old arrested larvae viewed with a confocal microscope. Ring glands are outlined in a dotted white line, as well as the top of the brain hemispheres. Heme precursors autofluoresce red when exposed to UV light. B) *Alas* expression was measured in ring glands from 9 day old arrested larvae via qPCR. *Alas* expression is normalized to *phm>DHR51*-RNAi (1). "White" ring glands refer to *phm>DHR51*-RNAi (1) *PPOX* ring glands that had no detectable autofluorescence, while "red" ring glands did have detectable autofluorescence. C) *Alas* expression was measured in ring glands from 44 hour post L2/L3 molt larvae. *Alas* expression in *PPOX* samples were normalized to w^{1118} samples (not *phm>*w^{1118} samples). *phm>* = *phm22-GAL4*, which expresses *GAL4* specifically in the prothoracic gland of the ring gland. * = P-value < 0.05. ** = P-value < 0.01. A Student's t-test was used to determine significance. Asterisks above the columns are relative to the *phm>*w^{1118} control. Asterisks above the bars are relative between the two samples at the end of the bar. *n.s.* = not significant.

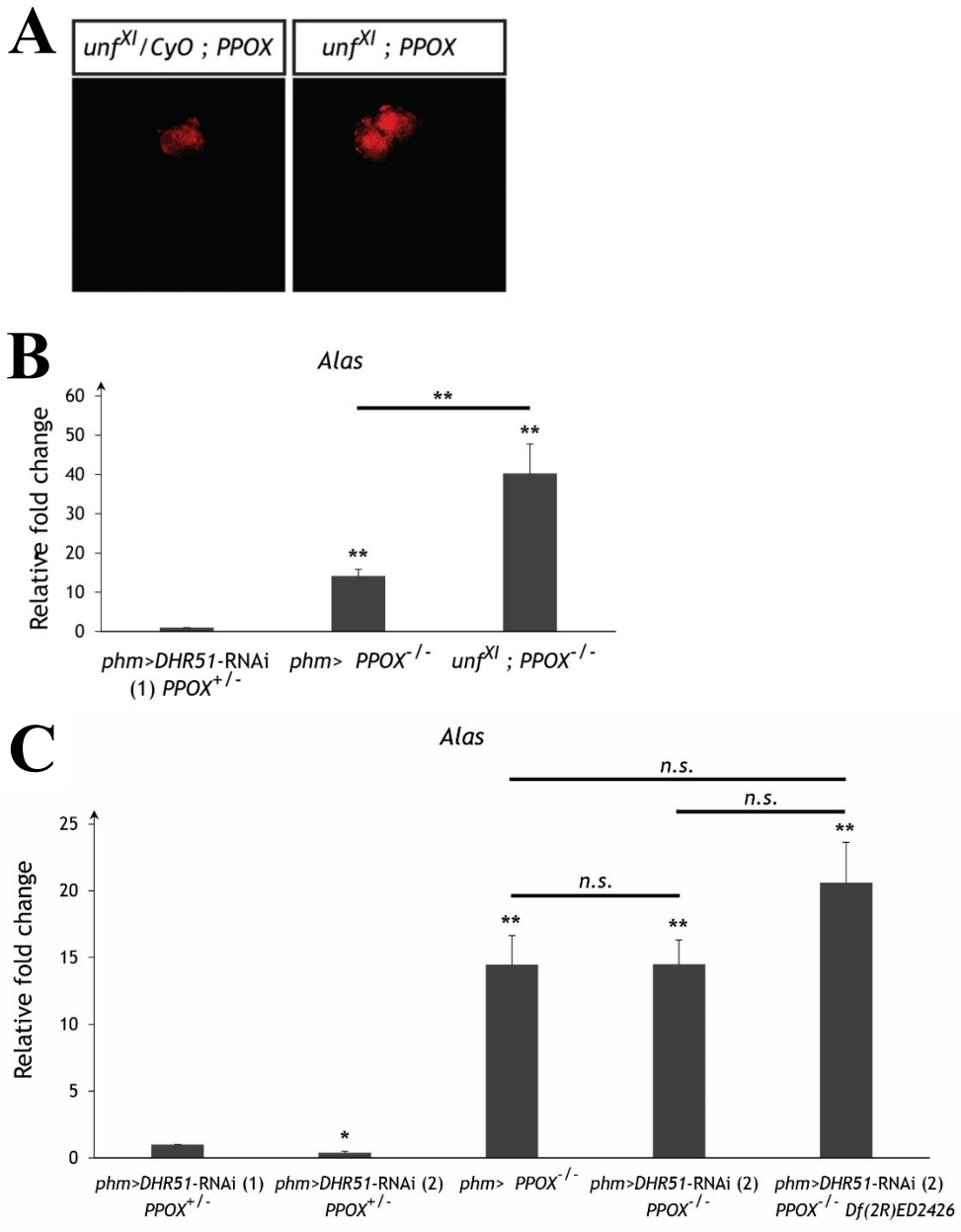

Figure 3-8. The *unf*^{XI} mutation did not attenuate *Alas* upregulation in a low heme background. A) Ring glands from 9 day old *PPOX* larvae viewed under UV light still autofluorescence red when a *DHR51* mutation (*unf*^{XI}) is present. B) *Alas* was upregulated in *unf*^{XI} ; *PPOX* ring glands from larvae 9 days after egg laying. qPCR values are normalized to *phm>DHR51*-RNAi (1) *PPOX*$^{+/-}$ heterozygotes. *PPOX* mutant ring glands express *phm22-GAL4* (*phm*) present as a control from another experiment (Figure 8B). C) *Alas* expression in ring glands from 9 day old larvae. *phm>DHR51*-RNAi (2) larvae are delayed, so they were dissected 6 days after egg laying for a reference. *Alas* expression was measured via qPCR. *Df(2R)ED2426* is a deficiency line that covers *DHR51* (FlyBase ID: FBab0033717). * = P-value < 0.05. ** = P-value < 0.01. A Student's t-test was used to determine significance. Asterisks above the columns are relative to the *phm>DHR51*-RNAi (1) *PPOX*$^{+/-}$ control. Asterisks above the bars are relative between the two samples at the end of the bar. *n.s.* = not significant.

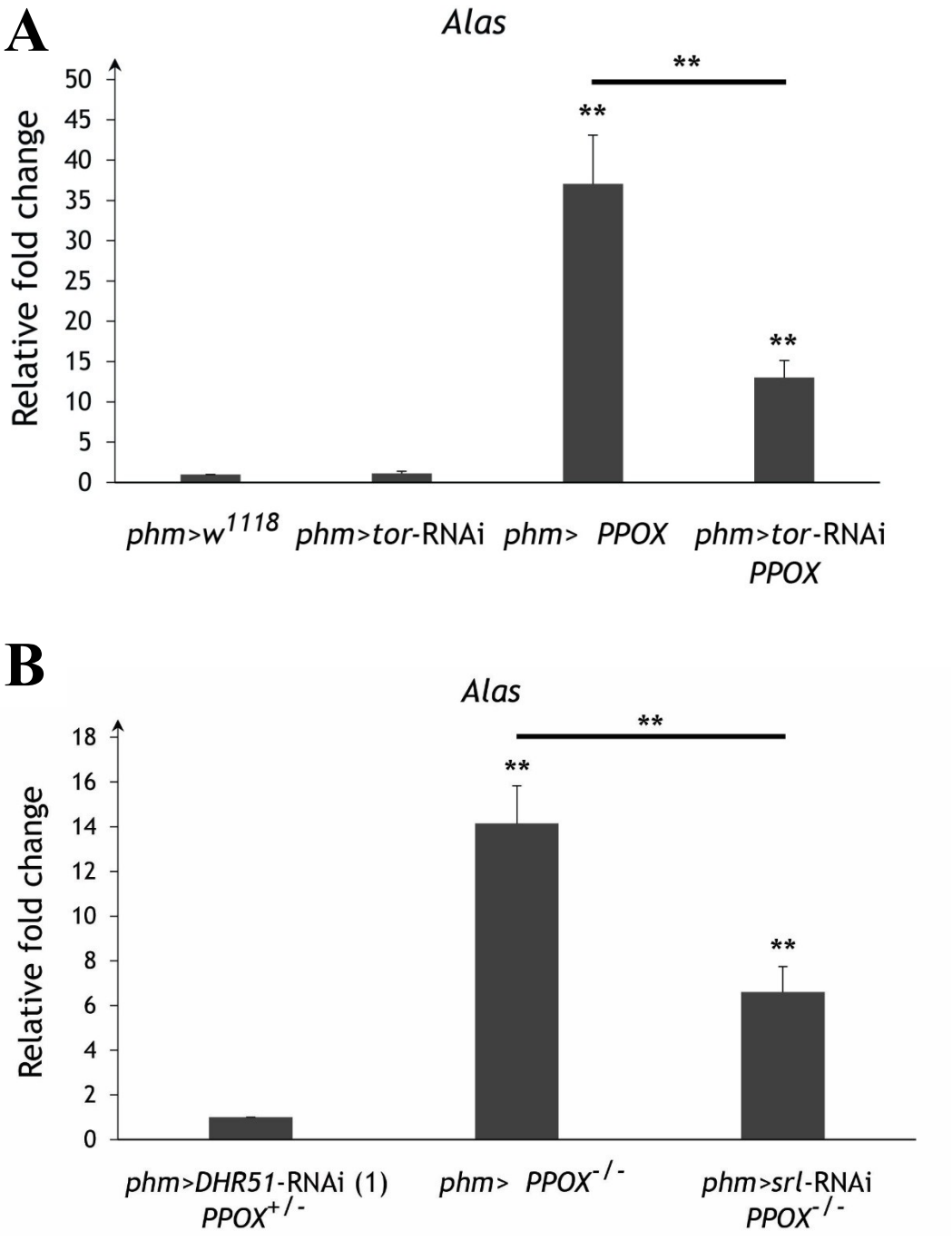

Figure 3-9. *torso*- and *spargel*-RNAi attenuated *Alas* upregulation in a *PPOX* mutant background. A) *Alas* expression was measured via qPCR in ring glands that were dissected from larvae 44 hours post L2/L3 molt. *tor* = *torso*. B) *Alas* expression was measured via qPCR in ring glands that were dissected from larvae 9 days after egg laying. *Alas* expression was normalized to *phm>DHR51*-RNAi (1) $PPOX^{+/-}$ heterozygotes. *srl* = *spargel*. *phm* = *phm22-GAL4*. ** = P-value < 0.01. A Student's t-test was used to determine significance. Asterisks above the columns are relative to $phm>w^{1118}$ or *phm>DHR51*-RNAi (1) $PPOX^{+/-}$. Asterisks above the bars are relative between the two samples at the end of the bar.

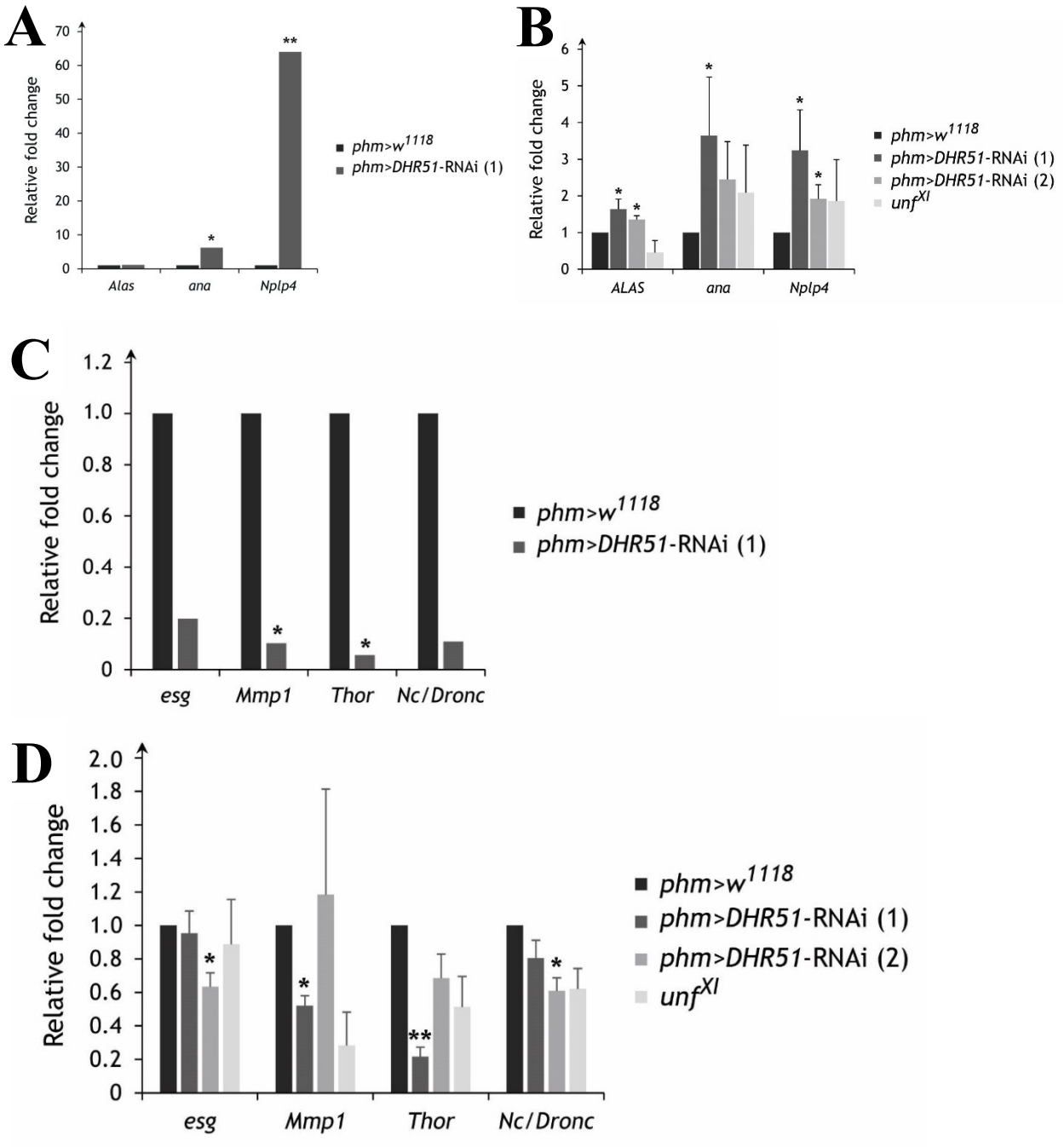

Figure 3-10. qPCR validation of *DHR51*-RNAi (1) RNA-Seq results. A) Selected upregulated genes as a result of *phm>DHR51*-RNAi (1) ring glands from larvae 44 hours post L2/L3 molt. Results are from the RNA-Seq. *Alas* was included out of interest. B) qPCR validation in brain-ring glands from larvae 44 hours post L2/L3 molt. unf^{XI} was normalized to the appropriate w^{1118} control. C) Selected downregulated genes from the RNA-Seq data. D) qPCR validation of RNA-Seq data with brain-ring glands from larvae 44 hours post L2/L3 molt. * = P-value < 0.05. ** = P-value < 0.01. *Alas = aminolevulinate synthase*. *ana = anachronism*. *Nplp4 = neuropeptide-like precursor 4*. *esg = escargot*. *Mmp1 = matrix metalloproteinase 1*. *Nc*/*Dronc = death regulator Nedd2-like caspase*. *phm = phm22-GAL4*. A Student's t-test was used to determine significance relative to the $phm>w^{1118}$ control for the expression of each gene.

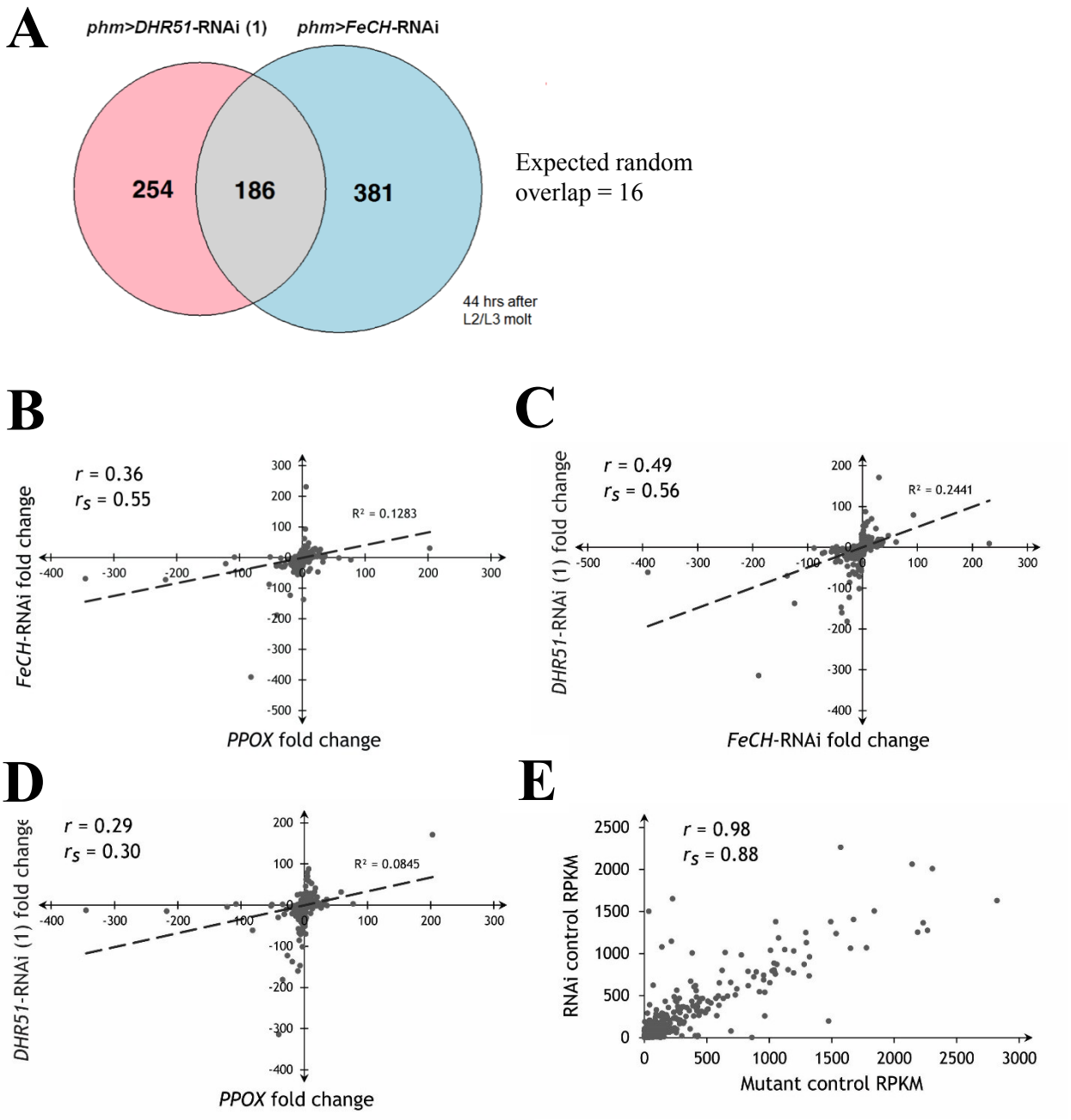

Figure 3-11. Correlation between *phm>DHR51*-RNAi (1) and lines that decrease cellular heme levels. A) Genes that are misregulated by greater than ± 3 fold in the ring gland from *phm>DHR51*- and *phm>FeCH*-RNAi larvae 44 hours after the L2/L3 molt. Genes were selected from the RNA-Seq data set. RPKM > 0.5. 186 genes are overlapping between these two RNAi lines that are similarly misregulated (either both upregulated or both downregulated). The overlap is approximately 12 times higher than random chance (16 randomly overlapping genes expected). P-value = 0.0. The P-value was calculated with a Chi-squared test between the observed and expected / random overlap given the number of genes recorded in the RNA-Seq (15771) in Microsoft Excel. B-D) Pearson correlation (r) and Spearman's rank correlation (r_s)

between *PPOX* mutants, *phm>FeCH*-RNAi, and *phm>DHR51*-RNAi (1) genes from the RNA-Seq data set. RPKM > 0.1. R^2 describes the fit of the trendline (dashed line) to the data. P-value << 0.01. E) Comparison of controls between two RNA-Seq experiments (one using RNAi lines and the other was an RNA-Seq of the *PPOX* mutant). RNAi control is *phm>*w^{1118} and mutant control is w^{1118}. 5 outliers have been removed from the graph for visibility but were used in the Pearson (r) and Spearman's rank (r_s) correlation analysis. P-value = 0. RPKM = Reads Per Kilobase of transcript per Million mapped reads. *phm* = *phm22-GAL4*. The P-values were calculated with a regression analysis in Microsoft Excel.

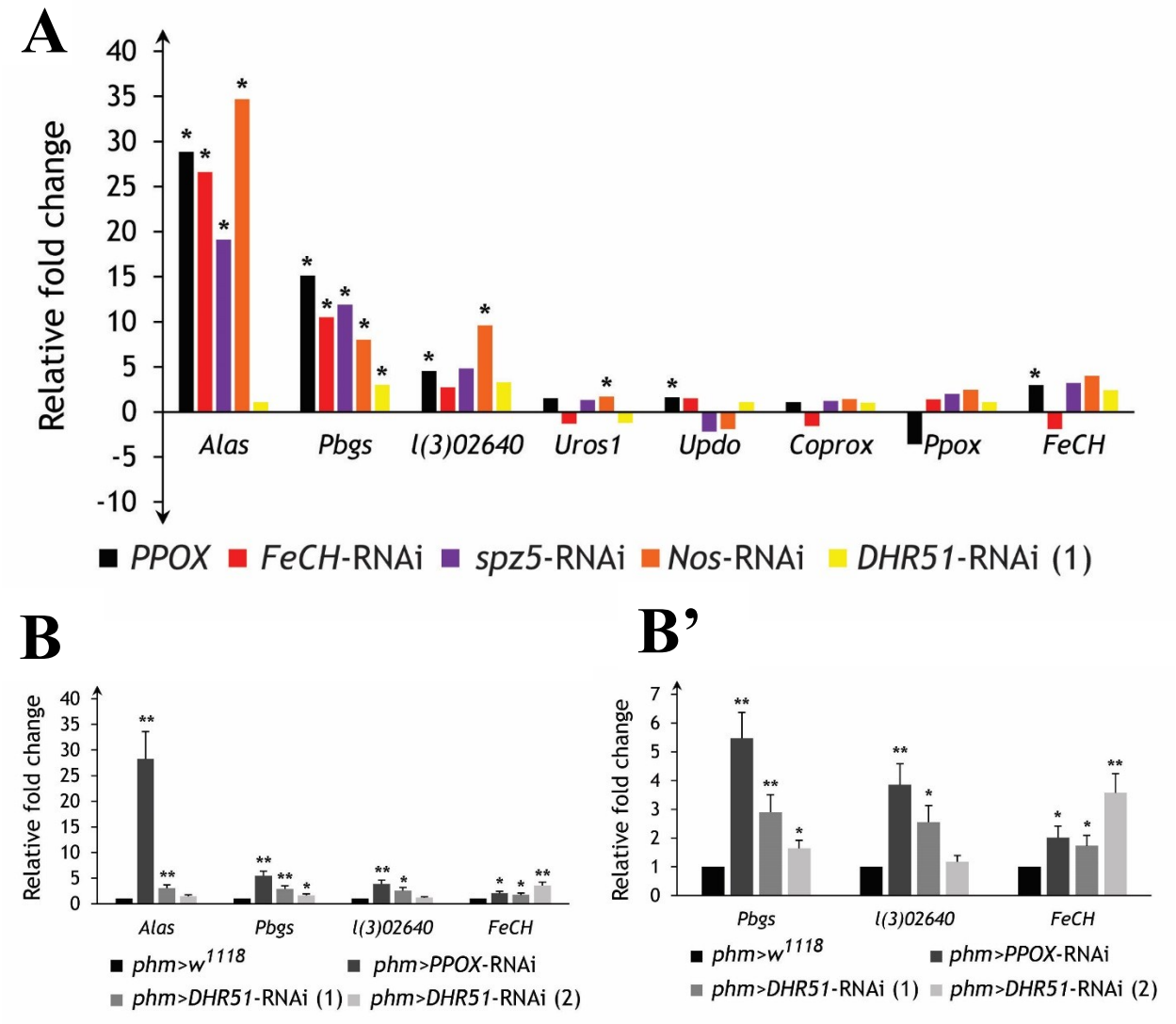

Figure 3-12. *Alas*, *Pbgs*, *l(3)02640*, and *FeCH* were upregulated when cellular heme levels were low. A) Results of all of the heme biosynthetic genes from the RNA-Seq. All genes are normalized to the appropriate control. All RNAi lines were expressed by *phm22-GAL4*. Negative values represent downregulation of the gene's transcript. B) qPCR of the four genes that are upregulated when cellular heme levels are low. Ring glands were dissected from larvae 68 hours after the L2/L3 molt. B' is a copy of B except that *Alas* has been removed so the graph is easier to view. *phm* = *phm22-GAL4*. * = P-value < 0.05. ** = P-value < 0.01. A Student's t-test was used to determine significance relative to the *phm*>w^{1118} control for the expression of each gene.

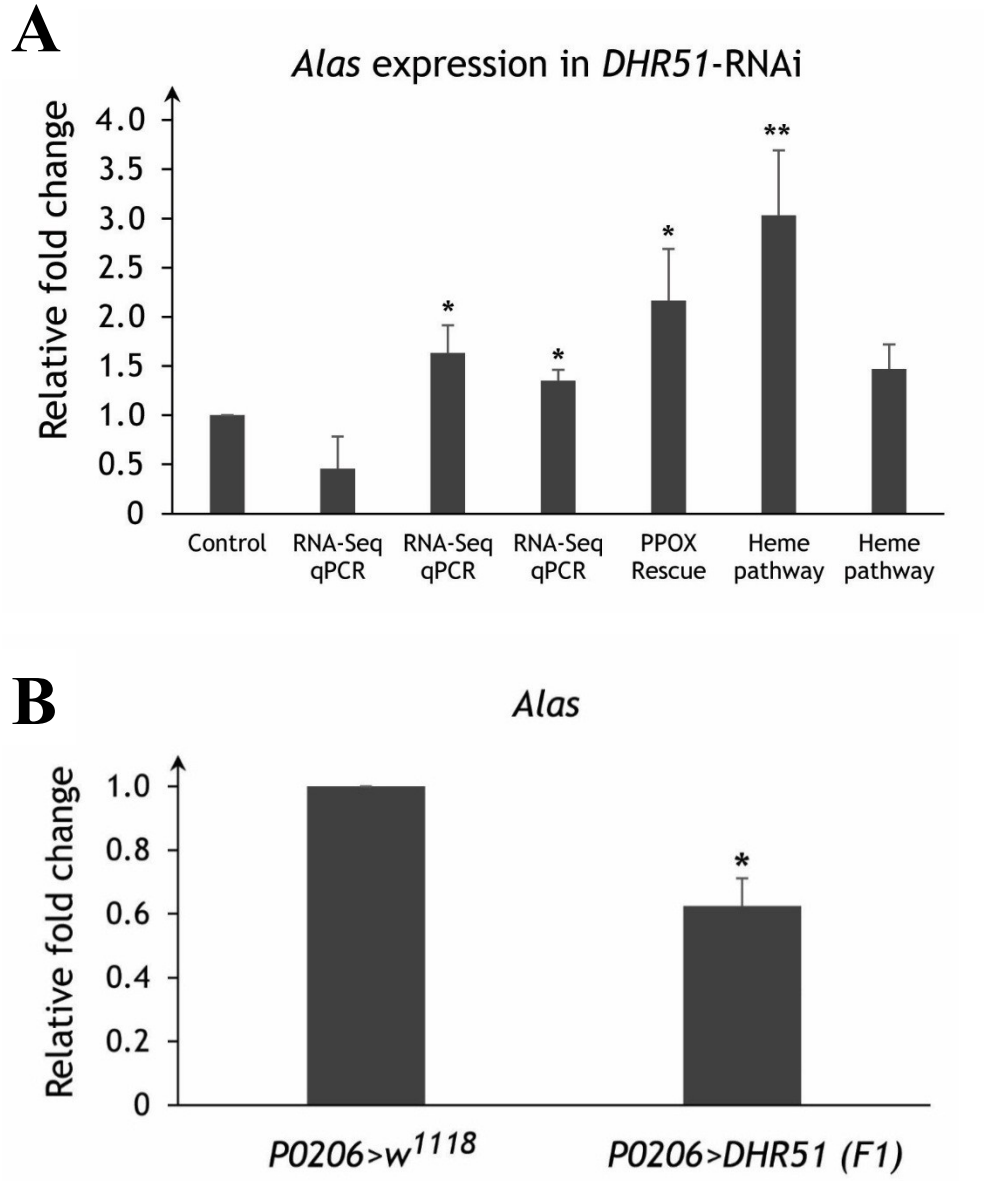

Figure 3-13. *DHR51*-RNAi increased *Alas* expression under normal conditions and *DHR51* overexpression decreased *Alas* expression. A) This graph was compiled from all the qPCR experiments mentioned on the X-axis. "RNA-Seq qPCR" is from the RNA-Seq validation qPCR in Figure 3-10B. The first bar is unf^{XI}, the second is *phm>DHR51*-RNAi (1), and the third is *phm>DHR51*-RNAi (2). Ring glands were collected from larvae 44 hours post L2/L3 molt. "*PPOX* Rescue" is from Figure 3-7C, ring glands were collected from *phm>DHR51*-RNAi (1) larvae 44 hours post L2/L3 molt. "Heme pathway" is from the experiment in Figure 3-12B. This first column is *phm>DHR51*-RNAi (1) and the second column is *phm>DHR51*-RNAi (2). For this, ring glands were dissected from larvae 68 hours post L2/L3 molt. Ring glands for the control were either dissected from $phm>w^{1118}$ or w^{1118} larvae. B) Brain-ring glands were dissected from larvae 24 hours after the L2/L3 molt. *DHR51* cDNA was overexpressed with the *P0206* ring gland *GAL4* driver. *DHR51 (F1)* was obtained from Dr. Steven Robinow. * = P-value < 0.05. ** = P-value < 0.01. A Student's t-test was used to determine significance relative to "Control" or $P0206>w^{1118}$.

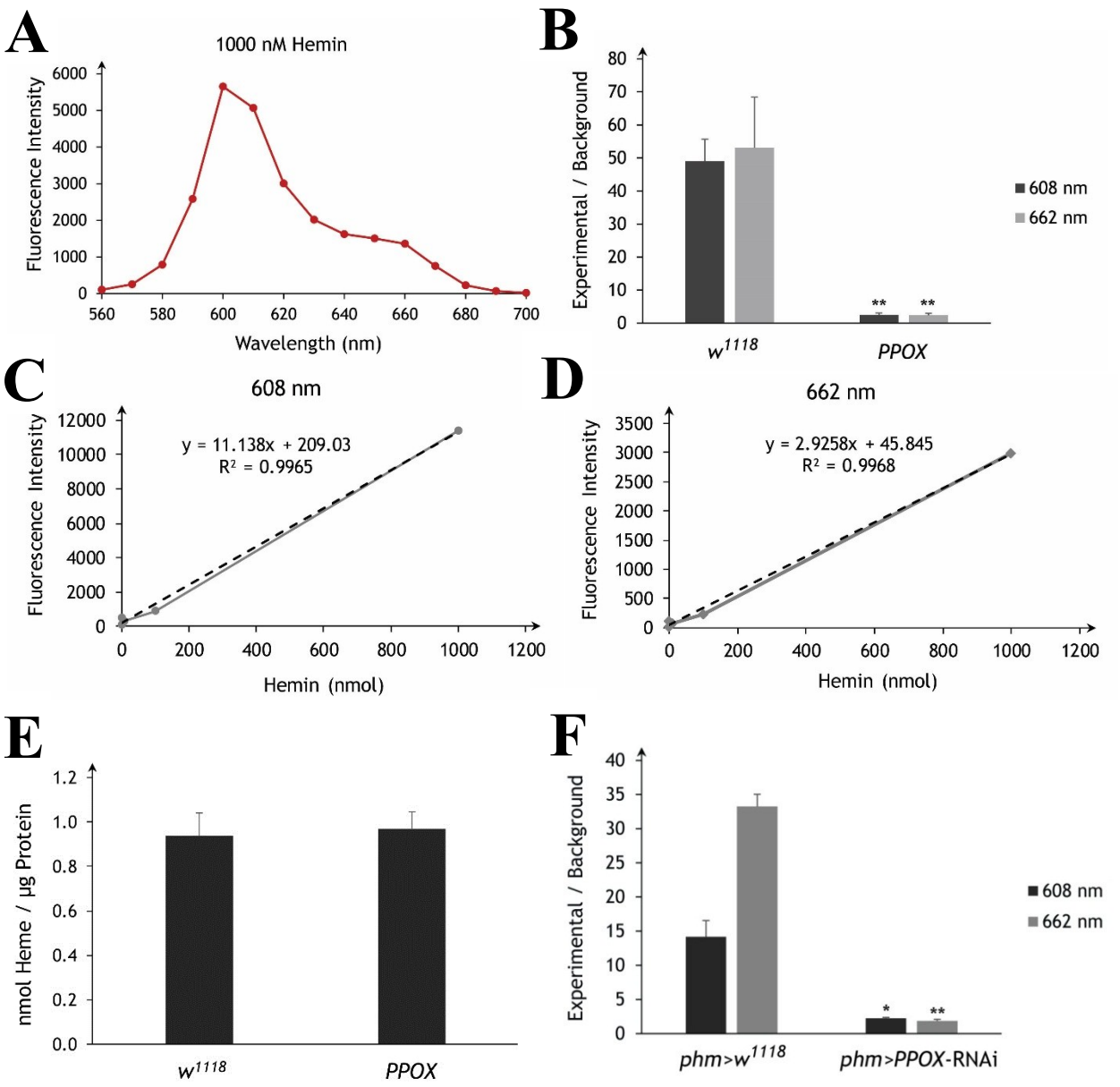

(Legend on next page)

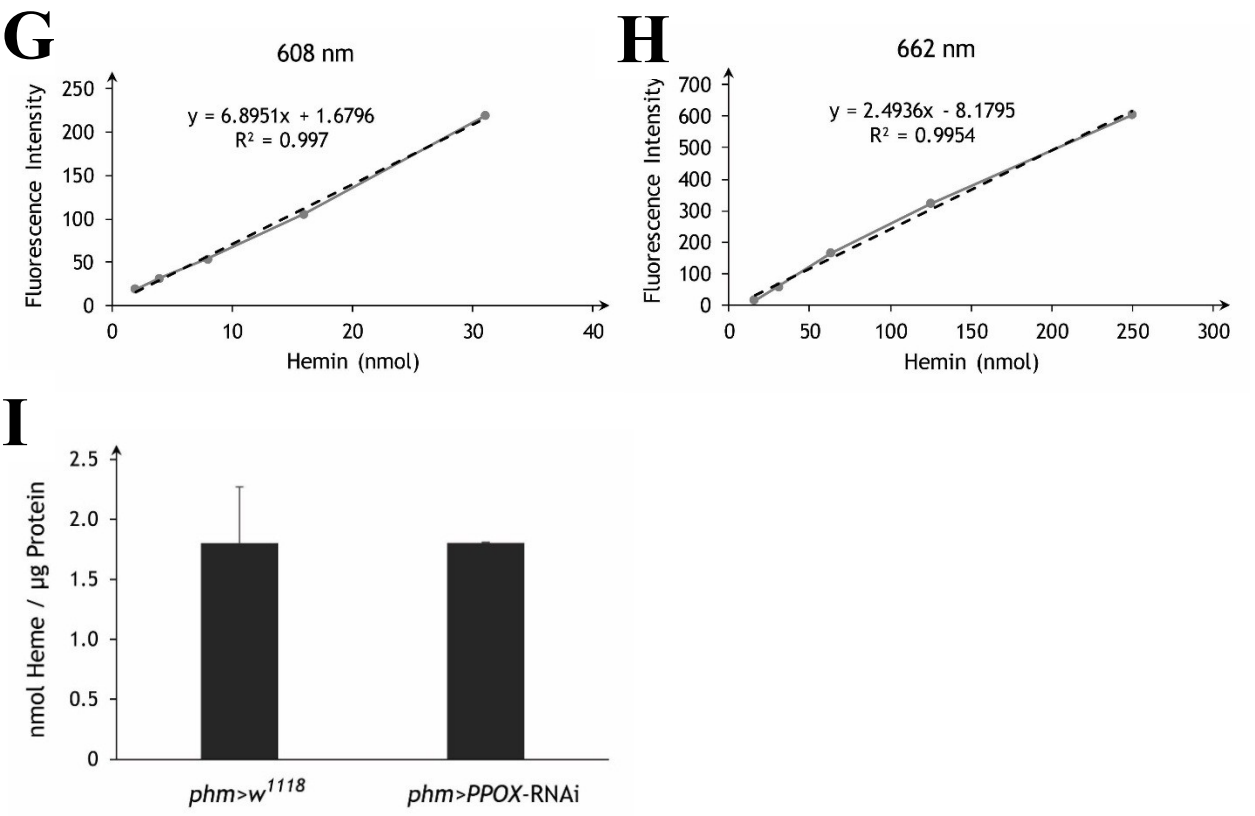

Figure 3-14. Heme can be measured in *Drosophila melanogaster* L3 larvae. A) 1000 nM hemin was measured at varying wavelengths to find the maximum fluorescence intensity after oxalic acid and heat treatment. Porphyrins are expected to have a major emission peak at 608 nm and a minor peak at 662 nm. Samples were excited at 400 nm. B) 5 day old whole body larvae were collected and fluorescence was measured after treating heme with oxalic acid with and without heat. The fluorescence ratio between the experimental fluorescence (oxalic acid and heat) and the background fluorescence (oxalic acid and no heat) was calculated. Fluorescence was measured at 608 nm and 662 nm. Hemin standard curve measured at 608 nm (C) and at 662 nm (D). The equation and R^2 value show the fit of the trendline (black). The standard curve was measured when performing whole body heme measurements. E) Whole body heme content was compared to a hemin standard curve (C-D) and normalized to the amount of protein per well. F) Fluorescence ratio for brain-ring gland (BRG) samples that were dissected from 5 day old larvae. The experiment followed a similar protocol to B. Hemin standard curve measured at 608 nm (G) and at 662 nm (H). The equation and R^2 value show the fit of the trendline (black). The standard curve was measured when performing BRG heme measurements. I) Heme was measured in BRGs by comparing fluorescence to a hemin standard curve (G-H) and then normalized to the amount of protein per well. Error bars represent the standard deviation. * = P-value < 0.05. ** = P-value < 0.01. A Student's t-test was used to determine significance relative to w^{1118} or *phm*>w^{1118} at the same wavelength.

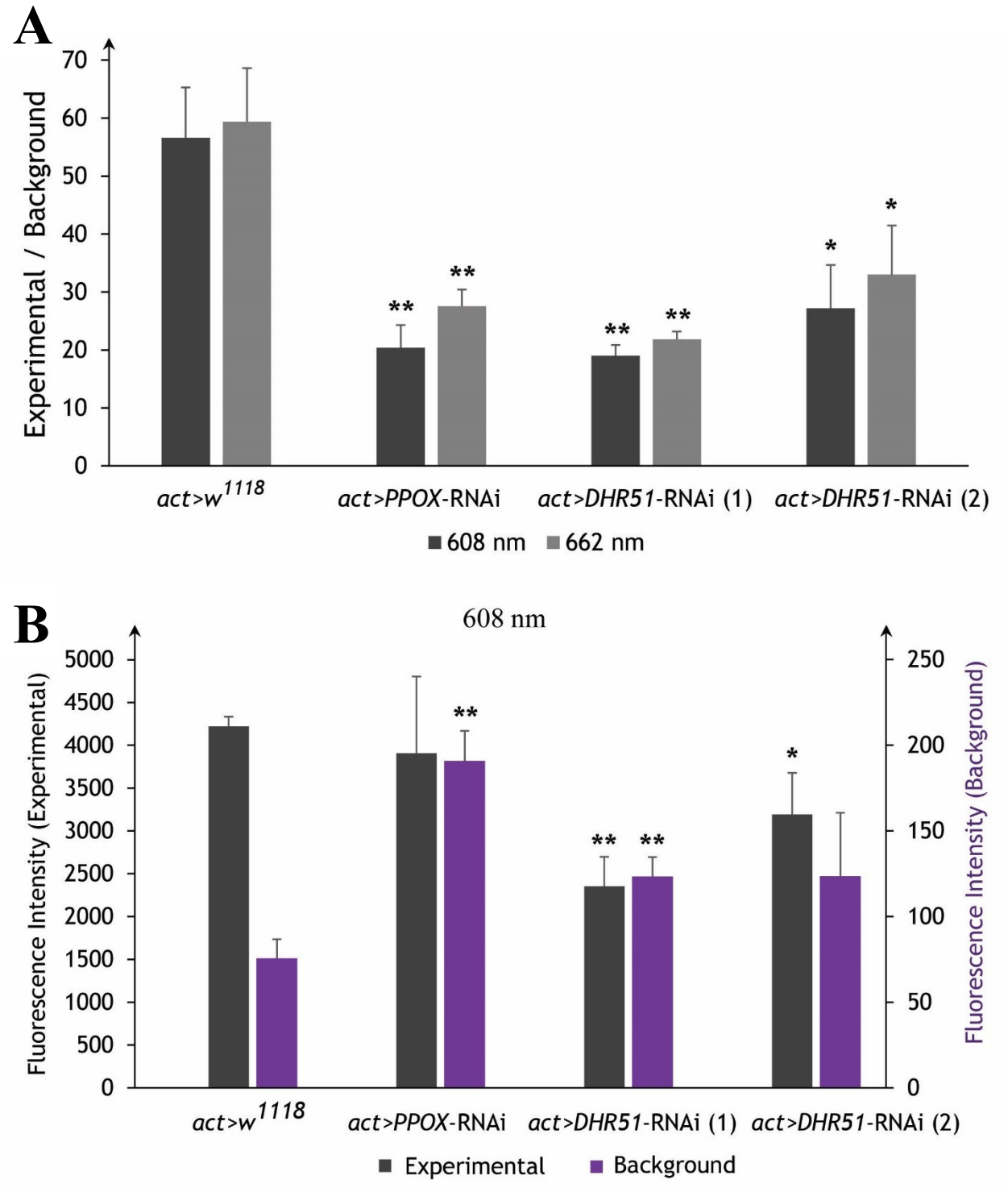

(Legend on next page)

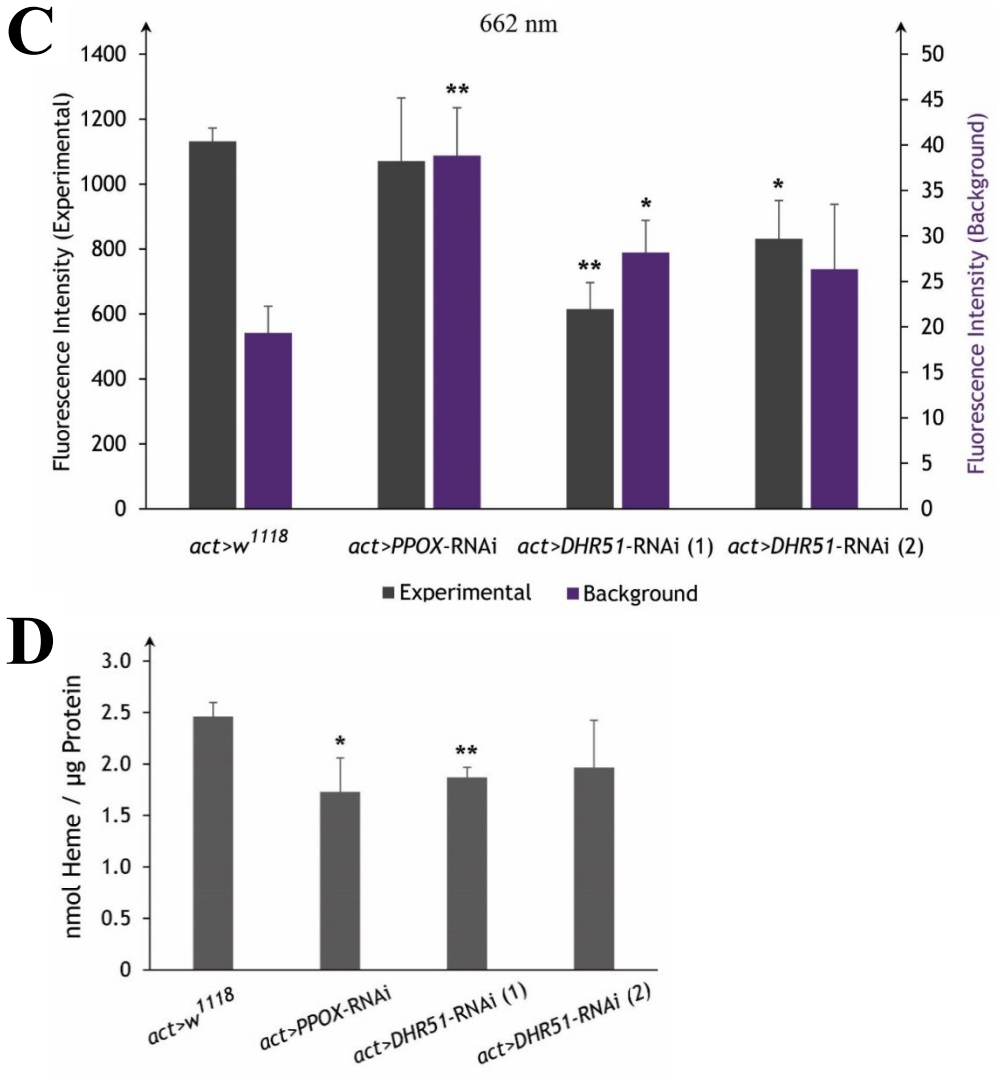

Figure 3-15. Whole body *DHR51*-RNAi reduced heme levels in L3 larvae. A) The fluorescence ratio (Experimental / Background) was calculated from fluorescence intensity in experimental samples (oxalic acid and heat) compared to the background (oxalic acid and no heat). RNAi was expressed ubiquitously with *actin* (*act*) – *GAL4* and 5 day old whole body larvae were collected. Ratios were calculated from values shown in B and C. A Student's t-test was used to determine significance relative to $act>w^{1118}$ at the same wavelength. B) Fluorescence intensities measured at 608 nm. Experimental values are shown in dark grey (using the left Y-axis) and background values are shown in purple (using the right Y axis). C) Fluorescence intensities measured at 662 nm. Experimental values are shown in dark grey (using the left Y-axis) and the background values are shown in purple (using the right Y axis). A Student's t-test was used to determine significance within the experimental fluorescence group and within the background fluorescence group relative to $act>w^{1118}$. D) Heme was measured by converting the fluorescence observed to concentration with a hemin standard curve and then normalized to the amount of protein per well. * = P-value < 0.05. ** = P-value < 0.01. Significance is being calculated relative to the $act>w^{1118}$ control at the same wavelength or condition. Error bars represent the standard deviation. A Student's t-test was used to determine significance relative to $act>w^{1118}$.

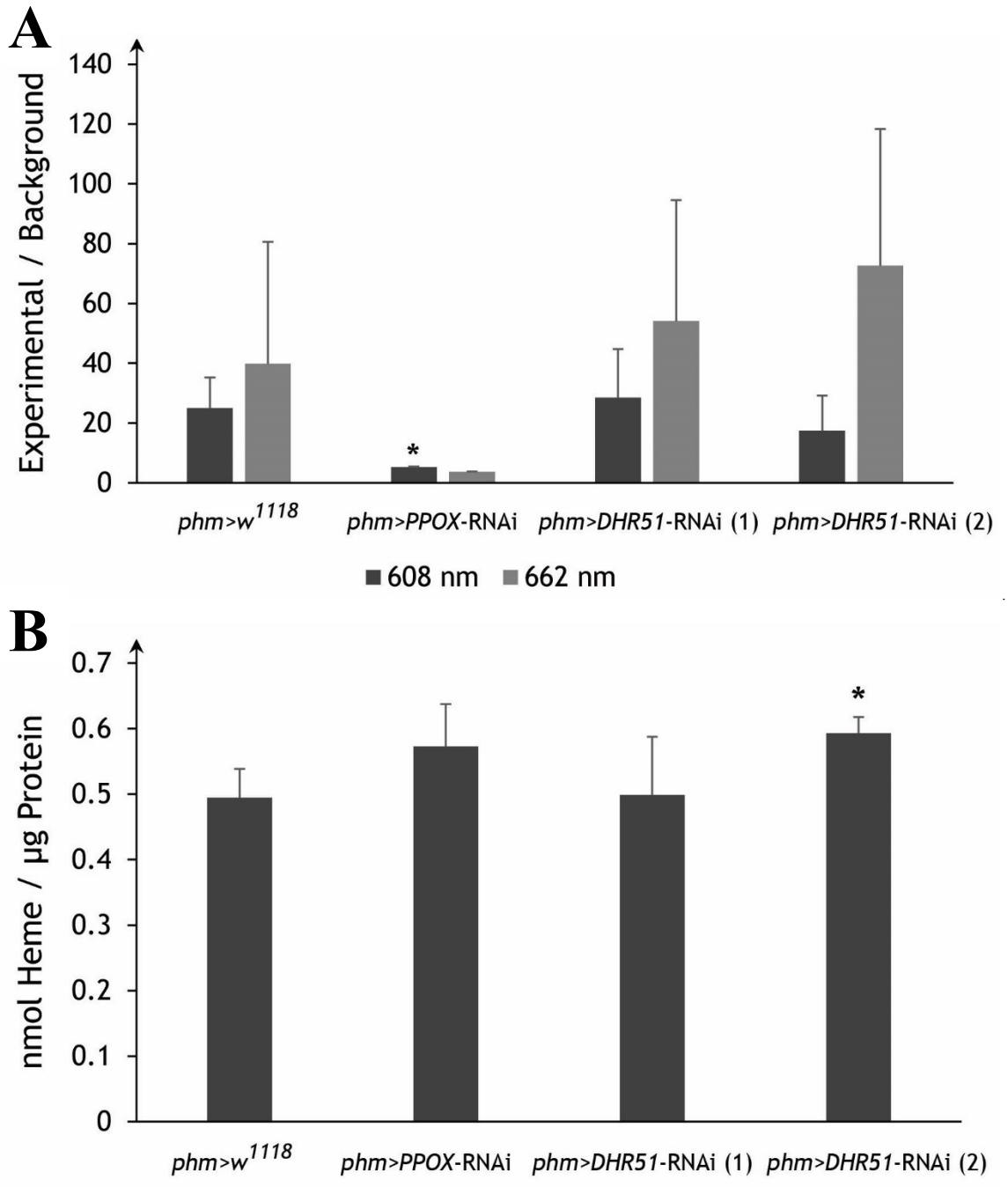

Figure 3-16. Loss-of-*DHR51* in the prothoracic gland did not decrease heme levels in brain-ring glands. A) Fluorescence ratio (Experimental / Background) calculated from fluorescence intensity in experimental samples (oxalic acid and heat) compared to the background (oxalic acid and no heat) fluorescence. RNAi was expressed in the prothoracic gland via *phm22-GAL4* (*phm*) and brain-ring glands were dissected from larvae 48 hours post L2/L3 molt. A Student's t-test was used to determine significance relative to *phm>w*^{1118} at the same wavelength. B) Heme was measured by converting the fluorescence observed to concentration with a hemin standard curve and then normalized to the amount of protein per well. * = P-value < 0.05. Error bars represent the standard deviation. A Student's t-test was used to determine significance relative to *phm>w*^{1118}.

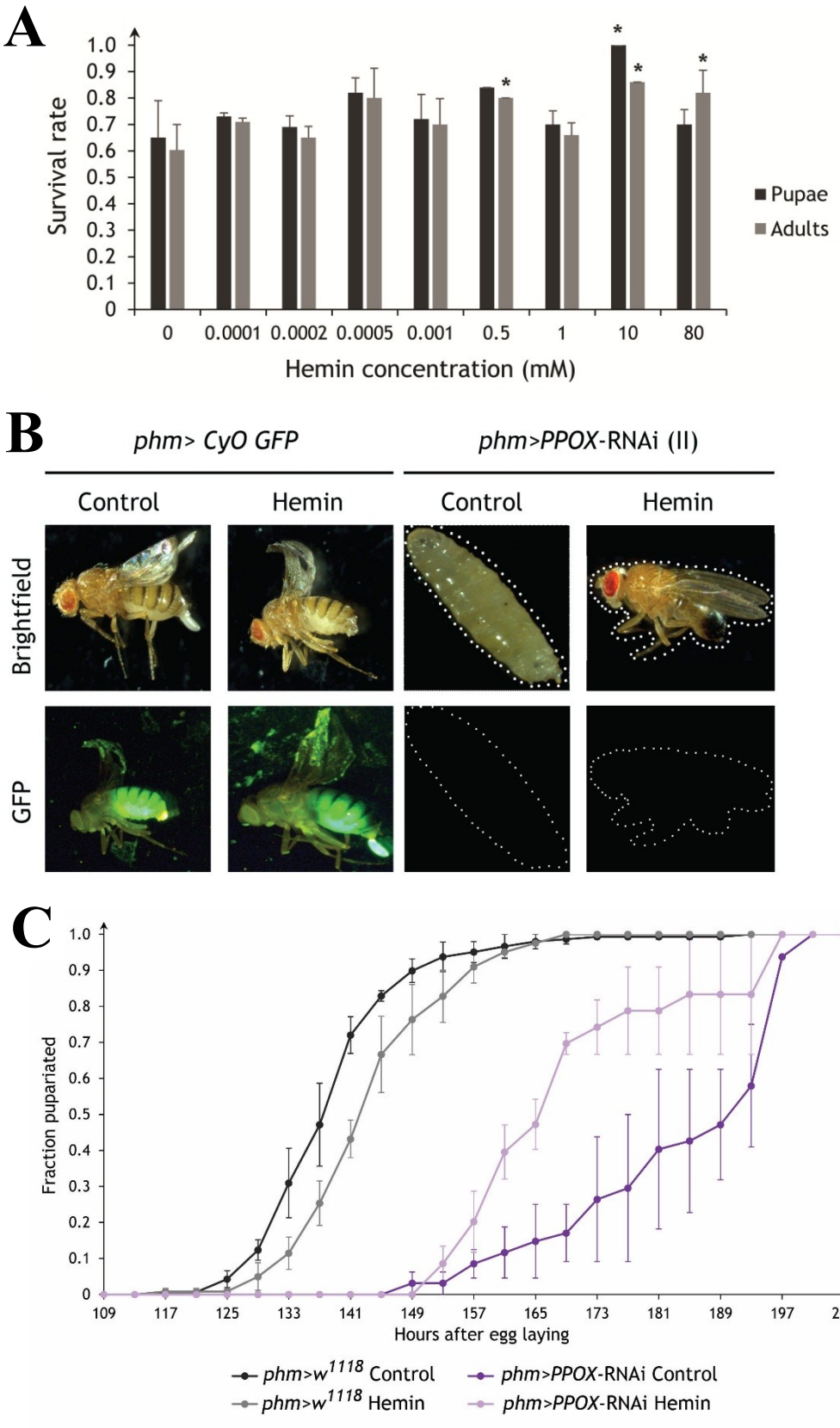

(Legend on next page)

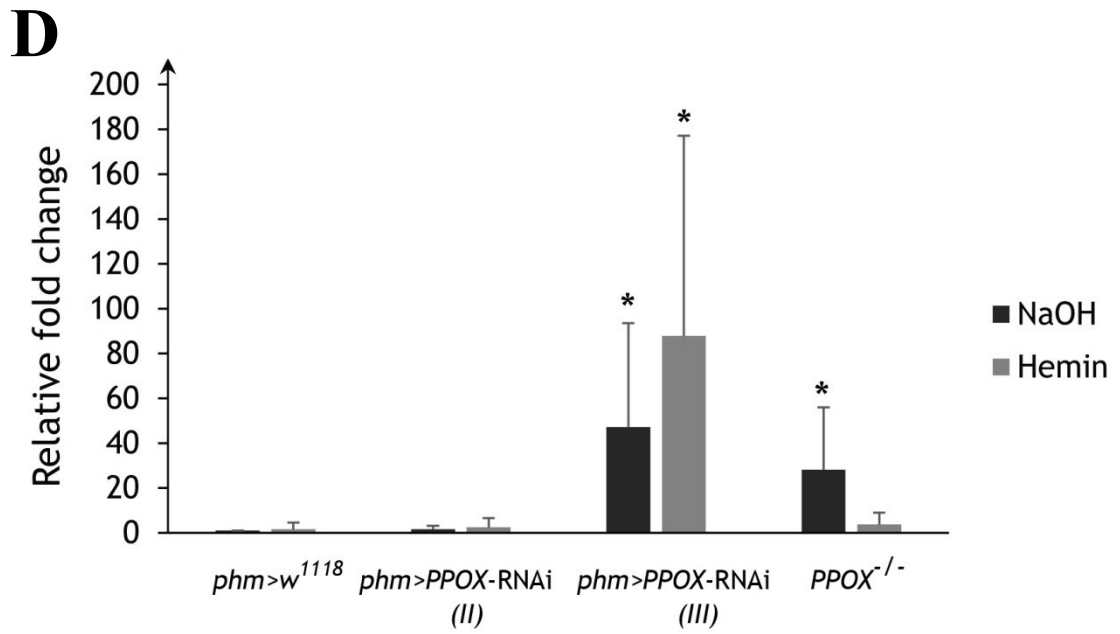

Figure 3-17. 1 mM hemin supplementation partially rescued *phm>PPOX*-RNAi animals. A) A wide range of hemin concentrations were tested looking for lethality in w^{1118} animals raised on standard agar cornmeal media supplemented with hemin. A Student's t-test was used to determine significance relative to survival on 0 mM hemin-supplemented media separately for pupae and adults. B) Since the *PPOX*-RNAi (II) stock is homozygous lethal, the balancer (*CyO GFP*) was used as an internal control. White dotted lines outline the animals when there is no GFP signal. Figure credit to Ami Soni. C) *phm*>w^{1118} and *phm*>*PPOX*-RNAi (III) larvae were timed from egg laying until they formed pupae. Fraction pupariated is relative to the final number of pupae observed. D) *Alas* expression was measured via qPCR in ring glands from 5 day old larvae. qPCR credit to Ami Soni. Hemin was dissolved in NaOH and used at a final concentration of 1 mM in the normal fly media. Control refers to control media that had equal amounts of NaOH added as the hemin-supplemented food. p*hm* = *phm22-GAL4*. * = P-value < 0.05. Error bars represent the standard deviation. A Student's t-test was used to determine significance relative to *phm*>w^{1118} on each type of media. There was no significant difference in *Alas* expression when larvae of the same genotype were raised on NaOH- or hemin-supplemented media due to high variance within the samples.

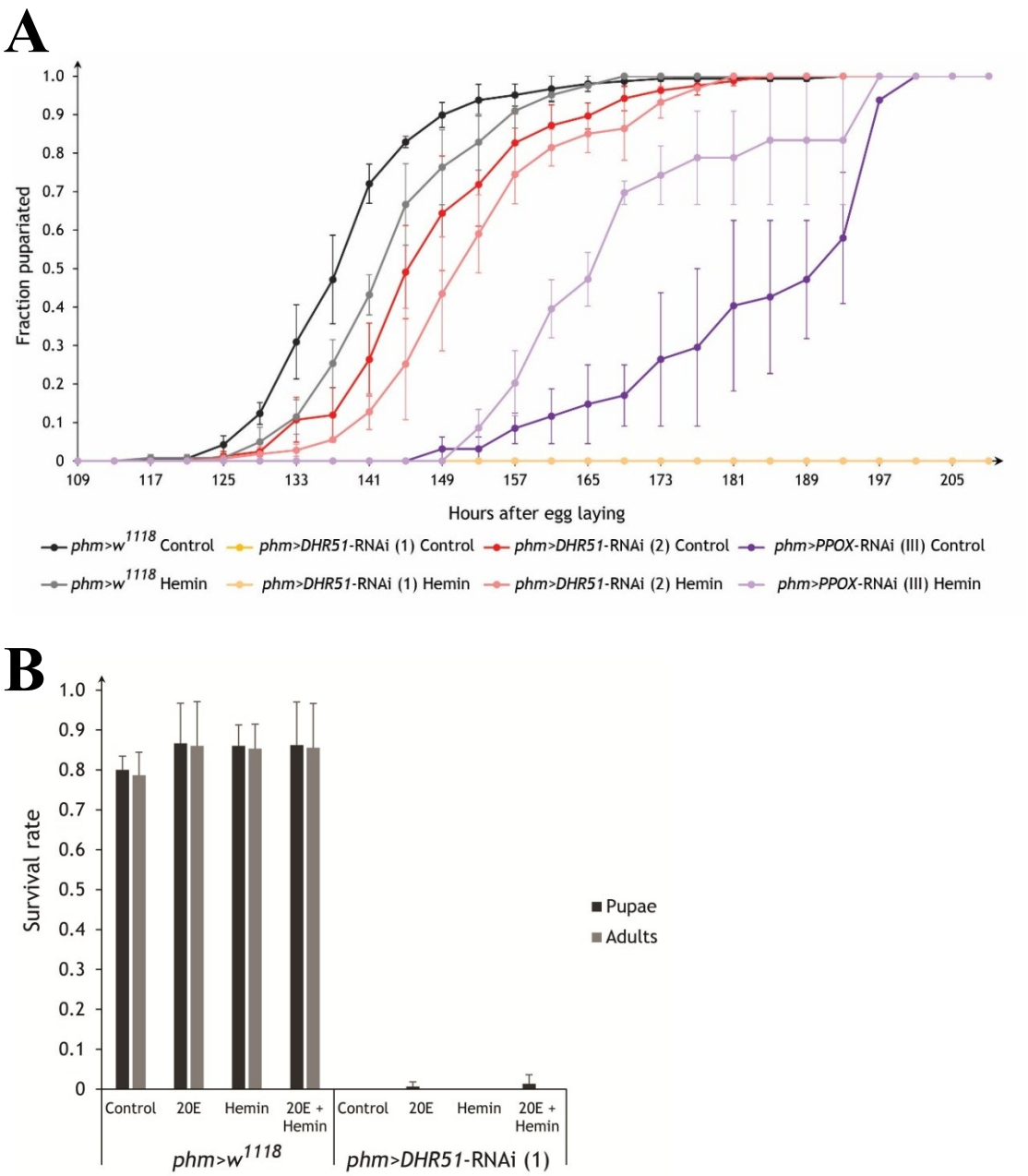

Figure 3-18. *phm>DHR51*-RNAi larvae cannot be rescued by hemin feeding. A) *phm>DHR51*- and *PPOX*-RNAi lines grown on control media and 1 mM hemin-supplemented media. The data is the same as Figure 3-17C as the experiments were done at the same time. Fraction pupariated is relative to the final number of pupae observed. *phm>DHR51*-RNAi (1) on either media type resulted in no pupae being observed, and as a result, the lines are overlapping. B) 50 embryos were transferred to control media, 20-hydroxyecdysone (20E) media (final concentration of 200 µg/ml), hemin media (1 mM final concentration), or a combination of 20E and hemin. *phm>DHR51*-RNAi (1) larvae on 20E resulted in wandering L3 larvae that attempted to form pupae and died on the walls; only normal looking pupae were included. p*hm = phm22-GAL4*. Error bars represent the standard deviation. A Student's t-test determined that there was no significant difference on survival when *phm>w*^{1118} or *phm>DHR51*-RNAi (1) animals were raised on 20E-, hemin-, or 20E- and hemin-supplemented media compared to control media.

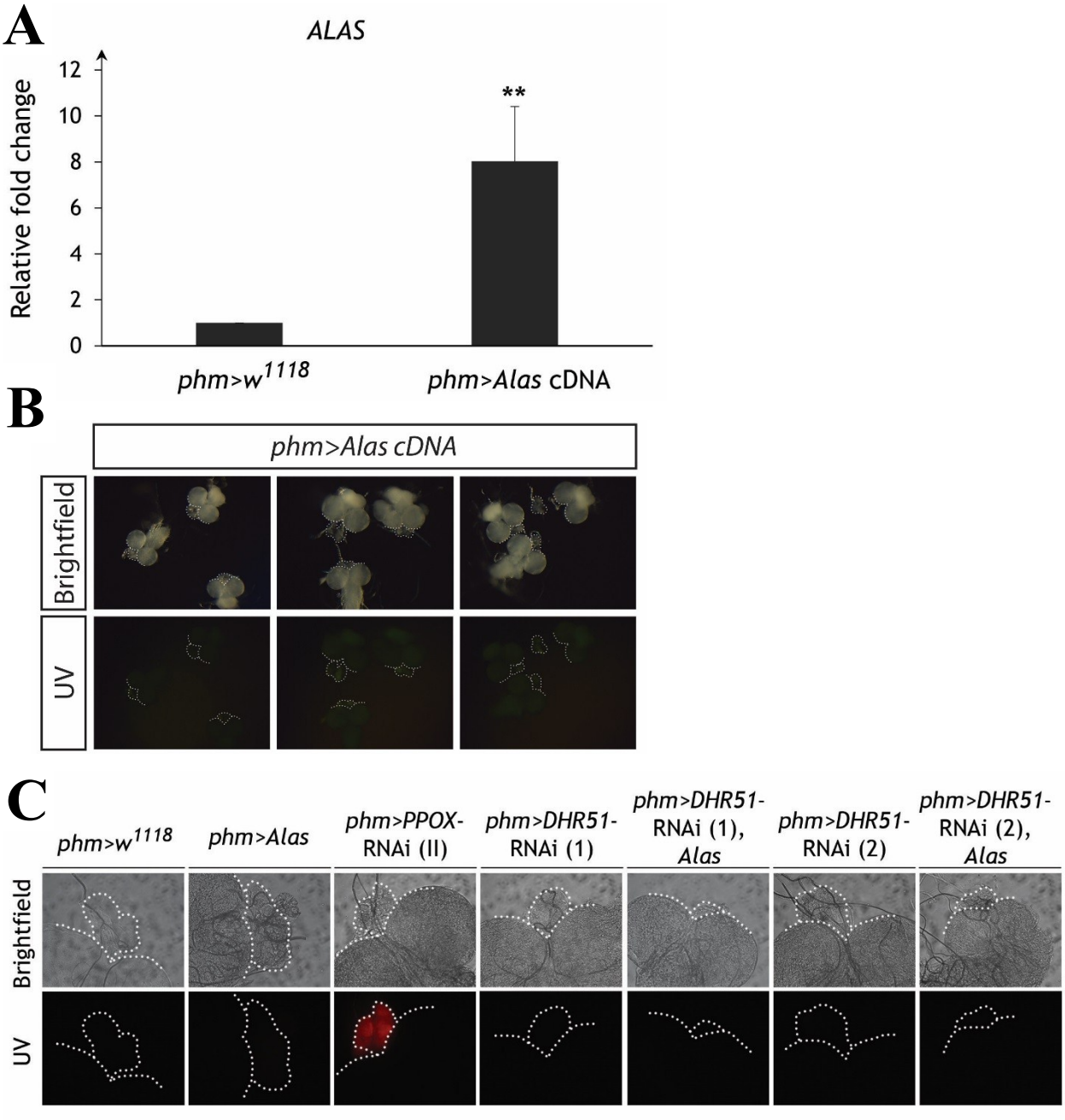

Figure 3-19. *phm>Alas* cDNA resulted in no observable phenotype and did not induce red autofluorescent ring glands by itself or in *DHR51*-RNAi larvae. A) qPCR of *Alas* expression in ring glands from wandering L3 larvae. ** = P-value < 0.01. A Student's t-test was used to determine significance relative to *phm>w*^{1118}. B) Brain-ring glands from wandering L3 larvae were viewed with a fluorescent microscope under normal light and UV light, which would show any red autofluorescence from accumulated heme precursors. Brain-ring glands were exposed to high exposure (3s) for 2-3 minutes. C) Brain-ring glands from late L3 larvae were observed with a confocal microscope. Photo credit to Ami Soni. Red autofluorescence was only observed in *PPOX*-RNAi ring glands. Ring glands are outlined with a white dotted line. p*hm = phm22-GAL4*.

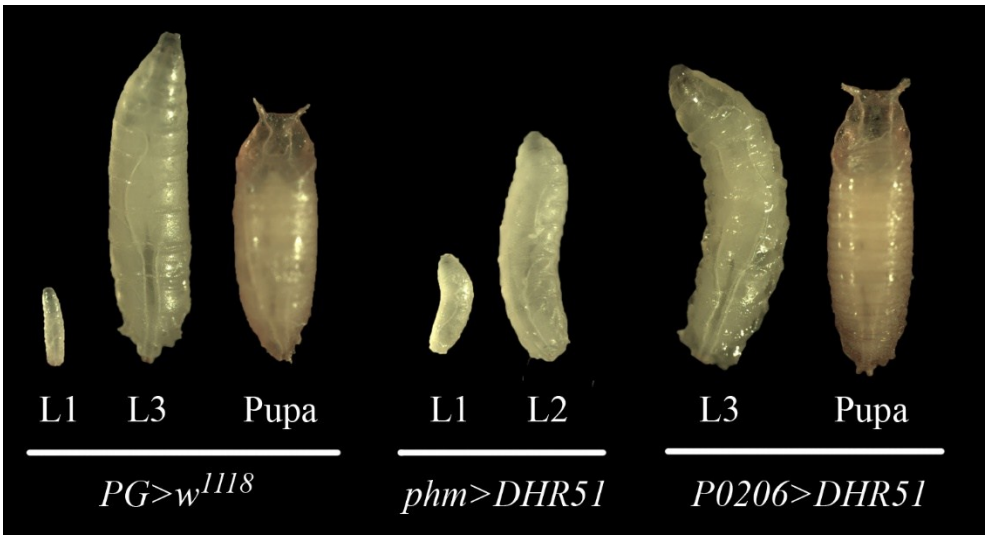

Figure 3-20. Overexpression of *DHR51 (F1)* caused developmental arrests. Overexpression of *UAS-DHR51* cDNA in the prothoracic gland with a strong *GAL4* driver, *phm22-GAL4* (*phm*), resulted in a major L1 arrest with only a small proportion of the larvae becoming arrested in the L2 stage. When a weaker ring gland *GAL4* driver is used (*P0206*), *UAS-DHR51* resulted in a major pupal arrest and minor L3 arrest. L1 = first instar. L2 = second instar. L3 = third instar.

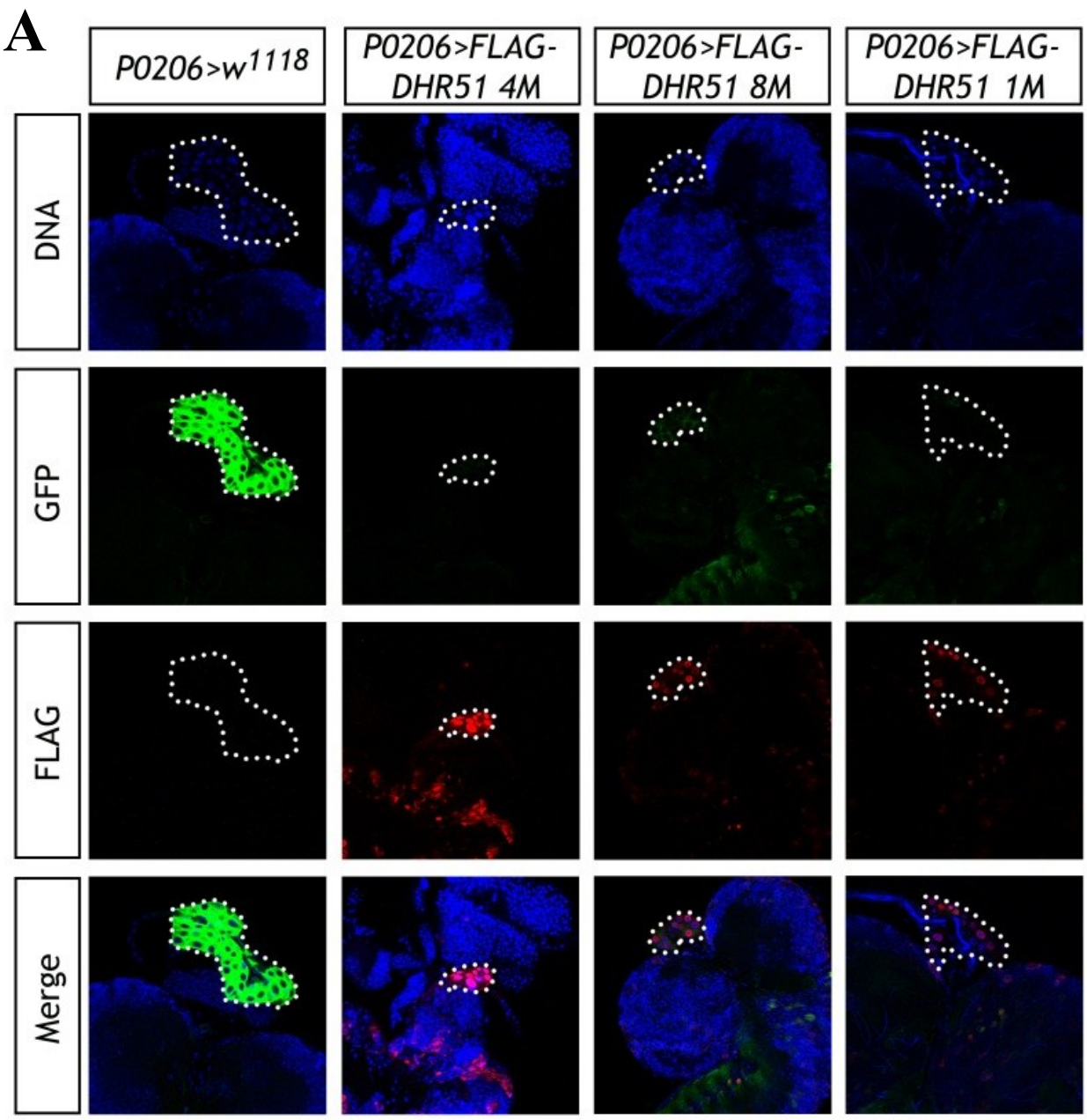

(Legend on next page)

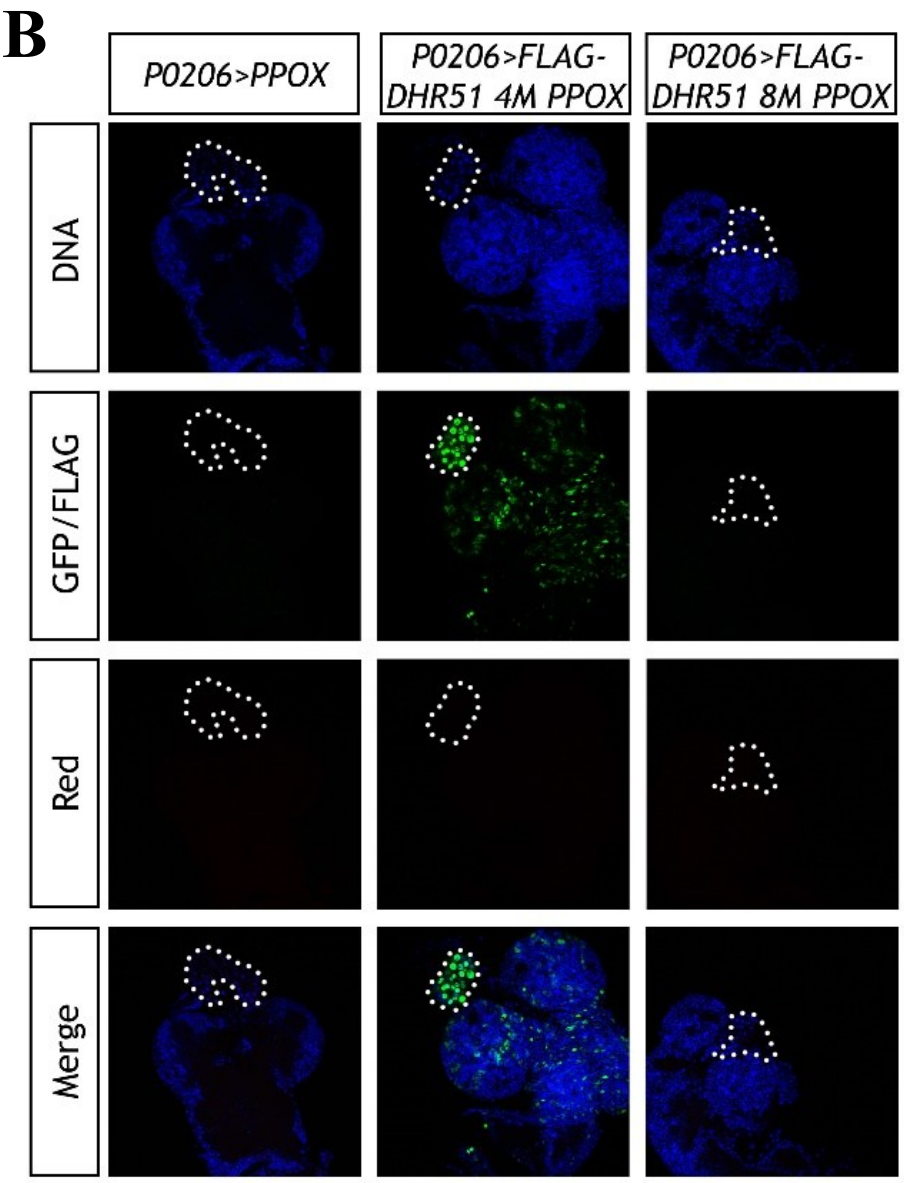

Figure 3-21. Overexpressed FLAG-DHR51 localized to the nucleus in prothoracic gland cells under normal and low cellular heme levels. A) Multiple lines of *FLAG-DHR51* (*4M*, *8M*, and *1M*) were expressed with the ring gland *GAL4* driver *P0206*. The *P0206* line also expresses cytoplasmic *GFP*. A primary FLAG antibody (1:800) was used in conjunction with a red fluorescent secondary antibody (1:2000). Brain-ring glands from the control, *P0206>w*^{1118}, and *P0206>FLAG-DHR51 1M* were dissected from L3 larvae and *P0206>FLAG-DHR51 4M* and *8M* were dissected from age-matched L2 arrested larvae. B) Two lines of *FLAG-DHR51* (*4M* and *8M*) were expressed with *P0206* in a low heme background (*PPOX* mutant background). All brain-ring glands were dissected from L2 larvae. *GFP* expression from the *P0206* line was not apparent in ring glands from L2 larvae or from ring glands that expressed the *FLAG-DHR51* transgenes. A primary FLAG antibody (1:800) was used in conjunction with a green fluorescent secondary antibody (1:2000). The red channel would show any autofluorescence from accumulated heme precursors in *PPOX*-deficient ring glands.

3.5 Tables

Table 3-1. Loss-of-*DHR51* phenotypes. Observed and published developmental phenotypes in prothoracic gland (PG) (*phm22-GAL4*) and ubiquitous (*act-GAL4*) *DHR51*-RNAi lines, and *DHR51* (*unf*) mutant lines. *Spok-Cas9* is PG specific. *unf* is another name for *DHR51*. Observed phenotypes are based on triplicate vials with greater than 20 animals. NOP = No obvious phenotype. *DHR51* 2xgRNA 6m and 12m behaved similarly, so they are grouped as 6/12m. [a] = (Sung, et al. 2009). [b] = (Yaniv, et al. 2012). - = no data available.

Genotype	Observed developmental phenotype	Published developmental phenotype
phm>DHR51-RNAi (1)	L3 arrest	-
phm>DHR51-RNAi (2)	14 hour delay during L3	-
act>DHR51-RNAi (1)	Pupal lethality, some larval lethality	-
act>DHR51-RNAi (2)	Pupal lethality, some adult escapers that die in food shortly after eclosing	-
unf^{Z0001}	NOP	75% uneclosed (pupal lethality), 25% adults with unexpanded wings. Infertile. [a]
unf^{X1} (*CyO GFP stock*)	~25% pupal lethality, 50% adults eclose and get stuck in food, 65% of adults have unexpanded wings (majority die in food)	44% uneclosed (pupal lethality), 17% adults with unexpanded wings, 39% NOP. Infertile. [a]
$unf^{LL04325}$	NOP	Lethal[b], then viable.
act-Cas9>DHR51 2xgRNA 3m	~4 day delay for eclosion. Adults get stuck in food and die. Many unexpanded wings. Free adults move very little and slowly, also seem to have tremor-like movements. ~20% pupal lethal.	-
act-Cas9>DHR51 2xgRNA 6/12m	~32 hour delay for eclosion. Adults get stuck in food and die. Many unexpanded wings. Free adults move very little and slowly, also seem to have tremor-like movements.	-
Spok-Cas9>DHR51 2xgRNA 3m	~3.5 day delay for eclosion. Adults appear normal.	-
Spok-Cas9>DHR51 2xgRNA 6/12m	NOP. Possible minor delay (less than half day delay).	-

Table 3-2. *DHR51* transgene locations. *DHR51* transgenes were made and integrated randomly into the genome. Transgenes were mapped due to transgene segregation from dominant markers. Multiple lines were received for *UAS-FLAG-DHR51* and the lines are distinguished by #M. Only one of each *hs* transgene was received. *UAS = upstream activation sequence*. *hs = heat shock* promoter.

Transgene	Chromosome
UAS-FLAG-DHR51 (1M)	3rd chromosome
UAS-FLAG-DHR51 (2M)	2nd chromosome
UAS-FLAG-DHR51 (4M)	3rd chromosome
UAS-FLAG-DHR51 (6M)	3rd chromosome
UAS-FLAG-DHR51 (7M)	3rd chromosome
UAS-FLAG-DHR51 (8M)	2nd chromosome
hs-DHR51	3rd chromosome
hs-FLAG-DHR51	3rd chromosome

Table 3-3. *DHR51* ring gland overexpression phenotypes. Overexpression of *DHR51* resulted in dose-dependent phenotypes, where higher expression of *DHR51* results in a more severe phenotype or earlier stage arrest. *phm* is a strong *GAL4* driver. *P0206* is a weak ring gland driver. Both *Mai60* and *Feb36* express *GAL4* strongly in the prothoracic gland (according to Bloomington Stock Center), but is likely not as strong as *phm*. Phenotypes are based on triplicate vials with greater than 20 animals. L1 = first instar. L2 = second instar. L3 = third instar. *UAS-DHR51 (F1)* and *(C1)* were obtained from Dr. Steven Robinow.

Transgene	***GAL4* Driver**	**Phenotype**
DHR51 (F1)	*phm*	Major L1 arrest, ~5% L2 arrest
	P0206	Major pupal lethality, ~15% L3 arrest, small ring glands
DHR51 (C1)	*phm*	Major L1 arrest, ~5% L2 arrest
	P0206	Major L3 arrest, ~5% L2 arrest, small ring glands
FLAG-DHR51 (4M)	*phm*	Major L1 arrest
	P0206	Major L2 arrest
	Mai60	Embryonic lethal
	Feb36	L3 arrest, but later changed to small larvae that were L2 arrested
FLAG-DHR51 (8M)	*phm*	Major L1 arrest
	P0206	Major L2 arrest
	Mai60	Embryonic lethal
	Feb36	Major L3 arrest, some smaller and dead L2, some pupal lethality, but changed to small larvae that were L2 arrest

Chapter 4

DHR51 regulates ecdysone production, potentially through the circadian rhythm

4.1 Introduction

4.1.1 DHR51 and the Ras/Raf/ERK pathway

I hypothesize that heme and heme regulation is related to ecdysone production in the PG and that DHR51 coordinates the regulation between heme and ecdysone biosynthesis. The PG must have a high demand for heme because cytochrome P450 enzymes are produced at a high rate and each cytochrome P450 enzyme requires heme to function. However, free heme is cytotoxic, so I suspect that heme and ecdysone production could be coordinated as heme cannot be efficiently stored. From previous work on DHR51, there are minor hints that DHR51 could be involved in the regulation of ecdysone production. Firstly, expressing *DHR51*-RNAi lines in the PG caused developmental defects. *phm>DHR51*-RNAi (1) caused an L3 arrest, while *phm>DHR51*-RNAi (2) caused a minor delay into puparium formation. These are classic phenotypes of insufficient ecdysone production. If larvae cannot produce sufficient ecdysone for the major ecdysone pulse at the end of the L3 stage, puparium formation and metamorphosis can be blocked or delayed. While disrupting one ecdysone regulatory pathway, like the MAPK Torso/Ras/Raf/ERK pathway, decreased ecdysone production, the PG was able to eventually synthesize enough ecdysone for an ecdysone pulse to initiate metamorphosis due to other ecdysone signaling pathways, but metamorphosis was delayed by a few days (Chapter 1, Figure 1-3) (McBrayer, et al. 2007; Rewitz, et al. 2009). The Ras/Raf/ERK pathway became a candidate mechanism for DHR51 to regulate ecdysone production as DHR51 was found to be a regulator of ERK signaling in cell culture (Friedman and Perrimon. 2006). *DHR51*-RNAi reduced ERK activation in S2 cells. Since insulin is also able to activate the Ras/Raf/ERK pathway, it is difficult to determine at what part of the pathway DHR51 functions, whether at the receptor level (which could be *torso*, or *Insulin-like receptor* (*InR*)), or downstream of the receptors (Clemens,

et al. 2000). That being said, both the Torso/Ras/Raf/ERK pathway and the IIS (Insulin/insulin-like growth factor signaling) pathway regulate ecdysone production in *Drosophila* (McBrayer, et al. 2007; Rewitz, et al. 2009; Colombani, et al. 2005; Mirth, C., et al. 2005; Mirth, C. K. and Shingleton. 2012). Given that DHR51 may regulate ERK activity, DHR51 could potentially interact with the Torso/Ras/Raf/ERK pathway to regulate ecdysone production.

4.1.2 DHR51 and the TOR pathway

The mushroom body is a center for learning and memory in the brain. During embryogenesis, γ neurons, the first subtype of mushroom body neurons appear, begin to extend, and continue until late in the L3 larvae. During metamorphosis, these larval-specific γ neurons are pruned back and adult-specific γ neurons re-extend (Bates, et al. 2015). DHR51 is required for the re-extension and guidance of the γ neurons (Lin, et al. 2009; Bates, et al. 2010; Yaniv, et al. 2012). Through a series of epistasis experiments, DHR51 was found to work through the TSC1/Rheb/TOR/S6K pathway to facilitate γ neuron re-extension but through an independent pathway from neuron guidance (Yaniv, et al. 2012). DHR51 was able to interact with the TOR pathway, however, DHR51 could also function independently of the TOR pathway. DHR51 was suggested to directly bind to and negatively regulate *Tsc1* (*Tuberous sclerosis complex 1*, an upstream regulator of TOR) based on homology to murine NR2E3. However, when I examined the data, *Nr2e3* mutant retinas were found to very weakly, but still considered statistically significant, upregulate *Tsc1*, and NR2E3 was not found to directly bind to *Tsc1* (Haider, et al. 2009). I suspect that the upregulation of *Tsc1* in *Nr2e3* mutant retinas was a false positive. Nevertheless, further experiments demonstrated that DHR51 induced the TOR pathway in *Drosophila* mushroom body γ neurons during re-extension. A suppressor screen of the lethality caused by the overexpression of *DHR51* in the mushroom body identified the TOR pathway

proteins *Tsc1* and *Rheb*, but not *S6K*, as able to rescue the lethality from *DHR51* overexpression, which demonstrated that DHR51 worked through the TOR pathway (Bates, et al. 2014). It was odd that *Tsc1* was identified in the screen to rescue lethality from mushroom bodies overexpressing *DHR51* because DHR51 was thought to negatively regulate *Tsc1*. This could suggest a more complex interaction between DHR51 and the TOR pathway.

During an assay of neuron sprouting in cultured mushroom body neurons, TOR was found to be required for neuron sprouting, while DHR51 was not (Marmor-Kollet and Schuldiner. 2016). PTEN (Phosphatase and tensin homolog) inhibited the TOR pathway to disrupt adult neuron sprouting, suggesting that TOR could be regulated by DHR51 during developmental re-extension, but regulated by PTEN during sprouting. PTEN is a negative regulator of insulin/insulin-like growth factor signaling (IIS), but also affects TOR (Nowak, et al. 2013; Mensah, et al. 2015). Despite the interaction between DHR51, TOR, and possibly the IIS pathway, these interactions seem restricted by developmental time, function (sprouting compared to developmental re-extension), assay (*in vivo* compared to cultured neurons), or possibly tissue type. As such, even though DHR51 could be a regulator of ERK activity, which can be activated by insulin, and that insulin can affect TOR, the IIS pathway (InR/PI3K/Akt) is not involved in the developmental regrowth of neurons following pruning (Friedman and Perrimon. 2006; Marmor-Kollet and Schuldiner. 2016). Together, DHR51 and the TOR pathway can interact during developmental regrowth, independently of the IIS pathway, but DHR51 and the TOR pathway are not completely dependent on each other and can function through other means.

The TOR pathway promotes growth and proliferation based on the nutrients available. Mutations in the TOR pathway resemble amino acid deprivation (Zhang, H., et al. 2000). TOR also couples nutrients and developmental timing. Developmental delays caused by poor nutrition

can be rescued by activating TOR in the PG (Layalle, et al. 2008). Disruption of TOR in the PG caused reduced ecdysone titers resulting in a delay of metamorphosis, similar to disruption of *torso*. Since DHR51 could interact with the TOR pathway in mushroom bodies, and TOR aids in regulating ecdysone production, this provided a candidate pathway through which DHR51 can regulate ecdysone production in the PG.

4.1.3 DHR51 and the circadian rhythm

The circadian rhythm is a sleep-wake cycle that controls many physiological processes and behaviours. The circadian rhythm is maintained by a transcriptional feedback loop that generates 24 hour cycles that takes in environmental cues (Figure 4-1), but also has a free-running clock that does not take in external factors. In *Drosophila*, protein levels of CLOCK (CLK) and CYCLE (CYC) accumulate during the early morning and peak later during the day. CLK and CYC form a heterodimer and activate the transcription of *period* (*per*) and *timeless* (*tim*). PER and TIM protein accumulate in the cytoplasm during the early night and protein levels peak late in the night, when PER and TIM eventually move into the nucleus. PER and TIM also form a heterodimer and inhibit their own transcription by repressing CLK and CYC. Finally, PER and TIM begin to degrade in the early morning, which allows for CLK and CYC to once again, begin transcribing *per* and *tim*. CLK, CYC, PER, and TIM form the core proteins of the feedback loop that maintains the circadian rhythm. A similar circadian rhythm is maintained in mammals, where CLOCK and BMAL1 replace CLOCK and CYCLE respectively, and PERIODs and CRYPTOCHROMEs replace PERIOD and TIMELESS respectively (circadian rhythm reviewed in (Hardin and Panda. 2013)).

DHR51 functions within the circadian rhythm. DHR51 is rhythmically expressed in the master pacemaker neurons that synchronize the various clocks in an organism. Mutant *DHR51*

adult flies were behaviourally arrhythmic and disruption of *DHR51* in developing pacemaker neurons abolished any free-running rhythms (Beuchle, et al. 2012). DHR51 directly bound to *per*, along with CLK and E75, and these three proteins were necessary for maximum *per* expression (Jaumouille, et al. 2015). Similarly, Rev-erbα is also expressed in a circadian manner in multiple tissues, including the liver (Yang, et al. 2006). Rev-erbα directly suppresses *Bmal1* expression, but also regulates *Clock*, *Cryptochrome1*, and *Npas2* (the heterodimer partner of BMAL1) (Preitner, et al. 2002; Crumbley and Burris. 2011; Ukai-Tadenuma, et al. 2011; Crumbley, et al. 2010). *Alas1* is expressed in a circadian rhythmic manner by BMAL1-NPAS2, as *Alas1* expression increased during the late day, peaked during the day-night transition, and began to decrease during the night (Kaasik and Lee. 2004). Heme levels cycle in a circadian manner and the rhythm of heme levels is likely due to *Alas1* regulation by Rev-erbα/BMAL1/ NPAS2 (Wu, et al. 2009). In turn, proteins in the circadian rhythm use heme as a cofactor, such as Rev-erbα, NPAS2, and PERIOD2 (Raghuram, et al. 2007; Dioum, et al. 2002; Kaasik and Lee. 2004). Many processes are under the influence of the circadian rhythm such as heme biosynthesis, but recently, in *Drosophila*, the circadian rhythm was found to be necessary for ecdysone production.

Eclosion, adult flies emerging from their pupal cases, is typically gated to the morning of each day. It was suggested that even if adults are ready to emerge earlier, the adults will remain in their pupal cases until the morning (Pittendrigh. 1967; Konopka and Benzer. 1971; Qiu, J. and Hardin. 1996). Eclosion gating suggested that eclosion may be under the control of the circadian rhythm. In addition, ecdysone pulses were found to have daily rhythms that peak during the night in the insect *Rhodnius prolixus* (the kissing bug) (Ampleford and Steel. 1985). The connection

between development, ecdysone, and the circadian rhythm led to the identification of a functional circadian rhythm in the PG.

In *Drosophila*, the PG was found to be necessary for eclosion gating, which was mediated by PDF (pigment-dispersing factor), a neuropeptide secreted from the pacemaker neurons (Myers, et al. 2003). Disruption of the circadian rhythm via RNAi specifically in the PG resulted in a range of developmental phenotypes ranging from L2 arrest to pupal lethality, even though mutants are generally considered viable (Di Cara and King-Jones. 2016). A possible explanation was that locally disrupting the circadian rhythm in the PG desynchronized the tissue from the rest of the body, whereas in a mutant, even if the circadian rhythm was disrupted, the clocks were synchronized. Ecdysteroidogenic enzymes were expressed during the night and *tim*- and *per*-RNAi downregulated genes involved in ecdysone production, such as *sad*, *phm*, and *dib*, and the cholesterol transport genes, *Npc1a* and *Start1*, during the night (Di Cara and King-Jones. 2016). The downregulation of these ecdysteroidogenic genes resulted in decreased ecdysone levels, which explained the developmental defects observed. This provided evidence that the circadian rhythm regulated ecdysone production within the PG. The connection between DHR51 and the circadian rhythm and the connection between the circadian rhythm and ecdysone production suggested that DHR51 could work within the circadian rhythm in the PG to regulate ecdysone production

4.2 Results

4.2.1 *DHR51*-RNAi reduced the expression of ecdysteroidogenic genes

Developmental defects, such as larval arrests or delays as seen in *phm>DHR51*-RNAi larvae, are classic phenotypes of ecdysone-deficiency. Therefore, it was plausible that DHR51 aided in ecdysone production. DHR51 also interacts with pathways in other tissues, as discussed in Chapter 4.1, that regulate ecdysone production in the PG. If insufficient ecdysone is synthesized, the major ecdysone pulse that triggers metamorphosis could be absent or delayed, resulting in a developmental arrest or delay. To determine whether DHR51 had a role in regulating ecdysone production, I identified gene ontology terms from the RG *phm>DHR51*-RNAi (1) RNA-Seq data , which was described in Chapter 3.2.4. "Larval development / ecdysone production" was one of the gene ontology terms found in the set of downregulated genes in *phm>DHR51*-RNAi (1) RGs, which supported my hypothesis that DHR51 was involved in regulating ecdysone production. Downregulated genes were at least 3-fold downregulated and had an RPKM greater than 0.5. The downregulated genes involved in ecdysone production covered a broad range of roles from cholesterol transport (*Start1* and *Npc1a*) to ecdysone signaling (*broad*, *tor*, and *CG11762* [*Ouib*]) to ecdysone production (*sad*, *dib*, and *phm*) (Roth, et al. 2004; Huang, et al. 2005; Moeller, et al. 2013; Rewitz, et al. 2009; Komura-Kawa, et al. 2015; Warren, et al. 2002; Warren, et al. 2004). *phm>DHR51*-RNAi (1) resulted in a widespread downregulation of genes involved in ecdysone production. As mentioned in Chapter 3.2.4, PG cells responded to *phm>DHR51*-RNAi (1) and *phm>FeCH*-RNAi in a similar manner, however, the downregulation of ecdysone-related genes was unique to *phm>DHR51*-RNAi (1) RGs. The ecdysteroidogenic genes downregulated by *DHR51*-RNAi (1) generally did not overlap with any of the low heme phenotype RNAi lines. This suggested

that the genes involved in ecdysone production were not downregulated when heme levels were low, despite that cytochrome P450 enzymes require heme. The downregulation of ecdysteroidogenic genes was specifically due to loss-of-*DHR51* and not due to possible reduced heme levels in *DHR51*-RNAi RGs.

As a result of the downregulation of many ecdysone-related genes in the *phm>DHR51*-RNAi (1) RNA-Seq data, I examined other genes involved in ecdysone production that may have been excluded from the initial list of downregulated genes. I found that most of the genes involved in synthesizing ecdysone were downregulated in the RNA-Seq data, which included: *nvd*, *sro*, *spok*, *phm*, *dib*, and *sad* (Figure 4-2A). The only exception was *Cyp6t3*, which was upregulated 4.5-fold. However, *Cyp6t3* may be unique because it has very low expression for a gene in the ecdysone production pathway, which suggested that Cyp6t3 could be a rate-limiting step in ecdysone production. Cyp6t3 functions in the "Black Box" where the rate-limiting step is known to occur (Ou, et al. 2011). *Cyp6t3* is also unique in that its expression was increased in the low heme phenotype RNAi lines: *spz5*-RNAi (*Cyp6t3* expression was increased 22.4-fold), *Nos*-RNAi (up 5.2-fold), *FeCH*-RNAi (up 13.2-fold), and the *PPOX* mutant (up 9.7-fold). Without sufficient heme, the cytochrome P450 enzymes in the ecdysone pathway would be non-functional leading to a deficit in ecdysone. If *Cyp6t3* encodes the rate-limiting enzyme in ecdysone production, *Cyp6t3* could then be upregulated in response to insufficient ecdysone production. RNA-Seq of *phm>DHR51*-RNAi (1) RGs provided evidence that DHR51 was required for the expression of ecdysteroidogenic genes and that loss-of-*DHR51* could impair ecdysone production.

In order to validate that DHR51 was required for the expression of the ecdysone biosynthetic genes, I used qPCR to examine these genes in both *DHR51*-RNAi lines. *DHR51*-

RNAi was expressed in the PG and BRGs were dissected 44 hours after the L2/L3 molt. Both *phm>DHR51*-RNAi lines significantly reduced the expression of the majority of the ecdysone biosynthetic genes in BRGs (Figure 4-2B). The main exception was *Cyp6t3*, where *phm>DHR51*-RNAi (2) seemed to have no impact on *Cyp6t3*'s expression. This data demonstrated that loss-of-*DHR51* reduced the expression of the ecdysone biosynthetic genes in the PG, which suggested that DHR51 was required for the proper expression of the ecdysone biosynthetic enzyme genes. A reduction in the ecdysone biosynthetic genes would likely reduce ecdysone levels in larvae, which could explain the developmental phenotypes observed in *phm>DHR51*-RNAi larvae.

4.2.2 DHR51 is required for ecdysone production

phm>DHR51-RNAi downregulated many ecdysteroidogenic genes, including the genes that encode the enzymes that synthesize ecdysone. Combined with the *phm>DHR51*-RNAi developmental phenotypes, it seemed plausible that disrupting *DHR51* in the PG impaired ecdysone titers during the L3 stage. Therefore, I directly measured whole body ecdysone titers with a 20E competitive enzyme immunoassay (the kit measures 20E and ecdysone equally well, I will just say ecdysone for simplicity). Whole body ecdysone titers were measured in larvae 4 hours, 28 hours, and 44 hours after the L2/L3 molt in *phm>w*^{1118} and *phm>DHR51*-RNAi larvae. 4 hours after the L2/L3 molt was included because ecdysone titers were at a minimum at this time point, while three minor ecdysone pulses occur between 8 to 28 hours after the L2/L3 molt (Warren, et al. 2006). The major ecdysone pulse should occur 44 hours after the L2/L3 molt. These time points were examined to determine whether only the major ecdysone pulse at the end of the L3 stage that initiates metamorphosis was affected or whether ecdysone production was disrupted throughout the L3 stage (including the minor ecdysone pulses). In addition, because

phm>DHR51-RNAi (1) resulted in an L3 arrest and *phm>DHR51*-RNAi (2) resulted in a prolonged L3 stage by approximately 14 hours, I also included a time point at 62 hours (44 hours plus 18 hours) only for *phm>DHR51*-RNAi larvae to determine whether *phm>DHR51*-RNAi (2) larvae eventually reached normal titers of circulating ecdysone or if the ecdysone pulse was lower but more sustained compared to wild type larvae.

Ecdysone levels were significantly decreased in *phm>DHR51*-RNAi larvae 28 hours and 44 hours after the L2/L3 molt, during the expected minor and major ecdysone pulses (Figure 4-3A). 4 hours after the L2/L3 molt, ecdysone levels were low in *phm*>DHR51-RNAi larvae, but not significantly different from ecdysone levels in $phm>w^{1118}$ control larvae. During the last minor ecdysone pulse at 28 hours post L2/L3 molt, ecdysone levels were significantly reduced in both *phm>DHR51*-RNAi lines (P-value = 0.043 and 0.036 for *DHR51*-RNAi (1) and (2), respectively). This suggested that DHR51 may have a more general function in ecdysone production and DHR51 was not limited to the major ecdysone pulse at the end of the L3 stage as suggested by the qPCR of the ecdysone biosynthetic genes, since the minor ecdysone pulse had a reduced titer. During the suspected major pulse at 44 hours post L2/L3 molt, ecdysone levels were even more significantly reduced in *phm>DHR51*-RNAi larvae compared to ecdysone levels in $phm>w^{1118}$ larvae (P-value = $9.0\text{x}10^{-4}$ and $8.0\text{x}10^{-4}$ for *DHR51*-RNAi (1) and (2), respectively). Although, *phm>DHR51*-RNAi (2) larvae had slightly higher ecdysone titers compared to *phm>DHR51*-RNAi (1) larvae. 18 hours after the suspected major ecdysone pulse, *phm>DHR51*-RNAi (2) larval ecdysone levels reached levels of control larvae at 44 hours, which suggested that *phm>DHR51*-RNAi (2) larvae do eventually reach normal titers of ecdysone, but the ecdysone pulse was delayed proportionally to puparium formation. *phm>DHR51*-RNAi (1) larvae continued to have low titers of ecdysone, even 18 hours after the

suspected major ecdysone pulse in control larvae. The ecdysone levels measured in these larvae nicely correlated with the developmental phenotypes seen in *phm>DHR51*-RNAi larvae, indicating that reduced ecdysone titers are likely the reason for the developmental timing defects.

One oddity I noticed when measuring ecdysone in the previous experiment was that the ecdysone titer was at approximately 10 pg/larvae 44 hours after the L2/L3 molt when the literature reported higher numbers in the range of 40-80 pg of ecdysone/larvae (Warren, et al. 2006; Ou, et al. 2011). In line with my lower ecdysone titer, when I re-examined the developmental timing of *phm>w*^{1118} larvae to form pupae from the L2/L3 molt, they began puparium formation around 70 hours after the L2/L3 molt, instead of the expected 48 hours after the L2/L3 molt. Since my larvae were forming pupae later, my ecdysone measurement at 44 hours post L2/L3 molt was likely prior to the peak of the major ecdysone pulse during the L3 stage, so I measured ecdysone in *phm>DHR51*-RNAi and *phm>w*^{1118} larvae 64 hours after the L2/L3 molt. Ecdysone titers in *phm>w*^{1118} larvae at 64 hours after the L2/L3 molt reached around 51 pg/animal, which indicated that I measured the major ecdysone pulse. Ecdysone titers in *phm>DHR51*-RNAi (2) larvae reached 40 pg/animal at 64 hours post L2/L3 molt, which was not significantly different compared to ecdysone titers in *phm>w*^{1118} control larvae (P-value = 0.34), while ecdysone titers were significantly reduced in *phm>DHR51*-RNAi (1) larvae (~17 pg of ecdysone/animal) (P-value = 0.019) (Figure 4-3B). Ecdysone titers in *phm>DHR51*-RNAi (2) larvae increased to 63 pg/animal at 78 hours post L2/L3 molt (64 plus 14 hours) but remained similar to control ecdysone titers at 64 hours post L2/L3 molt. Since only one time point was measured in *phm>w*^{1118} larvae, it is impossible to determine whether the ecdysone titer was increasing or decreasing at 64 hours, while the ecdysone titer in *phm>DHR51*-RNAi (2) larvae was increasing at 64 hours after the L2/L3 molt. If the ecdysone titer was decreasing in

phm>w^{1118} larvae while the *phm>DHR51*-RNAi (2) larval ecdysone titer was increasing, that would be a substantial difference in timing, but no significant difference in ecdysone titers may be detected with the ecdysone measurement. Given that ecdysone titers were reduced in the first 44 hours in *phm>DHR51*-RNAi (2) larvae, it is likely that *phm>DHR51*-RNAi (2) larvae had delayed ecdysone titers at 64 hours post L2/L3 molt as well. Ecdysone titers remained low in *phm>DHR51*-RNAi (1) larvae at all time points tested, which suggested that these larvae remained arrested in the L3 stage because they are unable to mount a major ecdysone pulse to trigger metamorphosis.

I combined the two ecdysone measurement experiments into one continuous graph to attempt to get a better view of the entire L3 stage (Figure 4-3C). The resulting graph had a jarring transition between the two measurements (4 to 62 hours were from the first experiment and 64 and 78 hours were from the second). The baseline ecdysone titer seemed to be off and a very large difference was observed in the span of what should be two hours. It could be that the larvae were not actually at the designated time or the enzyme immunoassay was done slightly different to give incompatible results. Despite the combined graph, the data from the individual experiments showed that *phm>DHR51*-RNAi decreased ecdysone titers throughout the L3 stage.

Since RNAi can have off-targets and even though two independent *DHR51*-RNAi lines were used, I tested the ecdysone titers in *w*^{1118} and *unf*^{XI} mutant larvae. Larvae were collected at 60 hours after the L2/L3 molt (a few hours before metamorphosis when the major ecdysone pulse should occur). *unf*^{XI} larvae had significantly reduced ecdysone titers compared to ecdysone titers in *w*^{1118} larvae (P-value = 0.0083) (Figure 4-3D). This confirmed that loss-of-*DHR51* larvae were unable to mount a proper major ecdysone pulse to trigger metamorphosis at the appropriate time and that DHR51 was required for proper and timely ecdysone production. As a

side experiment, I tested the assumption that reduced heme levels decreased ecdysone production by impairing cytochrome P450 enzyme function. *PPOX* mutant larvae at 60 hours after the L2/L3 molt had significantly reduced ecdysone titers compared to w^{1118} larvae (P-value = 0.0043) (Figure 4-3D). Reduced ecdysone titers in *PPOX* mutant larvae confirmed that without sufficient heme, cytochrome P450 enzymes were unable to function and could not produce ecdysone.

4.2.3 20-hydroxyecdysone feeding partially rescued *phm>DHR51*-RNAi larvae

Since loss-of-*DHR51* reduced ecdysone titers in L3 larvae, it seemed reasonable that the developmental timing defects were due to a lack of ecdysone. To test this, *phm*>w^{1118} and *phm>DHR51*-RNAi larvae were raised on food supplemented with 20E. 20E rescue experiments that feed larvae 20E are standard rescue experiments to determine whether a phenotype is due to insufficient ecdysone titers, like in larvae with mutant ecdysone biosynthetic genes (Yoshiyama, et al. 2006; Ono, et al. 2006; Niwa, et al. 2010). *phm>DHR51*-RNAi (1) and *phm*>w^{1118} larvae were raised on media supplemented with 330 µg/ml of 20E or on control media containing equal amounts of ethanol as the 20E-supplemented media. Animals were scored at the L3, pupal, and adult stages. *phm> DHR51*-RNAi (1) larvae raised on 20E-supplemented food were partially rescued to the pupal stage (Figure 4-4A). Typically, *phm>DHR51*-RNAi (1) larvae on control media resulted in a 100% L3 arrest, however, in some instances, there are very few escapers that start to pupate (<5%). When *phm>DHR51*-RNAi (1) larvae were raised on 20E-supplemented media, approximately 15% of the population formed relatively normal looking pupae (with some minor oddities) (Figure 4-4B). These pupae did not eclose as adults. In addition, there appeared to be some behavioural changes where *phm>DHR51*-RNAi (1) larvae on 20E-supplemented media began wandering when *phm*>w^{1118} animals were forming pupae, while *phm>DHR51*-

RNAi (1) larvae on control media remained in the food. Some of the wandering *phm>DHR51*-RNAi (1) larvae everted their anterior spiracles as they were preparing for puparium formation, although these larvae never actually formed pupae (and were not included in Figure 4-4A's pupae count). The wandering *phm>DHR51*-RNAi (1) larval population on 20E-supplemented media died within the following days after initiating wandering. *phm>w*^{1118} larvae did not appear to have any different behaviour when raised on 20E-supplemented media. *phm>DHR51*-RNAi (1) larvae were only partially rescued by 20E feeding, which suggested that part of the phenotype observed is due to reduced ecdysone titers.

phm>DHR51-RNAi (2) larvae were also raised on 20E-supplemented media to determine whether 20E feeding could rescue the loss-of-*DHR51* phenotype. Unlike *phm>DHR51*-RNAi (1), *phm>DHR51*-RNAi (2) resulted in a developmental delay, so I quantified how long it took for larvae to form pupae compared to *phm>w*^{1118} animals. On control media, puparium formation was delayed by 18 hours in *phm>DHR51*-RNAi (2) larvae compared to *phm>w*^{1118} larvae. When *phm>DHR51*-RNAi (2) larvae were raised on 20E-supplemented media, the 18 hour delay was reduced by more than 50%, to an 8 hour delay, compared to *phm>w*^{1118} larvae on 20E-supplemented media (Figure 4-4C). Thus, 20E feeding was able to partially rescue the developmental delay in *phm>DHR51*-RNAi (2) larvae, which confirmed that the developmental delay was due to reduced ecdysone titers in *phm>DHR51*-RNAi (2) larvae.

20E feeding was also used in an attempt to rescue *unf*^{XI} mutant animals, as *unf*^{XI} larvae were shown to have reduced ecdysone titers. Embryos from *unf*^{XI} */ CyO act-GFP* (*CyO GFP*) parents were laid on standard media and left there until the L2 stage when heterozygous L2 larvae could easily be screened for GFP and removed and *unf*^{XI} homozygous mutant larvae (no GFP) were transferred to control media or to media supplemented with 200 µg/ml of 20E. *unf*^{XI}

mutant animals showed no difference in phenotype when raised on 20E-supplemented media compared to control media (Figure 4-4D). There was a significant decrease in the number of unf^{XI} adults eclosing on both media types compared to w^{1118} controls (P-value = 0.031 and 0.0051 for control media and 20E-supplemented media, respectively), which indicated some pupal lethality in unf^{XI} animals. 20E-supplementation did not affect pupal lethality of unf^{XI} animals. The majority of unf^{XI} adults, about 70%, had unexpanded wings that characterized the *unf* phenotype, while w^{1118} adults fully expanded their wings. 20E-supplementation did not affect *unf* wing expansion, likely meaning wing expansion is not dependent on ecdysone. This experiment demonstrated that 20E is unable to rescue unf^{XI} animals, despite that unf^{XI} animals had reduced ecdysone titers. 20E was likely unable to rescue unf^{XI} animals due to DHR51's roles in other tissues, like aiding in mushroom body development (Bates, et al. 2015). The movement defect of unf^{XI} adults and getting stuck in the food was not noted at the time as I was unaware of the phenotype or the reproducibility of these phenotypes. I suspect 20E would not be able to rescue the coordination of unf^{XI} adult flies to keep them from getting stuck in the food as that phenotype would likely be due to disruptions of neurons in the brain and the phenotype was not observed in *Spok-Cas9>DHR51* 2xgRNA adults. With all the data taken together, it seems that 20E feeding can, at least, partially rescue developmental phenotypes due to PG loss-of-*DHR51*. This provided more evidence that DHR51 was required for normal ecdysone production and the timing of ecdysone pulses. I have provided evidence that DHR51 was required for ecdysone production and the proper regulation of ecdysteroidogenic genes, therefore, my next question became: how does DHR51 regulate ecdysone production and the ecdysteroidogenic genes in the PG?

4.2.4 DHR51 may not be involved in the Ras/Raf/ERK pathway

Based on the RNA-Seq data of *phm>DHR51*-RNAi (1) RGs, DHR51 seemed to have a role in the expression of a broad range of genes involved in ecdysone production, including the ecdysone biosynthetic enzyme genes. DHR51 could potentially regulate the ecdysone biosynthetic enzyme genes directly or DHR51 could function in one of the signaling pathways that stimulate ecdysone production. PTTH is released from the brain to properly time metamorphosis and stimulates ecdysone production by signaling through the Torso/Ras/Raf/ERK pathway. Ablating PTTH-producing neurons resulted in the majority, if not all, of the ecdysone biosynthetic genes not being properly upregulated at the end of the L3 stage, which resulted in a 5 day delay into puparium formation (McBrayer, et al. 2007). The Torso/Ras/Raf/ERK pathway was of interest to me because a previous RNAi screen for regulators for ERK signaling in cell culture identified DHR51 as a strong hit (Friedman and Perrimon. 2006). *DHR51*-RNAi reduced ERK activation in S2 cells, which suggested that DHR51 was required for ERK activation.

To determine whether DHR51 regulated ecdysone production through the Torso/Ras/Raf/ERK pathway in the PG, I attempted a genetic interaction experiment using *phm>DHR51*-RNAi and *UAS-Ras*^{V12}. *Ras*^{V12} is a constitutively active form of *Ras* (*Ras85D*) and PG expression resulted in the rare phenotype of developmental acceleration. *phm>Ras*^{V12} RGs were also massively overgrown and tumor-like. To determine whether DHR51 interacted with the Ras signaling pathway, I attempted to rescue the aberrant developmental timing caused by *phm>DHR51*-RNAi and *phm>Ras*^{V12} alone by co-expressing *phm>DHR51*-RNAi *Ras*^{V12} together and timing larval development. When *Ras*^{V12} was expressed with either *DHR51*-RNAi line in the PG, larvae had relatively normal developmental timing compared to either

phm>Ras^{V12} or *phm>DHR51*-RNAi alone (Figure 4-5A). *phm>DHR51*-RNAi (1) had an unusually high number of pupae that formed and the proportion of pupae was calculated based on the number of pupae and larvae while all the other samples were based on the final number of pupae. When *Ras*^{V12} was expressed along with *DHR51*-RNAi (1) in the PG, larvae had relatively normal developmental timing and significantly more larvae pupated compared to *phm>DHR51*-RNAi (1) alone (at least in one replicate, as the other replicate had very few larvae). RGs from *phm>Ras*^{V12} larvae were enlarged and RGs were small in *phm>DHR51*-RNAi (1) larvae, but RGs had a normal size in *phm>DHR51*-RNAi (1) *Ras*^{V12} larvae (Figure 4-5B). One issue was that three *DHR51*-RNAi (1) *Ras*^{V12} lines were made because it required recombination to combine the transgenes onto the same chromosome so that the transgenes could be crossed to *phm22-GAL4* flies. These three lines all had slightly different phenotypes, possibly due to the location that the recombination event occurred (one line was homozygous lethal while the others were viable) or there could have been an error in the crosses when making the lines. The other two *phm>DHR51*-RNAi (1) *Ras*^{V12} lines not included resulted in one replicate having a low number of larvae and the second replicate had no viable larvae, making it difficult to determine the phenotype and developmental timing of the larvae. The *phm>DHR51*-RNAi (1) *Ras*^{V12} line shown in the graph had one replicate with very few larvae and a healthy number of larvae in the second replicate.

phm>DHR51-RNAi (2) *; Ras*^{V12} also resulted in larvae with relatively normal developmental timing while either transgene alone resulted in aberrant developmental timing (Figure 4-5A). *phm>DHR51*-RNAi (2) *; Ras*^{V12} larvae had a range of body sizes; some were small (like *phm>Ras*^{V12} larvae), some were large (like *phm>DHR51*-RNAi (2) larvae), and others were normal. Despite the body size of the larvae, the RG was consistently overgrown,

similar to *phm>Ras*^{V12} RGs (Figure 4-5B). The general phenotypes of all the lines are listed in Table 4-1. Expression of *DHR51*-RNAi and *Ras*^{V12} in the PG was able to help restore normal developmental timing compared to *DHR51*-RNAi or *Ras*^{V12} expression alone in the PG. The effects on developmental timing seemed to be additive, rather than epistatic. This could mean that DHR51 and Ras were acting in parallel pathways to regulate ecdysone and overexpression of *Ras*^{V12} may compensate for reduced ecdysone biosynthetic gene expression due to loss-of-*DHR51*. However, it is still possible for DHR51 and Ras to function in the same pathway and the two proteins have a more complex relation. DHR51 was noted to reduce ERK activation after insulin stimulation in cell culture which suggested that DHR51 could function upstream of ERK (Friedman and Perrimon. 2006). However, the interaction between *DHR51*-RNAi and *Ras*^{V12} suggested that DHR51 could be one of the downstream effectors as well.

Since it seemed like DHR51 could interact in some way with Ras signaling, my question became 'how?". One possible connection was that *torso* (*tor*) was downregulated to 0.28-fold by *phm>DHR51*-RNAi (1) in the RNA-Seq data (P-value = 0.08) compared to *tor* expression in *phm>w*^{1118} RGs. Although *tor* is upstream of Ras/Raf/ERK signaling, I attempted to validate *tor* expression in both *DHR51*-RNAi lines with qPCR using BRGs from larvae 44 hours post L2/L3 molt since *tor* was highly enriched in the RG compared to whole body *tor* expression (Ou, et al. 2016). *tor* was only significantly downregulated in *phm>DHR51*-RNAi (1) BRGs (P-value = 0.034) and was unaffected in *phm>DHR51*-RNAi (2) BRGs (P-value = 0.060) (Figure 4-6A). This raised the possibility that *tor* was downregulated due to an off-target effect of *DHR51*-RNAi (1). However, since both *DHR51*-RNAi lines were able to help alleviate the *phm>Ras*^{V12} phenotype, this suggested that DHR51 could interact with the Ras/Raf/ERK pathway through another mechanism.

DHR51-RNAi was found to reduce ERK activation in cell culture when the cells were stimulated with insulin (Friedman and Perrimon. 2006). Insulin is recognized by Insulin-like receptor (InR) and can activate ERK. *InR* was downregulated in the RNA-Seq data of *phm>DHR51*-RNAi (1) RGs to 0.31-fold of normal expression (P-value = 0.16), which made *InR* a candidate gene for how DHR51 could interact with Ras/Raf/ERK signaling. I attempted to validate that *InR* was downregulated in both *DHR51*-RNAi lines using qPCR on RGs from larvae 44 hours after the L2/L3 molt. *phm>DHR51*-RNAi (1) significantly reduced *InR* to 0.57-fold of normal levels (P-value = 0.013), while *phm>DHR51*-RNAi (2) reduced *InR* expression to 0.72-fold but was not significantly different compared to *InR* expression in the control (P-value = 0.20) (Figure 4-6B). This suggested that *InR* could also be downregulated due to an off-target in the *DHR51*-RNAi (1) line, since *InR* was not be downregulated in *phm>DHR51*-RNAi (2) RGs. In addition, I found that *DHR51*-RNAi (1) targets a very similar sequence to the *DHR51*-RNAi that was used in the cell culture screen for regulators of ERK signaling (my RNAi was from VDRC, ID 37618 and the cell culture RNAi was from DRSC, ID DRSC06627) (Friedman and Perrimon. 2006). These two RNAi lines had the same predicted off-targets. If *tor* and *InR* are off-targets and downregulated in *DHR51*-RNAi (1), this calls into question whether DHR51 is actually an activator of ERK signaling as the reduced activation of ERK could be due to an off-target effect of *DHR51*-RNAi.

I have not found strong evidence that DHR51 regulates ecdysone production via the Ras/Raf/ERK pathway. Although *phm>DHR51*-RNAi was able to partially rescue the *phm>Ras^{V12}* phenotype, which suggested that DHR51 interact with the Ras/Raf/ERK pathway, this experiment did not rule out the possibility of DHR51 and Ras working in two parallel pathways to regulate ecdysone production. More experiments would be needed to differentiate

between the possibilities of DHR51 and Ras working in the same pathway or parallel pathways. There are also additional controls that need to be done to properly validate the results of the *phm>DHR51*-RNAi Ras^{V12} experiment, like having two *UAS* transgenes in the controls to keep the number of transgenes constant between all samples. *tor* and *InR* were not consistently downregulated in both *DHR51*-RNAi lines, which could make their downregulation in *phm>DHR51*-RNAi (1) due to off-target effects. This could also mean the reduced activation of ERK in cell culture was due to off-target effects and not specifically loss-of-*DHR51* as both RNAi lines were very similar. These data together may mean that DHR51 does not have a role in the Ras/Raf/ERK pathway, either as an upstream regulator (at least through Torso and InR) or downstream effector. Two other mechanisms remain as candidates for how DHR51 could regulate ecdysone production. Firstly, DHR51 was found to act upstream of the TOR pathway to regulate neuronal development (Yaniv, et al. 2012). Therefore, DHR51 may interact with the TOR pathway in the PG to regulate ecdysone production, but this has not been tested in the PG yet and will be discussed in the discussion section. Secondly, DHR51 may function in the circadian rhythm to regulate ecdysone production in the PG.

4.2.5 *DHR51*-RNAi disrupted the circadian rhythm in the PG

Previous research had demonstrated DHR51's role in the circadian rhythm. DHR51 was required in small ventral lateral neurons (s-LNvs), which are the master pacemaker neurons that generate free-running rhythms. Loss-of-*DHR51* in s-LNvs disrupted the ability to generate free-running rhythms (Beuchle, et al. 2012). Free-running rhythms maintain the circadian rhythm in the absence of external cues, like when in constant dark or light. DHR51 was later found to bind directly to the promoter of *period*, a core circadian rhythm gene, and *period* expression was significantly induced in cell culture with the addition of CLK, E75, and DHR51 (Jaumouille, et

al. 2015). Lastly, DHR51 was also found to bind to the promoter of *cyc*, which encodes another core circadian rhythm protein that works together with CLK, in a chromatin immunoprecipitation tiling array (ChIP-chip) (Kozlov, et al. 2017). This connection between DHR51 and the circadian rhythm was of interest because Dr. Francesca Di Cara, a previous postdoctoral fellow from our lab, identified that the circadian rhythm in the PG functioned in controlling developmental timing by regulating ecdysone production (Di Cara and King-Jones. 2016). Ecdysone biosynthetic genes had higher expression during the night compared to the day and *period*-RNAi or *timeless*-RNAi (Timeless works together with Period) in the PG during the night significantly reduced *phm*, *dib*, and *sad*, as well as genes related to cholesterol transport, *Start1* and *Npc1a*. This wide range of downregulated genes related to ecdysone production was similar to *phm>DHR51*-RNAi. When the RNA-Seq data for *phm>DHR51*-RNAi (1) was examined for circadian rhythm genes *tim* (*timeless*) appeared to be upregulated (2.8-fold, P-value = 0.07) and *per* (*period*) may have been downregulated (-2.5-fold, P-value = 0.47). This suggested that loss-of-*DHR51* could potentially disrupt the circadian rhythm in the PG. RGs for Qiuxiang Ou's RNA-Seq were dissected from larvae without regard for the circadian rhythm; they were likely not entrained to a light:dark cycle, raised in constant darkness, and dissected with bright lights. If loss-of-*DHR51* actually disrupted the circadian rhythm, the circadian rhythm could be the mechanism in which DHR51 regulates ecdysone production, as a dysfunctional circadian rhythm would have impaired ecdysone production.

I planned to use qPCR to examine the expression of *per* and *tim* in RGs two days after the L2/L3 molt in *phm>DHR51*-RNAi larvae to determine whether loss-of-*DHR51* disrupted the circadian rhythm. Animals were entrained to a 12 hour light:dark cycle (lights are turned on at ZT0 and turned off at ZT12) and RGs were dissected at various time points over a period of 24

hours (ZT1 – one hour after lights are turned on, ZT7 – seven hours after lights are turned on, ZT13 – one hour after lights are turned off, and ZT19 – seven hours after lights are turned off). First, I examined the expression of *per* and *tim* in *phm>w*^{1118} RGs at the stated time points to determine how *per* and *tim* expression oscillate in control RGs during this stage of L3 larvae. Normally, *per* and *tim* expression increase late during the day and hits maximum expression shortly after lights are turned off (~ZT13), followed by decreased expression during the rest of the night (Allada, et al. 1998; Jang, et al. 2015; Di Cara and King-Jones. 2016). Therefore, Period and Timeless protein levels peak later during the night. When I examined *per* and *tim* expression in RGs over 24 hours, I observed weak *per* circadian oscillations that followed the expected trend, however, *tim* had an unexpected rhythm that peaked at ZT1 and had a minor peak at ZT13 (Figure 4-7A). The degree of *per* and *tim* oscillations I observed were concerning because *per* and *tim* expression throughout the day were reported to have an expression range of at least tenfold (Jang, et al. 2015; Di Cara and King-Jones. 2016). I observed an expression range of about twofold for *per* and *tim*. *tim* expression also peaked at ZT1, when I had expected *tim* to peak at ZT13 based on previously reported *tim* expression data in the RG (Di Cara and King-Jones. 2016). One of my concerns was that the circadian rhythm could potentially dampen during late L3 larvae as the animals prepare for metamorphosis. The circadian rhythm was previously measured in RGs from early L3 larvae, but through personal communications with Dr. Di Cara, the circadian rhythm did not seem to be affected by developmental timing and the circadian rhythm should remain intact two days after the L2/L3 molt. Another potential source of error could come from dissecting larvae during the night / dark time points. My dissection process could have potentially exposed the larvae to too much light, despite trying to minimize light

exposure. Even still, I examined the circadian rhythm of *per* and *tim* in RGs from *phm>DHR51*-RNAi larvae.

phm>DHR51-RNAi (1) decreased *per* expression at all points throughout the 24 hours in the RG, however, *per* expression still appeared to oscillate to some extent with relatively normal timing, peaking at ZT13 and at a trough at ZT1 (Figure 4-7B). This confirmed the RNA-Seq data that *per* was downregulated in *phm>DHR51*-RNAi (1) RGs from larvae raised in constant darkness (*per* expression at 0.40 of controls, P-value = 0.47). *phm>DHR51*-RNAi (2) affected *per* expression differently, by shifting *per* expression. *per* expression peaked at ZT13 in control RGs, but *per* peaked later at ZT19 in *phm>DHR51*-RNAi (2) RGs. The circadian rhythm was disrupted by a similar phase shift when insulin signaling was impaired in the PG (Di Cara and King-Jones. 2016). Unfortunately, both *DHR51*-RNAi lines did not affect *per* in a similar fashion, however, both *DHR51*-RNAi lines did disrupt normal *per* expression; *phm>DHR51*-RNAi (1) dampened *per* expression and *phm>DHR51*-RNAi (2) caused a phase shift in *per* expression.

phm>DHR51-RNAi (1) caused minor upregulation of *tim* throughout the 24 hours RGs were collected and *tim* expression was shifted (Figure 4-7C). In control RGs, *tim* expression peaked at ZT1, but *tim* expression peaked at ZT19 in *phm>DHR51*-RNAi (1) RGs. Increased *tim* expression due to *phm>DHR51*-RNAi (1) validated the RNA-Seq data that *tim* was upregulated 2.8-fold (P-value = 0.07). *phm>DHR51*-RNAi (2) resulted in much higher *tim* expression than both control and *phm>DHR51*-RNAi (1) RGs. Unlike *tim* expression in *phm>DHR51*-RNAi (1) RGs, *tim* expression was not phase shifted in *phm>DHR51*-RNAi (2) RGs and had the same phase as *tim* in control RGs. *phm>DHR51*-RNAi consistently increased *tim* expression compared to control RGs, which suggested, like *per*, *tim* was also disrupted to some extent.

Taking *per* and *tim* together, it appeared that *DHR51*-RNAi likely disrupted the circadian rhythm in the PG by affecting the expression levels of *per* and *tim* and causing phase shifts in *per* and *tim* expression, although the exact mechanism was inconsistent between the two *DHR51*-RNAi lines. This suggested that DHR51 plays a role in the circadian rhythm in the PG. However, this experiment should be repeated to get more robust *per* and *tim* circadian expression in control RGs, possibly by dissecting larvae earlier after the L2/L3 molt. In addition, conditional CRISPR with the *DHR51* 2xgRNA lines can be used to create *DHR51* mutants in the PG to determine how mutant *DHR51* affects the expression of *per* and *tim*, since *per* and *tim* were affected differently depending on the *DHR51*-RNAi line used. I tried to examine protein levels of Period and Timeless to determine whether PER and TIM protein was normally accumulating in *phm>DHR51*-RNAi PGs using previously published Period and Timeless antibodies (Shafer, et al. 2002). However, when I attempted to view PER and TIM with immunofluorescence, there was no clear and consistent signal for both proteins at any time point tested in control RGs(data not shown). So, it remained unknown how PER and TIM are affected in the PG by *phm>DHR51*-RNAi. One potential source of error was that I attempted to entrain flies to two different 12 hour light:dark cycles to avoid sample collection in the middle of the night (in one schedule, ZT0 was at 10:00 AM and in the other schedule, ZT0 was at 2:00 PM). The free-running clock could potentially interrupt the altered schedule with ZT0 at 2:00 PM. Immunofluorescence of PER and TIM should be repeated with a single, standard light:dark cycle (ZT0 at 10:00 AM). *per* and *tim* expression were examined using the single, standard light:dark cycle.

I provided evidence that loss-of-*DHR51* disrupted the circadian rhythm in the PG, which suggested that DHR51 was required to maintain the circadian rhythm in the PG. Disruption of

the circadian rhythm could then cause the downregulation of genes that regulate and are involved in ecdysone production. The circadian rhythm could be the mechanism in which DHR51 regulates ecdysone production, as a disruption in the circadian rhythm would disrupt ecdysone production. However, DHR51 could potentially work in multiple pathways, so future experiments will still need to examine whether DHR51 interacts with the TOR pathway in the PG.

4.3 Discussion

4.3.1 DHR51 is required for ecdysone production

Loss-of-*DHR51* caused developmental defects that indicated that ecdysone production could have been impaired. RNA-Seq and qPCR on *phm>DHR51*-RNAi RGs showed that many genes involved in ecdysone production were downregulated. Loss-of-*DHR51* caused a broad downregulation of genes that included the ecdysone biosynthetic enzyme genes (*nvd*, *sro*, *spok*, *phm*, *dib*, *sad*) (Figure 4-2), genes involved in cholesterol transport (*Start1* and *Npc1a*), and genes that regulate ecdysone production (*broad*, *torso*, and *Ouib*) (Yoshiyama, et al. 2006; Niwa, et al. 2010; Ono, et al. 2006; Warren, et al. 2004; Warren, et al. 2002; Roth, et al. 2004; Huang, et al. 2005; Moeller, et al. 2013; Rewitz, et al. 2009; Komura-Kawa, et al. 2015). The downregulation of the ecdysone biosynthetic enzyme genes reduced the overall ecdysone titers in *phm>DHR51*-RNAi larvae during the mid and late L3 stage (Figure 4-3). DHR51 seemed to be responsible for ecdysone production throughout the entire L3 stage, including the minor ecdysone pulses at 28 hours after the L2/L3 molt (Warren, et al. 2006), rather than specifically for the major ecdysone pulse at the end of the L3 stage. This data provided evidence that DHR51 did not fine-tune ecdysone production by regulating a specific gene in preparation for the major ecdysone pulse, but that DHR51 regulated general ecdysteroidogenic genes throughout the L3 stage.

The second time when ecdysone was measured at 64 hours after the L2/L3 molt, only one time point was used for control ecdysone levels. Ecdysone levels at this time were not significantly different between *phm>w*^{1118} larvae and *phm>DHR51*-RNAi (2) larvae (Figure 4-3B). Since only a single time point was tested when I measured 64 hours after the L2/L3 molt, it is impossible to say at what point in the ecdysone pulse the controls were at. Ecdysone in

p*hm>DHR51*-RNAi (2) larvae was increasing at 64 hours after the L2/L3 molt because the ecdysone titer rose at 78 hours after the L2/L3 molt. However, if the ecdysone pulse in control larvae peaked at 64 hours or was declining, while the ecdysone pulse was still increasing in *phm>DHR51*-RNAi (2) larvae, the ecdysone titer could be similar between *phm>w*^{1118} and *phm>DHR51*-RNAi (2) larvae despite that the larvae were at different developmental times. To resolve this issue, more time points would need to be included in a single experiment.

A delay in the ecdysone pulse in *phm>DHR51*-RNAi (2) larvae was supported by feeding these larvae 20E. 20E feeding was able to rescue the delay in *phm>DHR51*-RNAi (2), indicating that the major ecdysone pulse was delayed (Figure 4-4). A 100% rescue of the developmental delay was not observed, possibly due to exogenous 20E was less efficient than endogenous 20E or the exogenous 20E concentration in the *phm>DHR51*-RNAi (2) larvae was still lower compared to normal 20E concentrations reached during the major ecdysone pulse. 20E feeding was also able to partially rescue *phm>DHR51*-RNAi (1) larvae. These experiments demonstrated that loss-of-*DHR51* disrupted ecdysone production, which leads to the developmental defective phenotypes observed in each of the RNAi lines.

Unlike the *DHR51*-RNAi lines, 20E feeding was unable to rescue *unf*^{XI} mutants (Figure 4-4D). *unf*^{XI} mutants have phenotypes that seem independent of ecdysone or DHR51 PG function, such as the wing expansion defect, motor defects, and defects in re-extension of adult γ neurons, as these phenotypes were not observed on *Spok-Cas9>DHR51* 2xgRNA 3m animals. In addition, the pupal lethality observed in *unf*^{XI} may also not be related to ecdysone as 20E feeding had about the same percentage of pupal lethality as *unf*^{XI} animals raised on control media. However, I have not tested whether *unf*^{XI} larvae are developmentally delayed like the *act-Cas9>DHR51* 2xgRNA CRISPR lines. In addition, *unf*^{XI} larvae had reduced ecdysone titers, so

development should be accurately timed. If there is a developmental delay, unf^{XI} larvae should be raised on 20E-supplemented media to determine whether 20E feeding is able to rescue a possible delay in unf^{XI} animals.

One interesting observation was that all the ecdysone biosynthetic enzyme genes were downregulated except for *Cyp6t3* (Figure 4-2). Cyp6t3 functions within the "Black Box" of ecdysone production (along with Spok and Sro), where the unknown rate-limiting step occurs (Ou, et al. 2011). *Cyp6t3* has low expression for an ecdysone biosynthetic enzyme gene which suggested that Cyp6t3 could function as a rate-limiting step in ecdysone production. However, overexpression of *Cyp6t3* was not sufficient to accelerate development by increasing ecdysone production, but increased *Cyp6t3* expression was required for the developmental acceleration of *DHR4* mutant animals (Ou, et al. 2011). Another unique feature of *Cyp6t3* was that *Cyp6t3's* expression was increased in the RG when cellular heme levels were low by at least tenfold, but the variability was very high between replicates (in *PPOX*-deficient, *phm> FeCH*-RNAi, *Nos*-RNAi, and *spz5*-RNAi RGs) according to the RNA-Seq data. *Cyp6t3* was the only ecdysteroidogenic gene to respond to low cellular heme levels, but *Cyp6t3* could be responding to low ecdysone levels. If *Cyp6t3* is responding to low ecdysone levels, that would provide further evidence that Cyp6t3 could be one of the rate-limiting enzymes in ecdysone production. However, *Cyp6t3* expression was unaffected in *phm>DHR51*-RNAi (2) RGs despite that the larvae had low ecdysone titers. If *Cyp6t3* is a specially regulated gene for ecdysone production, DHR51 does not seem to be responsible for regulating *Cyp6t3*.

4.3.2 DHR51 and ecdysone signaling

After identifying that DHR51 was required for ecdysone biosynthetic enzyme gene expression to mount a timely and sufficient ecdysone pulse, I attempted to determine how

DHR51 regulated ecdysone production and what signaling pathways DHR51 may be involved in. From the literature, there was evidence that DHR51 could interact with the Ras/Raf/ERK pathway, the TOR pathway, and the circadian rhythm, all of which can also influence ecdysone production (Friedman and Perrimon. 2006; Yaniv, et al. 2012; Beuchle, et al. 2012). Brain-derived PTTH is recognized by its receptor, Torso, and signals through the Ras/Raf/ERK pathway to initiate ecdysone production for the major ecdysone pulse at the end of the L3 stage (McBrayer, et al. 2007; Rewitz, et al. 2009). Co-expressing *phm>DHR51*-RNAi and Ras^{V12} together was able to even out the developmental timing, compared to each RNAi line separately, such that the larvae developed with relatively normal timing (Figure 4-5A). Co-expressing the two transgenes appeared to have an additive effect, rather than epistatic. This suggested that DHR51 and Ras could function in two parallel pathways to regulate ecdysone production, rather than the same pathway. Although, larvae should be examined in the reciprocal experiment (overexpressing *DHR51* and expressing *Ras*-RNAi) to rule out the possibility that DHR51 and Ras act in the same pathway.

If DHR51 and Ras do function within the same pathway, they would likely have a complex relationship. If DHR51 was solely upstream of Ras, larvae that expressed *DHR51*-RNAi and Ras^{V12} would be expected to have the Ras^{V12} phenotype (developmental acceleration). This could indicate that DHR51 is also downstream of the pathway and could form a feedback loop to help amplify the Ras/Raf/ERK signal, similar to EcR and Broad (Moeller, et al. 2013). The most likely explanation would be that DHR51 and Ras function in a separate, parallel signaling pathway, causing the additive effects observed. If one pathway is no longer inducing ecdysone production and another pathway is overactive signaling ecdysone production, the

effects could cancel out, leading to normal ecdysone production and normal developmental timing.

An issue with the *phm>DHR51*-RNAi Ras^{V12} experiment was low reproducibility between *DHR51*-RNAi (1) Ras^{V12} lines (multiple lines were created because a recombination event was required to get the transgenes on the same chromosome). Not only did some lines differ from the others, but technical replicates also varied, even though all the lines and replicates should have similar phenotypes. In some vials of replicates, few embryos were laid, the food dried out, and everything died within the vial, while other replicates appeared relatively healthy. The end result was that multiple of the *DHR51*-RNAi (1) Ras^{V12} lines only had one successful replicate so developmental timing could not be accurately quantified. Another issue was that the number of transgenes present in the animals was not controlled. Double transgene animals had two *UAS* promoters, while controls only had a single *UAS* promoter. GAL4 could have been "diluted" at each promoter in double transgene animals, weakening the RNAi or overexpression phenotype, which could mimic a rescue. However, *phm>DHR51*-RNAi (2) ; Ras^{V12} larvae still had enlarged RGs, similar to *phm>*Ras^{V12}, which indicated that the transgenes were still working to some extent (Figure 4-5B). Much later testing for a different experiment found that *phm>DHR51*-RNAi (1) ; *UAS-EGFP* larvae were still L3 arrested, suggesting that the RNAi line could still arrest larval development with a second *UAS* promoter present. Even still, the *phm>DHR51*-RNAi Ras^{V12} experiment should be repeated to control for the number of transgenes (including *UAS-EGFP* in the control lines) and increasing the number of technical replicates to get a more accurate view of developmental timing for each line.

If DHR51 does act in the same pathway as Ras/Raf/ERK, I attempted to identify how by trying to find potential upstream pathway proteins that DHR51 could regulate. I examined the

RNA-Seq data and found that *torso* and *InR* were downregulated in RGs expressing *phm>DHR51*-RNAi (1). *InR* was examined because InR can also activate Ras/Raf/ERK signaling (Clemens, et al. 2000). When I attempted to validate *tor* and *InR* expression with qPCR in both *DHR51*-RNAi lines, *tor* and *InR* were only significantly downregulated in *phm>DHR51*-RNAi (1) samples and unaffected in *phm>DHR51*-RNAi (2) samples (Figure 4-6). This suggested that *tor* and *InR* were off-target effects of *DHR51*-RNAi (1) and may not be true targets of DHR51. If *tor* and *InR* are off-targets of *DHR51*-RNAi (1), that could explain how *DHR51*-RNAi reduced ERK activation in cell culture as InR is required for insulin to stimulate ERK activation. The RNAi used in cell culture was very similar to *DHR51*-RNAi (1) and had the same predicted off-targets (Friedman and Perrimon. 2006). Given all this, it seemed unlikely that DHR51 is involved in Ras/Raf/ERK signaling and *phm>DHR51*-RNAi Ras^{V12} was able to rescue larvae due to interactions in two parallel pathways.

Future experiments could follow up on another candidate pathway that DHR51 could interact with in the PG, the TOR pathway. DHR51 functions upstream of the TOR pathway in mushroom body neurons during developmental remodeling (Yaniv, et al. 2012; Bates, et al. 2014; Rabinovich, et al. 2016). The TOR pathway promotes ecdysone production in the PG (Layalle, et al. 2008). The TOR pathway was originally investigated because *Tsc1* (a negative regulator of TOR) was reported as a direct target gene of murine NR2E3 (the vertebrate homolog of DHR51) (Haider, et al. 2009). However, I suspect that *Tsc1* was a false positive given the large number of genes examined to be misregulated in *Nr2e3* mutant retinas, the weak change in *Tsc1* expression in *Nr2e3* mutant retinas, and that *Tsc1* DNA was not identified in a chromatin immunoprecipitation followed by PCR. Nevertheless, I examined the expression of multiple TOR pathway genes in the *phm>DHR51*-RNAi (1) RNA-Seq data, but nothing was misregulated

(*Tsc1* expression was down to 0.81 relative to the control [P-value = 0.74]). Although there are no promising genes to follow up on, genetic interaction experiments with TOR pathway loss-of-function and gain-of-function mutants can be used in combination with *DHR51*-RNAi and *DHR51* cDNA to test for interactions and potential rescue of aberrant phenotypes, similar to what was done previously (Yaniv, et al. 2012). This would provide insight into whether DHR51 is upstream of the TOR pathway to regulate ecdysone production in the PG.

4.3.3 DHR51 is likely involved in the prothoracic gland circadian rhythm

DHR51 was found to be required in small ventral lateral neurons (s-LNvs), the master pacemaker neurons, for proper s-LNv function and to generate free-running rhythms (Beuchle, et al. 2012; Kozlov, et al. 2017). DHR51 had rhythmic protein levels in s-LNvs, peaking just after the lights are turned on (ZT2) and DHR51 protein was at a minimum after the lights turned off (ZT14). However, rhythmic DHR51 was dependent on tissue type, as rhythmic DHR51 protein levels were not observed in l-LNvs (Beuchle, et al. 2012). Additionally, *DHR51* mRNA levels did not appear to cycle in any of the LNvs (Kula-Eversole, et al. 2010). However, a cursory examination of Dr. Di Cara's RNA-Seq that compared control RGs from young L3 larvae between ZT0-4 and ZT18-22 showed that *DHR51* had a tenfold higher expression between ZT0-4 compared to ZT18-22, which complemented DHR51 protein levels in s-LNvs (Di Cara and King-Jones. 2016). This suggested that *DHR51* could have circadian expression in the PG, but *DHR51* transcripts or protein levels need to be verified with either qPCR or immunofluorescence, respectively. DHR51 does seem to function in the circadian rhythm as DHR51 bound to *per* regulatory sequences and enhanced CLK/CYC transcriptional upregulation of *per*, along with E75, in S2 cells (See Figure 4-1 for the circadian rhythm) (Jaumouille, et al.

2015). DHR51 and E75 were not involved in *tim* expression. These data suggested that DHR51 had a crucial role in establishing and maintaining the circadian rhythm.

Recently, the circadian rhythm was shown to be necessary for ecdysone production in the PG (Di Cara and King-Jones. 2016). Ecdysone was predominantly produced during the night when the expression of the ecdysone biosynthetic genes were at a maximum (ZT18-22). As a side note, *Cyp6t3* expression was higher during the day which could potentially explain why *Cyp6t3* expression behaved differently in *phm>DHR51*-RNAi RGs compared to the other ecdysone biosynthetic enzyme genes. *phm> per*-RNAi and *tim*-RNAi during the night resulted in a broad downregulation of ecdysteroidogenic genes in the RG, similar to *phm>DHR51*-RNAi (Di Cara and King-Jones. 2016). The majority of the ecdysone biosynthetic enzyme genes were downregulated in response to *phm>DHR51*-RNAi, *per*-RNAi, and *tim*-RNAi, as well as *Start1* and *Npc1a*, genes that are involved in cholesterol transport, were also downregulated. The broad downregulation of ecdysteroidogenic genes in *DHR51*-RNAi, *per*-RNAi, and *tim*-RNAi, as well as previously published experiments that demonstrated that DHR51 had a role in the circadian rhythm, made the circadian rhythm a prime candidate as a way for DHR51 to regulate ecdysone production.

I attempted to determine whether *phm>DHR51*-RNAi disrupted the circadian rhythm in RGs from larvae at least 48 hours after the L2/L3 molt by using qPCR to measure *per* and *tim* expression every six hours over 24 hours. In control RGs from *phm>*w^{1118} larvae, the circadian expression of *per* and *tim* seemed to be blunted, as *per* and *tim* did not have a wide range of expression (only about a twofold range in expression) (Figure 4-7A). Previous expression data on *per* and *tim* showed about a tenfold range in expression throughout a day (peaking at ZT13 and at a minimum at ZT1), which was observed in RGs from young L3 larvae (within 24 hours

of the L2/L3 molt) (Jang, et al. 2015; Di Cara and King-Jones. 2016). The dampened circadian expression of *per* and *tim* that I observed was worrying, as personal communication with Dr. Di Cara suggested that the circadian rhythm would be maintained in older (2 days old) L3 larvae. However, it seemed like *tim* expression may decrease throughout the L3 stage, and although *per* expression seemed to be relatively constant throughout the L3 stage, *per* had fairly high C_T values in my qPCR, indicating low expression (Ou, et al. 2016). If the expression of *tim* decreases throughout the L3 stage, that might explain the dampened circadian expression of *tim* and *per*. Despite the reduced range of expression for *per* and *tim*, *per* expression was cycling as expected (expression peaked at ZT13 – one hour after the lights are turned off and at a minimum early in the morning). However, *tim* expression peaked at ZT1, when I had expected *tim* expression to also peak at ZT13. This experiment will likely need to be repeated, either using larvae from newly molted L3 larvae or using immunofluorescence to observe PER and TIM protein levels and subcellular location.

With the oddities with *per* and *tim* expression in the RG that I observed, I still tested whether *phm>DHR51*-RNAi would disrupt the circadian rhythm in RGs dissected from late L3 larvae entrained to a 12 hour light:dark cycle. *phm>DHR51*-RNAi (1) decreased *per* expression throughout the 24 hours that samples were collected (Figure 4-7B). *per* expression may still have a circadian expression cycle, but the *per* expression range was dampened even more compared to the controls. *phm>DHR51*-RNAi (2) caused a phase shift so that *per* expression peaked six hours later at ZT19. *phm>DHR51*-RNAi (1) caused a phase shift such that *tim* expression peaked six hours earlier at ZT19 and overall *tim* expression was higher (Figure 4-7C). While *phm>DHR51*-RNAi (2) upregulated *tim*, the phase of *tim* expression was similar to *phm>*w^{1118} controls (peaked at ZT1). Both *DHR51*-RNAi lines disrupted *per* and *tim* expression in the RG,

evidenced by phase shifts or misregulation of *per* and *tim* expression that could desynchronize the circadian clock in the PG relative to other tissues. This data provided evidence that loss-of-*DHR51* in the PG could disrupt the circadian rhythm.

One issue was that the *DHR51*-RNAi lines did not similarly disrupt either per or tim. This experiment should be repeated, preferably in earlier L3 larvae that should have a more robust circadian expression of *per* and *tim* throughout a day and the *DHR51* 2xgRNA conditional CRISPR lines should be tested to determine how exactly loss-of-*DHR51* effects *per* and *tim* expression. In addition, PER and TIM protein can be examined with immunofluorescence. I attempted to do this, but I used two different 12 hour light:dark cycles so all dissections could be done during normal working hours (one cycle had lights on from 10:00 am to 10:00 pm and the other had lights on from 2:00 pm to 2:00 am). I did not observe strong or consistent PER or TIM staining using previously published antibodies against PER and TIM. The free-running clock may have been interfering with the light:dark cycle starting at 2:00 pm. This experiment should be repeated using a single 12 hour light:dark cycle. Given the data, it seemed that DHR51 was involved in the circadian rhythm in the PG and DHR51 regulated ecdysteroidogenic genes through the circadian rhythm, but more experiments are needed to confirm this result.

4.4 Figures

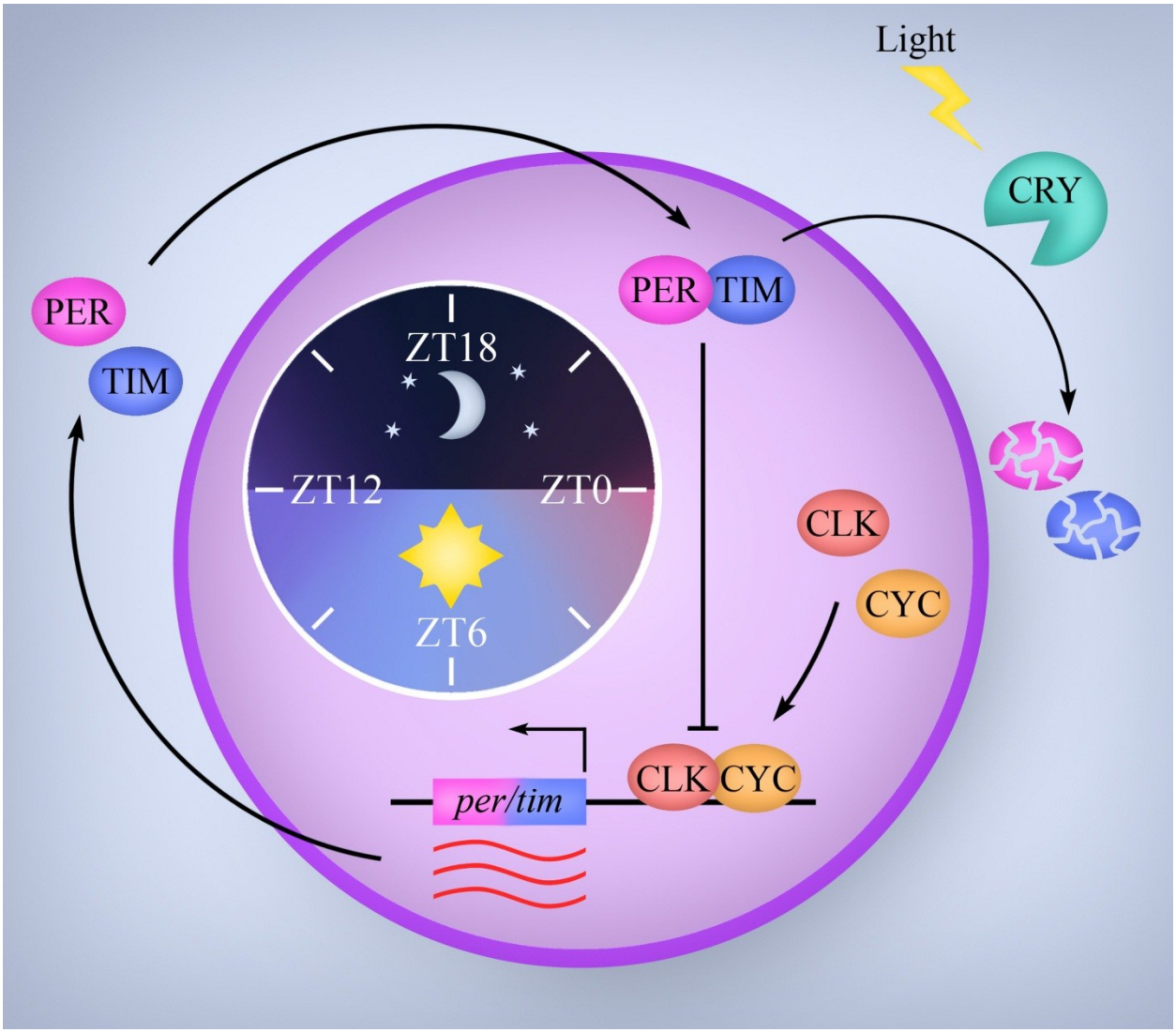

Figure 4-1. The core circadian rhythm components in *Drosophila melanogaster*. CLOCK (CLK) and CYCLE (CYC) protein build up in the early morning and bind to *timeless* (*tim*) and *period* (*per*) genes (represented as one gene), increasing transcription until the light:dark transition when expression is at a maximum. PER and TIM accumulate outside of the nucleus (large purple circle) until PER and TIM form a heterodimer and transition into the nucleus late during the night and inhibit their own expression via inhibition of CLK and CYC late in the night. Light activates CRYPTOCHROME (CRY), which degrades TIM protein (PER is degraded by another mechanism and not shown for simplicity). Flies were kept on a 12 hour light:dark cycle. ZT = Zeitgeber time. ZT0 = lights turn on. ZT12 = lights turn off. In mammals, CYCLE is replaced by BMAL1 and TIMELESS is replaced by CRYPTOCHROME. The circadian rhythm is reviewed in (Hardin and Panda. 2013).

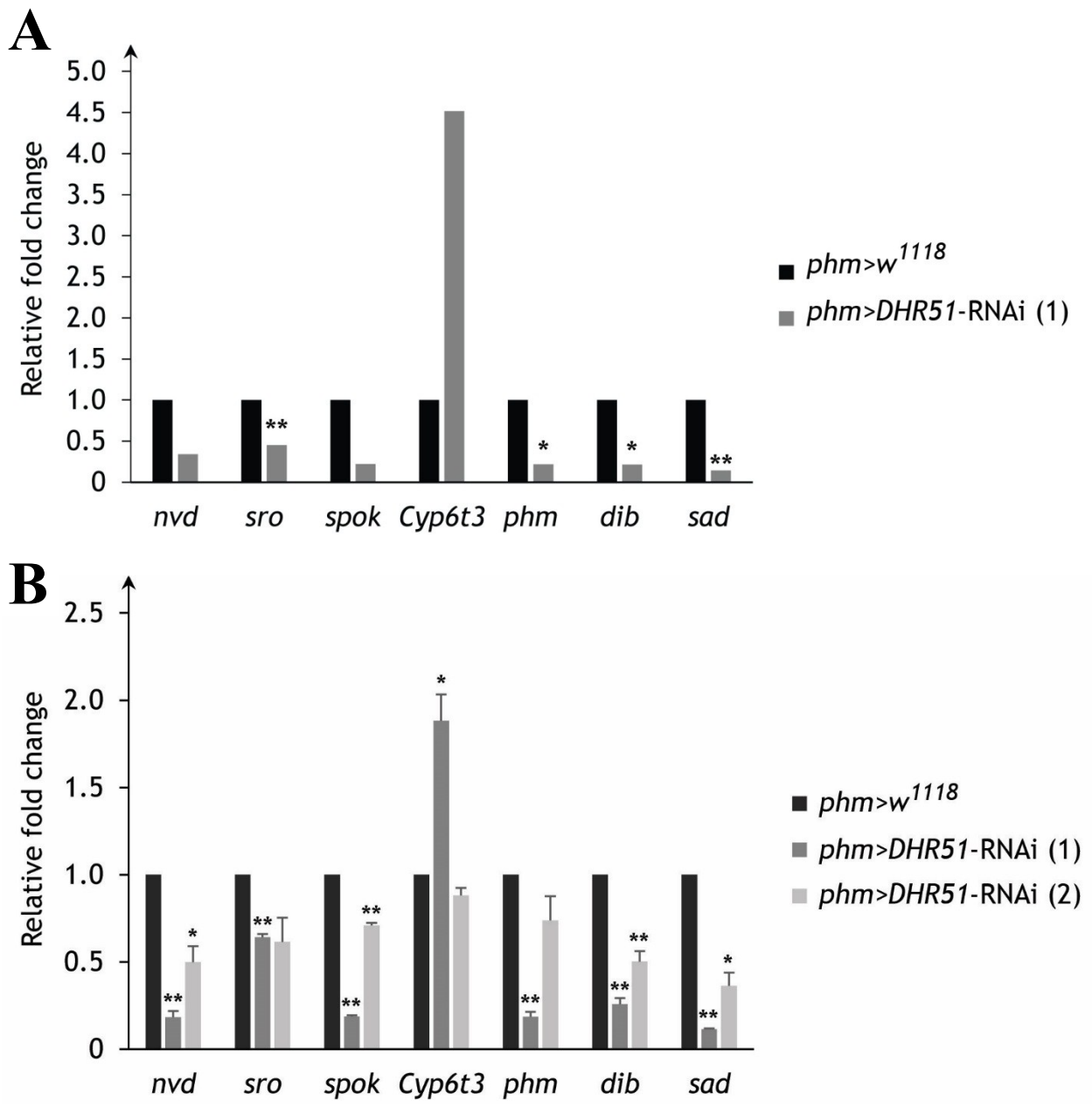

Figure 4-2. DHR51 was required for the expression of the ecdysone biosynthetic genes. A) RNA-Seq data of ring glands from 44 hour post L2/L3 molt larvae. B) qPCR of brain-ring glands from 44 hour post L2/L3 molt larvae. *phm>* = *phm22-GAL4*. *nvd* = *neverland*. *sro* = *shroud*. *spok* = *spookier*. *phm* = *phantom*. *dib* = *disembodied*. *sad* = *shadow*. * = P-value < 0.05. ** = P-value < 0.01. A Student's t-test was used to determine significance relative to *phm>w*^{1118} for the expression of each gene.

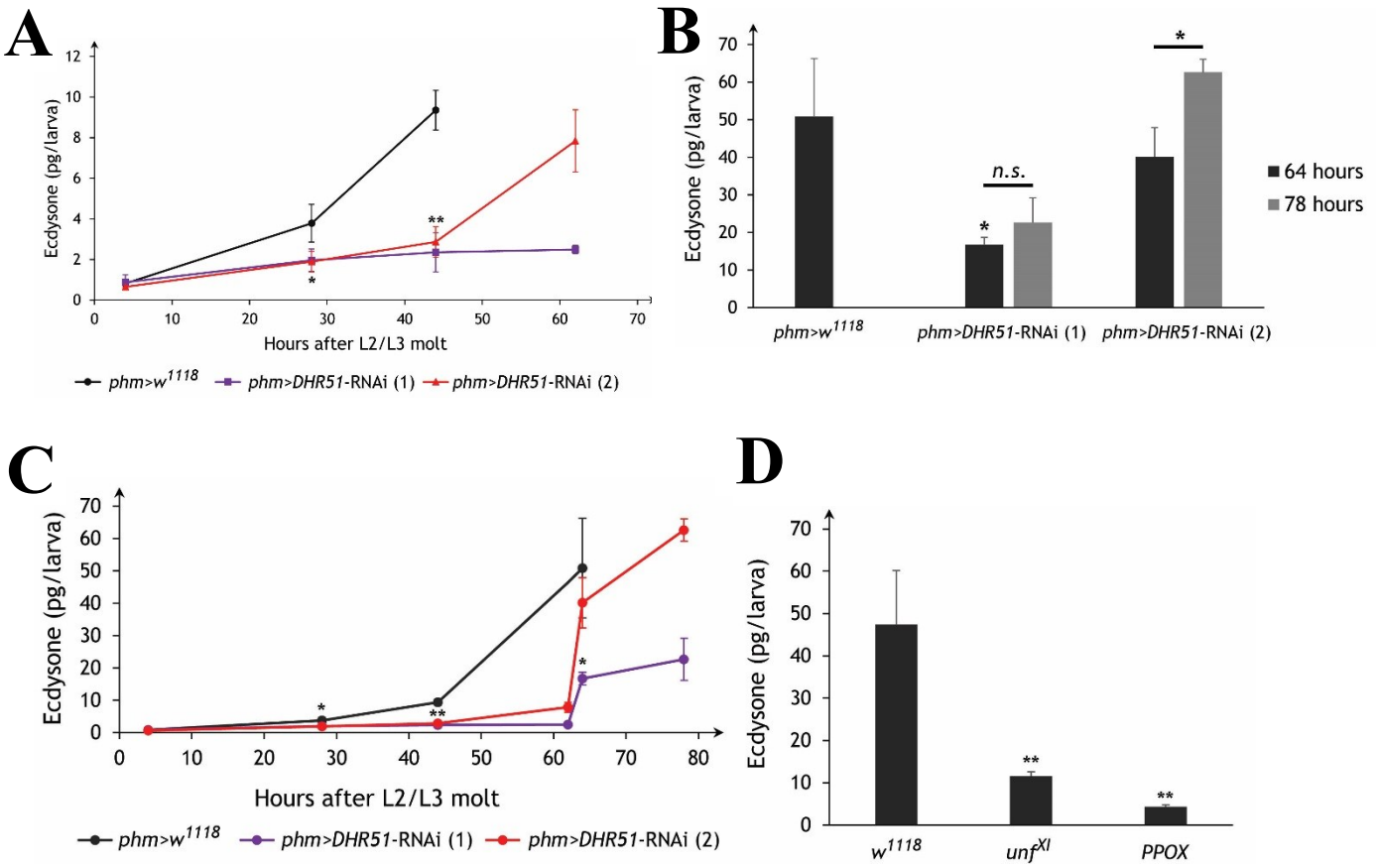

Figure 4-3. Loss-of-*DHR51* in the prothoracic gland reduced ecdysone in whole body larvae. A) Larvae were staged at the L2/L3 molt prior to being collected. Whole body larvae were used for the ecdysone measurement. * applies to both *DHR51*-lines. B) Ecdysone was re-measured in later larvae since the major ecdysone pulse was not measured in A. Larvae were collected 64 and 78 (64+14 hours, when control larvae have formed pupae) after the L2/L3 molt. Significance is relative to *phm>w*^{1118} at 64 hours. C) Data from A and B compiled into one graph. Experiments were done at different times on two separate plates, so the numbers do not align and there is a massive shift from one experiment to the other. *phm>* = *phm22-GAL4*. D) Ecdysone was measured in whole body *unf*^{XI} and *PPOX* mutant larvae 60 hours after the L2/L3 molt. Error bars represent the standard deviation. * = P-value < 0.05. ** = P-value < 0.01. A Student's t-test was used to determine significance. Asterisks above the columns are relative to the *phm>w*^{1118} control at the same time point. Asterisks above the bars are relative between the two samples at the end of the bar. *n.s.* = not significant.

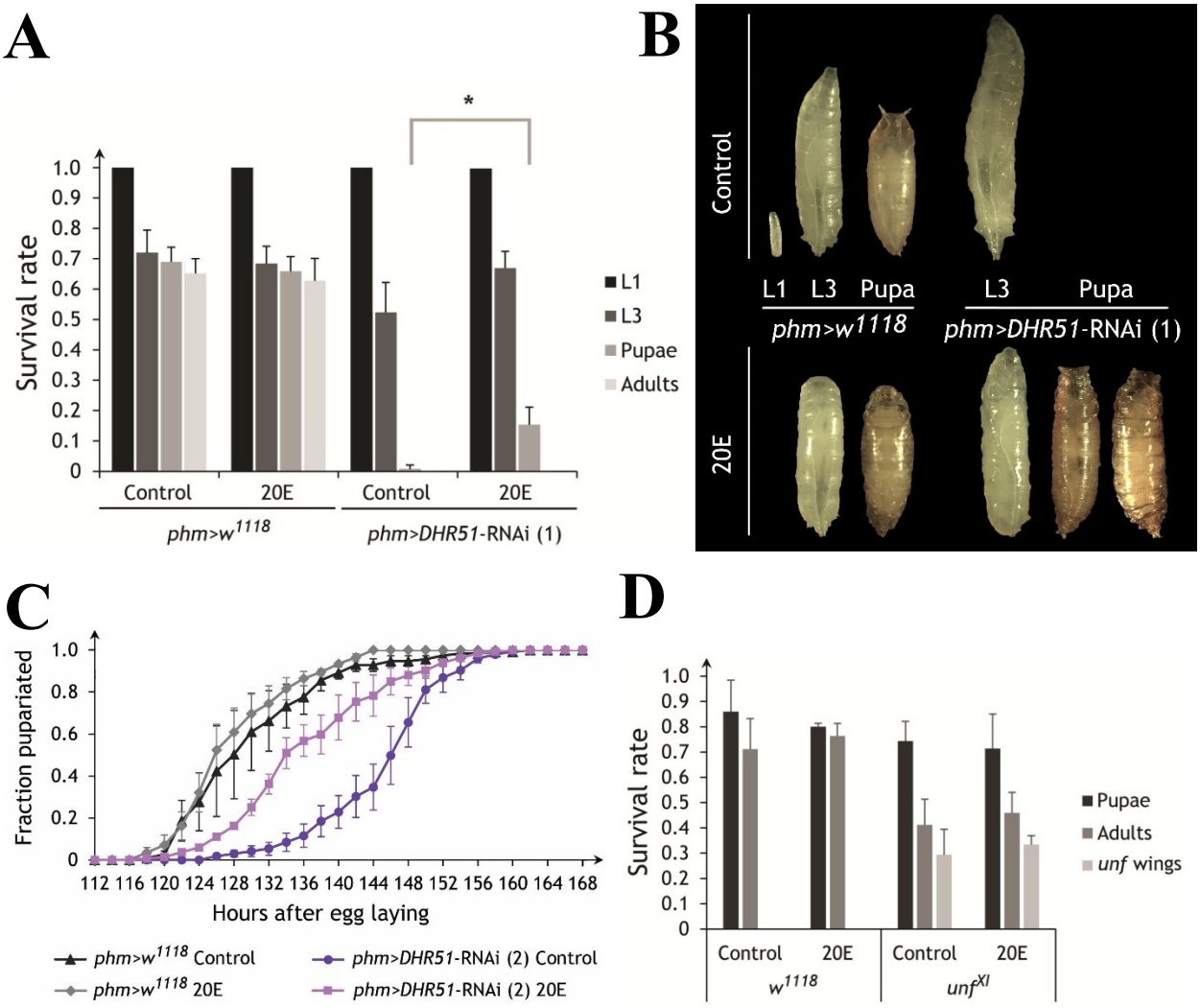

Figure 4-4. *phm>DHR51*-RNAi larvae were partially rescued by 20-hydroxyecdysone feeding. A) 50 L1 larvae were transferred to either media supplemented with 330 µg/ml of 20E (20-hydroxyecdysone) or control media (with equal amounts of ethanol as 20E food). L1 larvae were counted and then moved onto fresh control or 20E-supplemented media. The grey bracket at the top measured significance between *phm>DHR51*-RNAi (1) pupae on control media compared to pupae on 20E-supplemented media via a Student's t-test. Survival was measured as a fraction of initial L1. * = P-value < 0.05. B) Images of *phm>w*^{1118} and *phm>DHR51*-RNAi (1) animals raised on control and 20E-supplemented media. *phm>DHR51*-RNAi (1) larvae are arrested on control media but attempt to form pupae when on 20E-supplemented media. C) 50 embryos were transferred to media supplemented with 330 µg/ml 20E or control food. Larvae were timed until puparium formation. D) *unf*^{XI} larvae were grown on normal media until identified (non-GFP larvae) at the L2 stage. Both *unf*^{XI} and *w*^{1118} L2 larvae were transferred to control media or media supplemented with 200 µg/ml of 20E. Survival was determined relative to the number of L2 larvae transferred. *unf* wings refer to the characteristic unexpanded wings observed in *unf* mutants. Error bars represent the standard deviation. A Student's t-test determined that animals raised on 20E-supplemented media did not significantly differ from animals raised on control media. *unf = DHR51*. *phm> = phm2-GAL4*.

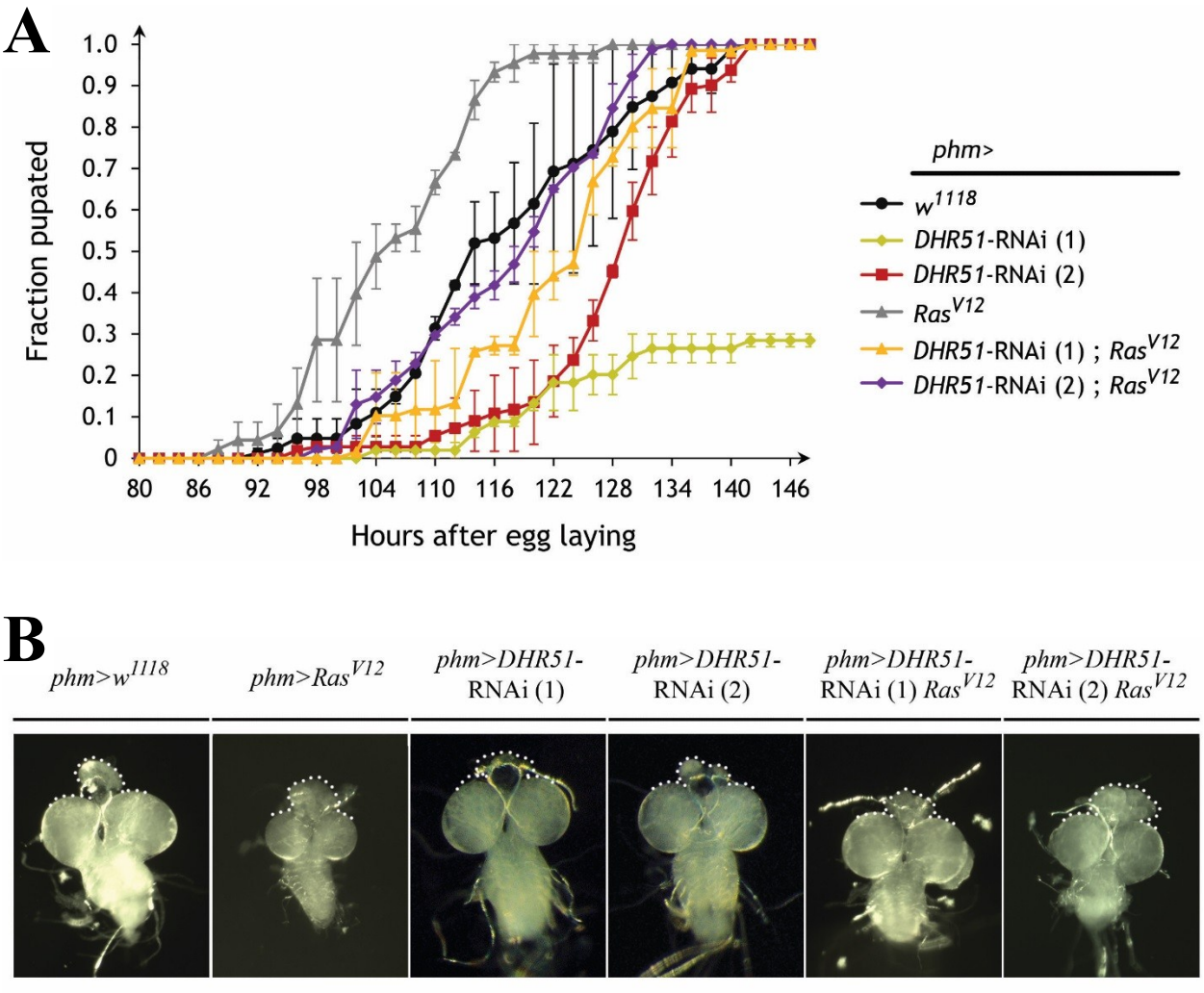

Figure 4-5. *DHR51*-RNAi rescued the *Ras^{V12}* overexpression developmental acceleration phenotype. A) *DHR51*-RNAi and *Ras^{V12}* were expressed in the PG with *phm22-GAL4* (*phm>*). Pupae were counted as larvae began metamorphosis. The fraction of pupae was calculated based on the final number of pupae observed, except for *phm>DHR51*-RNAi (1) since that resulted in an L3 arrest, however, some pupae were observed. Error bars represent the standard deviation. B) Brain-ring glands were dissected 5 days after egg laying. Ring glands are outlined in a dotted white line. Ras^{V12} is a constitutively active form of Ras.

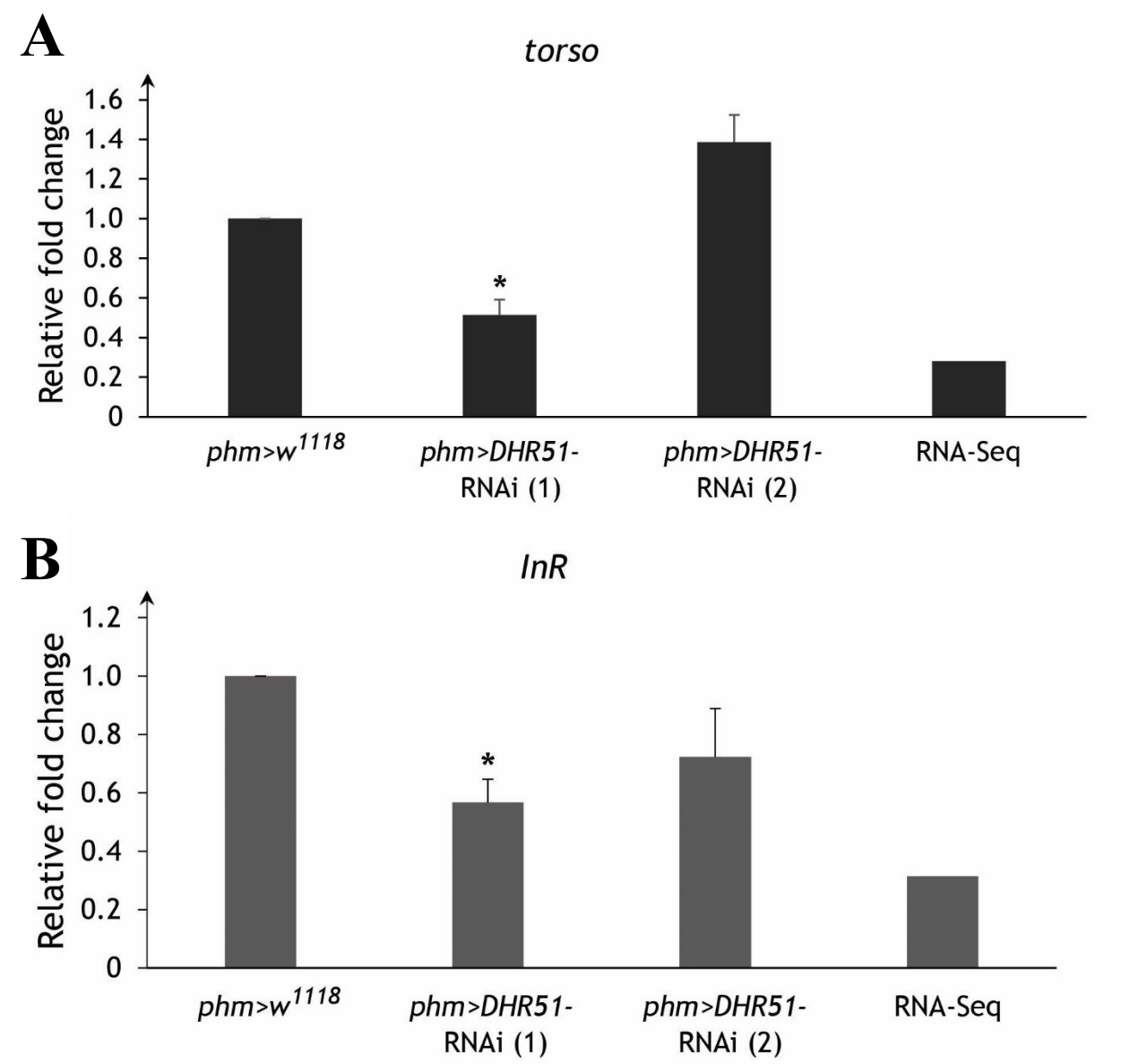

Figure 4-6. *phm>DHR51*-RNAi did not consistently downregulate *torso* and *InR* in the ring gland. A) qPCR of brain-ring gland samples from *phm>DHR51*-RNAi larvae 44 hours after the L2/L3 molt. *torso* is highly enriched in the ring gland compared to the whole body by greater than 20-fold. B) qPCR to determine *InR* (*Insulin-like Receptor*) in *phm>DHR51*-RNAi ring glands from larvae 44 hours post L2/L3 molt. The RNA-Seq data was of *phm>DHR51*-RNAi (1) ring glands from larvae 44 hours after the L2/L3 molt. * = P-value < 0.05. *phm>* = *phm22-GAL4*. A Student's t-test was used to determine significance relative to the *phm>w*^{1118} control

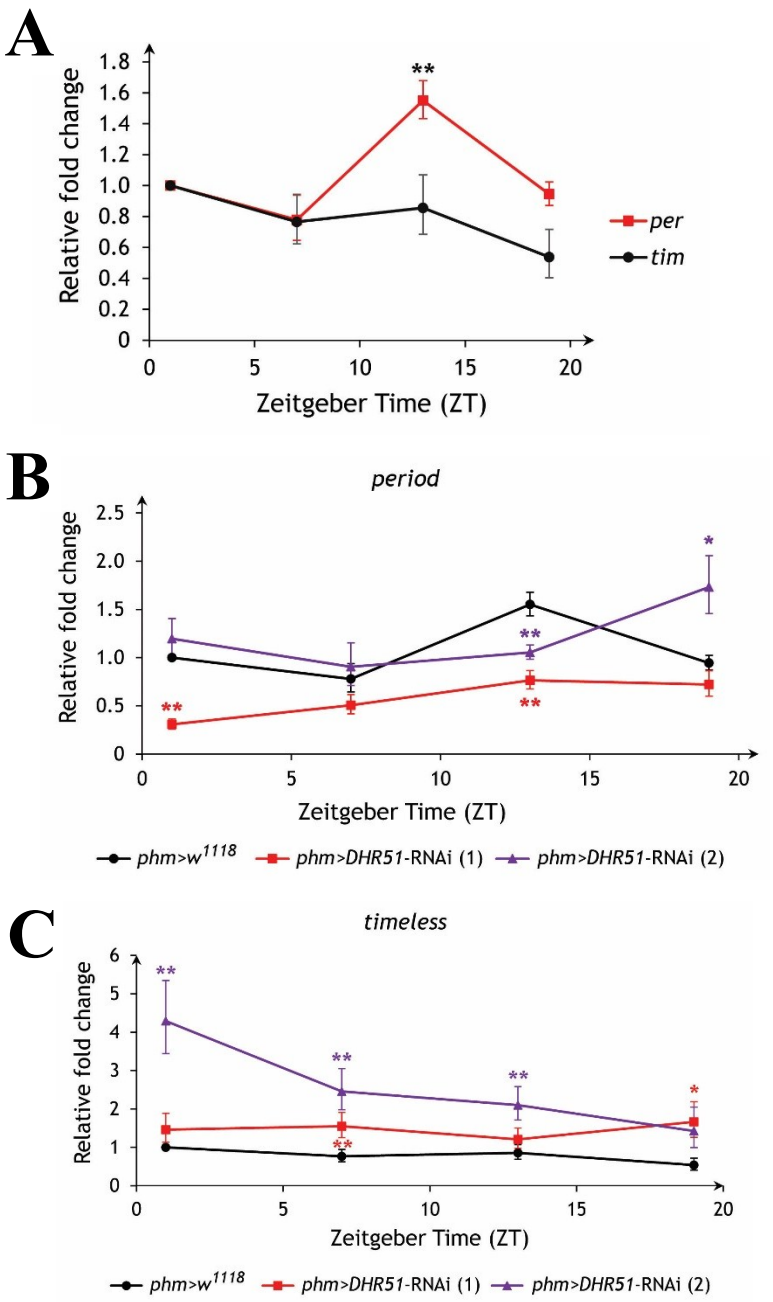

Figure 4-7. Loss-of-*DHR51* disrupted the circadian rhythm in the prothoracic gland. A) Animals were entrained to a 12 hour light:dark cycle (lights on at ZT0 and lights off at ZT12). Larval ring glands were dissected 2 days after larvae were staged at the L2/L3 molt, starting at ZT1 and then every six hours over the course of 24 hours. qPCR was used to quantify *period* (*per*) and *tim* (*timeless*) expression in *phm>w*^{1118} ring glands. B) *DHR51*-RNAi was expressed in ring glands and *period* expression was quantified with qPCR using the protocol above. C) *DHR51*-RNAi was expressed in ring glands and *timeless* expression was quantified with qPCR. ZT1 indicates one hour after lights turn on, while ZT7 is seven hours after the lights have been on. ZT13 is 1 hour after lights turn off, while ZT19 is seven hours after the lights have turned off. * = P-value < 0.05. ** = P-value < 0.01. Significance (*) was colour-coded according to the legend for readability. *phm>* = *phm22-GAL4*. A Student's t-test was used to determine significance relative to *phm>w*^{1118} for the expression of each gene at the same Zeitgeber time.

4.5 Tables

Table 4-1. *DHR51*-RNAi rescued *Ras^{V12}* developmental acceleration and viability in the prothoracic gland. Developmental timing was based on time to puparium formation. Multiple lines of *DHR51*-RNAi (1) *Ras^{V12}* were made due to the requirement of recombination to get both transgenes on the same chromosome. Exact proportions of L3 arrested larvae and pupal lethality was not quantified due to difficulty with total larval numbers per replicate and variability between replicates. *phm> = phm22-GAL4*. Phenotypes are based off Figure 4-5. Ras^{V12} is a constitutively active form of Ras.

Genotype (*phm*>)	**Phenotypes**
w^{1118}	Normal development and ring gland size.
DHR51-RNAi (1)	L3 arrest. In some cases, some escapers form pupae that never make it to adulthood. Larvae are large due to prolonged feeding. Ring glands are small.
DHR51-RNAi (2)	Minor delay in development by ~15 hours. A slight increase in body size. Animals make it to adulthood.
Ras^{V12}	Accelerated development by ~9 hours. Form small lethal pupae with some escapers. Very large ring glands.
DHR51-RNAi (1) *Ras^{V12}*	Relatively normal developmental timing. In general, there may be some L3 arrested larvae, some pupal lethality, and some animals make it to adulthood. Ring glands were normal sized in one line, but small in another.
DHR51-RNAi (2) ; *Ras^{V12}*	Normal developmental timing. A range in body sizes were observed between small to large. Small larvae tended to make lethal pupae, otherwise viable to adulthood. All larvae had very large ring glands.

Chapter 5

Conclusions and future directions

5.1 Tools to disrupt DHR51 function

The main tools that I used were *DHR51*-RNAi lines (one from VDRC and the other from Dr. Tzumin Lee's lab). Based on the VDRC website, *DHR51*-RNAi (1) is predicted to have ten potential off-targets, so caution is needed when using this RNAi line, which is why most of my experiments were done in combination with *DHR51*-RNAi (2). dsCheck, a program that predicts RNAi off-targets, found two targets for *DHR51*-RNAi (2): *DHR51* and *CG32579* (Naito, et al. 2005). *CG32579* has an unknown function, but according to Flybase.org, *CG32579* may have a role in apoptosis and is highly expressed during early embryonic stages and in the ovaries. *CG32579* has low expression during the larval stages. RNAi against *CG32579* (VDRC ID: 110645) in the PG resulted in no obvious phenotype (Danielsen, et al. 2016). It seems likely that *CG32579* would not have a role in the PG, however, *CG32579*-RNAi was used in a screen and the RNAi was not validated to be functional.

In addition to predicted off-targets, *phm>DHR51*-RNAi (1) seemed to disrupt *tor* and *InR* expression, while *phm>DHR51*-RNAi (2) did not (Figure 4-6). This suggested that *tor* and *InR* may not be regulated by DHR51 and misregulation of *tor* and *InR* may be due to an off-target of *DHR51*-RNAi (1). The L3 arrest phenotype of *phm>DHR51*-RNAi (1) larvae may also be due to an off-target as *Spok-Cas9>DHR51* 2xgRNA 3m caused a developmental delay, similar to *phm>DHR51*-RNAi (2), but more severe. However, *DHR51*-RNAi (1) was still able to disrupt *DHR51* expression (Figure 3-2C), so I believe my data are still valid as long as the results from *DHR51*-RNAi (1) and (2) are in agreement.

Future experiments can use my conditional *DHR51* 2xgRNA CRISPR lines as a replacement for *DHR51*-RNAi (1) due to the risk of off-targets in *DHR51*-RNAi (1). However, since the *DHR51* 2xgRNA 3m line differed from the 6/12m lines, quality control measures will

need to be done prior to use. The efficiency of the 2xgRNA lines to disrupt *DHR51* expression will need to be measured via qPCR. If the *DHR51* 2xgRNA 3m line proves to be useful, future experiments can be conducted with both *DHR51*-RNAi (2) and *DHR51* 2xgRNA 3m. This would allow disrupting DHR51 function using two independent mechanisms, greatly minimizing the risk of off-targets and non-specific effects from overexpressing *GAL4* / RNAi in general and *Cas9*.

5.2 Coordination between ecdysone and heme biosynthesis

My hypothesis was that DHR51 coordinated ecdysone and heme biosynthesis in the PG to produce the major ecdysone pulse at the end of L3 larvae to initiate metamorphosis. I first tested whether DHR51 acted as a heme sensor to ensure cytochrome P450 enzymes had sufficient heme for ecdysone production. Although I never came to a definitive conclusion whether DHR51 was a heme sensor, it seemed like DHR51 had a role in heme homeostasis. Loss-of-*DHR51* seemed to reduce cellular heme levels based on correlation analyses with *FeCH*-RNAi and *PPOX* mutants, upregulation of the heme biosynthesis pathway (with the exception of *Alas*), and whole body heme measurements. Evidence also suggested that did, at least, partly regulate *Alas* expression, but those experiments should be validated with the *DHR51* 2xgRNA conditional CRISPR lines. More experiments are needed to determine whether DHR51 truly binds heme *in vivo* and if heme binding is related to DHR51 activity to maintain heme homeostasis. If DHR51 is shown to bind heme, that could prompt a serious examination of NR2E3 to determine whether NR2E3 also binds heme, similar to how Rev-erbα/β were found to bind heme based on E75 (Raghuram, et al. 2007; Yin, et al. 2007).

Secondly, I provided evidence that DHR51 was required for the proper timing of the major ecdysone pulse and that loss-of-*DHR51* reduced ecdysone titers due to a reduction in the

expression of ecdysone biosynthetic enzyme genes and likely other ecdysteroidogenic genes. The impairment of ecdysone production in *phm>DHR51*-RNAi PGs may have been caused by disrupting the circadian rhythm when DHR51 function was impaired. Further tests will need to be completed to confirm the role of DHR51 in the PG circadian rhythm, but the circadian rhythm is my prime candidate for how DHR51 regulates ecdysone production. The circadian rhythm could be the mechanism in which ecdysone and heme biosynthesis are coordinately regulated. As previously noted, *Alas1* (the housekeeping *Alas*, similar to *Drosophila Alas*) was regulated by the circadian proteins BMAL1-PNAS2 in mammals and *Alas1* expression peaked at ZT12 (when lights are turned off) (Kaasik and Lee. 2004). Based on Francesca Di Cara's RNA-Seq of control RGs from ZT0-4 and ZT18-22, *Alas* expression was approximately 2 fold higher at night (Di Cara and King-Jones. 2016), which suggests that *Alas* could also be under the control of the circadian rhythm similar to *Alas*1. However, *Alas* expression in the RG needs to be confirmed with qPCR.

Rev-erbα is a heme sensor that regulates *Alas1* and functions within the circadian rhythm (Wu, et al. 2009; Preitner, et al. 2002). In turn, many circadian proteins use heme as a cofactor, such as Rev-erbα, NPAS2, and PERIOD2 (Raghuram, et al. 2007; Yin, et al. 2007; Dioum, et al. 2002; Kaasik and Lee. 2004). Ecdysone production is also under the control of the circadian rhythm and the expression of the ecdysone biosynthetic enzyme genes peaked during the night (Di Cara and King-Jones. 2016). Although the expression profile of the ecdysone biosynthetic enzyme genes are not as finely tuned during a 24 hour period as *Alas1* expression, it does seem like heme biosynthesis could immediately precede the upregulation of the ecdysone biosynthetic enzyme genes during the night if *Alas* has a similar expression profile as *Alas1*. Despite that DHR51 protein levels peaked at ZT2, more DHR51 was bound to DNA at ZT14 compared to

ZT2 in the heads of adult *Drosophila* flies (Kozlov, et al. 2017). So, when DHR51 is the most transcriptionally active during the beginning of the night, ecdysone biosynthetic enzyme genes and *Alas* expression are also peaking. However, more circadian rhythm-based experiments are needed to confirm whether *DHR51* is responsible for the circadian coordination of ecdysone production and heme biosynthesis in the PG.

In mammals, Rev-erbα acts as a heme sensor and as a component of the circadian rhythm. I am proposing that DHR51 fills a similar role in *Drosophila*. Although DHR51 may seem more functionally related to Rev-erbα than NR2E3 (the *DHR51* vertebrate homolog), NR2E3 may not be that different. NR2E3 is typically associated with mutations that cause enhanced S-cone syndrome and autosomal dominant retinitis pigmentosa (Haider, et al. 2000; Gerber, et al. 2000; Coppieters, et al. 2007). However, NR2E3 may not be so specific to photoreceptors because a recent paper identified that NR2E3 is present in the liver of mice via a western blot. Specifically, NR2E3 in the liver was found to be associated with a good prognosis in liver cancers and that NR2E3 positively regulated AHR (aryl hydrocarbon receptor) (Khanal, et al. 2017). AHR is a ligand-dependent transcription factor that can bind environmental toxins, phytochemicals, and some endogenous ligands (Denison and Nagy. 2003; Denison, et al. 2011). Notably, AHR target genes include cytochrome P450 enzyme genes for detoxification (Gonzalez and Fernandez-Salguero. 1998). Thus, knockdown of *Nr2e3* decreased the expression of some cytochrome P450 enzyme genes in the liver (Khanal, et al. 2017). Typically, when cytochrome P450 genes are induced for drug metabolism or detoxification, heme biosynthesis is also induced to match the demand of cytochrome P450 enzymes for heme (which is why drugs that induce cytochrome P450 gene expression cause acute porphyria attacks and are avoided by porphyria patients) (Correia, et al. 2011; Tracy and Dyck. 2014).

In light of my research, it was interesting to see NR2E3 indirectly regulate cytochrome P450 genes in the liver, which has the second highest demand for heme after erythrocytes, and the majority of heme in the liver is used for cytochrome P450 enzymes. However, there has yet to be a connection between NR2E3 and heme. Given that NR2E3 and Rev-erbα can physically interact in the retina, it is plausible that the NR2E3 – Rev-erbα interaction occurs in the liver to coordinate levels of cytochrome P450 enzymes and heme in response to toxins (Cheng, et al. 2004; Mollema, et al. 2011). However, this is a lot of speculation and many experiments would need to be done to confirm whether NR2E3 also regulates heme biosynthesis in the liver or functions in the circadian rhythm. If strong evidence is found that DHR51 regulates heme biosynthesis and the circadian rhythm, that will give a more compelling reason to explore NR2E3 function within the liver to possibly also regulate heme biosynthesis and the circadian rhythm.

There does seem to be an evolutionarily conserved relationship between nuclear receptors, the circadian rhythm, cytochrome P450 enzymes, and heme regulation. While some interactions are stronger than others, nuclear receptors, the circadian rhythm, cytochrome P450 enzymes, and heme regulation all work in concert towards the same biological function, whether for detoxification or steroid hormone production. Although I cannot quite confirm my hypothesis that DHR51 coordinates ecdysone and heme biosynthesis through the circadian rhythm, I have provided evidence that DHR51 regulates ecdysone production, potentially through the circadian rhythm and that DHR51 likely has a role in heme homeostasis, possibly by regulating *Alas* expression.

5.3 Future directions

The major direction that my project should go is to determine whether DHR51 acts as a heme sensor in the PG. Identifying direct target genes of DHR51 via ChIP would be a major step. Identifying whether DHR51 binds directly to *Alas* under low cellular heme levels or if DHR51 binds to a known regulator of *Alas* could provide confirmation that DHR51 does regulate *Alas*. Not only would ChIP provide data for how DHR51 could maintain heme homeostasis, but ChIP would also provide further evidence for how DHR51 regulates ecdysone production. Does DHR51 only function within the circadian rhythm or does it also bind the ecdysone biosynthetic enzyme genes directly? A fairly small DHR51 binding peak was observed near *sro* in the heads of adult flies at ZT14 but not at ZT2, which would be consistent with ecdysone production occurring during the night (Kozlov, et al. 2017). The authors never mentioned anything about this peak as the ecdysone biosynthetic enzyme genes are not expressed in adults (except during oogenesis). This could be a hint that DHR51 can bind to *sro*, but *sro* is still inactive at that stage and time (adulthood). ChIP could also determine whether DHR51 is involved in the TOR pathway in the PG.

Additional to determining whether DHR51 regulates *Alas*, identifying heme as a natural, *in vivo* ligand for DHR51 is also a critical step. Multiple approaches can be taken such as identifying direct target genes of DHR51 and if DHR51's DNA-binding capability is heme-dependent would provide strong evidence that heme is a relevant ligand. ChIP can be performed in low, normal, or even high heme levels, preferably in RGs. Low cellular heme levels can be achieved in a *PPOX* mutant background or, if in cell culture, presumably by adding sufficient concentrations of succinylacetone. Hemin can be added to cell culture or fed to larvae to increase cellular heme levels. If DHR51 DNA binding is not affected by changes in cellular heme levels,

then the expression of DHR51 target genes can be measured under varying levels of cellular heme levels to determine whether DHR51 regulates the gene differently dependent on cellular heme conditions. Since DHR51 is localized to the nucleus regardless of cellular heme levels, DHR51 may always be bound to DNA, similar to a Type II nuclear receptor.

Ligand binding can affect not only nuclear receptor DNA binding, but can also affect protein-protein interactions and co-regulator recruitment. Mass spectrometry (mass spec) can be used to identify DHR51's protein binding partners under varying levels of heme. If heme is DHR51's *in vivo* ligand, heme binding should affect the proteins that DHR51 interacts with, especially co-regulators. Mass spec could be performed in cell culture or either whole body larvae or BRGs. I was preparing to do a mass spec in whole body larvae, but multiple whole-body *GAL4* drivers (*tubulin-GAL4*, *actin-GAL4*, *daughterless-GAL4*, and *ubiquitin-GAL4*) resulted in embryonic lethality when overexpressing *FLAG-DHR51*. Temperature sensitive *GAL80* could be used to repress *GAL4* expression until the L3 stage and then larvae could be collected for mass spec.

The conditional *DHR51* 2xgRNA CRISPR lines were received late into my program, so I was unable to use them for my experiments. First, *DHR51* expression should be examined in the RG of the *DHR51* 2xgRNA lines to determine how efficient these lines are at disrupting *DHR51* expression. Once checked, the *DHR51* 2xgRNA lines can be used to replicate all of my critical experiments. The first experiment that should be replicated would be to use the *DHR51* 2xgRNA lines to disrupt *DHR51* in a *PPOX* mutant background to determine whether loss-of-*DHR51* does attenuate *Alas* expression in a low heme background independently of RNAi. Heme measurements in *DHR51* 2xgRNA larvae could also be replicated. If heme levels are to be re-

measured in BRGs, I would advise collecting more BRGs per replicate, as 50 may have been too low.

Ecdysone levels should be measured in the *DHR51* 2xgRNA lines to confirm that these lines also have reduced ecdysone levels. Lastly, the *DHR51* 2xgRNA lines could be used to determine the effect of loss-of-*DHR51* on the circadian rhythm in the PG. Both of the *DHR51*-RNAi lines affected the expression of *per* and *tim* in different ways, so a third knockdown of *DHR51*, independent of RNAi, can be used as a deciding factor for the effect of loss-of-*DHR51* on the circadian rhythm. If qPCR is used to measure *per* and *tim* expression again, RGs may need to be collected from early L3 larvae instead of older L3 larvae, in hopes of having a more robust circadian rhythm in control RGs. In combination, PER and TIM protein should be examined with immunofluorescence to determine whether protein accumulation in the nucleus is phase shifted or if PER and TIM protein levels are reduced or do not cycle. Further experiments could be done to test whether DHR51's regulation of heme biosynthesis and ecdysone production are dependent on circadian time. For example, are the ecdysone biosynthetic enzyme genes more strongly downregulated by loss-of-*DHR51* in the night or the day?

References

Allada, R., White, N.E., So, W.V., Hall, J.C., Rosbash, M., 1998. A Mutant Drosophila Homolog of Mammalian Clock Disrupts Circadian Rhythms and Transcription of Period and Timeless. Cell 93, 791-804.

Ampleford, E.J., Steel, C.G., 1985. Circadian Control of a Daily Rhythm in Hemolymph Ecdysteroid Titer in the Insect Rhodnius Prolixus (Hemiptera). Gen Comp Endocrinol 59, 453-459.

Ashburner, M., Richards, G., 1976. Sequential Gene Activation by Ecdysone in Polytene Chromosomes of Drosophila Melanogaster. III. Consequences of Ecdysone Withdrawal. Dev Biol 54, 241-255.

Ashburner, M., 1974. Sequential Gene Activation by Ecdysone in Polytene Chromosomes of Drosophila Melanogaster. II. the Effects of Inhibitors of Protein Synthesis. Dev Biol 39, 141-157.

Balwani, M., Desnick, R.J., 2012. The Porphyrias: Advances in Diagnosis and Treatment. Hematology Am Soc Hematol Educ Program 2012, 19-27.

Barrangou, R., Fremaux, C., Deveau, H., Richards, M., Boyaval, P., Moineau, S., Romero, D.A., Horvath, P., 2007. CRISPR Provides Acquired Resistance Against Viruses in Prokaryotes. Science 315, 1709-1712.

Bassett, A.R., Liu, J.L., 2014. CRISPR/Cas9 and Genome Editing in Drosophila. J Genet Genomics 41, 7-19.

Bassett, A.R., Tibbit, C., Ponting, C.P., Liu, J.L., 2013. Highly Efficient Targeted Mutagenesis of Drosophila with the CRISPR/Cas9 System. Cell Rep 4, 220-228.

Bates, K.E., Molnar, J., Robinow, S., 2015. The Unfulfilled Gene and Nervous System Development in Drosophila. Biochim Biophys Acta 1849, 217-223.

Bates, K.E., Sung, C., Hilson, L., Robinow, S., 2014. Unfulfilled Interacting Genes Display Branch-Specific Roles in the Development of Mushroom Body Axons in Drosophila Melanogaster. G3 (Bethesda) 4, 693-706.

Bates, K.E., Sung, C.S., Robinow, S., 2010. The Unfulfilled Gene is Required for the Development of Mushroom Body Neuropil in Drosophila. Neural Dev 5, 4-8104-5-4.

Berrabah, W., Aumercier, P., Lefebvre, P., Staels, B., 2011. Control of Nuclear Receptor Activities in Metabolism by Post-Translational Modifications. FEBS Lett 585, 1640-1650.

Beuchle, D., Jaumouille, E., Nagoshi, E., 2012. The Nuclear Receptor Unfulfilled is Required for Free-Running Clocks in Drosophila Pacemaker Neurons. Curr Biol 22, 1221-1227.

Bialecki, M., Shilton, A., Fichtenberg, C., Segraves, W.A., Thummel, C.S., 2002. Loss of the Ecdysteroid-Inducible E75A Orphan Nuclear Receptor Uncouples Molting from Metamorphosis in Drosophila. Dev Cell 3, 209-220.

Biason-Lauber, A., 2016. The Battle of the Sexes: Human Sex Development and its Disorders. Results Probl Cell Differ 58, 337-382.

Birk, O.S., Casiano, D.E., Wassif, C.A., Cogliati, T., Zhao, L., Zhao, Y., Grinberg, A., Huang, S., Kreidberg, J.A., Parker, K.L., Porter, F.D., Westphal, H., 2000. The LIM Homeobox Gene Lhx9 is Essential for Mouse Gonad Formation. Nature 403, 909-913.

Brouns, S.J., Jore, M.M., Lundgren, M., Westra, E.R., Slijkhuis, R.J., Snijders, A.P., Dickman, M.J., Makarova, K.S., Koonin, E.V., van der Oost, J., 2008. Small CRISPR RNAs Guide Antiviral Defense in Prokaryotes. Science 321, 960-964.

Brudevoll, J.E., Liestol, K., Walloe, L., 1979. Menarcheal Age in Oslo during the Last 140 Years. Ann Hum Biol 6, 407-416.

Bumsted O'Brien, K.M., Cheng, H., Jiang, Y., Schulte, D., Swaroop, A., Hendrickson, A.E., 2004. Expression of Photoreceptor-Specific Nuclear Receptor NR2E3 in Rod Photoreceptors of Fetal Human Retina. Invest Ophthalmol Vis Sci 45, 2807-2812.

Butenandt, A., Karlson, P. 1954. Über die Isolierung eines Metamorphose-Hormons der Insekten in kristallisierter Form. Z. Naturforsch 9b, 389-391.

Caceres, L., Necakov, A.S., Schwartz, C., Kimber, S., Roberts, I.J., Krause, H.M., 2011. Nitric Oxide Coordinates Metabolism, Growth, and Development Via the Nuclear Receptor E75. Genes Dev 25, 1476-1485.

Chan, L., O'Malley, B.W., 1976. Mechanism of Action of the Sex Steroid Hormones (First of Three Parts). N Engl J Med 294, 1322-1328.

Chen, F., Figueroa, D.J., Marmorstein, A.D., Zhang, Q., Petrukhin, K., Caskey, C.T., Austin, C.P., 1999. Retina-Specific Nuclear Receptor: A Potential Regulator of Cellular Retinaldehyde-Binding Protein Expressed in Retinal Pigment Epithelium and Muller Glial Cells. Proc Natl Acad Sci U S A 96, 15149-15154.

Chen, J., Rattner, A., Nathans, J., 2005. The Rod Photoreceptor-Specific Nuclear Receptor Nr2e3 Represses Transcription of Multiple Cone-Specific Genes. J Neurosci 25, 118-129.

Cheng, H., Khanna, H., Oh, E.C., Hicks, D., Mitton, K.P., Swaroop, A., 2004. Photoreceptor-Specific Nuclear Receptor NR2E3 Functions as a Transcriptional Activator in Rod Photoreceptors. Hum Mol Genet 13, 1563-1575.

Christesen, D., Yang, Y.T., Somers, J., Robin, C., Sztal, T., Batterham, P., Perry, T., 2017. Transcriptome Analysis of Drosophila Melanogaster Third Instar Larval Ring Glands Points to Novel Functions and Uncovers a Cytochrome p450 Required for Development. G3 (Bethesda) 7, 467-479.

Chung, H., Sztal, T., Pasricha, S., Sridhar, M., Batterham, P., Daborn, P.J., 2009. Characterization of Drosophila Melanogaster Cytochrome P450 Genes. Proc Natl Acad Sci U S A 106, 5731-5736.

Clemens, J.C., Worby, C.A., Simonson-Leff, N., Muda, M., Maehama, T., Hemmings, B.A., Dixon, J.E., 2000. Use of Double-Stranded RNA Interference in Drosophila Cell Lines to Dissect Signal Transduction Pathways. Proc Natl Acad Sci U S A 97, 6499-6503.

Clever, U., Karlson, P., 1960. Induction of Puff Changes in the Salivary Gland Chromosomes of Chironomus Tentans by Ecdysone. Exp Cell Res 20, 623-626.

Colombani, J., Bianchini, L., Layalle, S., Pondeville, E., Dauphin-Villemant, C., Antoniewski, C., Carre, C., Noselli, S., Leopold, P., 2005. Antagonistic Actions of Ecdysone and Insulins Determine Final Size in Drosophila. Science 310, 667-670.

Cong, L., Ran, F.A., Cox, D., Lin, S., Barretto, R., Habib, N., Hsu, P.D., Wu, X., Jiang, W., Marraffini, L.A., Zhang, F., 2013. Multiplex Genome Engineering using CRISPR/Cas Systems. Science 339, 819-823.

Coppieters, F., Leroy, B.P., Beysen, D., Hellemans, J., De Bosscher, K., Haegeman, G., Robberecht, K., Wuyts, W., Coucke, P.J., De Baere, E., 2007. Recurrent Mutation in the First Zinc Finger of the Orphan Nuclear Receptor NR2E3 Causes Autosomal Dominant Retinitis Pigmentosa. Am J Hum Genet 81, 147-157.

Correia, M.A., Sinclair, P.R., De Matteis, F., 2011. Cytochrome P450 Regulation: The Interplay between its Heme and Apoprotein Moieties in Synthesis, Assembly, Repair, and Disposal. Drug Metab Rev 43, 1-26.

Crumbley, C., Burris, T.P., 2011. Direct Regulation of CLOCK Expression by REV-ERB. PLoS One 6, e17290.

Crumbley, C., Wang, Y., Kojetin, D.J., Burris, T.P., 2010. Characterization of the Core Mammalian Clock Component, NPAS2, as a REV-ERBalpha/RORalpha Target Gene. J Biol Chem 285, 35386-35392.

d'Anglemont de Tassigny, X., Colledge, W.H., 2010. The Role of Kisspeptin Signaling in Reproduction. Physiology (Bethesda) 25, 207-217.

Danielsen, E.T., Moeller, M.E., Yamanaka, N., Ou, Q., Laursen, J.M., Soenderholm, C., Zhuo, R., Phelps, B., Tang, K., Zeng, J., Kondo, S., Nielsen, C.H., Harvald, E.B., Faergeman, N.J., Haley, M.J., O'Connor, K.A., King-Jones, K., O'Connor, M.B., Rewitz, K.F., 2016. A Drosophila Genome-Wide Screen Identifies Regulators of Steroid Hormone Production and Developmental Timing. Dev Cell 37, 558-570.

de Rosny, E., de Groot, A., Jullian-Binard, C., Borel, F., Suarez, C., Le Pape, L., Fontecilla-Camps, J.C., Jouve, H.M., 2008. DHR51, the Drosophila Melanogaster Homologue of the Human Photoreceptor Cell-Specific Nuclear Receptor, is a Thiolate Heme-Binding Protein. Biochemistry 47, 13252-13260.

Denison, M.S., Soshilov, A.A., He, G., DeGroot, D.E., Zhao, B., 2011. Exactly the Same but Different: Promiscuity and Diversity in the Molecular Mechanisms of Action of the Aryl Hydrocarbon (Dioxin) Receptor. Toxicol Sci 124, 1-22.

Denison, M.S., Nagy, S.R., 2003. Activation of the Aryl Hydrocarbon Receptor by Structurally Diverse Exogenous and Endogenous Chemicals. Annu Rev Pharmacol Toxicol 43, 309-334.

Di Cara, F., King-Jones, K., 2016. The Circadian Clock is a Key Driver of Steroid Hormone Production in Drosophila. Curr Biol 26, 2469-2477.

Dioum, E.M., Rutter, J., Tuckerman, J.R., Gonzalez, G., Gilles-Gonzalez, M.A., McKnight, S.L., 2002. NPAS2: A Gas-Responsive Transcription Factor. Science 298, 2385-2387.

Ebert, P.S., Hess, R.A., Frykholm, B.C., Tschudy, D.P., 1979. Succinylacetone, a Potent Inhibitor of Heme Biosynthesis: Effect on Cell Growth, Heme Content and Delta-Aminolevulinic Acid Dehydratase Activity of Malignant Murine Erythroleukemia Cells. Biochem Biophys Res Commun 88, 1382-1390.

Edel, Y., Mamet, R., 2018. Porphyria: What is it and Who should be Evaluated? Rambam Maimonides Med J 9, 10.5041/RMMJ.10333.

Escher, P., Gouras, P., Roduit, R., Tiab, L., Bolay, S., Delarive, T., Chen, S., Tsai, C.C., Hayashi, M., Zernant, J., Merriam, J.E., Mermod, N., Allikmets, R., Munier, F.L., Schorderet, D.F., 2009. Mutations in NR2E3 can Cause Dominant Or Recessive Retinal Degenerations in the Same Family. Hum Mutat 30, 342-351.

Faller, M., Matsunaga, M., Yin, S., Loo, J.A., Guo, F., 2007. Heme is Involved in microRNA Processing. Nat Struct Mol Biol 14, 23-29.

Friedman, A., Perrimon, N., 2006. A Functional RNAi Screen for Regulators of Receptor Tyrosine Kinase and ERK Signalling. Nature 444, 230-234.

Fristrom, D., Liebrich, W., 1986. The Hormonal Coordination of Cuticulin Deposition and Morphogenesis in Drosophila Imaginal Discs in Vivo and in Vitro. Dev Biol 114, 1-11.

Gasiunas, G., Barrangou, R., Horvath, P., Siksnys, V., 2012. Cas9-crRNA Ribonucleoprotein Complex Mediates Specific DNA Cleavage for Adaptive Immunity in Bacteria. Proc Natl Acad Sci U S A 109, E2579-86.

Gerber, S., Rozet, J.M., Takezawa, S.I., dos Santos, L.C., Lopes, L., Gribouval, O., Penet, C., Perrault, I., Ducroq, D., Souied, E., Jeanpierre, M., Romana, S., Frezal, J., Ferraz, F., Yu-Umesono, R., Munnich, A., Kaplan, J., 2000. The Photoreceptor Cell-Specific Nuclear Receptor Gene (PNR) Accounts for Retinitis Pigmentosa in the Crypto-Jews from Portugal (Marranos), Survivors from the Spanish Inquisition. Hum Genet 107, 276-284.

Gibbens, Y.Y., Warren, J.T., Gilbert, L.I., O'Connor, M.B., 2011. Neuroendocrine Regulation of Drosophila Metamorphosis Requires TGFbeta/Activin Signaling. Development 138, 2693-2703.

Gonzalez, F.J., Fernandez-Salguero, P., 1998. The Aryl Hydrocarbon Receptor: Studies using the AHR-Null Mice. Drug Metab Dispos 26, 1194-1198.

Gratz, S.J., Rubinstein, C.D., Harrison, M.M., Wildonger, J., O'Connor-Giles, K.M., 2015. CRISPR-Cas9 Genome Editing in Drosophila. Curr Protoc Mol Biol 111, 31.2.1-20.

Gratz, S.J., Ukken, F.P., Rubinstein, C.D., Thiede, G., Donohue, L.K., Cummings, A.M., O'Connor-Giles, K.M., 2014. Highly Specific and Efficient CRISPR/Cas9-Catalyzed Homology-Directed Repair in Drosophila. Genetics 196, 961-971.

Gratz, S.J., Cummings, A.M., Nguyen, J.N., Hamm, D.C., Donohue, L.K., Harrison, M.M., Wildonger, J., O'Connor-Giles, K.M., 2013. Genome Engineering of Drosophila with the CRISPR RNA-Guided Cas9 Nuclease. Genetics 194, 1029-1035.

Gratz, S.J., Wildonger, J., Harrison, M.M., O'Connor-Giles, K.M., 2013. CRISPR/Cas9-Mediated Genome Engineering and the Promise of Designer Flies on Demand. Fly (Austin) 7, 249-255.

Haider, N.B., Mollema, N., Gaule, M., Yuan, Y., Sachs, A.J., Nystuen, A.M., Naggert, J.K., Nishina, P.M., 2009. Nr2e3-Directed Transcriptional Regulation of Genes Involved in Photoreceptor Development and Cell-Type Specific Phototransduction. Exp Eye Res 89, 365-372.

Haider, N.B., Jacobson, S.G., Cideciyan, A.V., Swiderski, R., Streb, L.M., Searby, C., Beck, G., Hockey, R., Hanna, D.B., Gorman, S., Duhl, D., Carmi, R., Bennett, J., Weleber, R.G., Fishman, G.A., Wright, A.F., Stone, E.M., Sheffield, V.C., 2000. Mutation of a Nuclear Receptor Gene, NR2E3, Causes Enhanced S Cone Syndrome, a Disorder of Retinal Cell Fate. Nat Genet 24, 127-131.

Handschin, C., Lin, J., Rhee, J., Peyer, A.K., Chin, S., Wu, P.H., Meyer, U.A., Spiegelman, B.M., 2005. Nutritional Regulation of Hepatic Heme Biosynthesis and Porphyria through PGC-1alpha. Cell 122, 505-515.

Hanukoglu, I., 1992. Steroidogenic Enzymes: Structure, Function, and Role in Regulation of Steroid Hormone Biosynthesis. J Steroid Biochem Mol Biol 43, 779-804.

Hardin, P.E., Panda, S., 2013. Circadian Timekeeping and Output Mechanisms in Animals. Curr Opin Neurobiol 23, 724-731.

Huang, X., Suyama, K., Buchanan, J., Zhu, A.J., Scott, M.P., 2005. A Drosophila Model of the Niemann-Pick Type C Lysosome Storage Disease: Dnpc1a is Required for Molting and Sterol Homeostasis. Development 132, 5115-5124.

Huynh, N., Zeng, J., Liu, W., King-Jones, K., 2018. A Drosophila CRISPR/Cas9 Toolkit for Conditionally Manipulating Gene Expression in the Prothoracic Gland as a Test Case for Polytene Tissues. G3 (Bethesda) .

Hwang, W.Y., Fu, Y., Reyon, D., Maeder, M.L., Tsai, S.Q., Sander, J.D., Peterson, R.T., Yeh, J.R., Joung, J.K., 2013. Efficient Genome Editing in Zebrafish using a CRISPR-Cas System. Nat Biotechnol 31, 227-229.

Ishino, Y., Shinagawa, H., Makino, K., Amemura, M., Nakata, A., 1987. Nucleotide Sequence of the Iap Gene, Responsible for Alkaline Phosphatase Isozyme Conversion in Escherichia Coli, and Identification of the Gene Product. J Bacteriol 169, 5429-5433.

Jang, A.R., Moravcevic, K., Saez, L., Young, M.W., Sehgal, A., 2015. Drosophila TIM Binds Importin Alpha1, and Acts as an Adapter to Transport PER to the Nucleus. PLoS Genet 11, e1004974.

Jaumouille, E., Machado Almeida, P., Stahli, P., Koch, R., Nagoshi, E., 2015. Transcriptional Regulation Via Nuclear Receptor Crosstalk Required for the Drosophila Circadian Clock. Curr Biol 25, 1502-1508.

Jinek, M., Chylinski, K., Fonfara, I., Hauer, M., Doudna, J.A., Charpentier, E., 2012. A Programmable Dual-RNA-Guided DNA Endonuclease in Adaptive Bacterial Immunity. Science 337, 816-821.

Jurgens, G., Wieschaus, E., Nusslein-Volhard, C., Kluding, H., 1984. Mutations Affecting the Pattern of the Larval Cuticle inDrosophila Melanogaster : II. Zygotic Loci on the Third Chromosome. Wilehm Roux Arch Dev Biol 193, 283-295.

Kaasik, K., Lee, C.C., 2004. Reciprocal Regulation of Haem Biosynthesis and the Circadian Clock in Mammals. Nature 430, 467-471.

Kanda, A., Swaroop, A., 2009. A Comprehensive Analysis of Sequence Variants and Putative Disease-Causing Mutations in Photoreceptor-Specific Nuclear Receptor NR2E3. Mol Vis 15, 2174-2184.

Kataoka, H., Nagasawa, H., Isogai, A., Ishizaki, H., Suzuki, A., 1991. Prothoracicotropic Hormone of the Silkworm, Bombyx Mori: Amino Acid Sequence and Dimeric Structure. Agric Biol Chem 55, 73-86.

Kauppinen, R., Mustajoki, P., 1992. Prognosis of Acute Porphyria: Occurrence of Acute Attacks, Precipitating Factors, and Associated Diseases. Medicine (Baltimore) 71, 1-13.

Kawakami, A., Kataoka, H., Oka, T., Mizoguchi, A., Kimura-Kawakami, M., Adachi, T., Iwami, M., Nagasawa, H., Suzuki, A., Ishizaki, H., 1990. Molecular Cloning of the Bombyx Mori Prothoracicotropic Hormone. Science 247, 1333-1335.

Khan, A.A., Quigley, J.G., 2011. Control of Intracellular Heme Levels: Heme Transporters and Heme Oxygenases. Biochim Biophys Acta 1813, 668-682.

Khanal, T., Choi, K., Leung, Y.K., Wang, J., Kim, D., Janakiram, V., Cho, S.G., Puga, A., Ho, S.M., Kim, K., 2017. Loss of NR2E3 Represses AHR by LSD1 Reprogramming, is Associated with Poor Prognosis in Liver Cancer. Sci Rep 7, 10662-017-11106-2.

Kim, H.J., Khalimonchuk, O., Smith, P.M., Winge, D.R., 2012. Structure, Function, and Assembly of Heme Centers in Mitochondrial Respiratory Complexes. Biochim Biophys Acta 1823, 1604-1616.

Kimberland, M.L., Hou, W., Alfonso-Pecchio, A., Wilson, S., Rao, Y., Zhang, S., Lu, Q., 2018. Strategies for Controlling CRISPR/Cas9 Off-Target Effects and Biological Variations in Mammalian Genome Editing Experiments. J Biotechnol 284, 91-101.

King, W.J., Greene, G.L., 1984. Monoclonal Antibodies Localize Oestrogen Receptor in the Nuclei of Target Cells. Nature 307, 745-747.

King-Jones, K., Charles, J.P., Lam, G., Thummel, C.S., 2005. The Ecdysone-Induced DHR4 Orphan Nuclear Receptor Coordinates Growth and Maturation in Drosophila. Cell 121, 773-784.

King-Jones, K., Thummel, C.S., 2005. Nuclear Receptors--a Perspective from Drosophila. Nat Rev Genet 6, 311-323.

Klatt, P., Schmidt, K., Mayer, B., 1992. Brain Nitric Oxide Synthase is a Haemoprotein. Biochem J 288 (Pt 1), 15-17.

Koelle, M.R., Talbot, W.S., Segraves, W.A., Bender, M.T., Cherbas, P., Hogness, D.S., 1991. The Drosophila EcR Gene Encodes an Ecdysone Receptor, a New Member of the Steroid Receptor Superfamily. Cell 67, 59-77.

Komura-Kawa, T., Hirota, K., Shimada-Niwa, Y., Yamauchi, R., Shimell, M., Shinoda, T., Fukamizu, A., O'Connor, M.B., Niwa, R., 2015. The Drosophila Zinc Finger Transcription Factor Ouija Board Controls Ecdysteroid Biosynthesis through Specific Regulation of Spookier. PLoS Genet 11, e1005712.

Konopka, R.J., Benzer, S., 1971. Clock Mutants of Drosophila Melanogaster. Proc Natl Acad Sci U S A 68, 2112-2116.

Kozlov, A., Jaumouille, E., Machado Almeida, P., Koch, R., Rodriguez, J., Abruzzi, K.C., Nagoshi, E., 2017. A Screening of UNF Targets Identifies Rnb, a Novel Regulator of Drosophila Circadian Rhythms. J Neurosci 37, 6673-6685.

Kula-Eversole, E., Nagoshi, E., Shang, Y., Rodriguez, J., Allada, R., Rosbash, M., 2010. Surprising Gene Expression Patterns within and between PDF-Containing Circadian Neurons in Drosophila. Proc Natl Acad Sci U S A 107, 13497-13502.

Larsen, R., Gouveia, Z., Soares, M.P., Gozzelino, R., 2012. Heme Cytotoxicity and the Pathogenesis of Immune-Mediated Inflammatory Diseases. Front Pharmacol 3, 77.

Layalle, S., Arquier, N., Leopold, P., 2008. The TOR Pathway Couples Nutrition and Developmental Timing in Drosophila. Dev Cell 15, 568-577.

Li, J., Al-Azzawi, F., 2009. Mechanism of Androgen Receptor Action. Maturitas 63, 142-148.

Lin, S., Huang, Y., Lee, T., 2009. Nuclear Receptor Unfulfilled Regulates Axonal Guidance and Cell Identity of Drosophila Mushroom Body Neurons. PLoS One 4, e8392.

Mak, P.J., Denisov, I.G., 2018. Spectroscopic Studies of the Cytochrome P450 Reaction Mechanisms. Biochim Biophys Acta Proteins Proteom 1866, 178-204.

Makarova, K.S., Haft, D.H., Barrangou, R., Brouns, S.J., Charpentier, E., Horvath, P., Moineau, S., Mojica, F.J., Wolf, Y.I., Yakunin, A.F., van der Oost, J., Koonin, E.V., 2011. Evolution and Classification of the CRISPR-Cas Systems. Nat Rev Microbiol 9, 467-477.

Mali, P., Yang, L., Esvelt, K.M., Aach, J., Guell, M., DiCarlo, J.E., Norville, J.E., Church, G.M., 2013. RNA-Guided Human Genome Engineering Via Cas9. Science 339, 823-826.

Mangelsdorf, D.J., Thummel, C., Beato, M., Herrlich, P., Schutz, G., Umesono, K., Blumberg, B., Kastner, P., Mark, M., Chambon, P., Evans, R.M., 1995. The Nuclear Receptor Superfamily: The Second Decade. Cell 83, 835-839.

Marmor-Kollet, N., Schuldiner, O., 2016. Contrasting Developmental Axon Regrowth and Neurite Sprouting of Drosophila Mushroom Body Neurons Reveals Shared and Unique Molecular Mechanisms. Dev Neurobiol 76, 262-276.

McBrayer, Z., Ono, H., Shimell, M., Parvy, J.P., Beckstead, R.B., Warren, J.T., Thummel, C.S., Dauphin-Villemant, C., Gilbert, L.I., O'Connor, M.B., 2007. Prothoracicotropic Hormone Regulates Developmental Timing and Body Size in Drosophila. Dev Cell 13, 857-871.

Mensah, L.B., Davison, C., Fan, S.J., Morris, J.F., Goberdhan, D.C., Wilson, C., 2015. Fine-Tuning of PI3K/AKT Signalling by the Tumour Suppressor PTEN is Required for Maintenance of Flight Muscle Function and Mitochondrial Integrity in Ageing Adult Drosophila Melanogaster. PLoS One 10, e0143818.

Mirth, C., Truman, J.W., Riddiford, L.M., 2005. The Role of the Prothoracic Gland in Determining Critical Weight for Metamorphosis in Drosophila Melanogaster. Curr Biol 15, 1796-1807.

Mirth, C.K., Shingleton, A.W., 2012. Integrating Body and Organ Size in Drosophila: Recent Advances and Outstanding Problems. Front Endocrinol (Lausanne) 3, 49.

Moeller, M.E., Danielsen, E.T., Herder, R., O'Connor, M.B., Rewitz, K.F., 2013. Dynamic Feedback Circuits Function as a Switch for Shaping a Maturation-Inducing Steroid Pulse in Drosophila. Development 140, 4730-4739.

Mollema, N.J., Yuan, Y., Jelcick, A.S., Sachs, A.J., von Alpen, D., Schorderet, D., Escher, P., Haider, N.B., 2011. Nuclear Receptor Rev-Erb Alpha (Nr1d1) Functions in Concert with Nr2e3 to Regulate Transcriptional Networks in the Retina. PLoS One 6, e17494.

Morrison, G.R., 1965. Fluorometric Microdetermination of Heme Protein. Anal Chem 37, 1124-1126.

Much, J.W., Slade, D.J., Klampert, K., Garriga, G., Wightman, B., 2000. The Fax-1 Nuclear Hormone Receptor Regulates Axon Pathfinding and Neurotransmitter Expression. Development 127, 703-712.

Myers, E.M., Yu, J., Sehgal, A., 2003. Circadian Control of Eclosion: Interaction between a Central and Peripheral Clock in Drosophila Melanogaster. Curr Biol 13, 526-533.

Nagababu, E., Rifkind, J.M., 1998. Formation of Fluorescent Heme Degradation Products during the Oxidation of Hemoglobin by Hydrogen Peroxide. Biochem Biophys Res Commun 247, 592-596.

Naito, Y., Yamada, T., Matsumiya, T., Ui-Tei, K., Saigo, K., Morishita, S., 2005. dsCheck: Highly Sensitive Off-Target Search Software for Double-Stranded RNA-Mediated RNA Interference. Nucleic Acids Res 33, W589-91.

Namiki, T., Niwa, R., Sakudoh, T., Shirai, K., Takeuchi, H., Kataoka, H., 2005. Cytochrome P450 CYP307A1/Spook: A Regulator for Ecdysone Synthesis in Insects. Biochem Biophys Res Commun 337, 367-374.

Niwa, R., Niwa, Y.S., 2014. Enzymes for Ecdysteroid Biosynthesis: Their Biological Functions in Insects and Beyond. Biosci Biotechnol Biochem 78, 1283-1292.

Niwa, R., Namiki, T., Ito, K., Shimada-Niwa, Y., Kiuchi, M., Kawaoka, S., Kayukawa, T., Banno, Y., Fujimoto, Y., Shigenobu, S., Kobayashi, S., Shimada, T., Katsuma, S., Shinoda, T., 2010. Non-Molting Glossy/Shroud Encodes a Short-Chain Dehydrogenase/Reductase that Functions in the 'Black Box' of the Ecdysteroid Biosynthesis Pathway. Development 137, 1991-1999.

Nowak, K., Seisenbacher, G., Hafen, E., Stocker, H., 2013. Nutrient Restriction Enhances the Proliferative Potential of Cells Lacking the Tumor Suppressor PTEN in Mitotic Tissues. Elife 2, e00380.

Nusslein-Volhard, C., Wieschaus, E., Kluding, H., 1984. Mutations Affecting the Pattern of the Larval Cuticle inDrosophila Melanogaster : I. Zygotic Loci on the Second Chromosome. Wilehm Roux Arch Dev Biol 193, 267-282.

Ogawa, K., Sun, J., Taketani, S., Nakajima, O., Nishitani, C., Sassa, S., Hayashi, N., Yamamoto, M., Shibahara, S., Fujita, H., Igarashi, K., 2001. Heme Mediates Derepression of Maf Recognition Element through Direct Binding to Transcription Repressor Bach1. EMBO J 20, 2835-2843.

Okamoto, N., Viswanatha, R., Bittar, R., Li, Z., Haga-Yamanaka, S., Perrimon, N., Yamanaka, N., 2018. A Membrane Transporter is Required for Steroid Hormone Uptake in Drosophila. Dev Cell 47, 294-305.e7.

Ono, H., Rewitz, K.F., Shinoda, T., Itoyama, K., Petryk, A., Rybczynski, R., Jarcho, M., Warren, J.T., Marques, G., Shimell, M.J., Gilbert, L.I., O'Connor, M.B., 2006. Spook and Spookier Code for Stage-Specific Components of the Ecdysone Biosynthetic Pathway in Diptera. Dev Biol 298, 555-570.

Ou, Q., Zeng, J., Yamanaka, N., Brakken-Thal, C., O'Connor, M.B., King-Jones, K., 2016. The Insect Prothoracic Gland as a Model for Steroid Hormone Biosynthesis and Regulation. Cell Rep 16, 247-262.

Ou, Q., Magico, A., King-Jones, K., 2011. Nuclear Receptor DHR4 Controls the Timing of Steroid Hormone Pulses during Drosophila Development. PLoS Biol 9, e1001160.

Palanker, L., Necakov, A.S., Sampson, H.M., Ni, R., Hu, C., Thummel, C.S., Krause, H.M., 2006. Dynamic Regulation of Drosophila Nuclear Receptor Activity in Vivo. Development 133, 3549-3562.

Park-Sarge, O.K., Sarge, K.D., 2009. Detection of Sumoylated Proteins. Methods Mol Biol 464, 255-265.

Parvy, J.P., Blais, C., Bernard, F., Warren, J.T., Petryk, A., Gilbert, L.I., O'Connor, M.B., Dauphin-Villemant, C., 2005. A Role for betaFTZ-F1 in Regulating Ecdysteroid Titers during Post-Embryonic Development in Drosophila Melanogaster. Dev Biol 282, 84-94.

Peng, G.H., Ahmad, O., Ahmad, F., Liu, J., Chen, S., 2005. The Photoreceptor-Specific Nuclear Receptor Nr2e3 Interacts with Crx and Exerts Opposing Effects on the Transcription of Rod Versus Cone Genes. Hum Mol Genet 14, 747-764.

Perissi, V., Rosenfeld, M.G., 2005. Controlling Nuclear Receptors: The Circular Logic of Cofactor Cycles. Nat Rev Mol Cell Biol 6, 542-554.

Petryk, A., Warren, J.T., Marques, G., Jarcho, M.P., Gilbert, L.I., Kahler, J., Parvy, J.P., Li, Y., Dauphin-Villemant, C., O'Connor, M.B., 2003. Shade is the Drosophila P450 Enzyme that Mediates the Hydroxylation of Ecdysone to the Steroid Insect Molting Hormone 20-Hydroxyecdysone. Proc Natl Acad Sci U S A 100, 13773-13778.

Pittendrigh, C.S., 1967. Circadian Systems. I. the Driving Oscillation and its Assay in Drosophila Pseudoobscura. Proc Natl Acad Sci U S A 58, 1762-1767.

Port, F., Chen, H.M., Lee, T., Bullock, S.L., 2014. Optimized CRISPR/Cas Tools for Efficient Germline and Somatic Genome Engineering in Drosophila. Proc Natl Acad Sci U S A 111, E2967-76.

Preitner, N., Damiola, F., Lopez-Molina, L., Zakany, J., Duboule, D., Albrecht, U., Schibler, U., 2002. The Orphan Nuclear Receptor REV-ERBalpha Controls Circadian Transcription within the Positive Limb of the Mammalian Circadian Oscillator. Cell 110, 251-260.

Qiu, J., Hardin, P.E., 1996. Developmental State and the Circadian Clock Interact to Influence the Timing of Eclosion in Drosophila Melanogaster. J Biol Rhythms 11, 75-86.

Qiu, Y., Tittiger, C., Wicker-Thomas, C., Le Goff, G., Young, S., Wajnberg, E., Fricaux, T., Taquet, N., Blomquist, G.J., Feyereisen, R., 2012. An Insect-Specific P450 Oxidative Decarbonylase for Cuticular Hydrocarbon Biosynthesis. Proc Natl Acad Sci U S A 109, 14858-14863.

Rabinovich, D., Yaniv, S.P., Alyagor, I., Schuldiner, O., 2016. Nitric Oxide as a Switching Mechanism between Axon Degeneration and Regrowth during Developmental Remodeling. Cell 164, 170-182.

Raghuram, S., Stayrook, K.R., Huang, P., Rogers, P.M., Nosie, A.K., McClure, D.B., Burris, L.L., Khorasanizadeh, S., Burris, T.P., Rastinejad, F., 2007. Identification of Heme as the Ligand for the Orphan Nuclear Receptors REV-ERBalpha and REV-ERBbeta. Nat Struct Mol Biol 14, 1207-1213.

Redfern, C.P., 1984. Evidence for the Presence of Makisterone A in Drosophila Larvae and the Secretion of 20-Deoxymakisterone A by the Ring Gland. Proc Natl Acad Sci U S A 81, 5643-5647.

Reinking, J., Lam, M.M., Pardee, K., Sampson, H.M., Liu, S., Yang, P., Williams, S., White, W., Lajoie, G., Edwards, A., Krause, H.M., 2005. The Drosophila Nuclear Receptor e75 Contains Heme and is Gas Responsive. Cell 122, 195-207.

Rewitz, K.F., Yamanaka, N., Gilbert, L.I., O'Connor, M.B., 2009. The Insect Neuropeptide PTTH Activates Receptor Tyrosine Kinase Torso to Initiate Metamorphosis. Science 326, 1403-1405.

Richards, G., 1981. The Radioimmune Assay of Ecdysteroid Titres in Drosophila Melanogaster. Mol Cell Endocrinol 21, 181-197.

Riddiford, L.M., 1993. In: In The Development of Drosophila melanogaster. Bate, M., Arias, A.M., editor. New York: Cold Spring Harbor Press. Hormones and Drosophila development; pp. 899-939.

Rilk-van Gessel, R., Kayser, H., 2007. Porphobilinogen Synthase from the Butterfly, Pieris Brassicae: Purification and Comparative Characterization. J Insect Sci 7, 1-13.

Roduit, R., Escher, P., Schorderet, D.F., 2009. Mutations in the DNA-Binding Domain of NR2E3 Affect in Vivo Dimerization and Interaction with CRX. PLoS One 4, e7379.

Roth, G.E., Gierl, M.S., Vollborn, L., Meise, M., Lintermann, R., Korge, G., 2004. The Drosophila Gene Start1: A Putative Cholesterol Transporter and Key Regulator of Ecdysteroid Synthesis. Proc Natl Acad Sci U S A 101, 1601-1606.

Segraves, W.A., Hogness, D.S., 1990. The E75 Ecdysone-Inducible Gene Responsible for the 75B Early Puff in Drosophila Encodes Two New Members of the Steroid Receptor Superfamily. Genes Dev 4, 204-219.

Sever, R., Glass, C.K., 2013. Signaling by Nuclear Receptors. Cold Spring Harb Perspect Biol 5, a016709.

Shafer, O.T., Rosbash, M., Truman, J.W., 2002. Sequential Nuclear Accumulation of the Clock Proteins Period and Timeless in the Pacemaker Neurons of Drosophila Melanogaster. J Neurosci 22, 5946-5954.

Shanmugam, D., Wu, B., Ramirez, U., Jaffe, E.K., Roos, D.S., 2010. Plastid-Associated Porphobilinogen Synthase from Toxoplasma Gondii: Kinetic and Structural Properties Validate Therapeutic Potential. J Biol Chem 285, 22122-22131.

Sinclair, P.R., Gorman, N., Jacobs, J.M., 2001. Measurement of Heme Concentration. Curr Protoc Toxicol Chapter 8, Unit 8.3.

Sluder, A.E., Maina, C.V., 2001. Nuclear Receptors in Nematodes: Themes and Variations. Trends Genet 17, 206-213.

Soliman, A., De Sanctis, V., Elalaily, R., 2014. Nutrition and Pubertal Development. Indian J Endocrinol Metab 18, S39-47.

Sun, F., Cheng, Y., Chen, C., 2015. Regulation of Heme Biosynthesis and Transport in Metazoa. Sci China Life Sci 58, 757-764.

Sung, C., Wong, L.E., Chang Sen, L.Q., Nguyen, E., Lazaga, N., Ganzer, G., McNabb, S.L., Robinow, S., 2009. The Unfulfilled/DHR51 Gene of Drosophila Melanogaster Modulates Wing Expansion and Fertility. Dev Dyn 238, 171-182.

Tanner, J.M., 1986. Normal Growth and Techniques of Growth Assessment. Clin Endocrinol Metab 15, 411-451.

Tracy, J.A., Dyck, P.J., 2014. Porphyria and its Neurologic Manifestations. Handb Clin Neurol 120, 839-849.

Ukai-Tadenuma, M., Yamada, R.G., Xu, H., Ripperger, J.A., Liu, A.C., Ueda, H.R., 2011. Delay in Feedback Repression by Cryptochrome 1 is Required for Circadian Clock Function. Cell 144, 268-281.

Wang, H., Yang, H., Shivalila, C.S., Dawlaty, M.M., Cheng, A.W., Zhang, F., Jaenisch, R., 2013. One-Step Generation of Mice Carrying Mutations in Multiple Genes by CRISPR/Cas-Mediated Genome Engineering. Cell 153, 910-918.

Wang, J.W., Beck, E.S., McCabe, B.D., 2012. A Modular Toolset for Recombination Transgenesis and Neurogenetic Analysis of Drosophila. PLoS One 7, e42102.

Warren, J.T., Yerushalmi, Y., Shimell, M.J., O'Connor, M.B., Restifo, L.L., Gilbert, L.I., 2006. Discrete Pulses of Molting Hormone, 20-Hydroxyecdysone, during Late Larval Development of Drosophila Melanogaster: Correlations with Changes in Gene Activity. Dev Dyn 235, 315-326.

Warren, J.T., Petryk, A., Marques, G., Parvy, J.P., Shinoda, T., Itoyama, K., Kobayashi, J., Jarcho, M., Li, Y., O'Connor, M.B., Dauphin-Villemant, C., Gilbert, L.I., 2004. Phantom Encodes the 25-Hydroxylase of Drosophila Melanogaster and Bombyx Mori: A P450 Enzyme Critical in Ecdysone Biosynthesis. Insect Biochem Mol Biol 34, 991-1010.

Warren, J.T., Petryk, A., Marques, G., Jarcho, M., Parvy, J.P., Dauphin-Villemant, C., O'Connor, M.B., Gilbert, L.I., 2002. Molecular and Biochemical Characterization of Two P450 Enzymes in the Ecdysteroidogenic Pathway of Drosophila Melanogaster. Proc Natl Acad Sci U S A 99, 11043-11048.

White, K.A., Marletta, M.A., 1992. Nitric Oxide Synthase is a Cytochrome P-450 Type Hemoprotein. Biochemistry 31, 6627-6631.

White, K.P., Hurban, P., Watanabe, T., Hogness, D.S., 1997. Coordination of Drosophila Metamorphosis by Two Ecdysone-Induced Nuclear Receptors. Science 276, 114-117.

Wieschaus, E., Nusslein-Volhard, C., Jurgens, G., 1984. Mutations Affecting the Pattern of the Larval Cuticle inDrosophila Melanogaster : III. Zygotic Loci on the X-Chromosome and Fourth Chromosome. Wilehm Roux Arch Dev Biol 193, 296-307.

Wightman, B., Ebert, B., Carmean, N., Weber, K., Clever, S., 2005. The C. Elegans Nuclear Receptor Gene Fax-1 and Homeobox Gene Unc-42 Coordinate Interneuron Identity by Regulating the Expression of Glutamate Receptor Subunits and Other Neuron-Specific Genes. Dev Biol 287, 74-85.

Wilkenfeld, S.R., Lin, C., Frigo, D.E., 2018. Communication between Genomic and Non-Genomic Signaling Events Coordinate Steroid Hormone Actions. Steroids 133, 2-7.

Wu, N., Yin, L., Hanniman, E.A., Joshi, S., Lazar, M.A., 2009. Negative Feedback Maintenance of Heme Homeostasis by its Receptor, Rev-Erbalpha. Genes Dev 23, 2201-2209.

Xue, Z., Wu, M., Wen, K., Ren, M., Long, L., Zhang, X., Gao, G., 2014. CRISPR/Cas9 Mediates Efficient Conditional Mutagenesis in Drosophila. G3 (Bethesda) 4, 2167-2173.

Yang, X., Downes, M., Yu, R.T., Bookout, A.L., He, W., Straume, M., Mangelsdorf, D.J., Evans, R.M., 2006. Nuclear Receptor Expression Links the Circadian Clock to Metabolism. Cell 126, 801-810.

Yaniv, S.P., Issman-Zecharya, N., Oren-Suissa, M., Podbilewicz, B., Schuldiner, O., 2012. Axon Regrowth during Development and Regeneration Following Injury Share Molecular Mechanisms. Curr Biol 22, 1774-1782.

Yao, T.P., Segraves, W.A., Oro, A.E., McKeown, M., Evans, R.M., 1992. Drosophila Ultraspiracle Modulates Ecdysone Receptor Function Via Heterodimer Formation. Cell 71, 63-72.

Yin, L., Wu, N., Curtin, J.C., Qatanani, M., Szwergold, N.R., Reid, R.A., Waitt, G.M., Parks, D.J., Pearce, K.H., Wisely, G.B., Lazar, M.A., 2007. Rev-Erbalpha, a Heme Sensor that Coordinates Metabolic and Circadian Pathways. Science 318, 1786-1789.

Yoshiyama, T., Namiki, T., Mita, K., Kataoka, H., Niwa, R., 2006. Neverland is an Evolutionally Conserved Rieske-Domain Protein that is Essential for Ecdysone Synthesis and Insect Growth. Development 133, 2565-2574.

Yu, W., Hardin, P.E., 2006. Circadian Oscillators of Drosophila and Mammals. J Cell Sci 119, 4793-4795.

Yu, Z., Ren, M., Wang, Z., Zhang, B., Rong, Y.S., Jiao, R., Gao, G., 2013. Highly Efficient Genome Modifications Mediated by CRISPR/Cas9 in Drosophila. Genetics 195, 289-291.

Zhang, H., Stallock, J.P., Ng, J.C., Reinhard, C., Neufeld, T.P., 2000. Regulation of Cellular Growth by the Drosophila Target of Rapamycin dTOR. Genes Dev 14, 2712-2724.

Zhang, Z., Burch, P.E., Cooney, A.J., Lanz, R.B., Pereira, F.A., Wu, J., Gibbs, R.A., Weinstock, G., Wheeler, D.A., 2004. Genomic Analysis of the Nuclear Receptor Family: New Insights into Structure, Regulation, and Evolution from the Rat Genome. Genome Res 14, 580-590.

Appendix A

Creating a DHR51 antibody and DHR51 CRISPR plasmids

A.1 Introduction

I began designing a DHR51 antibody that could hopefully be used in future ChIP experiments to identify direct target genes of DHR51. In case the antibody would be unsuccessful, I also began cloning CRISPR plasmids that could be used to add a FLAG tag to the endogenous DHR51 locus. This would allow ChIP to be done with commercially available antibodies without the need to overexpress DHR51, which would reduce the possibility of DHR51 binding to off-target sites. Since adding a tag to endogenous DHR51 could interfere with protein function, designing a DHR51 antibody was the preferred method to conduct a DHR51 ChIP. ChIP would provide valuable insight into DHR51 function in the PG and further the work of my two aims, answering questions of how DHR51 could regulate heme biosynthesis and how DHR51 regulates ecdysone production. Does DHR51 directly bind to *Alas* or a known regulator of *Alas*? Does DHR51 bind to *per* in the PG and other circadian rhythm genes? Does DHR51 bind to genes that encode other known regulators of ecdysone production, like TOR pathway genes? Do lower cellular heme levels affect DHR51 binding to target genes? If not, do lower heme levels affect gene expression of direct DHR51 target genes? Manipulating cellular heme levels and testing DHR51's DNA binding capability and transcriptional regulation of direct target genes could provide strong evidence whether heme is a ligand for DHR51 *in vivo* and whether DHR51 is truly a heme sensor in the PG. A *PPOX* mutant background could create low cellular heme levels, while raising wild type larvae on hemin-supplemented media would increase cellular heme levels in the PG. Normal heme levels could be achieved with wild type larvae on standard media. This appendix will outline my quality control steps for my DHR51 antibody.

A.1.1 CRISPR

CRISPR (Clustered Regularly Interspaced Short Palindromic Repeats) was first modified from the adaptive immune system of bacteria after it was discovered in 1987 (Ishino, et al. 1987). CRISPR is used in prokaryotes as a defensive mechanism against invading phages by using short viral-derived RNA sequences to gain resistance against the phage via *cas* genes, which encode for proteins that use the viral-derived RNA to target foreign nucleic acids (Barrangou, et al. 2007). The CRISPR system in the host is set up in an array of repetitive sequences, some which are palindromic, and interspersed with unique spacer sequences derived from foreign nucleic acids. *cas* genes were adjacent to the CRISPR array (Makarova, et al. 2011). Cas proteins can be divided into different types, but type II, which includes Cas9, has been the most widely used for genome editing due to their simplicity as type II Cas proteins are a single large endonuclease that can generate CRISPR RNA and cut DNA (Makarova, et al. 2011). Type I and III Cas proteins require large protein complexes to function, making them less suitable for genome editing in various model organisms.

The type II CRISPR/Cas9 system originally used three components. The host-derived *trans*-activating CRISPR RNA (tracrRNA) recruits the phage-derived CRISPR RNA (crRNA) to the Cas9 endonuclease (Brouns, et al. 2008; Gasiunas, et al. 2012; Jinek, et al. 2012). tracrRNA, crRNA, and Cas9 form a complex that cuts viral DNA complementary to the crRNA, causing double-strand breaks. Based on the RNA structure of both the tracrRNA and crRNA, the two RNA fragments were able to be fused into one single synthetic guide RNA (gRNA) that would still work with Cas9 to cut DNA (Jinek, et al. 2012). The creating of gRNA, along with Cas9, led to the development of CRISPR as a genome-editing tool, a relatively cheap and easy genome-editing technique that could work for a variety of models like human cells, mice, zebrafish, and

Drosophila (Mali, et al. 2013; Wang, H., et al. 2013; Cong, et al. 2013; Hwang, et al. 2013; Bassett, et al. 2013; Gratz, Cummings, et al. 2013; Yu, Z., et al. 2013). Cas9 uses gRNA to target specific DNA sequences that are adjacent to a short protospacer adjacent motif (PAM) sequence (NGG) to cut DNA, causing double-strand breaks three to eight base pairs upstream of the PAM sequence (Jinek, et al. 2012). Once the DNA is cut, insertion and deletion mutations can occur from error-prone NHEJ. One major benefit of CRISPR is that off-target cuts seem to be extremely rare, although there is still some debate about the extent of CRISPR off-targets (Bassett, et al. 2013; Gratz, et al. 2014; Kimberland, et al. 2018).

Modified CRISPR techniques exist so more can be done to edit the genome than just mutagenesis with insertions and deletions. When the DNA is cut and a donor plasmid is provided that has homology arms around the cut site and a desired DNA modification, homologous recombination (homology-directed repair) can use the donor plasmid as a template to edit an endogenous gene with the DNA modification carried on the donor plasmid. This way, endogenous genes can be edited with specific mutations, incorporate recombination sites, or incorporate a tag to an endogenous gene (Gratz, Wildonger, et al. 2013; Bassett and Liu. 2014). I designed CRISPR plasmids to facilitate homology-directed repair to knock-in a FLAG tag to the endogenous *DHR51* locus to create a tool that could be used in chromatin immunoprecipitation (ChIP). The protocol I used to generate the CRISPR plasmids to add a tag to the *DHR51* locus was based on previously published protocols (Gratz, et al. 2014; Gratz, et al. 2015).

A.2 Results

A.2.1 Designing a ChIP-grade DHR51 antibody

A.2.1.1 Testing *hs-DHR51* and *hs-FLAG-DHR51* transgenes

As discussed in Chapter 3.2.8, FLAG-tagged and untagged *heat shock* (*hs*)-*DHR51* cDNA fly lines were made to have temporal control of *DHR51* overexpression. These lines were primarily used to help test whether my DHR51 antibody was specific to DHR51 and suitable for ChIP. Before discussing their use, I will briefly outline some quality control steps to determine whether the lines were working as intended. Only one line of *hs-DHR51* and *hs-FLAG-DHR51* were obtained after embryo injections by BestGene. DHR51 protein levels were assessed after heat shock with western blotting to test whether the *hs-(FLAG-)DHR51* transgenes produced a protein.

DHR51 protein levels were tested in whole body L3 larvae before heat shock and 0 hours, 3 hours, and 6 hours after a one hour heat shock. My experimental DHR51 primary antibody was used for the western blot with *hs-DHR51*, while a commercially available FLAG antibody was used for *hs-FLAG-DHR51*. DHR51 was expected to have a size of 63.33 kDa based on the 582 amino acids that make up the DHR51 protein. However, DHR51-FLAG was found to have a size of approximately 70 kDa in cell culture (Rabinovich, et al. 2016). 3xFLAG should only add about 3 kDa to the expected size, so the difference could be due to post-translational modifications. When I tested *hs-DHR51*, there was an unexpected doublet around 70 kDa that was only present after heat shock and 3 to 6 hours of recovery before protein extraction. The lighter band was at 70 kDa and the heavier band was around ~85 kDa (Figure A-1A). This doublet had the highest protein level following a 3 hour recovery after heat shock and began to decrease, but was still present, after a 6 hour recovery. There was no detectable protein when

larvae were not heat shocked, nor immediately after heat shock, which suggested that the doublet was a heat shock product, likely to be DHR51 since the doublet was identified with a primary antibody designed to target DHR51. Curiously, the lighter band of the doublet was not detected when I tested *hs-FLAG-DHR51*, which only had one band at ~85 kDa (Figure A-1B). This suggested that there may be more than one protein product from heat shocking the *hs-DHR51* line, possibly due to an alternative start codon producing a differently sized protein. The single protein product of *hs-FLAG-DHR51* had little protein product immediately after a one hour heat shock and the protein level was significantly higher four hours after heat shock. Together, the *hs-DHR51* and *hs-FLAG-DHR51* lines expressed transgenic protein, likely to be DHR51, that reached peak protein levels 3 to 4 hours after heat shock. However, a larger protein product was produced than expected (70 kDa). Additional quality control steps may need to be taken for these *hs-(FLAG-) DHR51* lines to determine what exactly the larger sized protein band was.

A.2.1.2 Generating a DHR51 antibody for ChIP

GenScript was hired to generate a primary polyclonal antibody targeting DHR51's LBD. I commissioned the DHR51 antibody so that it could be used in future ChIP experiments. For full details on the production of the antibody, see Chapter 2.1.14.1. A DHR51 protein antigen of the following amino acid sequence was used to generate an immune response and antibody against DHR51 in rabbits:

```
                                    394    MAVKWAK NLPSFARLSF RDQVILLEES
421 WSELFLLNAI QWCIPLDPTG CALFSVAEHC NNLENNANGD TCITKEELAA DVRTLHEIFC
481 KYKAVLVDPA EFACLKAIVL FRPETRGLKD PAQIENLQDQ AHVMLSQHTK TQFTAQIARF
541 GRLLLMLPLL RMISSHKIES IYFQRTIGNT PMEKVLCDMY KN
```

This sequence starts just before the annotated LBD and continues to the end of the protein (Sung, et al. 2009). This region was chosen for protein accessibility (compared to the DBD which would be bound to DNA in a ChIP) and hopefully low resemblance to other nuclear receptor family

proteins. A protein BLAST of the DHR51-LBD protein antigen sequence returned the top three most similar hits after DHR51 as the nuclear receptors *dissatisfaction* (*dsf*), *seven up* (*svp*), and *tailless* (*tll*) which had an identity of 45%, 42%, and 28%, respectively (Figure A-2). There were some 6-8 strings of similar amino acids that could potentially form an epitope for my DHR51 antibody, but the DBD of nuclear receptors are more highly conserved compared to the LBD, so the LBD was used. DSF and SVP are currently not known to have a function or be expressed in the RG. There was also a large decrease in protein similarity to the DHR51-LBD protein antigen after DSF and SVP. The LBD of DHR51 used as a protein antigen seemed to be the best sequence to use to produce a suitable DHR51 antibody.

Two rabbits were injected with the protein antigen and a test bleed was sent to me after the third immunization for in-house testing. If the antibody was sufficient from my in-house testing, a fourth immunization and purification of the antibody would be done. I tested the antibody from two different rabbits (#295 and #298) using western blotting. Wandering *hs-DHR51* L3 larvae were heat shocked for 1 hour at 37.5°C and larvae were allowed to recover for 0 hours, 3 hours, and 6 hours before protein was extracted from whole body larvae. A no heat shock control was also included. Western blotting was done with the pre-immune serum, which should not have any DHR51 antibody, and post-immune serum, which should contain antibodies against DHR51. As mentioned in the previous section, DHR51 was expected to have a size of about 70 kDa. The pre-immune serum (#295) did not recognize any protein in any of the conditions tested as expected. The post-immune serum (#295) had a very high background smear above 70 kDa in all protein extracts, including extracts from larvae that were not heat shocked (Figure A-3A). I decided against the antibody from this rabbit (#295) due to the high background smears that I observed when testing this serum. The post-immune serum (#298) was more

promising. The pre-immune serum (#298) also did not detect any protein, nor have any background signal, as expected because the pre-immune serum should not contain antibodies against DHR51. The post-immune serum had some background smears above approximately 100 kDa and a clear doublet was observed at and just above 70 kDa (Figure A-3B). The doublet was most prominent after a 3 hour recovery following heat shock and began to fade after a 6 hour recovery. The doublet was not observed immediately after heat shock nor in the absence of a heat shock, which suggested that the doublet was a heat shock product. The antibodies that targeted DHR51 from this rabbit (#298) seemed sufficient to purify as I hoped the affinity-purification would reduce some of the background smearings.

Once the final affinity-purified DHR51 antibody was obtained (from rabbit #298 only), I again tested the affinity-purified antibody with the same protocol as the test bleed samples. Wandering *hs-DHR51* L3 larvae were heat shocked and allowed to recover for 0 hours, 3 hours, and 6 hours, plus larvae that were not heat shocked were used as a control. The affinity-purified antibody behaved similarly to the post-immune serum (#298) except it did not have the background smear above 100 kDa. A doublet was observed at about 70 kDa and 80 kDa, peaking after a 3 hour recovery following heat shock and the doublet began to fade after 6 hours of recovery time (Figure A-3C). The protein was undetectable when larvae had 0 hours to recover after a heat shock and when larvae were not heat shocked. This suggested that the affinity-purified antibody recognized DHR51 and had low background. Since each band in the doublet behaved similar to the other, both peaking and fading to the same degree at the same times, I think it is likely that both protein bands are DHR51. The size difference could be due to post-translational modifications, as DHR51 shares conserved phosphorylation and SUMOylation sites

in the LBD with NR2E3 (Bates, et al. 2015). The affinity-purified antibody targeted DHR51 with no observable off-targets.

A.2.1.3 Testing whether the DHR51 antibody can pull-down DHR51

Before using the DHR51 antibody with ChIP, I first wanted to ensure I could pull DHR51 protein down with a pull-down assay. My plan was to carefully test each stage to ensure my DHR51 antibody would be suitable for ChIP before an actual ChIP experiment would be done. Late L3 *hs-FLAG-DHR51* larvae were used for the pull-down assay to allow for a comparison between my DHR51 antibody and a ChIP-verified commercial FLAG antibody. Larvae were heat shocked for 1 hour at 37.5°C and allowed to recover for 0 hours and 4 hours before protein extraction. 4 hours was used because it was near the peak observed at 3 hours and I knew the protein would be present as protein was still present 6 hours after heat shock. A denaturing lysis buffer was initially used, but I later switched to a non-denaturing lysis buffer to more closely mimic the conditions for ChIP.

I first confirmed my pull-down protocol by pulling down FLAG-DHR51 with a FLAG antibody. FLAG-DHR51 protein was detected on a western blot that used my DHR51 antibody. A single protein band at approximately 85-90 kDa was observed in the total lysate and after the pull-down with the FLAG antibody (Figure A-4A). The band at 85-90 kDa was faintly present 0 hours after a one hour heat shock but was stronger 4 hours after heat shock. This band is very likely FLAG-DHR51, as the size matched what was previously observed in the *hs-FLAG-DHR51* line. Unexpectedly, non-specific bands were present at about 55 kDa and another set was present at about 25 kDa and 35 kDa. These non-specific bands were only in the pull-down extract and absent in the original crude protein (total) extract, which suggested the bands were introduced during the pull-down assay. These bands were later identified to be IgG heavy chain

and light chain from the large excess of the primary antibody used in the pull-down, as these non-specific bands still appeared when no protein extract was used (see control western blot Figure A-4C). However, since a band around 85-90 kDa that likely corresponded to FLAG-DHR51 was detected, this suggested that my protocol could pull-down DHR51. Using the same protein extracts from above, I performed the pull-down assay with my DHR51 antibody and used the FLAG antibody for detection with a western blot. My DHR51 antibody pulled down a protein with an approximate size of 85-90 kDa (Figure A-4B). The 85-90 kDa protein was very likely the same protein identified with the FLAG antibody, which suggested that this band is indeed FLAG-DHR51. The band was faintly present after a 0 hour recovery after a one hour heat shock and strongly present 4 hours after heat shock. Again, a large band was observed at 55 kDa, however, the smaller band at 25 kDa and 35 kDa was not observed. As will be explained in my control western blot, these bands are likely excess antibody used to pull-down FLAG-DHR51. These pull-down assays demonstrated that my DHR51 antibody was able to specifically pull-down DHR51.

The IgG heavy chain was expected to be around 55 kDa and the light chain was expected to be approximately 25 kDa. These sizes line up with what I observed in my pull-down assays, except the predicted light chain produced what looked like a doublet, one band at 25 kDa and one near 35 kDa. Also, both primary antibodies used in the pull-down assay and western blot originated from rabbit, which allowed the secondary antibody used in the western blot to recognize both primary antibodies. To avoid this issue, the primary antibodies used in the pull-down assay and western blot should have originated from different animals. To identify whether these non-specific bands at 55 kDa and 35 kDa were excess antibodies, I performed a control western blot that ran no protein pull-down controls (Figure A-4C). In the pull-down assay with

protein, FLAG-DHR51 was observed at approximately 85-90 kDa after a 4 hour recovery following heat shock, along with the non-specific bands at 55 kDa and 25 and 35 kDa. When no protein was included in the pull-down assay with either the DHR51 or FLAG antibody, the non-specific bands were still observed, which indicated that the non-specific bands are not from the larval protein extracts. Oddly, the smaller set of non-specific bands were observed when the DHR51 antibody was used in the pull-down assay as this was not observed originally. When no protein and no antibody to pull-down FLAG-DHR51 was present in the pull-down assay, the larger 55 kDa band was absent, which indicated that the larger non-specific band was likely the IgG heavy chain, however, the lower set of bands were present. The non-specific bands at 25 kDa and 35 kDa could, therefore, be denatured light chains from the Protein G beads used in the pull-down assay. Also of note, a faint 100 kDa band was observed in the DHR51 antibody pull-down with no protein. This approximate 100 kDa band was likely a small amount of non-denatured heavy and light chain IgG (55 kDa + 35 kDa). This non-denatured band was more apparent in later western blots that used non-denaturing conditions, which further supports the band at approximately 100 kDa is non-denature heavy and light chain IgG. The no protein pull-down assay demonstrated that the non-specific bands observed did not originate from the larval protein extract used and was very likely excess antibody used during the pull-down itself. Together, this data showed that FLAG-DHR51 could be pulled down under denaturing conditions and no other protein appeared to be pulled down with FLAG-DHR51 using my DHR51 antibody.

During the ChIP protocol, proteins are not denatured during initial primary antibody binding. I then performed my pull-down assay using a non-denaturing lysis buffer to recreate conditions more closely related to ChIP. Other than changing the lysis buffer to non-denaturing,

my protocol remained unchanged. *hs-FLAG-DHR51* L3 larvae were heat shocked and allowed to recover for 0 hours and 4 hours. A no heat shock control was also included. An 85-90 kDa band that was likely FLAG-DHR51 was only pulled down after heat shock with my DHR51 antibody (Figure A-4D). The FLAG-DHR51 band was faint immediately after heat shock, but a strong band was observed after a 4 hour recovery following heat shock. The FLAG-DHR51 band was not present in non-heat shocked samples. A 100 kDa band was observed in all pull-down lanes at the same intensity which indicated the band was not a heat shock product. As mentioned from the control western blot, the 100 kDa band likely corresponded to the non-denatured IgG heavy chain and light chain. Since a non-denaturing lysis buffer was used, more non-denatured antibody would be expected compared to the previous western blots that used a denaturing lysis buffer. The 100 kDa band was not observed in the total protein lysate, which indicated that the band was not from the larval protein extract. Taken together, my DHR51 antibody was successfully able to pull-down FLAG-DHR51 under non-denaturing conditions, meaning my DHR51 antibody could be suitable for ChIP experiments.

A.2.1.4 Optimization of sonication

Before testing whether my DHR51 antibody can be used for a DHR51 ChIP, I needed to optimize my sonication protocol to obtain DNA fragments of about 300 bp in length. I first began testing sonication efficiency in whole body larvae because my plan was to test DHR51 ChIP-qPCR in whole body larvae to determine whether my DHR51 antibody is actually suitable for ChIP. Whole body w^{1118} L3 larvae were used to optimize the sonication duration and protocol. Initially, long uniform smears of DNA were obtained after sonication, even at longer sonication times. Various protocols were used in an attempt to get consistent shearing of DNA. These protocols varied in buffers used, the concentration and duration of the fix, and some of the

steps and washes. After lots of troubleshooting, I determined that a higher percent of SDS (1% compared to 0.1%) significantly improved sonication efficiency and consistency (Figure A-5A). After identifying increased SDS concentrations vastly improved sonication, I could consistently shear DNA and finally settled on a sonication protocol listed in Chapter 2.1.14.4. With this done, I was able to start optimizing the sonication duration for the whole body L3 larval extracts. Sonication times were tested in 5 min intervals ranging from 5 min to 20 min. To obtain a peak of DNA fragments at 300 bp, a sonication time of 15 min was selected as an optimal sonication duration (Figure A-5B). With an optimized sonication duration, I was able to actually test my DHR51 antibody for ChIP, doing a ChIP-qPCR in whole body larval extracts.

A.2.1.5 DHR51 ChIP-qPCR

Since my DHR51 antibody was successfully able to pull-down DHR51, I began testing whether my DHR51 antibody was suitable for ChIP. FLAG-DHR51 ChIP-qPCR was attempted with a ChIP-verified FLAG antibody to determine whether my ChIP protocol with FLAG-DHR51 was working. Previous research demonstrated that DHR51-FLAG directly bound to the promoter of *period* (*per*) in S2 cells, so I used the *per* promoter as a positive control. However, DHR51-FLAG has only been demonstrated to bind to *per* with co-expression of *Clock* (*Clk*) since DHR51-FLAG only induced *per* expression with CLK present (further induction occurred with the addition of E75 as well) (Jaumouille, et al. 2015). DHR51 was found to bind to *E5* (*CRS – circadian regulatory sequence*), *RORE* (*retinoid-related orphan receptors element*), and *E8* of *per*, but not to *Lim1* (*Lim1* is a negative control sequence) (Jaumouille, et al. 2015). This previous work would hopefully allow me to use these *per* sequences (*E5*, *RORE*, and *E8*) as a positive control and the *Lim1* sequence as a negative control during my own FLAG-DHR51 ChIP-qPCR. Wandering *hs-FLAG-DHR51* L3 larvae were heat shocked and allowed to recover

for 4 hours. I performed ChIP with my DHR51 antibody and a ChIP-verified FLAG antibody. ChIP-qPCR with my DHR51 antibody resulted in a high percent of DNA recovered compared to the amount of input DNA for all sequences tested (Figure A-6A). Unfortunately, this was also true for my negative control, *Lim1*. This could mean that the DHR51 antibody was able to purify all DNA sequences (or at least *Lim1* and the expected positive control sequences) or there was high background in the ChIP samples, which gave a high percent of DNA recovered relative to the input. However, the percent of input I observed (about 0.3%) matched very closely with what was obtained from the ChIP in S2 cells (approximately 0.2% of the input for positive hits) (Jaumouille, et al. 2015).

To test whether my DHR51 antibody was not suitable for ChIP or whether my protocol was not working, I also performed ChIP-qPCR with the FLAG antibody. The protocol was done similar to the DHR51 ChIP-qPCR protocol, but I also included a mock ChIP sample that was done without the FLAG antibody. Similar to the results of the DHR51 antibody ChIP, I observed a high percent of DNA being recovered from the input DNA for all sequences being tested (about 0.3%, except 3.9% for *E5* (*CRS*)), including the negative control, *Lim1* (Figure A-6B). The mock ChIP, which included no primary antibody, did not recover any DNA and the percent of DNA recovered was so low that it did not appear visible on the graph (on average, about 0.008%). With the mock ChIP, I also calculated the relative fold change between the ChIP samples compared to the mock ChIP. All DNA sequences tested, including *Lim1*, were highly enriched in the ChIP samples, however, no sequence differed in enrichment compared to *Lim1* (Figure A-6C). This data suggested that the FLAG antibody was recovering DNA sequences from the extract, including the negative control. Besides *Lim1*, I also tested another negative control while troubleshooting my protocol, *E1*, which is near *per*. However, like *Lim1*, *E1* was

also recovered from ChIP samples with the FLAG antibody. From this data, my ChIP-qPCR protocol was not working as intended as negative control sequences appeared to be bound by FLAG-DHR51.

More troubleshooting to get a working ChIP-qPCR protocol is necessary, but, unfortunately, I ran out of time during my program to properly troubleshoot my ChIP protocol. There was also the possibility that the heat shock interferes with normal DHR51 function or whole body larvae are unsuitable for this experiment and did not accurately match the conditions in the S2 cells. Co-expression of *Clk* may be necessary to recapitulate DHR51 target binding in S2 cells. Larvae were raised in constant darkness, but DHR51 may only bind *per* at a certain circadian time. Too many assumptions were being made for the ChIP-qPCR in whole body larvae, so a better step would be to replicate the DHR51 ChIP-qPCR in S2 cells to determine whether my DHR51 antibody is suitable for ChIP.

A.2.1.6 1 mM Succinylacetone did not upregulate *Alas* expression in cell culture

Since my FLAG-DHR51 ChIP-qPCR in whole body larvae did not work, I had planned to replicate the DHR51 ChIP in S2 cells. I contacted Dr. Emi Nagoshi, University of Geneva, and received their S2 cell plasmids for *DHR51-FLAG, Clk*, and *E75* (Jaumouille, et al. 2015). Ultimately, I wanted to use my DHR51 antibody for ChIP to determine DHR51 target genes and whether cellular heme levels affected DHR51 DNA binding. As I was preparing to work with S2 cells, I tested whether cellular heme levels could be reduced in S2 cells by treating the cells with succinylacetone. Succinylacetone is an inhibitor of ALAD (aminolevulinic acid dehydratase in vertebrates, or PBGS, porphobilinogen synthase in *Drosophila*), which is the second enzyme in the heme biosynthesis pathway (Ebert, et al. 1979). Succinylacetone inhibits ALAD/PBGS by mimicking ALA (aminolevulinic acid, the substrate of ALAD/PBGS). Succinylacetone was used

at concentrations generally between 0.5 mM and 5 mM for 16 to 24 hours and was able to decrease cellular heme levels in cell culture, which resulted in *Alas1* upregulation, in mammalian cell lines (Raghuram, et al. 2007; Wu, et al. 2009).

I was not aware of any previous use of succinylacetone in S2 cells, so I tested whether a 24 hour treatment of 1 mM of succinylacetone was able to induce *Alas* expression in S2 cells and therefore, cellular heme levels. I examined *Alas* expression with qPCR, as well as the other three heme biosynthetic genes that were upregulated when cellular heme levels were low: *Pbgs*, *l(3)02640*, and *FeCH*. *DHR51* expression was also examined to determine whether heme levels affected *DHR51* expression in S2 cells. When S2 cells were treated for 24 hours with 1 mM succinylacetone, there was no difference in expression of any of the heme biosynthetic genes or *DHR51* expression (Figure A-7). A 1 mM succinylacetone treatment was insufficient to induce *Alas* expression in S2 cells, thus heme levels did not appear to be lowered by a 1 mM succinylacetone treatment. A wide range of succinylacetone concentrations will need to be used to determine what concentration is necessary to adequately inhibit PBGS in S2 cells to induce low cellular heme levels and induce *Alas* expression. Unfortunately, I was not able to complete testing the necessary range of succinylacetone concentrations due to program time constraints. I did not pursue the FLAG-DHR51 ChIP in S2 cells because I was unable to determine whether succinylacetone disrupted heme biosynthesis in S2 cells as *Alas* was not upregulated.

Unfortunately, this is where my work ended testing my DHR51 antibody. A DHR51 antibody was generated and the DHR51 antibody was capable of binding to DHR51 with no observed non-specific binding in whole body L3 larvae. The DHR51 antibody was suitable for pull-down experiments, but the antibody still needs to be tested for its potential in ChIP in either

larval samples or cell culture. It will be up to future researchers to identify DHR51 target genes in the PG.

A.2.2 Using CRISPR to add a FLAG tag to the endogenous *DHR51* locus

As mentioned at the beginning of this results section, my secondary plan was to use CRISPR to FLAG tag the endogenous *DHR51* locus. CRISPR plasmids were designed to add either an N-terminal or C-terminal FLAG tag using homology-directed repair, similar to what was previously described in *Drosophila* (Gratz, et al. 2015). Two gRNA sequences were targeted relatively near the start codon of DHR51 for the addition of an N-terminal tag. These sequences are 5'-CCGCCAAAGCTCAACAAA ATGAA-3' and 5'-ACACCCACGATTAATTAGGACGG-3' (the PAM sequences are underlined) (Figure A-8A). The sequences 5'-TCTATTTTCAGCGCACTATTGGG-3' and 5'-CCAAGCTGGTTTCGCTACCGTCC-3' were targeted by the gRNAs for the C-terminal tag, which targeted near the stop codon of DHR51 (Figure A-8B). Each of the two gRNAs were cloned into a single pCFD4 plasmid. Once the genomic DNA was cut by Cas9 near the targeted PAM sequences, the genomic DNA would hopefully align with the 1 kb homology arms of the CRISPR pHD plasmid and homology-directed repair would knock-in a FLAG tag to the endogenous DHR51 locus and a selectable *DsRed* marker. *DsRed* was flanked by *LoxP* sites so *DsRed* could be removed by the addition of *Cre* recombinase. The exact cloning method used is outlined in Chapter 2.1.16.1. The final pHD-*DsRed* Flag-tagged *DHR51* plasmids that I constructed are shown in Figure A-9.

Once both the pHD-*DsRed* Flag-tagged *DHR51* plasmids that add a FLAG tag to the N-terminus or C-terminus of *DHR51* and the corresponding 2xgRNA pCFD4 plasmids were constructed, all the plasmids were sent to GenetiVision for injection into the *vasa-Cas9* strain

#51323. Unfortunately, GenetiVision was unable to identify any successful transformants due to high lethality and sterility in the injected embryos. A member of our lab, Nhan Huynh, briefly did another round of injections with the N-terminal Flag-tagged DHR51 plasmids while demonstrating the injection protocol. I identified viable larvae and quickly transferred the newly hatched larvae to fresh food. The larvae that made it to adulthood were crossed to w^{1118} flies of the opposite sex. G_1 progeny were screened for DsRed fluorescence in the abdomen of adults. No adults were observed with DsRed fluorescence. I conducted a small PCR screen on possible DsRed positive flies, but no flies had the CRISPR modification (data not shown). It is difficult to determine whether the CRISPR plasmids were lethal or whether the transformation was just inefficient. A greater number of *Drosophila* embryos may need to be injected to find successful transformants. Since I was near the end of my program at this time, I was unable to devote sufficient time to learn how to perform *Drosophila* embryo injections to inject my CRISPR plasmids and screen for successful transformants.

A.3 Discussion

A.3.1 DHR51 antibody and ChIP

My DHR51 polyclonal antibody was designed using a protein antigen of DHR51's LBD to reduce the chance of non-specific binding by the antibody. Nuclear receptors tend to have highly conserved DBDs while the LBDs are less well conserved (King-Jones and Thummel. 2005). A protein BLAST of the protein antigen used returned DHR51 followed by DSF (45% identity), SVP isoforms (42% identity), and thirdly, TLL (28% identity) (Figure A-2). While there are some strings of 6-8 conserved amino acids that could possibly form an epitope, the LBD was the best DHR51 sequence to use for the protein antigen. The purified DHR51 antibody was able to recognize a heat shock product from my *hs-(FLAG-)DHR51* lines that likely are DHR51 (Figure A-4). However, two heat shock products were produced in *hs-DHR51*, one at 70 kDa and the other at approximately 80-85 kDa, while only one product was recognized with a FLAG antibody in *hs-FLAG-DHR51* larvae at ~85 kDa (Figure A-1). The two products from *hs-DHR51* were present in approximately equal amounts after a heat shock and behaved similarly, both peaking and fading at the same time. This led me to think that both products were transgenic, possibly due to an alternative start codon. If true, my DHR51 antibody seemed to be specific for DHR51, although there is still a chance that there is non-specific binding below my western blot detection limit since *DHR51* was highly expressed throughout the whole body of the larvae following heat shock.

Other non-specific bands, that were not DHR51, that were observed in my pull-down assays were shown not to originate from my larval protein extracts and are likely from the antibody used to pull-down FLAG-DHR51 (Figure A-4C). All of my primary antibodies were from rabbits, so the HRP secondary antibody would recognize both the western primary antibody

and the antibody that pulled down FLAG-DHR51. A non-rabbit FLAG antibody should have been used to alleviate this issue. My DHR51 antibody was also capable of binding all the DHR51 in the protein extract as no DHR51 protein was found in the absorbed fraction, which indicated that my DHR51 antibody had a high affinity for DHR51. Taken together, my DHR51 antibody was able to bind DHR51 with a high affinity and no non-specific binding by my DHR51 antibody was observed.

Based on the 582 amino acids that make up DHR51, DHR51 was expected to have a size of 63.33 kDa, but DHR51 ran at 70 kDa in a previous experiment (Rabinovich, et al. 2016). After heat shock, *hs-DHR51* produced a 70 kDa protein product and a ~85 kDa protein product, while *hs-FLAG-DHR51* produced a single ~85-90 kDa protein product (Figure A-1). These protein products were recognized by my DHR51 antibody and a FLAG antibody. The difference in size could come from an alternative start codon, but that would mean only the alternative start codon was used in the *hs-FLAG-DHR51* line. The size difference could also arise from post-transcriptional modifications, as DHR51 shares a conserved phosphorylation and SUMOylation site with NR2E3 (Bates, et al. 2015). Although phosphorylation adds relatively little mass, SUMOylation adds approximately 11 kDa, but when run on an SDS-PAGE gel SUMOylation adds an apparent 15-17 kDa (Park-Sarge and Sarge. 2009). However, if DHR51 is SUMOylated, then all of FLAG-DHR51 is SUMOylated, but only half of the transgenic DHR51 protein is SUMOylated. It is difficult to determine why DHR51 had a larger apparent size without performing additional experiments. One possible approach would be to determine whether DHR51 expressed from *UAS-(FLAG-)DHR51* has a similar size as DHR51 from the heat shock lines. Since *UAS-DHR51* was able to rescue the *unf* mutants, the transgenic DHR51 was functionally equivalent. In a similar approach, *(FLAG-)DHR51* could be heat shocked at a

critical moment in an *unf* mutant in an attempt to rescue a mutant phenotype. It may be best to determine the functionality of the *hs-(FLAG-)DHR51* lines rather than why the lines have a protein size difference.

I was unable to determine whether my DHR51 was suitable for ChIP due to my difficulties performing a FLAG-DHR51 ChIP qPCR in whole body larvae. However, my antibody does seem promising for ChIP. The ChIP-qPCR in whole body L3 larvae after a heat shock seemed to have pulled down all the DNA sequences that I tested, including the negative control, with either the DHR51 antibody or with a ChIP-verified FLAG antibody, which indicated that my protocol was not working or that the *hs-FLAG-DHR51* line I was using was not suitable for ChIP (Figure A-6). If the lysis buffer was too harsh due to high concentrations of SDS, DHR51 or the antibodies could have been denatured. A new lysis buffer that works with a lower concentration of SDS or a gentler lysis buffer could be used as long as DNA can continue to be sheared by sonication reliably. The best way to determine whether my DHR51 antibody is suitable for ChIP may be to replicate the ChIP in S2 cells that demonstrated that DHR51 bound to the *per* promoter with CLK (Jaumouille, et al. 2015). After my DHR51 antibody was produced, another DHR51 (UNF) antibody was found to be suitable for ChIP in the heads of adult *Drosophila*, which could provide an alternative to my DHR51 antibody (Kozlov, et al. 2017). So if there are sufficient quantities of the UNF antibody, the UNF antibody could be used for ChIP in the PG once a working ChIP protocol is established.

A.3.2 Succinylacetone treatment of S2 cells

Before trying to attempt ChIP in S2 cells, I wanted to determine whether I could reduce cellular heme levels with succinylacetone (an inhibitor of ALAD/PBGS) (Ebert, et al. 1979). Being able to manipulate cellular heme levels in cell culture would allow for determining

whether reducing cellular heme levels affected DHR51's DNA binding capability. However, a 24 hours treatment of 1 mM of succinylacetone was insufficient to induce *Alas* expression in S2 cells (Figure A-7). Higher concentrations of succinylacetone should be tested, possibly up to 5 mM or higher as long as cell viability is not significantly diminished. There was a chance succinylacetone was unable to inhibit *Drosophila* PBGS, however, succinylacetone inhibited PBGS in the cabbage butterfly, *Pieris brassicae*, and a eukaryotic intracellular parasite, *Toxoplasma gondii* (Rilk-van Gessel and Kayser. 2007; Shanmugam, et al. 2010). Given how conserved the heme biosynthesis pathway is, that succinylacetone mimics the substrate of ALAD/PBGS, ALA, and the range of eukaryotic ALAD/PBGS enzymes that succinylacetone is capable of inhibiting, it seems probable that succinylacetone can inhibit *Drosophila* PBGS. Nevertheless, if succinylacetone does not affect S2 cells, ChIP could still be done in S2 cells to determine whether my DHR51 antibody is suitable for ChIP.

An intriguing alternative possibility why succinylacetone did not induce *Alas* expression was that S2 cells could not have a heme sensor to recognize that cellular heme levels are low. I never measured heme levels in S2 cells; I just noted that *Alas* expression was not induced after succinylacetone treatment. Heme levels can be measured in S2 cells using my heme protocol in Chapter 2.1.11 that used a high concentration of oxalic acid and heat. If heme levels are reduced, but *Alas* expression is not induced, that would argue for the absence of a heme sensor. If this is the case, *DHR51* cDNA could be expressed to determine whether DHR51 can recognize the low cellular heme levels and induce *Alas* expression. If succinylacetone-treated cells do indeed have low cellular heme levels, expressing *DHR51* could be an elegant experiment to test whether DHR51 is a heme sensor. The heme pathway is not regulated similarly in all tissues as only three tissues in *Drosophila* accumulated red autofluorescent heme precursors when heme levels were

low (in *PPOX* mutant larvae): the PG, gut, and oenocytes (Figure 1-5). This suggested that *Alas* may be regulated differently in other tissues or *Alas* does not get as highly induced when cellular heme levels are low as in tissues that have a very high demand for heme. Since S2 cells are derived from late-stage embryos, the heme pathway may not be regulated in the same manner as the PG, gut, or oenocytes, so no functional heme sensor may be present. If future experiments are unable to induce *Alas* expression with higher concentrations of succinylacetone, it would be worth measuring cellular heme levels to determine whether heme levels are reduced. If heme levels are reduced, but *Alas* expression is not induced in S2 cells, exogenous *DHR51* could be expressed to determine whether DHR51 can act as a heme sensor by recognizing low cellular heme levels and upregulating *Alas*.

A.3.3 FLAG knock-in CRISPR

I designed a set of CRISPR plasmids to knock-in a FLAG tag to the N-terminus of DHR51 and another set of CRISPR plasmids to knock-in a FLAG tag to the C-terminus of DHR51 (Figure A-9). The 2xgRNAs were designed to target near the start or stop codon, where the FLAG tag sequence would hopefully be copied into, and the gRNAs were approximately 300 bps apart (Figure A-8). I followed a similar protocol to what has been described in *Drosophila* (Gratz, et al. 2014; Gratz, et al. 2015). *DsRed* was used as a selectable marker and was flanked by LoxP sites that could be combined with Cre recombinase to remove the *DsRed* marker. Unfortunately, the first round of injections of the CRISPR plasmids (a plasmid containing the 2xgRNA and a donor plasmid with *DHR51* homology arms, the knock-in FLAG tag, and the *DsRed* marker) into *Drosophila* embryos performed by GenetiVision did not produce a successfully transformed fly that expressed the *DsRed* selectable marker. A second, smaller

round of injections was performed by Nhan Huynh, a graduate student in our lab, but I was unable to identify any successfully transformed flies.

If the survival rate of the transformed flies after injection is low, then several hundred or a thousand embryos may need to be injected instead of a couple hundred. The designed CRISPR plasmids could be lethal or just inefficient. Inefficiency could arise due to the targeted locus, inefficient repair of double-stranded breaks, or a preference for NHEJ over homology-directed repair. Unfortunately, I did not have the time needed to learn the proper embryo injection techniques and screen for transformants. If anyone has interests in tagging the endogenous DHR51 locus, then these CRISPR plasmids could be of use. In the unlikely event that these CRISPR plasmids are lethal, DHR51 could be overexpressed if ChIP is to be done, but that would increase the incidence of off-target DNA binding. Alternatively, a *DHR51-GFP* knock-in that has DNA ~3 kb upstream of *DHR51* could be used for ChIP as the expression of the *DHR51-GFP* construct will not be as high as overexpression of *DHR51* with *UAS-GAL4* (Spokony, R. and White, K. (2012.5.22) Spokony insertions). The *DHR51-GFP* construct at least has a similar expression pattern to the *DHR51 in situ* hybridization pattern (data not shown) (Sung, et al. 2009). I initially attempted to rescue the 100% lethality in unf^{XI} mutants (when kept as an unf^{XI} / *CyO* stock) by crossing in the *DHR51-GFP* construct. I did observe rescue from 100% lethality, but later when I kept the unf^{XI} stock over a *CyO GFP* balancer, the 100% lethality also became less severe and adults were observed. Thus, I cannot determine whether *DHR51-GFP* was capable of rescuing unf^{XI} mutants or if the change in genetic background rescued the mutants. Another experiment to rescue unf^{XI} (from the *CyO GFP* stock) will need to be done. As long as DHR51-GFP retains normal DHR51 function, DHR51-GFP could be a replacement for endogenously tagged DHR51.

A.4 Figures

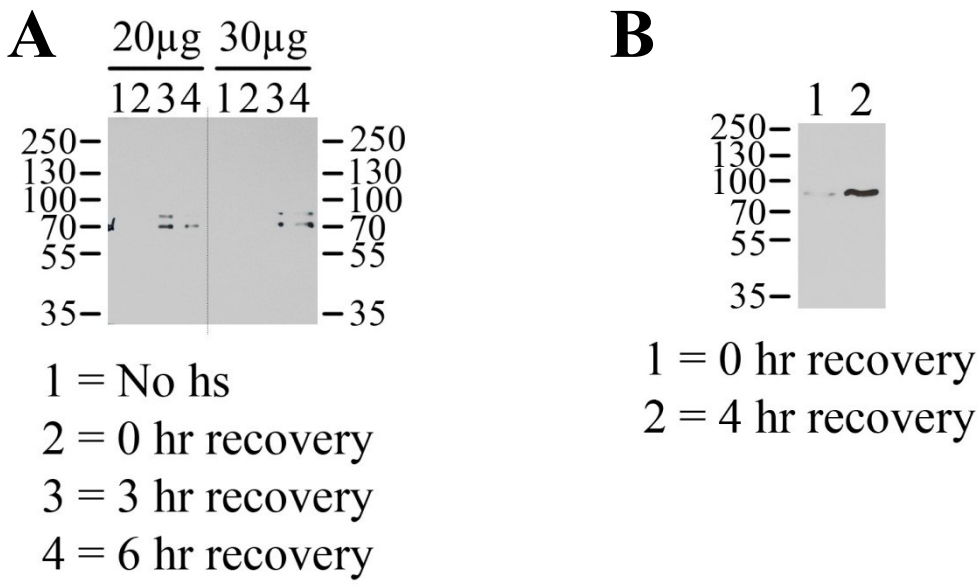

Figure A-1. Testing transgene expression of *hs-DHR51* and *hs-FLAG-DHR51* cDNA. A) A western blot using my DHR51 antibody. Protein was extracted from whole body wandering *heat shock* (*hs*)-*DHR51* L3 larvae. Larvae were either not heat shocked (hs) (Lane 1), or were heat shocked for one hour at 37.5°C. Larvae were allowed to recover for 0 hours (Lane 2), 3 hours (Lane 3), or 6 hours (Lane 4). 20 µg of protein extract was loaded into the left side of the gel and 30 µg of protein extract was loaded into the right side of the gel. The western blot was performed with my rabbit DHR51 antibody (1:500) and a goat anti-rabbit HRP secondary antibody was used (1:8000). The blot was exposed to X-ray film for 5 min. In Lane 1, at 70 kDa, there is a "d" that I had written on the X-ray film. B) A western blot using a rabbit FLAG antibody. Protein was extracted from whole body wandering *hs-FLAG-DHR51* L3 larvae. Larvae were heat shocked for one hour at 37.5°C and allowed to recover for 0 hours (Lane 1) or 4 hours (Lane 2). The western blot was performed with a rabbit FLAG antibody (1:1000) and a goat anti-rabbit HRP secondary antibody was used (1:7000). The blot was exposed to X-ray film for 30 seconds. DHR51 is expected to have a size of approximately 70 kDa. On the sides is a PageRuler Plus Prestained Protein Ladder, 10 to 250 kDa. The ladder is in kDa.

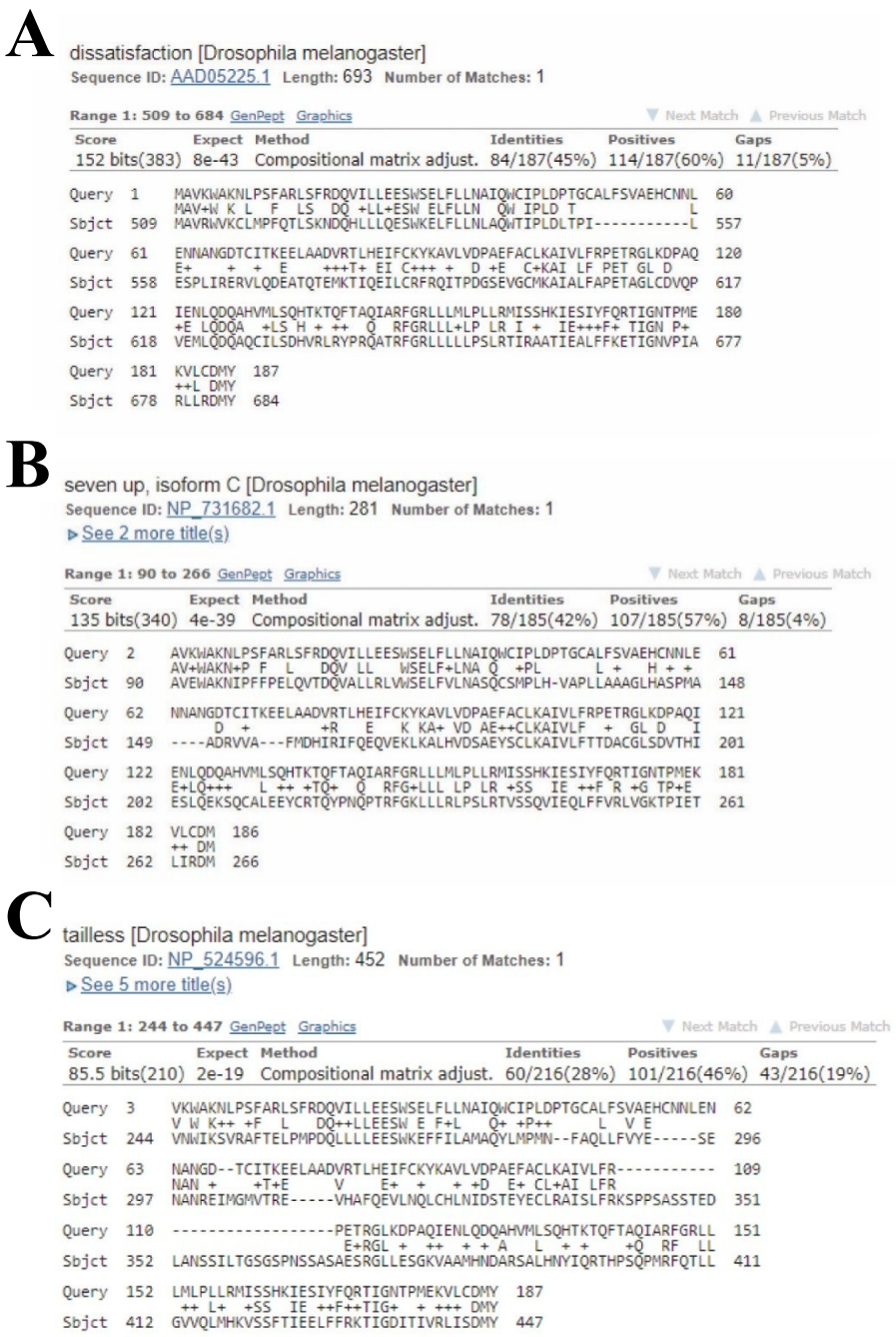

Figure A-2. Protein BLAST searches of the DHR51-LBD protein antigen. Protein BLAST results generated from NCBI (National Center for Biotechnology Information) shows the sequence alignments. The Query is the antigen sequence from DHR51-LBD (ligand binding domain) that was used to generate a DHR51 antibody. The top three protein hits, after DHR51 itself, are shown above in order of most similar to least: *dissatisfaction* (A), *seven up* (B), and *tailless* (C). + mark conservative amino acid changes.

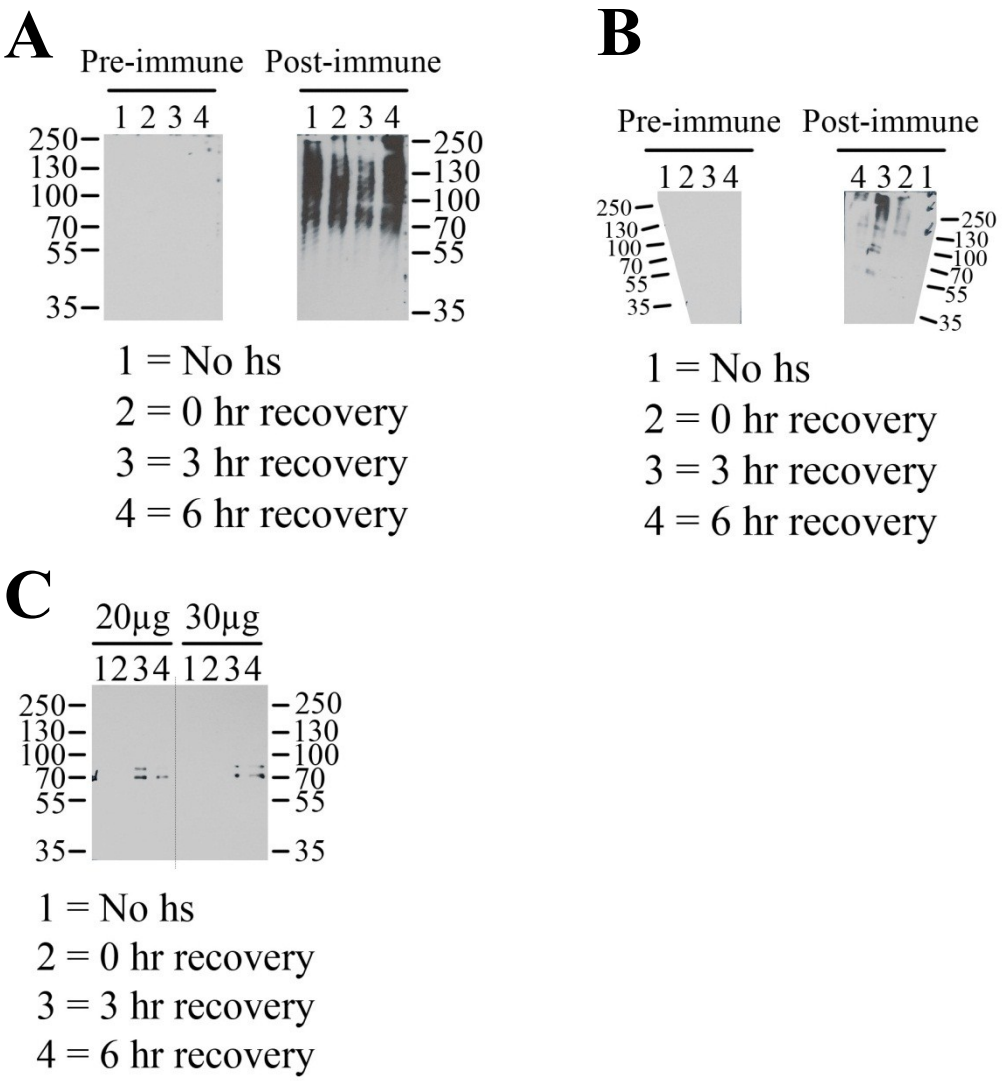

Figure A-3. Trial of rabbit immune serums before final antibody purification. Wandering *hs-DHR51* L3 larvae were either not heat shocked (hs) (Lane 1) or were heat shocked for one hour at 37.5°C and allowed to recover for 0 hours (Lane 2), 3 hours (Lane 3), or 6 hours (Lane 4). DHR51 is expected to have a size of approximately 70 kDa. A) A western blot using a trial rabbit DHR51 antibody (#295) (used at 1:300) is shown on the right (post-immune). The pre-immune serum (1:50), which should not have a DHR51 antibody is shown on the left. A goat anti-rabbit HRP secondary antibody was used (1:5000). 20 µg of protein was loaded into each lane. The blot was exposed to X-ray film for 30 seconds. B) A western blot using a trial rabbit DHR51 antibody (#298) (used at 1:500) is shown on the right. The pre-immune serum (1:50), which should not have a DHR51 antibody is shown on the left. A goat anti-rabbit HRP secondary antibody was used (1:8000). 20 µg of protein was loaded into each lane. The blot was exposed to X-ray film for 5 min. The gel ran a little crooked. C) A western blot using the affinity-purified DHR51 antibody from rabbit #298 (1:500). A goat anti-rabbit HRP secondary antibody was used (1:8000). The blot was exposed to X-ray film for 5 min. The left side of the blot was loaded with 20 µg of protein and 30 µg was loaded on the right side. This is the same blot from Figure A-1A. On the sides is a PageRuler Plus Prestained Protein Ladder, 10 to 250 kDa. The ladder is in kDa.

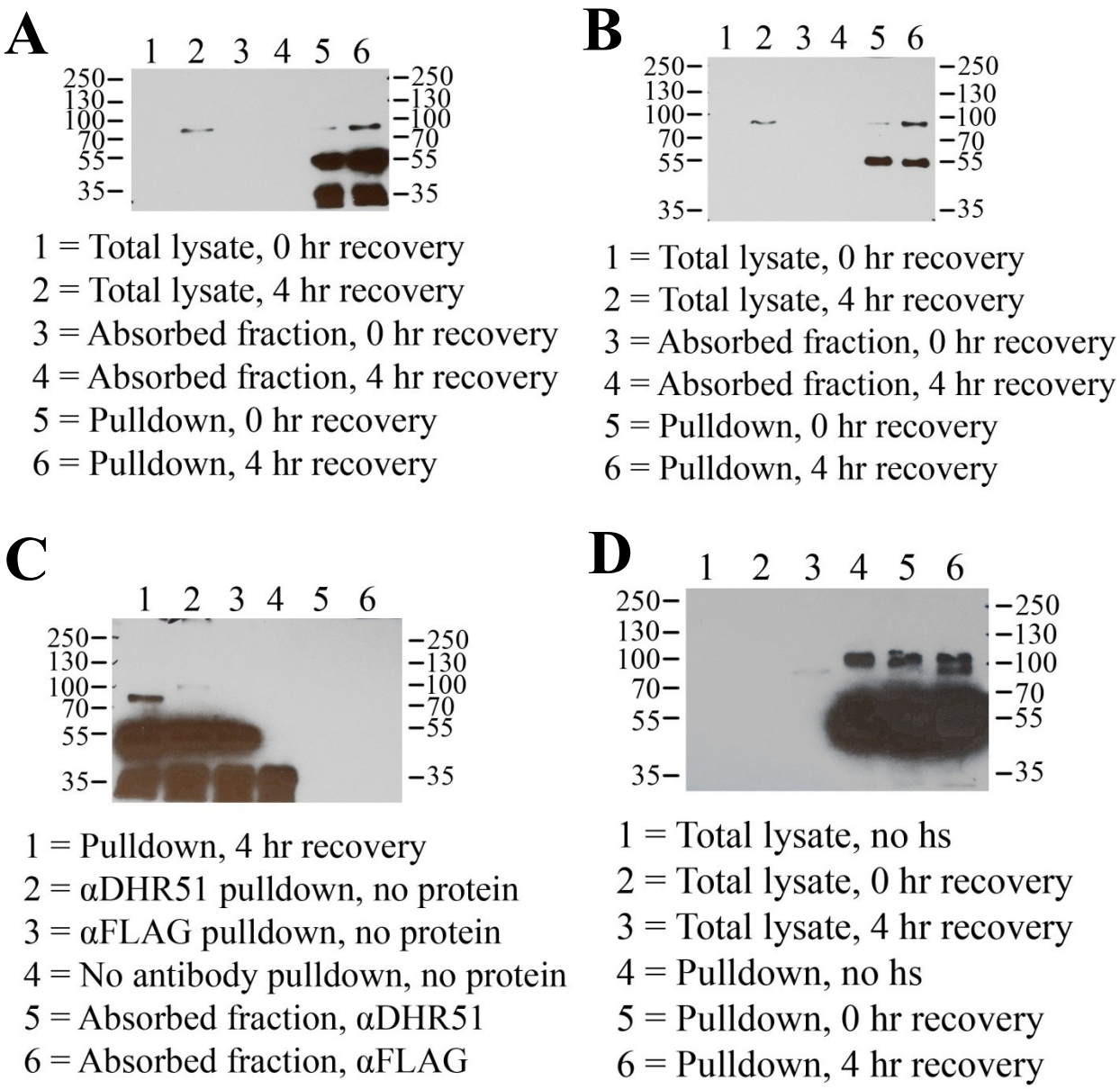

Figure A-4. Pull-down of FLAG-DHR51 with a FLAG and DHR51 antibody. Wandering *hs-FLAG-DHR51* L3 larvae were either not heat shocked (hs) or were heat shocked for one hour at 37.5°C and allowed to recover for 0 hours or 4 hours. DHR51 is expected to have a size of approximately 70 kDa. Total lysate is the input protein extract. The absorbed fraction is the protein extract after being exposed to the pull-down antibody and IgG bound protein G beads. A) DHR51 was pulled down with a rabbit FLAG antibody (1:50) and IgG bound Protein G beads. A western blot was performed with my rabbit DHR51 antibody (1:400) and a goat anti-rabbit HRP secondary antibody (1:7000). The blot was exposed to X-ray film for 30 seconds. B) DHR51 was pulled down with my rabbit DHR51 antibody (4 µg). A western blot was performed with a rabbit FLAG antibody (1:1000) and a goat anti-rabbit HRP secondary antibody (1:7000). The blot was exposed to X-ray film for 30 seconds. The total lysate was shown in Figure A-1B at a longer exposure. C) A control pull-down / western blot was done to identify the unexpected (non-specific) bands in the previous pull-downs. Lane 1 is the only lane that has a protein extract

input, which is from a FLAG pull-down. A western blot was performed with my rabbit DHR51 antibody (1:400) and a goat anti-rabbit HRP secondary antibody (1:7000). The blot was exposed to X-ray film for 20 seconds. α = anti. D) Protein extraction and pull-down were done under non-denaturing conditions. DHR51 was pulled down with my rabbit DHR51 antibody (3.5 μg). A western blot was performed with a rabbit FLAG antibody (1:1000) and a goat anti-rabbit HRP secondary antibody (1:7000). The blot was exposed to X-ray film for 1 min. On the sides is a PageRuler Plus Prestained Protein Ladder, 10 to 250 kDa. The ladder is in kDa.

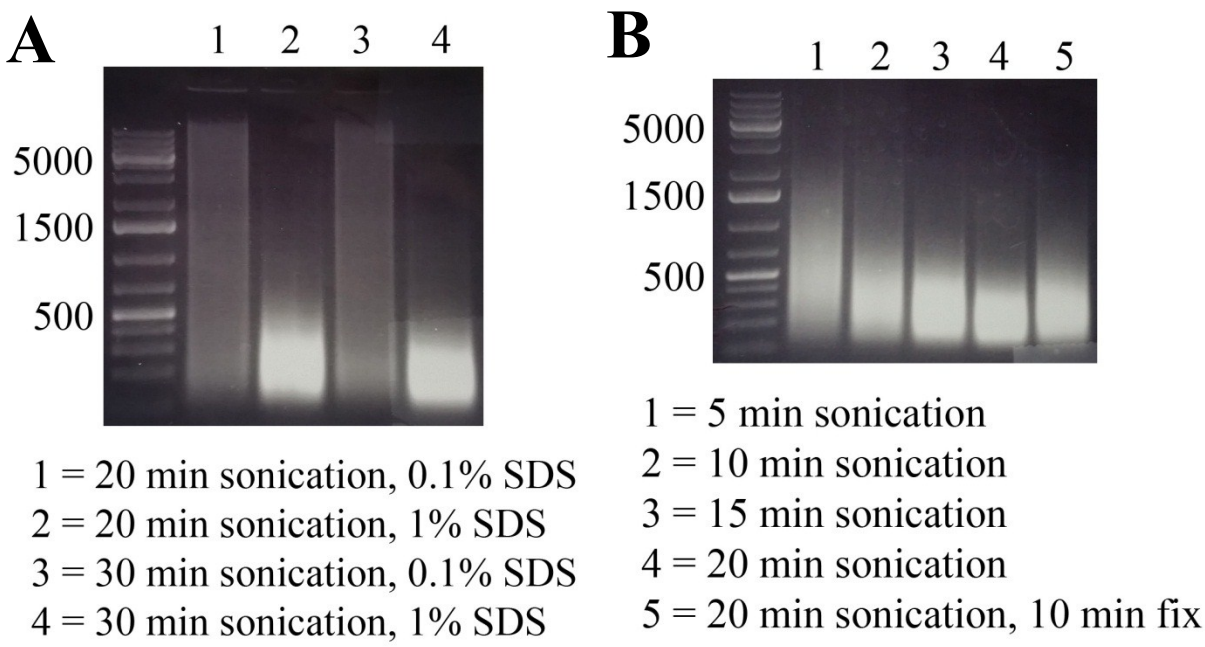

Figure A-5. Optimization of *Drosophila* whole body L3 larvae sonication prior to ChIP. DNA from wandering w^{1118} whole body L3 larvae was extracted. The protocol for sample preparation and the sonicator settings are outlined in Chapter 2.1.14.4. A) Optimization of the protocol and buffers. SDS (sodium dodecyl sulfate) concentration was found to be critical for sonication. B) A range of sonication times were used to obtain the optimal size of DNA fragments around 300 bps. DNA was fixed for 5 min, unless otherwise stated. DNA was run on an agarose gel. The ladder used is the GeneRuler 1kb Plus DNA Ladder. The thick white bands of the ladder are marked on the left of the gel (in base pairs).

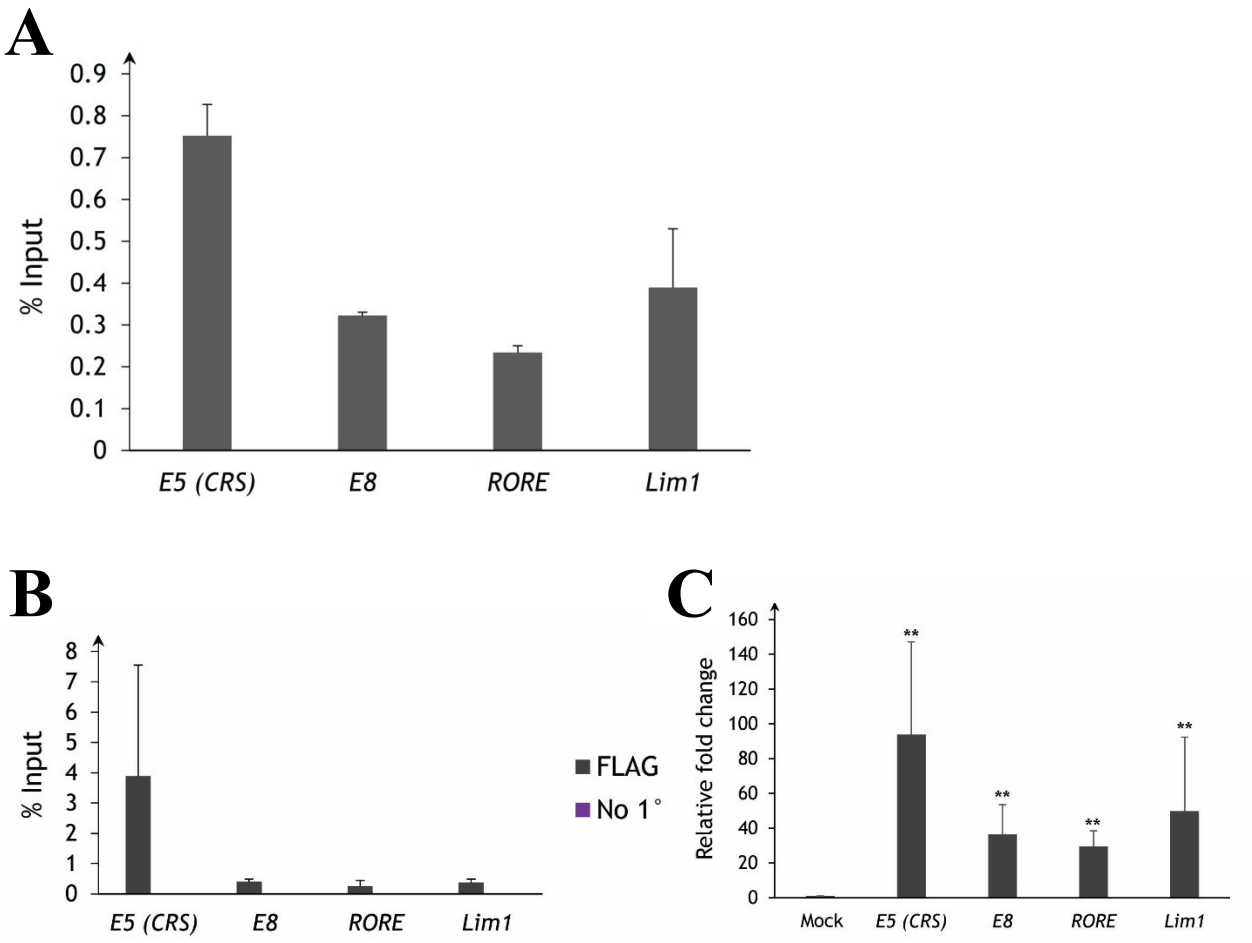

Figure A-6. DHR51 ChIP-qPCR of *period* with a DHR51 and FLAG antibody was unsuccessful. A) DHR51 ChIP-qPCR using my constructed DHR51 antibody. Wandering *hs-FLAG-DHR51* L3 larvae were heat shocked and allowed to recover for 4 hours. Whole body larvae were used for the ChIP. Previous research demonstrated that DHR51 bound to *E5* (*CRS*), *E8*, and *RORE* DNA sequences from the *period* locus and that DHR51 did not bind to *Lim1*. B) DHR51 ChIP-qPCR using a FLAG antibody and mock, no primary antibody (No 1°) ChIP was included as a control. Wandering *hs-FLAG-DHR51* L3 larvae were heat shocked and allowed to recover for 4 hours. Whole body larvae were used for the ChIP. The no primary antibody is included in the graph, but the values are so low that they are not visible. C) Relative fold change was calculated comparing the ChIP and mock (no primary antibody) ChIP data from (B). A Student's t-test was used to determine significance relative to the no antibody (mock) ChIP. ** = P-value < 0.01.

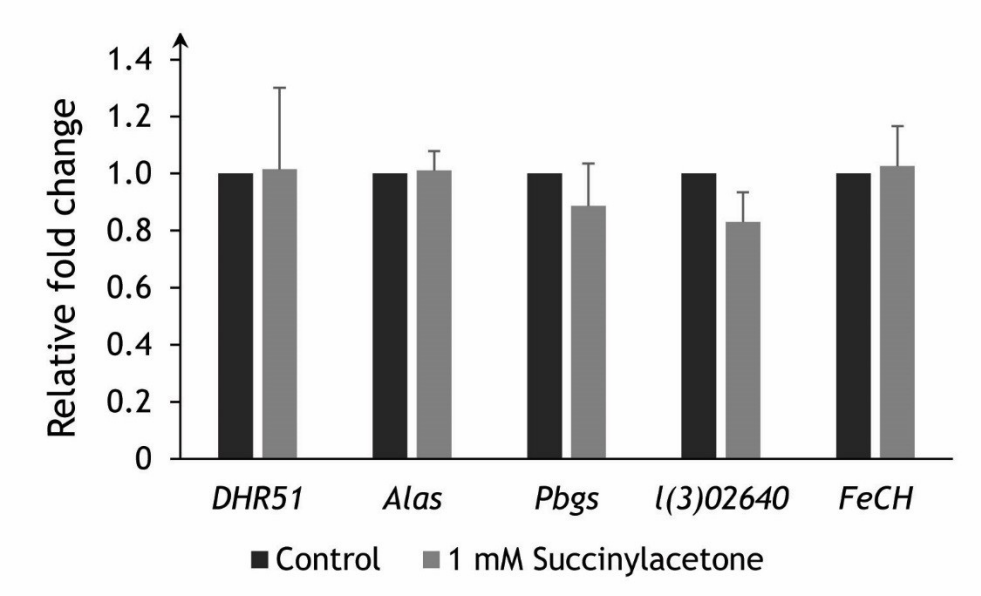

Figure A-7. 1 mM succinylacetone treatment of S2 cells did not induce *Alas* or other heme biosynthetic genes. S2 cells were incubated in 1 mM succinylacetone for 24 hours prior to RNA extraction and qPCR. The control had equal volumes of water added as the succinylacetone treatment. A Student's t-test determined that gene expression between control S2 cells and 1 mM succinylacetone-treated S2 cells was not significantly different.

A

AATCTGAAATCGTACATCGAGACGTTAACATCATCATCGCGGCACACTCGCAGCGCC
GTCGGATCGGATTGGTTCGGTTTCATCAGCGGGAATCAGAGGACCGTCCACTTGCCG
TCGCCTCTCCACGATTGCAAATTAATATGGAGCCTACTGCGATGAACCCGAAAAGTG
CCATTTAAAAGTGGTGTTTTAGAAATTCTTACAAATAGTGTCAATTGTTAATAAACTT
TTCAACGAGGTGTGATCTTTAATCGCAGT**CCG**CCAAAGCTCAACAAAATGAATAAG
GAAGAAAATTCCTCCGAAACACGACCATCTTCTCAAGGTAAATTAGTGTGTTAATAA
AAACATGAGTATGGTGATGAAATATATTTATTAAGCTGTAAACACAAAGGTGTGGTT
TCCTTACTTAAATACATAAAAAAATAAATATACAAGATGGCCCTAATGGTGGCTAAA
AATTCCTTTACCAACAAATTTTAAAAAGGACAATATCACGTTTGTTGGGAAATTGTG
CGTGAAATATAATTACGTTTCTTACACCCACGATTAATTAGGA**CGG**…

B

…GTGATGCTGTCGCAGCACACAAAGACGCAGTTCACCGCCCAGATAGCCAGATTCG
GACGACTCCTTCTCATGCTGCCGTTGCTGCGCATGATCAGCTCCCACAAGATTGAGT
CCATCTATTTTCAGCGCACTATT**GGG**AACACGCCCATGGAAAAGGTGCTCTGTGACA
TGTATAAGAACTAGTTAACTCGAGCTTTAAGTTACAACAAATTTAAATAAATATGTT
TTTGTGTCTTGAATGTTAGATGGCGTGACTTTTGATTTTTCCAGTTTTTCACCACTAGT
TGCATATAATTTCATATAAAAATGCTATAGAAAACAAAGTTAAAAAAAAAAAAAAA
TTTGATCGAAAATTATGTGTACTTTTTTTATCTGTACAAAGAACAAGACGCCATGAA
TTAACGTATGAATTTGAATTTTTTAATGAGTTAGCGCCAAAAGTTTTAGTGTTCAATA
ACATACACGGTGCTGTGTTGTAAAATGTATATTTCTATACAA**CCA**AGCTGGTTTCGC
TACCGTCC

Figure A-8. Target sequences of gRNAs for CRISPR to insert FLAG tags to the endogenous *DHR51* locus. A) gRNA target sequences for the N-terminal tag for DHR51. The grey highlight is Exon 1. The non-highlighted sequence is Intron 1. The Turquoise ATG is the DHR51 start codon. B) gRNA target sequences for the C-terminal tag for DHR51. The grey highlight is the last exon, Exon 10. The non-highlighted sequence is non-coding sequence. The Turquoise TAG is the DHR51 stop codon. The yellow highlights mark the two gRNA target sites. Bold letters are the targeted PAM sequence (NGG).

A

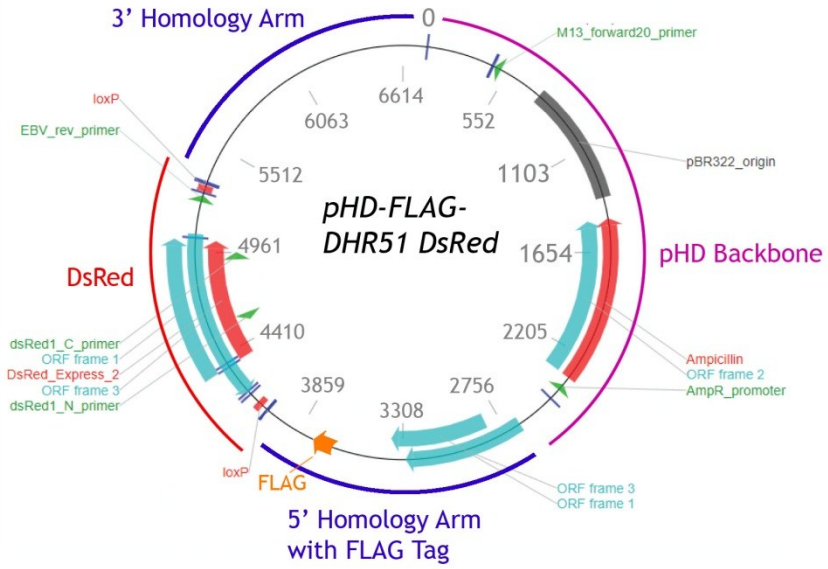

B

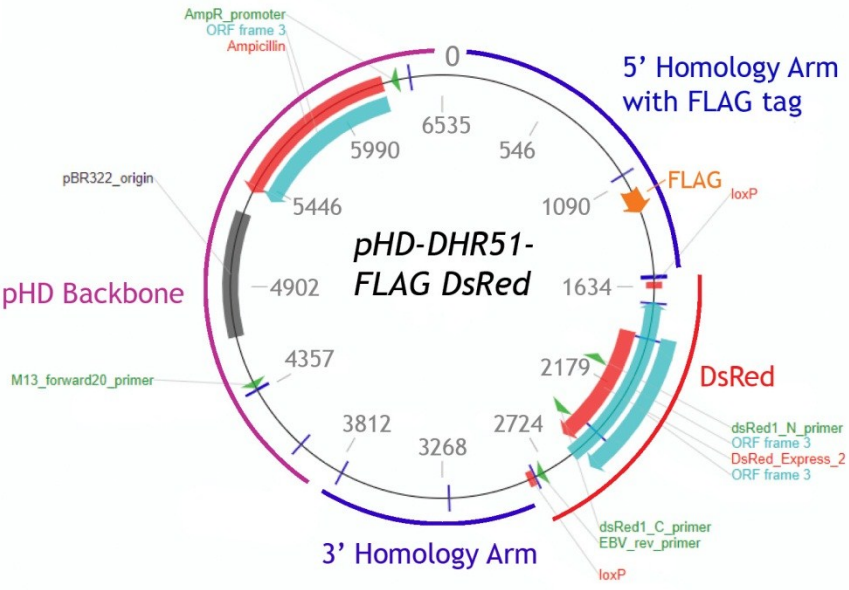

Figure A-9. pHD-*DsRed* Flag-tagged *DHR51* CRISPR plasmids designed for homology-directed repair to add a FLAG tag to the endogenous *DHR51* locus and *DsRed* selectable marker. A) A CRISPR plasmid to add a FLAG tag to the N-terminal of DHR51. B) A CRISPR plasmid to add a FLAG tag to the C-terminal of DHR51. Sections of the plasmid are labeled with coloured curved lines. Plasmid figures were designed by inputting the plasmid sequence into the Analyze Sequence resource on addgene.org and then modified.